Polimery w Medycynie

Polymers in Medicine

BIANNUAL ISSN: 0370-0747 e-ISSN: 2451-2699 polimery.umw.edu.pl

2025, Vol. 55, No. 2 (July–December)

Ministry of Science and Higher Education – 70 pts.
Index Copernicus (ICV) – 121.14 pts.

Wroclaw Medical University

Polimery w Medycynie

Polymers in Medicine

Polimery w Medycynie
Polymers in Medicine

ISSN 0370-0747 (PRINT) ISSN 2451-2699 (ONLINE) polimery.umw.edu.pl

BIANNUAL
2025, Vol. 55, No. 2
(July–December)

"Polymers in Medicine" is an independent, multidisciplinary forum to exchange scientific and clinical information, which publishes original papers (technical, analytical, experimental, clinical), preliminary reports and reviews regarding the use of polymers (natural and synthetic) and biomaterials in different specialties of medicine (biochemistry, clinical medicine, pharmacology, dentistry, implantology), biotechnology and veterinary science.

Address of Editorial Office
Marcinkowskiego 2–6
50-368 Wrocław, Poland
Tel.: +48 71 784 11 33
E-mail: redakcja@umw.edu.pl

Publisher
Wroclaw Medical University
Wybrzeże L. Pasteura 1
50-367 Wrocław, Poland

Online edition is the original version of the journal

Editorial Policy

During the review process, the Editorial Board conforms to the "Uniform Requirements for Manuscripts Submitted to Biomedical Journals: Writing and Editing for Biomedical Publication" approved by the International Committee of Medical Journal Editors (http://www.icmje.org/). Experimental studies must include a statement that the experimental protocol and informed consent procedure were in compliance with the Helsinki Convention and were approved by the ethics committee.

For more information visit the following page: https://polimery.umw.edu.pl

Indexed in: Scopus, OCLC, WorldCat, PBL, EBSCO, MEDLINE, Index Copernicus

Typographic design: Monika Kolęda, Piotr Gil
Cover: Monika Kolęda
DTP: Wroclaw Medical University Press

Circulation: 11 copies

Polimery w Medycynie

Polymers in Medicine

BIANNUAL 2025, Vol. 55, No. 2 (July–December)

ISSN 0370-0747 (PRINT)
ISSN 2451-2699 (ONLINE)
polimery.umw.edu.pl

Contents

PREFACE

Dear Readers,

The scientific community welcomes with great enthusiasm and curiosity the new discoveries honored by the Nobel Committee. In medicine, the groundbreaking work of Mary E. Brunkow, Fred Ramsdell and Shimon Sakaguchi has the potential to revolutionize the treatment of autoimmune and cancer diseases and to significantly influence the development of transplantology. In chemistry, the pioneering achievements of Susumu Kitagawa, Richard Robson and Omar M. Yaghi may provide invaluable contributions to the design of new drug carriers based on materials with exceptionally large specific surface areas. Both of these research areas clearly relate to the chemistry of polymeric protein structures as well as to polymer chemistry. Our authors likewise contribute to this growing field, presenting studies on polymer structures relevant to medicine and pharmacy. Their research encompasses the use of polymers in pharmaceutical dosage forms such as metronidazole tablets, topical creams and ointments, and ophthalmic preparations. Two noteworthy articles in this issue are devoted to polymeric materials applied in dentistry. Also significant are two articles that examine the stability of polymeric substances relevant to medicine and pharmacology. The first analyzes the impact of ethylene oxide sterilization on the properties of polymeric materials of crucial importance in medical applications, while the second focuses on photodynamic therapy. Equally compelling is the article exploring the potential use of plant viruses as innovative drug carriers.

An important milestone for our journal was the conference held on December 4–5, 2025, at Wrocław Medical University under the patronage of *Polimery w Medycynie – Polymers in Medicine*. The event, entitled "Pharmaceutical Sciences – Physical Chemistry and Biophysics for Pharmacy 2025," led to an increase in submissions and further strengthened the journal's position in the scientific community. I would like to take this opportunity to remind our readers that the highly regarded CiteScore achieved by *Polimery w Medycynie – Polymers in Medicine* (currently 3.5) should encourage researchers from around the world to contribute their work to our journal – we warmly invite you to submit your manuscripts!

The world of science continues its creative and constructive work despite a growing sense of global uncertainty, ongoing armed conflicts and potential threats to international security. We all hope for effective, just and peaceful solutions to the challenges the world has faced over the past year. As the holiday season approaches and we prepare to welcome the new year 2026, may this time offer moments of rest – and perhaps also the opportunity to explore the articles presented in this issue of *Polimery w Medycynie – Polymers in Medicine*.

I extend my warmest wishes to all our readers and to the entire Editorial Team of *Polimery w Medycynie – Polymers in Medicine* for a prosperous New Year 2026 and a peaceful holiday season. All the best!

Prof. Witold Musiał, PhD, DSc
Editor-in-Chief
Polimery w Medycynie – Polymers in Medicine

WSTĘP

Drodzy Czytelnicy,

świat nauki z radością i zaciekawieniem przyjmuje nowe odkrycia nagradzane przez Komitet Noblowski. W świecie medycyny odkrycia Mary E. Brunkow, Freda Ramsdella i Shimona Sakaguchiego mogą zrewolucjonizować terapię chorób autoimmunologicznych i nowotworowych oraz wpłynąć na rozwój transplantologii. W obszarze chemii pionierskie prace Susumu Kitagawy, Richarda Robsona i Omara M. Yaghiego są ważne dla tworzenia nowych nośników leków opartych o materiały o olbrzymiej powierzchni właściwej. Oba te kierunki badań są wyraźnie związane z chemią polimerowych struktur białkowych i chemią polimerów. Również nasi autorzy włączają się w nurt badań nad strukturami polimerowymi istotnymi z punktu widzenia medycyny i farmacji – tematy badawcze obejmują zastosowanie polimerów w takich postaciach leku, jak tabletki z metronidazolem, kremy i maści stosowane na skórę oraz leki do oczu. Dwa ważne artykuły poświęcono materiałom polimerowym stosowanym w stomatologii. Warto też zwrócić uwagę na dwa inne artykuły poruszające tematykę stabilności substancji polimerowych istotnych dla medycyny i farmakologii. Pierwszy z nich omawia wpływ sterylizacji tlenkiem etylenu na właściwości materiałów polimerowych o istotnym znaczeniu w medycynie, a drugi skupia się na terapii fotodynamicznej. Równie ciekawie prezentuje się artykuł nt. potencjalnego wykorzystaniu wirusów roślinnych jako nośników leków.

Ważnym wydarzeniem w życiu naszego czasopisma była konferencja zorganizowana w dniach 4–5 grudnia 2025 w Uniwersytecie Medycznym we Wrocławiu pod patronatem naszego wydawnictwa pt. „Nauki Farmaceutyczne – Chemia Fizyczna i Biofizyka dla Farmacji 2025", która zaowocowała zgłoszeniem szeregu nowych artykułów i przyczyniła się do umocnienia pozycji *Polimerów w Medycynie – Polymers in Medicine*. Przypominam Państwu przy okazji, że istotny parametr CiteScore, wynoszący dla naszego czasopisma 3,5, powinien zachęcać naukowców z całego świata do składania prac do naszego czasopisma – serdecznie zapraszamy!

Świat nauki nie zaprzestaje twórczej, konstruktywnej pracy mimo poczucia nadchodzących zmian, tlących się konfliktów zbrojnych oraz potencjalnych zagrożeń globalnego bezpieczeństwa. Wszyscy chyba mamy nadzieję na skuteczne, sprawiedliwe i pokojowe rozwiązanie problemów towarzyszących nam na całym świecie w mijającym roku. Zaczynamy już okres świąteczny, a wkrótce przywitamy nowy rok 2026. Niech ten świąteczny czas będzie okazją do odpoczynku, ale może i lektury artykułów zawartych w niniejszym wydaniu *Polimerów w Medycynie – Polymers in Medicine*. Naszym Czytelnikom, a także zespołowi redakcyjnemu składam serdecznie życzenia wszelkiej pomyślności w Nowym Roku 2026 oraz spokojnego okresu świątecznego. Wszystkiego dobrego!

Prof. dr hab. Witold Musiał
Redaktor Naczelny
Polimery w Medycynie – Polymers in Medicine

Comparison of the optical and mechanical properties of plastics before and after ethylene oxide sterilization

Hans de Brouwer[1,A–F], Muhammad Maqsood[2,A–F]

[1] SABIC, Technology & Innovation, Bergen op Zoom, the Netherlands
[2] SABIC, Technology & Innovation, Geleen, the Netherlands

A – research concept and design; B – collection and/or assembly of data; C – data analysis and interpretation;
D – writing the article; E – critical revision of the article; F – final approval of the article

Polymers in Medicine, ISSN 0370-0747 (print), ISSN 2451-2699 (online) *Polim Med*. 2025;55(2):79–87

Address for correspondence
Hans de Brouwer
E-mail: hans.debrouwer@sabic.com

Funding sources
None declared

Conflict of interest
None declared

Acknowledgements
The authors would like to thank Jos de Heer for measuring the infrared spectra.

Received on April 8, 2025
Reviewed on June 23, 2025
Accepted on July 9, 2025

Published online on December 19, 2025

Abstract

Background. Ethylene oxide (EO) sterilization is the most used sterilization method for disposable medical devices. Its popularity is based on the fact that it can be executed on industrial scale on full pallets of packed products and the fact that many materials are compatible with this sterilization technique.

Objectives. This article describes an introduction to EO as a sterilization technique and further studies on the compatibility of medical grade plastics with EO sterilization.

Materials and methods. Fourteen different healthcare polymer grades have been exposed to EO. This includes frequently used polyethylenes, polypropylenes, polyesters, and polycarbonates. Their mechanical and optical properties before and after exposure with EO were determined.

Results. After both the statistical analysis and a comparison with the accuracy of the measurement system, it can be concluded that all tested polymers retained their mechanical properties as measured by tensile and Izod impact testing after 1 sterilization cycle. Optical measurements showed that only 2 of the polymer grades had a minor discoloration, while all other materials had a very limited color change.

Conclusions. It has been shown that all families of plastics typically used in disposable medical products can be sterilized with EO without significant change in properties as determined on standardized test specimen.

Key words: infection control, sterilization, polymers, plastics, ethylene oxide

Cite as
de Brouwer H, Maqsood M. Comparison of the optical and mechanical properties of plastics before and after ethylene oxide sterilization. *Polim Med*. 2025;55(2):79–87. doi:10.17219/pim/208083

DOI
10.17219/pim/208083

Highlights

- Ethylene oxide (EO) sterilization effectively preserves the mechanical properties and performance of medical-grade polymers.
- Common polymers such as polyethylenes, polypropylenes, polyesters, and polycarbonates show excellent compatibility with EO sterilization.
- Minimal color change or discoloration occurs in most polymer materials after a single EO sterilization cycle.
- EO sterilization ensures safe and reliable processing of disposable medical devices without degrading polymer structure or integrity.

Background

Treating patients in a hospital requires sterile medical devices. Care must be taken to ensure that their health benefits from treatment and does not deteriorate due to the infamous "hospital-acquired infections". Patients are vulnerable human beings who can easily contract infections, especially when their natural barrier, i.e., the skin, is open or damaged through surgery or wounds. Every tool used under these circumstances must be sterile. Devices may be reusable (cleaned and sterilized) or single-use (pre-sterilized and discarded). Sterilization is defined as the process that eliminates microbial life, including transmissible agents such as fungi, bacteria, viruses, and spores, from a surface, fluid or any material that will come into contact with a patient.[1–3] Sterilization can be performed using various methods, each with its own advantages and disadvantages. The most common terminal techniques are listed in Table 1. Terminal sterilization refers to the process in which the sterilizing step is applied after the production and packaging of the devices or drug formulation. The packaging maintains the product's sterility until use once the sterilization process is complete. Material compatibility with sterilization techniques has been widely discussed in journal publications, books and industrial guidelines.[1,4–6]

For each technique, typical application areas are indicated in Table 1. The industrial space refers to large-scale production environments, such as those for medical devices or pharmaceutical formulations. The professional space includes dedicated sterilization departments in hospitals or external sterilization service providers. The general space refers to local medical practices, dental offices and similar settings. While the location and scale of sterilization are not necessarily critical, it is within the industrial application space that single-use devices, primarily composed of plastics, are sterilized. Here, approx. 45% of sterilization is performed using radiation techniques and 50% using ethylene oxide (EO).[7–9] For this reason, it is of paramount importance to establish material compatibility with these sterilization methods. The professional and general application areas mainly involve reusable tools, which are typically manufactured from metal or, in some cases, from high-end engineering plastics.

Radiation techniques are widely used, with gamma sterilization being the most common method today. It is estimated that around 40% of all single-use medical devices are sterilized by gamma radiation.[8] The advantage of this method is that it can be applied under ambient conditions and to full pallets of products in their primary and secondary packaging as the final step before shipment. This

Table 1. Overview of most common sterilization techniques

Sterilization technique	Mechanism	Application space		
		industrial	professional	general
Ethylene oxide	gas	✓	✓	–
Hydrogen peroxide	gas	–	✓	✓
Ozone	gas	–	✓	✓
Gamma	radiation	✓	–	–
Electron beam	radiation	✓	–	–
X-ray	radiation	✓	–	–
UV-C	radiation	–	✓	✓
Dry heat	temperature 150–180°C	✓	✓	✓
Autoclaving	temperature 100–140°C	✓	✓	✓
Disinfectant (wipes)	chemical	–	✓	✓

technique is typically performed at dedicated facilities, as it requires a cobalt-60 (^{60}Co) radioactive source, which necessitates specific permits, expertise and safety measures. Plastics show variable compatibility with gamma radiation.[4]

Most materials retain their performance but may exhibit a color change. A few, however, can deteriorate and lose functionality. Notably, polypropylene (PP) requires specific stabilization, as it is highly sensitive to radiation. Electron beam and X-ray sterilization are alternative applications of ionizing radiation and have effects on materials similar to those of gamma radiation.[5] UVC radiation is commonly used for water and air disinfection but gained prominence in medical applications during the COVID-19 pandemic.[6]

Temperature-based sterilization can be performed using either dry heat or steam exposure. The excellent heat transfer properties of steam allow for shorter sterilization cycles at lower temperatures compared with dry heat. However, both heat and humidity can significantly influence material properties. The advantage of these techniques is their wide availability and compatibility with most metals, ceramics and glass, making them the preferred methods in doctors' offices, hospital sterilization departments and sterilization service facilities.

Chemical disinfection is not strictly a sterilization technique but is related in that it aims to disinfect surfaces by eliminating or reducing the microbial load. A variety of chemical wipes are used to clean stationary surfaces and equipment in medical environments. Material compatibility varies greatly and depends on the specific chemicals used.

In gas-based sterilization, EO is the only method used on an industrial scale for single-use devices. Its use in sterilizing single-use medical devices is roughly comparable to that of gamma radiation, accounting for an estimated 40–50%.[8,9] The use of other gases is increasing, but their application remains relatively limited. Hydrogen peroxide, in vapor or plasma form,[10,11] and ozone[12] can oxidize organic molecules and attack DNA, proteins and other microbial components, thereby preventing their transmission and replication. These gases can be generated in situ, offering logistical advantages and leaving no residues on sterilized devices.

Objectives

This article briefly discusses the fundamentals of EO sterilization. For more detailed information, several comprehensive review papers are available.[7,13] In addition, the effects of EO on commonly used plastics are examined.

Materials and methods

Outline

Ethylene oxide readily alkylates polar groups such as hydroxyl and carboxyl groups. The reaction is exothermic and occurs rapidly at ambient temperatures. This reactivity gives EO its sterilizing capability: When polar groups in proteins and DNA are alkylated, the microbes carrying them are rendered nonviable and unable to replicate or multiply. However, this strong sterilizing action also makes EO gas toxic. It must be handled under strictly controlled conditions with extreme care. Another associated risk of EO is its flammability. Despite these hazards, the use of EO for sterilization offers many advantages. Unlike gamma radiation, it does not require the handling of dangerous or highly regulated radioactive isotopes. It can also be applied to temperature- and radiation-sensitive devices. Most materials are reported to be compatible with EO sterilization. The Advancing Safety in Health Technology (AAMI) Technical Information Report: *Compatibility of Materials Subject to Sterilization* lists many material classes and provides an initial indication of their compatibility. In the section covering EO, only acrylics received a rating lower than "excellent".[4] All terminal sterilization techniques are applied to packaged products. In the case of EO sterilization, the gas must be able to enter and exit the packaging easily to achieve an acceptable sterilization cycle duration. A practical solution is to use packaging that is at least partially made of permeable materials such as paper or nonwoven plastic fabrics. These materials must meet strict pore size specifications to ensure that gases can penetrate efficiently while preventing microbial passage. Otherwise, sterility cannot be maintained during transport and storage.

A typical EO sterilization cycle proceeds as follows[14]:
– The load to be sterilized is placed in an airtight sterilization chamber.
– Air is removed using a vacuum and replaced with an inert gas such as nitrogen.
– A humidification step is carried out by injecting steam.
– EO is then introduced into the chamber. Typical concentrations are within the range of 450–1200 mg/L, at temperatures between 37°C and 63°C and relative humidity of 40–80%, for a duration of 1–6 h. Higher concentrations may cause difficulties in removing residual EO from the product, while lower concentrations may result in incomplete sterilization.

The products are degassed using alternating vacuum and nitrogen cycles. To further reduce residual EO levels, the sterilized items may be stored in an aeration chamber for 8 h up to 1 week. Sterilization efficiency depends on careful control of EO concentration, humidity, temperature, and exposure time. For each product and packaging combination, the speed and depth of the vacuum must be optimized. When the secondary packaging

Fig. 1. Several examples of packaging compatible with EO sterilization

is also compatible with the process, sterilization can be applied to full pallets or containers. Figure 1 shows examples of gas-permeable packaging. The packaging consists of 2 parts: 1) a transparent polyethylene film, and 2) a white, opaque, gas-permeable layer made of either paper or nonwoven fabric. DuPont's Tyvek®, a nonwoven material made from HDPE fibers, is frequently used for this purpose.[15] The 2nd part allows air, water vapor and EO gas to pass in and out of the package during the various stages of the sterilization cycle without causing damage. Additionally, the pore sizes in this layer must be small enough to prevent the entry of microbes, viruses, spores, and bacteria after sterilization. The shelf life of sterilized products typically ranges from 3 to 5 years, requiring the packaging to maintain its integrity throughout this period.[16] One disadvantage specific to EO sterilization is the presence of undesirable residual chemicals in sterilized products.[17,18] These products may contain traces of EO, ethylene glycol (EG), and ethylene chlorohydrin (ECH).[17] All 3 substances are toxic, and EO additionally possesses carcinogenic properties. Ethylene glycol forms through the reaction of EO with water (humidity), while ECH is produced when EO comes into contact with free chloride ions, such as those present in polyvinyl chloride. Patients may develop allergic reactions upon exposure to these residues, particularly with repeated use.[19,20] For patients with chronic conditions requiring regular treatment, such as those undergoing dialysis, EO-sterilized devices are typically avoided, and radiation-sterilized consumables are preferred. Because of these disadvantages, as well as the dangers and environmental impact of EO emissions, the U.S. Food and Drug Administration (FDA) has launched a program to support reducing EO concentrations and exploring alternative sterilization methods.[21] Nevertheless, EO sterilization remains indispensable due to its large-scale applicability and broad material compatibility. With approx. 20 billion medical devices sterilized annually by EO in the USA alone, concerns have arisen that facility closures driven by environmental regulations could significantly impact the availability of essential medical devices.[2]

Methods

The plastic materials were molded according to ISO 294-1:2017 using an Engel 90t injection molding machine to produce tensile bars with ISO 527/1A dimensions and impact bars measuring 80 × 10 × 4 mm. Samples for color measurements were also prepared to evaluate color changes following EO sterilization. The materials were sterilized with EO in accordance with the ISO 11135:2014 standard testing method, and the samples were packed in open plastic bags.

Tensile properties were measured at a crosshead speed of 50 mm/min following ISO 527-1:2019, while impact strength was determined according to ISO 180:2023. Color measurements were performed using a Konica Minolta

CM-5 spectrophotometer (Konica Minolta Co., Ltd, Tokyo, Japan) in accordance with ASTM E313-96, employing illuminant D65 in the CIELAB color space.

The 3 coordinates represent color positions along the following axes: L* (lightness, 0 = black, 100 = white), a* (negative = green, positive = red) and b* (negative = blue, positive = yellow). The Yellowness Index (YI) is a calculated parameter used to describe shifts in color toward the yellow spectrum.

Materials

Dedicated healthcare grades from SABIC's portfolio were tested. These materials are manufactured under Good Manufacturing Practice (GMP) to meet the stringent quality standards of the medical industry. The selected materials are used in a wide range of applications, including drug delivery devices (e.g., inhalers, injection pens, insulin pumps), diagnostic devices (e.g., glucose monitors, wearables), syringes, ampoules (e.g., for eye drops), primary pharmaceutical packaging, tubes, intravenous (IV) bags, and blood filters, among others. Although SABIC does not supply materials for implant applications, other HDPE grades are known to be used in that field, e.g., as bone replacement materials.[22] Many of these applications can employ EO for sterilization purposes. The following materials were used: PCG07 low-density polyethylene (LDPE), PCG453 and PCG863 high-density polyethylene (HDPE), PCGR40 polypropylene random copolymer with ethylene (PP r), 58MNK10 polypropylene impact copolymer with ethylene (PP icp), PCGH19 polypropylene homopolymer (PP h), CYCOLAC™ HMG94MD and HMG47MD acrylonitrile–butadiene–styrene copolymers (ABS), VALOX™ HX325HP and HX312C polybutylene terephthalate (PBT) polyesters, LEXAN™ HP2REU and HP4REU polycarbonate (PC), CYCOLOY™ HC1204HF PC/ABS blend, and XYLEX™ HX7509HP blend of PC and polycyclohexylenedimethylene terephthalate glycol-modified (PCTG) polyester. All materials were processed according to their respective datasheet recommendations, including temperature settings and pre-drying conditions.

Statistical analyses

Statistical analyses were performed using Minitab® v. 17.1.0 (Minitab Inc., State College, USA). Mechanical testing was typically conducted on 5 samples for each material before and after EO exposure. The 5 individual measurements were used to calculate an average value, which served as the single data point for each impact or tensile test. In the subsequent statistical analyses, the individual measurements and their results were evaluated. For all datasets (n = 5), normality tests were performed. The Anderson–Darling, Ryan–Joiner, and Kolmogorov–Smirnov tests generally yielded consistent outcomes. When normality was confirmed, an F-test was used to compare variances between 2 datasets collected before and after EO exposure. A two-sample t-test was performed on the same 2 datasets to test the null hypothesis that their means were equal. When equal variances were confirmed, the "assume equal variances" option was applied for the t-test. These analyses were conducted for all impact and tensile test results. For tensile elongation at break, an error occurred during some tests, causing the procedure to stop once 100% elongation was reached. This affected several unexposed samples. For these cases, a comparison was made between the 5 post-exposure measurements and the average value of unexposed samples obtained from historical data, using a one-sample t-test. Table 3 indicates which samples this applies to. Further details on hypothesis testing can be found in standard references on process improvement methodologies.[23]

Results and Discussion

Mechanical properties

The data obtained before and after EO exposure were first compared statistically using the approach described in the Materials section. This process eliminated most apparent differences. Average values for impact and tensile properties are presented in Tables 2 and 3. Differences between the 2 datasets are reported only when the statistical analysis (two-sample t-test) indicated significance at the 95% confidence level ($p < 0.05$). It should be noted that statistically significant differences do not necessarily correspond to the numerically largest absolute or relative changes. For all datasets comparing results before and after EO exposure, where statistical analysis confirmed significance, the practical significance of each difference was evaluated. This was done by comparing the magnitude of the change to the long-term standard deviation (SD) of a repeatedly measured Statistical Quality Control (SQC) sample. Table 4 presents the values obtained for a LEXAN™ PC sample measured over a 9-month period. The variation observed represents the inherent variability of the measurement system itself over that timeframe, independent of any sample variation. It is important to note that the SQC data were obtained in accordance with the relevant ISO test protocols, meaning that 5 measurements were taken to produce 1 average value, representing a single data point. The averages and standard deviations (SDs) presented in Table 4 are based on 36 such data points. In contrast, the statistical analyses in this report used individual measurements rather than averages of 5. One could argue that either the absolute or relative value of the SQC SD should be considered when comparing observed differences between samples to measurement variation across different material types. In any case, the differences observed in the notched Izod impact results are not practically relevant. For unnotched Izod impact, the values for the PP

Table 2. Statistical comparison of Izod impact energy before and after ethylene oxide (EO) exposure

Grade	Polymer	Notched impact [kJ/m²]			Unnotched [kJ/m²]		
		before	after	Δ*)	before	after	Δ*)
PCG07	LDPE	39	35	–	33	30	–
PCG453	HDPE	10	10	–0.3	85	60	–
PCG863	HDPE	7	7	–	86	99	–
PCGR40	PP r	3	4	0.6	102	94	–8
58MNK10	PP icp	12	12	–	110	107	–
PCGH19	PP h	2	2	–	60	60	–
HMG94MD	ABS	19	18	–	86	77	–
HMG47MD	ABS	23	23	–	155	166	–
HX325HP	PBT	4	4	–	144	143	–
HX312C	PBT	3	4	–	125	113	–12
HC1204HF	PC/ABS	49	47	–	166	171	–
HX7509HP	PC/PCTG	11	n.a.	n.a.	170	165	–
HP2REU	PC	38†	33†	–	176	169	–
HP4REU	PC	74†	53†	–	174	177	–

* Delta values are given only for datasets that show a statistically significant difference ($p < 0.05$); † broad distribution due to material ductile-brittle transition. PCG07 – low-density polyethylene (LDPE); PCG453 and PCG863 – high-density polyethylene (HDPE); PCGR40 – polypropylene random copolymer with ethylene (PP r); 58MNK10 – polypropylene impact copolymer with ethylene (PP icp); PCGH19 – polypropylene homopolymer (PP h); CYCOLAC™ HMG94MD and HMG47MD – acrylonitrile–butadiene–styrene copolymers (ABS); VALOX™ HX325HP and HX312C – polybutylene terephthalate (PBT) polyesters; LEXAN™ – HP2REU and HP4REU polycarbonate (PC); CYCOLOY™ – HC1204HF PC/ ABS blend; XYLEX™ HX7509HP – blend of PC and polycyclohexylenedimethylene terephthalate glycol-modified (PCTG) polyester.

Table 3. Tensile properties before and after sterilization with ethylene oxide (EO)

Grade	Polymer	Chord modulus [MPa]			Stress@Yield [MPa]			Strain@Yield [%]			Stress@Break [MPa]			Strain@Break [%]		
		before	after	Δ*)	before	after	Δ*)	before	after	Δ*)	before	after	Δ*)	before	after	Δ*)
PCG07	LDPE	141	135	–	9	9	–0.2	84.1	77.4	–6.6	8	8	–	96	90	–
PCG453	HDPE	896	822	–74	22	22	–0.5	10.4	10.8	0.4	13	15	–	578‡	782‡	–
PCG863	HDPE	1208	1137	–71	27	26	–1.0	8.7	8.9	0.3	13	11	–	275	647	–
PCGR40	PP r	1220	1231	–	30	29	–0.7	12.3	12.3		16	15	–1	97	96	–
58MNK10	PP icp	1484	1427	–	25	25	–0.5	4.4	4.4	0.1	18	19	–	91†	306	–
PCGH19	PP h	1722	1652	–70	37	36	–0.9	7.7	7.7		27	29	2	18	17	–
HMG94MD	ABS	2381	2430	–	46	46	–0.2	2.3	2.3	0.0	34	34	–	33	34	–
HMG47MD	ABS	2272	2362	89	48	47	–0.7	2.6	2.5	–0.1	33	34	–	18	15	–
HX325HP	PBT	2664	2691	–	58	58	0.6	10.3	9.2	–1.1	21	20	–	64	54	–
HX312C	PBT	2501	2559	–	56	57	0.7	3.8	4.0	0.2	51	49	–	12	15	–
HC1204HF	PC/ABS	2282	2270	–	55	55	–0.4	5.0	4.8	–0.2	51	52	–	107†	96	–
HX7509HP	PC/PCTG	2271	2238	–	60	59	–0.6	5.9	5.6	–0.3	56	59	–	99†	115	–
HP2REU	PC	2415	2444	–	64	64	–0.6	6.1	5.9	–0.2	62	66	4	114†	112	–
HP4REU	PC	2455	2452	–	64	63	–0.6	6.1	5.9	–0.1	63	63	–	94	97	–

* Delta values are given only for datasets that show a statistically significant difference ($p < 0.05$); † average of historical data. Value used as target value for 1 sample t-test; ‡ too few datapoints to determine statistical significance of difference. PCG07 – low-density polyethylene (LDPE); PCG453 and PCG863 – high-density polyethylene (HDPE); PCGR40 – polypropylene random copolymer with ethylene (PP r); 58MNK10 – polypropylene impact copolymer with ethylene (PP icp); PCGH19 – polypropylene homopolymer (PP h); CYCOLAC™ HMG94MD and HMG47MD – acrylonitrile–butadiene–styrene copolymers (ABS); VALOX™ HX325HP and HX312C – polybutylene terephthalate (PBT) polyesters; LEXAN™ – HP2REU and HP4REU polycarbonate (PC); CYCOLOY™ – HC1204HF PC/ABS blend; XYLEX™ HX7509HP – blend of PC and polycyclohexylenedimethylene terephthalate glycol-modified (PCTG) polyester.

Table 4. 2024 Statistical quality control data of a LEXAN polycarbonate material

Statistic	Izod impact strength [kJ/m²]	Chord modulus [MPa]	Stress@Yield [MPa]	Strain@Yield [%]	Strain@Break [%]
Average value	23.0	2428	48.5	2.77	23.9
Standard deviation	0.81	33	0.50	0.04	1.12
Relative standard deviation	3.5%	1.4%	1.0%	1.5%	4.7%

impact copolymer decreased by 8 kJ/m², while those for one of the PBT materials (HX312C) decreased by 12 kJ/m². The relative difference was below 10% in both cases and less than 3 times the relative SD of the SQC measurements. However, the absolute difference exceeded 3 times the SD. A few values for modulus and most values for stress and strain at the yield point showed statistically significant changes following sterilization, but the magnitude of these changes was limited – less than 3 times the SQC SD. The strain at break was not recorded for the SQC material due to the high variability between measurements. In the literature, stress at yield and strain at break are commonly used to assess the compatibility of materials with sterilization techniques or chemical exposure. Although strain at break is highly sensitive to small material changes, it also exhibits relatively high variability (SD), often rendering observed differences statistically insignificant. Based on the data showing statistical differences, all tested materials can be classified as "compatible."

Color retention

Color differences before and after EO sterilization of plastic parts were compared. Unpigmented or natural polymers are typically either colorless (transparent) or opaque (white). The development of yellowness in an unpigmented polymer or plastic part often indicates degradation. High temperatures or exposure to UV light or chemicals can cause chemical or physical changes in the polymer, resulting in yellow discoloration. During the polymer compounding process, yellowing may also occur due to factors such as photo-oxidation and thermal degradation.

A change in the Yellowness Index (ΔYI) can serve as a quality control specification when manufacturing unpigmented plastic parts, such as blow-molded bottles or extruded sheets. Table 5 presents the color measurements for the materials investigated. Five measurements were taken for each sample, and the averages were recorded both before and after EO sterilization. Delta values are reported

Table 5. Color data before and after ethylene oxide (EO) exposure

Grade	Polymer	L*			a*			b*			YI†)		
		before	after	Δ*)	before	after	Δ*)	before	after	Δ*)	before	after	Δ*)
PCG07	LDPE	85.7	85.5	–	1.6	1.6	–	4.6	4.5	–	10.8	10.7	–
PCG453	HDPE	79.4	79.2	–0.2	1.6	1.6	–0.1	6.2	6.4	0.2	15.0	15.4	0.4
PCG863	HDPE	75.4	75.6	–	0.7	0.5	–0.2	10.5	11.1	0.6	23.7	24.7	1.1
PCGR40	PP r	91.0	90.8	–0.2	0.9	0.9	–	1.3	1.4	–	3.2	3.4	–
58MNK10	PP icp	77.5	77.3	–0.2	0.8	0.7	–0.1	4.7	4.9	–	11.3	11.5	–
PCGH19	PP h	94.2	93.8	–	0.8	0.8	–	4.4	4.6	–	9.0	9.3	–
HMG94MD	ABS	64.0	63.9	–	1.6	1.8	0.2	26.4	27.4	1.0	59.8	61.9	2.1
HMG47MD	ABS	62.5	62.2	–0.3	2.7	3.1	0.4	31.3	32.4	1.1	70.3	72.6	2.3
HX325HP	PBT	35.9	36.2	–	3.1	3.0	–0.1	21.7	21.8	–	74.9	74.7	–
HX312C	PBT	44.9	45.3	0.4	3.8	3.7	–0.1	21.9	21.8	–0.1	67.7	66.9	-0.8
HC1204HF	PC/ABS	60.8	61.2	–	2.2	2.2	–	31.6	31.6	–	71.5	71.1	–
HX7509HP	PC/PCTG	95.1	95.1	–	0.0	0.0	–	0.3	0.3	–	0.6	0.6	–
HP2REU	PC	95.5	95.5	–	0.1	0.1	–	–0.2	-0.2	–	–0.4	–0.4	–
HP4REU	PC	86.9	87.4	0.5	1.3	1.3	–	4.4	4.5	–	10.1	10.3	–

* Delta values are given only for datasets that show a statistically significant difference ($p < 0.05$); † Yellowness index. PCG07 – low-density polyethylene (LDPE); PCG453 and PCG863 – high-density polyethylene (HDPE); PCGR40 – polypropylene random copolymer with ethylene (PP r); 58MNK10 – polypropylene impact copolymer with ethylene (PP icp); PCGH19 – polypropylene homopolymer (PP h); CYCOLAC™ HMG94MD and HMG47MD – acrylonitrile–butadiene–styrene copolymers (ABS); VALOX™ HX325HP and HX312C – polybutylene terephthalate (PBT) polyesters; LEXAN™ – HP2REU and HP4REU polycarbonate (PC); CYCOLOY™ – HC1204HF PC/ABS blend; XYLEX™ HX7509HP – blend of PC and polycyclohexylenedimethylene terephthalate glycol-modified (PCTG) polyester.

only for datasets in which the difference between "before" and "after" values was statistically significant ($p < 0.05$). As shown in Table 5, most samples exhibited similar YI values before and after sterilization, with only minor differences, except for 3 materials – 1 HDPE (PCG863) and the 2 ABS samples. The ΔYI for these 3 materials were greater than those of the others, indicating an increase in yellowness following EO sterilization. All other samples maintained their YI values after sterilization. Photographs of the parts before and after sterilization, provided in the supplementary information, confirm the absence of visible changes in appearance. The supplementary material also includes Fourier transform infrared spectroscopy (FTIR) spectra for the 3 samples with statistically significant ΔYI values, showing no detectable chemical changes or signs of molecular degradation.

Limitations

The conclusions of this study should be interpreted with the usual caution. The results are based on a single set of experiments and have not been replicated over time. Although the experimental conditions reflect typical real-life applications, variations in molding or sterilization parameters may yield different outcomes. Therefore, it is essential that users of these materials conduct their own evaluation to confirm the suitability of the material for the intended application.

Conclusions

Ethylene oxide remains the most widely used sterilization technique for single-use medical devices due to its large-scale applicability and broad material compatibility. This study confirms the general statements from the literature, demonstrating that EO sterilization is indeed compatible with a wide range of medical-grade plastics.[4]

The study focused on material stability parameters most relevant to end-use applications: tensile strength, impact resistance, and color retention. Based on statistical evaluations and comparisons with long-term measurement variation, only minimal changes were observed as a result of the sterilization process. The variations detected were minor, and according to commonly applied criteria (<10% change), all tested plastics can be classified as compatible with a single cycle of EO sterilization..

Supplementary data

The supplementary materials are available at https://doi.org/10.5281/zenodo.15681248. The package includes the following files:

20250611 EO full data.csv : The full dataset of measurements both mechanical and optical

Supplementary Fig. 1. Photographs of samples 1–7 before and after EO sterilization.

Supplementary Fig. 2. Photographs of samples 8–14 before and after EO sterilization.

Supplementary Fig. 3. Comparison of ATR FTIR spectra of PCG863 HDPE before and after EO sterilization.

Supplementary Fig. 4. Comparison of ATR FTIR spectra of HMG94MD ABS before and after EO sterilization.

Supplementary Fig. 5. Comparison of ATR FTIR spectra of HMG47MD ABS before and after EO sterilization.

Data Availability Statement

The datasets generated and/or analyzed during the current study are available from the corresponding author on reasonable request.

Consent for publication

Not applicable.

Use of AI and AI-assisted technologies

Not applicable.

ORCID iDs

Hans de Brouwer https://orcid.org/0000-0002-9100-4706
Muhammad Maqsood https://orcid.org/0000-0002-3056-4742

References

1. Bharti B, Li H, Ren Z, Zhu R, Zhu Z. Recent advances in sterilization and disinfection technology: A review. *Chemosphere* 2022;308; 136404. doi:10.1016/j.chemosphere.2022.136404
2. Rutala WA, Weber DJ. Disinfection, sterilization, and antisepsis: Principles, practices, current issues, new research, and new technologies. *Am J Infect Control*. 2019;47:A1–A2. doi:10.1016/j.ajic.2019.03.035
3. Garvey M. Medical device-associated healthcare infections: Sterilization and the potential of novel biological approaches to ensure patient safety. *Int J Mol Sci*. 2023;25(1):201. doi:10.3390/ijms25010201
4. Advancing Safety in Health Technology (AAMI). *Compatibility of Materials Subject to Sterilization*. Arlington, USA: Association for the Advancement of Medical Instrumentation; 2018. ISBN:978-1-57020-700-6.
5. de Brouwer H. Comparison of the effects of x-ray and gamma irradiation on engineering thermoplastics. *Radiat Phys Chem*. 2022;193:109999. doi:10.1016/j.radphyschem.2022.109999
6. de Brouwer H, Anbuchezhian N. The effects of UVC irradiation on the properties of thermoplastics. *Polym Degrad Stab*. 2024;222:110703. doi:10.1016/j.polymdegradstab.2024.110703
7. McEvoy B, Wiehle SB, Gordon K, Kearns G, Laranjeira P, McLees N. Advancing the sustainable use of ethylene oxide through process validation. *Biomed Instrum Technol*. 2021;55(Suppl 3):35–44. doi:10.2345/0899-8205-55.s3.35
8. Comben M. The future of gamma irradiation for medical device sterilization. Santa Monica, USA: Medical Device and Diagnostic Industry; 2021. https://www.mddionline.com/sterilization/the-future-of-gamma-irradiation-for-medical-device-sterilization. Accessed November 22, 2024.
9. Gamma Industry Processing Alliance (GIPA), International Irradiation Association (IIA). White paper: A Comparison of Gamma, E-beam, X-ray and Ethylene Oxide Technologies for the Industrial Sterilization of Medical Devices and Healthcare Products. Gamma Industry Processing Alliance (GIPA) and International Irradiation Association (IIA); 2017. https://gipalliance.net/wp-content/uploads/2013/01/GIPA-WP-GIPA-iia-Sterilization-Modalities-FINAL-Version-2017-October-308772.pdf. Accessed November 22, 2024.
10. Kempf L, Rauschnabel J, Langowski HC. Influencing parameters of vaporized hydrogen peroxide on the sterilization of polyethylene terephthalate bottles. *Food Packaging and Shelf Life*. 2023;36:101053. doi:10.1016/j.fpsl.2023.101053

11. Meleties M, Cooper BM, Marcano-James D, Bhalla AS, Shameem M. Vaporized hydrogen peroxide sterilization in the production of protein therapeutics: Uptake and effects on product quality. *J Pharm Sci*. 2023;112(12):2991–3004. doi:10.1016/j.xphs.2023.09.012
12. Galante R, Ghisleni D, Paradiso P, et al. Sterilization of silicone-based hydrogels for biomedical application using ozone gas: Comparison with conventional techniques. *Mater Sci Eng C Mater Biol Appl*. 2017;78:389–397. doi:10.1016/j.msec.2017.04.073
13. Mendes GCC, Brandão TRS, Silva CLM. Ethylene oxide sterilization of medical devices: A review. *Am J Infect Control*. 2007;35(9):574–581. doi:10.1016/j.ajic.2006.10.014
14. McKeen L. Introduction to food irradiation and medical sterilization. In: *The Effect of Sterilization Methods on Plastics and Elastomers*. Norwich, USA: William Andrew Publishing (Elsevier); 2018:1–40. doi:10.1016/b978-0-12-814511-1.00001-9
15. Kim D, Seo J. A review: Breathable films for packaging applications. *Trends Food Sci Technol*. 2018;76:15–27. doi:10.1016/j.tifs.2018.03.020
16. du Plessis TA. The shelf life of sterile medical devices. *S Afr Orthopaed J*. 2014;13(4):32–24. https://saoj.org.za/index.php/saoj/article/view/136/127.
17. Van Cauwenbergh T, Theys E, Stroeykens D, et al. The effect of gamma and ethylene oxide sterilization on a selection of active pharmaceutical ingredients for ophthalmics. *J Pharm Sci*. 2022;111(7):2011–2017. doi:10.1016/j.xphs.2022.01.020
18. Wang D, Zhang A, Guo W, Zhu B, Yu H, Chen Y. Identification of residues in ethylene oxide sterilized hard gelatin capsule shells by gas chromatography-mass spectrometry and development of a simple gas chromatography-flame ionization detector method for the determination of residues. *J Chromatogr Open*. 2022;2:100061. doi:10.1016/j.jcoa.2022.100061
19. Cooling L, Sherbeck J. Ethylene oxide-type hypersensitivity reactions in G-CSF mobilized, peripheral blood hematopoietic progenitor cell donors and review. *J Clin Apher*. 2023;38(4):427–436. doi:10.1002/jca.22046
20. Poothullil J, Shimizu A, Day RP, Dolovich J. Anaphylaxis from the product(s) of ethylene oxide gas. *Ann Intern Med*. 1975;82(1):58–60. doi:10.7326/0003-4819-82-1-58
21. U.S. Food and Drug Administration (FDA). Notice of ethylene oxide sterilization master pilot program, November 26, 2019. Silver Spring, USA: U.S. Food and Drug Administration (FDA); 2019. https://www.federalregister.gov/d/2019-25631. Accessed March 15, 2025.
22. Balaji Ayyanar C, Marimuthu K. Investigation on the morphology, thermal properties, and in vitro cytotoxicity of the fish scale particulates filled high-density polyethylene composite. *Polymers and Polymer Composites*. 2020;28(4):285–296. doi:10.1177/0967391119872877
23. Peña-Rodríguez MA. Chapter 8: Hypothesis testing. In: *Process Monitoring and Improvement Handbook*. 2nd ed. Milwaukee, USA: Quality Press; 2018:79–104. ISBN: 978-0-87389-974-1 978-1-953079-07-7.

Physico-chemical properties and composition govern adhesion of resin-based dental fissure sealants: A preliminary in vitro study

Właściwości fizykochemiczne i skład warunkują adhezję polimerowych laków szczelinowych – wstępne badanie in vitro

Aleksandra Piszko[1,A–F], Justyna Marcula[2,B–D], Paweł J. Piszko[3,B–D], Anna Nikodem[2,B–E], Maria Krystyna Szymonowicz[4,A,E,F], Maciej Dobrzyński[1,A,C,E,F]

[1] Department of Pediatric Dentistry and Preclinical Dentistry, Wroclaw Medical University, Poland
[2] Department of Mechanics, Materials and Biomedical Engineering, Faculty of Mechanical Engineering, Wroclaw University of Science and Technology, Poland
[3] Department of Biomedical Engineering, Faculty of Fundamental Problems of Technology, Wroclaw University of Science and Technology, Poland
[4] Pre-clinical Research Centre, Wroclaw Medical University, Poland

A – research concept and design; B – collection and/or assembly of data; C – data analysis and interpretation;
D – writing the article; E – critical revision of the article; F – final approval of the article

Polymers in Medicine, ISSN 0370-0747 (print), ISSN 2451-2699 (online) *Polim Med*. 2025;55(2):89–103

Address for correspondence
Aleksandra Piszko
E-mail: aleksandra.piszko@student.umw.edu.pl

Funding sources
None declared

Conflict of interest
None declared

Received on August 27, 2025
Reviewed on September 8, 2025
Accepted on September 16, 2025

Published online on December 19, 2025

Cite as
Piszko A, Marcula J, Piszko PJ, Nikodem A, Szymonowicz MK, Dobrzyński M. Physico-chemical properties and composition govern adhesion of resin-based dental fissure sealants: A preliminary in vitro study. *Polim Med*. 2025;55(2):89–103 doi:10.17219/pim/210966

DOI
10.17219/pim/210966

Abstract

Background. Dental sealants are used to caulk fissures and pits in order to prevent caries development both in deciduous and permanent dentition. Loss of sealant integrity leads to the formation of marginal gaps, consequently increasing the risk of caries.

Objectives. This study aimed to compare the physicochemical and clinically relevant properties of 3 commercially available resin-based pit and fissure sealants: Arkona Fissure Sealant (AFS; Arkona, Nasutów, Poland), Flow-Color (FC; Arkona, Nasutów, Poland) and Flow-It ALC (FIA; Pentron, Orange, USA).

Materials and methods. After polymerization in dedicated molds, the materials were characterized using attenuated total reflectance Fourier-transform infrared spectroscopy (ATR-FTIR), surface free energy (SFE) measurements and micromechanical testing to evaluate structural and mechanical properties. Scanning electron microscopy (SEM) coupled with energy-dispersive spectroscopy (EDS) was employed to visualize sample morphology and determine elemental composition. An in vitro fluoride release study was conducted in artificial saliva at varying pH values (4.5, 5.5, 7.0, 7.5), with deionized water as a reference. Measurements were recorded at 1, 3, 24, 48, 72, and 96 h, and then weekly for up to 7 weeks.

Results. AFS exhibited the highest values of SFE (38.4 mJ/m^2), Vickers hardness (51.93 HV) and indentation modulus (11.93 kN/mm^2). All sealants demonstrated cumulative fluoride release over the incubation period, with the highest release observed for AFS in artificial saliva at pH = 7.5 (0.772 ppm). FTIR spectra of all materials confirmed the presence of polymer backbones as declared by the manufacturers.

Conclusions. Presented findings provide insight into material-dependent properties influencing adhesion, mechanical performance and ion release of resin-based dental sealants. Among the tested materials, AFS exhibited the most favorable overall profile, combining high filler content, optimized particle architecture, superior mechanical strength, elevated surface energy, and sustained fluoride release, which together support robust adhesion, resistance to occlusal forces and effective caries prevention.

Abstract (in Polish)

Wprowadzenie. Laki stomatologiczne są przeznaczone do uszczelniania bruzd i szczelin zębów w celu zapobiegania rozwojowi próchnicy zarówno w uzębieniu mlecznym, jak i stałym. Zmiany strukturalne zaaplikowanego laku prowadzą do utraty szczelności brzeżnej, co w konsekwencji zwiększa ryzyko rozwoju próchnicy.

Cel pracy. Celem badania była charakterystyka oraz porównanie właściwości fizykochemicznych, mechanicznych oraz adhezyjnych trzech komercyjnie dostępnych laków szczelinowych z matrycą polimerową: Arkona Fissure Sealant (AFS; Arkona, Nasutów, Polska), Flow-Color (FC; Arkona, Nasutów, Polska) oraz Flow-It ALC (FIA; Pentron, Orange, CA, USA).

Materiał i metody. Po fotopolimeryzacji materiałów w dedykowanych formach materiały poddano analizie za pomocą spektroskopii w podczerwieni (ATR-FTIR), pomiarom energii swobodnej powierzchni (SFE) oraz ewaluacji właściwości strukturalnych i mikromechanicznych. Morfologia próbek i ich morfologię oraz skład pierwiastkowy określono za pomocą elektronowej mikroskopii skaningowej (SEM) sprzężonej z dyspersyjną spektroskopią rentgenowską (EDS). Wyniki badania in vitro uwalniania fluoru przeprowadzono w sztucznej ślinie o różnych wartościach pH (4.5; 5.5; 7.0; 7.5) oraz w wodzie dejonizowanej jako próbie kontrolnej, z pomiarami wykonywanymi po 1, 3, 24, 48, 72, 96 godzinach oraz co tydzień do 7 tygodnia.

Wyniki. Wśród badanych materiałów AFS wykazał najwyższą wartość energii swobodnej powierzchni (38.4 mJ/m^2), twardości Vickersa (51.93 HV) oraz modułu indentacji (11.93 kN/mm^2). Wszystkie laki wykazały kumulatywne uwalnianie fluoru w trakcie inkubacji, przy czym najwyższe stężenie fluoru odnotowano dla AFS w sztucznej ślinie o pH 7.5 (0.772 ppm). Widma FTIR wszystkich materiałów potwierdziły obecność łańcuchów polimerowych zgodnie z deklaracjami producentów.

Wnioski. Przedstawione wyniki dostarczają wiedzy na temat właściwości wpływających na adhezję, właściwości mechanicznych oraz uwalniania jonów fluorkowych w lakach szczelinowych opartych na matrycach polimerowych. Spośród badanych materiałów AFS wykazał najbardziej korzystny profil, łącząc wysoką zawartość wypełniacza, morfologię powierzchni, wysoką wytrzymałość mechaniczną, podwyższoną energię powierzchniową oraz wysokie kumulatywne uwalnianie fluoru, co wspiera trwałą adhezję, odporność na siły okluzyjne oraz potencjalnie najskuteczniejszą profilaktykę próchnicy.

Key words: physico-chemical properties, caries prevention, fluoride release, dental fissure sealant, adhesion to dental tissues

Słowa kluczowe: właściwości fizykochemiczne, uwalnianie fluoru, stomatologiczny lak szczelinowy, prewencja próchnicy, adhezja do szkliwa

Highlights

- Arkona Fissure Sealant (AFS shows superior performance): Comparative analysis of 3 resin-based sealants identified AFS as the top performer, with the highest surface free energy, Vickers hardness, and fluoride release — making it highly effective for potential caries prevention.
- Fluoride release depends on pH and composition: All tested sealants demonstrated cumulative fluoride release, with AFS achieving the highest levels at pH 7.5, confirming the role of pH-sensitive release in long-term caries protection.
- Mechanical strength supports AFS longevity: Higher indentation modulus and surface hardness in AFS indicate stronger resistance to masticatory forces, ensuring extended durability in both primary and permanent teeth.
- Advanced material testing validates structural integrity: ATR-FTIR, SEM-EDS, and micromechanical analysis confirmed robust polymer networks and optimized filler architecture, with AFS demonstrating superior adhesion for clinical use.

Background

Dental caries is a widespread, chronic, non-communicable microbial disease that can affect individuals at any age, resulting from a complex, multifactorial process that leads to the demineralization of dental tissues.[1,2] In the span of 20 years, it has affected approx. 2.4 billion individuals worldwide.[3] Therefore, effective preventive strategies are essential, with fluoride-based interventions being the cornerstone of modern caries management. Fluoride exerts its anticaries effects through multiple mechanisms, including the inhibition of demineralization, promotion of enamel remineralization and suppression of bacterial metabolism.[4]

Fluoride is capable of affecting dental health in pre-eruptive, posteruptive, systemic and topical mechanisms.[5] On a structural level, it modifies the enamel surface by converting hydroxyapatite crystals into more chemically stable fluorapatite, enhancing resistance to acid attack and maintaining a protective barrier against cariogenic challenges.[6]

A variety of fluoride-containing products are available for caries prevention, including toothpastes, mouth rinses, gels, and sealants. Clinical evidence indicates that both fluoride varnishes and fluoride-containing fissure sealants are

effective caries-preventive measures.[7] However, the long-term clinical performance of fissure sealants is critically dependent on their ability to form a durable bond with dental tissues. Adhesion to enamel and dentin is influenced by a complex interplay of material properties, including surface energy, wettability, microstructural homogeneity, and chemical composition.

Variations in these physico-chemical characteristics can affect a material's ability to penetrate fissures, adapt to the tooth surface, and withstand mechanical and chemical challenges in the oral environment. Furthermore, the chemical constituents of the sealant, including monomer composition, filler type and fluoride content, may modulate both the initial bonding efficiency and the sustained release of protective ions, thereby influencing the material's anticariogenic potential.

Dental sealants are employed to caulk occlusal fissures, pits and foramina caeca to prevent caries development both in deciduous and permanent dentition. Nevertheless, their use is contraindicated in patients with known allergies or hypersensitivities to any component of the sealant material.[4] Sealing is a painless procedure which may be carried out by professional dentists or dental hygienists. Dental sealants are divided into glass ionomer and resin-based materials. Among resin-based materials, ultraviolet-activated, auto-polymerized and light-cured formulations may be outlined.[8] Materials for sealing pits and fissures are distributed under the name of dental sealants or composite or glass-ionomer materials with sealing indications. A systematic review by Azarpazhooh et al.[8] indicates that resin-based sealants should be preferred by clinicians due to their better retention.

The effectiveness of fissure sealants depends not only on the intrinsic properties of the material but also on the method of application.[9] Critical physico-chemical features include the ability to penetrate fissures and adhere strongly to enamel, while mechanical properties such as microhardness and wear resistance further determine long-term performance.[10,11] Among these factors, one of the most decisive for clinical success is the maintenance of marginal integrity throughout the service life of the sealant. Loss of marginal integrity leads to gap formation, providing niches for bacterial colonization and consequently increasing the risk of secondary caries.[12]

Furthermore, the efficacy of sealing is also dependent on anatomical factors. The morphology of occlusal fissures, pits and foramina caeca is a key factor in the retention rate of dental sealants. The geometry of fissures influences both the penetration and retention of the material.[13] Finally, thinner enamel layer and wider dentinal tubules facilitate rapid progression of carious lesions, directly contributing to the accelerated development of the disease.[14]

A major mechanism underlying the loss of sealant integrity is polymerization shrinkage. During the curing process, monomers are converted into a cross-linked polymer network, which is accompanied by a reduction in material volume.[15] When the contraction forces exceed the adhesive strength to enamel, micro-separation may occur at the interface between the sealant and the tooth surface. The resulting microgaps create favorable conditions for bacterial penetration, thereby facilitating the initiation and progression of carious lesions in the compromised area.[16]

Despite the proven effectiveness of fissure sealants in caries prevention, certain limitations remain regarding their long-term application. The most prominent challenge is the loss of marginal integrity at the material–enamel interface, which contributes to gap formation and reduces the durability of the protective barrier. For this reason, ongoing research is focused on identifying material and application strategies that can minimize shrinkage effects, improve adhesion, and ensure a stable and effective seal over time.

Objectives

The objective of this study was to make a comparison between the physicochemical and clinical-relevant properties of 3 commercially available resin-based pit and fissure sealants. The following resin-based sealants were examined: Arkona Fissure Sealant (AFS; Arkona, Nasutów, Poland), Flow-Color (FC; Arkona), and Flow-It ALC (FIA; Pentron, Orange, USA).

Materials and methods

In the present study, 3 commercially available composite resin-based materials for pit and fissure sealing (AFS, FC and FIA) were selected and subjected to a comprehensive experimental evaluation. The assessment included physico-chemical characterization by attenuated total reflectance Fourier-transform infrared spectroscopy (ATR-FTIR) and water contact angle (WCA) measurements, as well as the determination of mechanical and physical properties relevant to clinical performance. In addition, the fluoride release potential of the tested materials was investigated in order to assess their anticariogenic capacity. A detailed overview of the materials, including their composition and manufacturer-reported characteristics, is provided in Table 1, while their macroscopic appearance is illustrated in Fig. 1.

Specimen preparation and experimental design

Since fissure sealants are originally liquid polymeric materials, polymerized specimens were prepared for the experimental procedures. Two main groups of cylindrical samples were fabricated to assess the physico-chemical,

Table 1. Comparative characterization and chemical composition of the investigated commercial fissure sealants, including resin matrix formulation as declared by the manufacturers

Study material	Producer	Chemical composition	Reference
AFS Arkona Fissure Sealant	Arkona, Nasutów, Poland	Bisphenol A diglycide ether dimethacrylate, urethane dimethacrylate, triethylene glycol dimethacrylate, barium-aluminum-silicon glass, barium-aluminum-boron-fluorine glass, pyrogenic silica, titanium dioxide, photoinitiators, inhibitors, catalysts, stabilizers, pigments	[17]
FC Flow-Color	Arkona, Nasutów, Poland	Dimethacrylate resins: Bis-GMA, TEGDMA, UDMA, Bis-EMA, Mineral fillers, Al-Ba-B-Si glass, Ba-Al-B-F-Si glass, pyrogenic silica, pigments	[18]
FIA Flow-It ALC	Pentron, Orange, USA	Filler, 2,2′-ethylenedioxy dimethanol dimethacrylate, Poly(oxy-1,2-ethanediyl), Bis (1,2,2,6,6-pentamethyl-4-piperidyl) sebacate	[19]

AFS – Arkona Fissure Sealant (Arkona, Nasutów, Poland); FC – Flow-Color (Arkona); FIA – Flow-It ALC (Pentron, Orange, USA).

Fig. 1. Comparative images of the investigated commercial fissure sealants in their original syringes/tubes: A. AFS; B. FC; C. FIA, as used for the experimental measurements

AFS – Arkona Fissure Sealant (Arkona, Nasutów, Poland); FC – Flow-Color (Arkona); FIA – Flow-It ALC (Pentron, Orange, USA).

mechanical and functional properties of the tested materials.

The 1st group consisted of cylinders with a diameter of 12 mm and a height of 5 mm, dedicated to physico-chemical analyses. The 2nd group comprised smaller specimens (5 mm in diameter and 2 mm in height), prepared in dedicated polytetrafluoroethylene (PTFE) molds,[20] specifically designed for the evaluation of fluoride ion release. All specimens were produced under identical conditions and light-cured strictly according to the manufacturers' instructions: AFS and FIA for 10 s, and FC for 30 s, using an LED curing lamp Elipar II (3M ESPE, St. Paul, USA).

For physico-chemical characterization, due to the requirement of flat and parallel surfaces, each polymerized specimen was subsequently embedded in heat-curing acrylic resin (Duracryl® Plus). The embedded samples were sectioned using a precision metallographic cutter (STRUERS® Accutom-5) and carefully polished to obtain reproducible, smooth surfaces suitable for measurement. These prepared specimens were then subjected to a set of analyses, including microhardness testing, surface morphology evaluation using scanning electron microscopy (SEM) coupled with energy-dispersive X-ray spectroscopy (EDS), Fourier-transform infrared spectroscopy (FTIR), and determination of contact angle and surface free energy.

In order to investigate the adhesion of fissure sealants to dental tissues, extracted premolars were included in the study. The teeth were prepared in accordance with clinical recommendations, and sealants were applied to the pits and fissures of the occlusal surfaces of the premolar's crowns (Fig. 2). Following polymerization, the sealed teeth were subjected to advanced imaging and characterization techniques, including micro-computed tomography (micro-CT) and SEM, to visualize and evaluate the interfacial adaptation and integrity of the material–tooth interface.

ATR-FTIR

The ATR-FTIR analysis was performed on cured sealant samples. Spectra were acquired using a Nicolet iZ10 infrared spectrometer (Thermo Fisher Scientific, Waltham, USA) equipped with an ATR accessory. The measurements spanned a spectral range of 4000–550 cm^{-1}, with a resolution of 4 cm^{-1}, and each spectrum was averaged over 32 scans.

Scanning electron microscopy

The surface morphology of the tested fissure sealants was examined using a SEM (Phenom ProX; Thermo Fisher Scientific Observations were carried out under high-vacuum conditions at various magnifications, which enabled a detailed assessment of both surface topography and the homogeneity of the investigated materials. The evaluation focused on the presence of morphological features such as pores, cracks, material discontinuities, and the quality

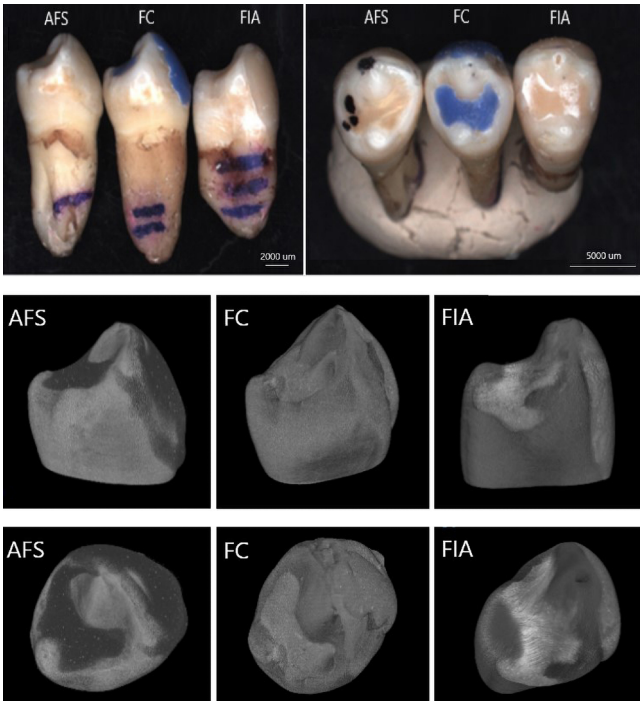

Fig. 2. Lateral and occlusal views of premolars with fissure sealants (AFS, FC and FIA) applied, showing the filling of cuspal grooves. Images obtained using stereomicroscopy (Discovery V.20; Carl Zeiss AG, Jena, Germany) and micro-computed tomography (micro-CT) (SkyScan 1172; Bruker)

AFS – Arkona Fissure Sealant (Arkona, Nasutów, Poland); FC – Flow-Color (Arkona); FIA – Flow-It ALC (Pentron, Orange, USA).

of adhesion between the sealant and the underlying substrate. To complement the structural observations, an elemental composition analysis was performed using EDS. This approach allowed for the identification and qualitative assessment of the main chemical elements present on the surface of the fissure sealants, thereby providing additional insight into the material characteristics relevant to their clinical performance.

Surface wettability analysis

To quantitatively characterize the wettability of the investigated sealants, contact angle measurements and subsequent determination of surface free energy (SFE) were performed, providing insight into the hydrophilic or hydrophobic character of the tested materials. The method relied on the analysis of the shape of a liquid droplet deposited on the sample surface under controlled conditions. Measurements were conducted using an optical contact angle goniometer (Surftense Universal; OEG GmbH, Frankfurt am Main, Germany). The surface free energy was calculated using the Owens–Wendt approach,[21] which is based on contact angle values obtained for at least 2 probe liquids of known surface tension parameters. The surface energy components of the different liquids used in this study are summarized in Table 2.

Table 2. Reference values of surface energy components used liquids, including total surface energy (γ_L), dispersive component (γ_L^d), and polar component (γ_L^p)[22]

Liquid	γ_L [mJ/m^2]	γ_L^d [mJ/m^2]	γ_L^p [mJ/m^2]
Water	72.8	21.8	51.0
Diiodomethane	50.8	50.4	0.4

This method allows the decomposition of SFE into its dispersive and polar components, thereby enabling a comprehensive assessment of the surface characteristics and their potential influence on adhesive interactions. For each specimen, 5 independent measurements were performed using 2 probe liquids: distilled water (polar liquid) and diiodomethane (non-polar liquid, purity 99%). A single droplet of 0.80 ±0.01 µL of the respective liquid was carefully dispensed onto the polished specimen surface for each measurement, and the contact angle was recorded within 1 s after droplet deposition to minimize the effects of evaporation or spreading.

Microhardness testing

Hardness is one of the fundamental parameters of dental materials, reflecting their resistance to localized deformation and surface wear. Microhardness and reduced elastic modulus were evaluated using instrumented indentation in accordance with ISO 14577, employing a Berkovich indenter (65.3° apex angle, <150 nm tip radius) mounted on a MicroCombi Tester (CSM Instruments SA, Peseux, Switzerland). The measurements were carried out under a load of 400 mN, and data acquisition was performed following the Oliver–Pharr method. This approach enabled not only the determination of Vickers hardness values, but also provided detailed insight into the mechanical response of the material during deformation. In this procedure, after reaching the maximum load, the indenter was held in contact with the specimen for a defined dwell time, producing a characteristic load–displacement curve.[23] From this curve, a comprehensive set of mechanical parameters was derived, including Vickers hardness (HV), instrumented hardness (H_{IT}), reduced modulus of elasticity (E_r), instrumented modulus of elasticity (E_{IT}), work ratio (η_{IT}) and indentation depth (h_r) and at peak load. A minimum of 5 indentations (n = 5) were performed per area. All measurements were conducted at room temperature (~22°C) and relative humidity of 40–50%.

Fluoride release

Fluoride ion release was evaluated using an Orion 9609 ion-selective electrode (Thermo Fisher Scientific) connected to a CPI-551 pH/ion meter (Elmetron, Zabrze, Poland). Prior to each measurement, the system was calibrated with standard fluoride solutions to ensure accuracy

and reproducibility. The electrode setup was subsequently employed to monitor fluoride ion leaching from the sealant matrices under different experimental conditions. Fluoride release was assessed at the following time intervals: 3, 24, 48, 72, 96, and 168 h, with 4 independent replicates per material. The release was determined in both deionized water and artificial saliva solutions at different pH values (4.5, 5.5, 7.0, and 7.5). The artificial saliva formulation, based on previously reported protocols,[24,25] did not contain calcium ions in order to avoid precipitation phenomena. It was prepared in deionized water and consisted of the following components: 0.4 g/L sodium chloride (NaCl), 0.4 g/L potassium chloride (KCl), 0.005 g/L sodium bisulfate ($Na_2S{\cdot}9H_2O$), 0.78 g/L sodium dihydrogen phosphate ($NaH_2PO_4{\cdot}2H_2O$), and 1.0 g/L urea. All reagents were supplied by Chempur (Piekary Śląskie, Poland). The initial burst release (IBR) was defined as the fraction of the cumulative fluoride released within the first 24 h relative to the total cumulative fluoride release index (CFRI) after 7 weeks. The half-release time ($t_{1/2}$) was determined as the time range at which 50% of the total fluoride release had occurred.

Adhesion to dental tissues

To evaluate the adhesion of fissure sealants to dental tissues, extracted premolars were employed. The occlusal fissures of the teeth were sealed following standard clinical protocols using the tested materials. The prepared specimens were subsequently analyzed using micro-CT (1172 SkyScan; Bruker, Kontich, Belgium) to assess interfacial adaptation. Scanning parameters were set at 95 kV and 100 µA, with a rotation step of 0.21° over a full 360° rotation, using a 0.5 mm Al filter and an exposure time of 2,000 ms per projection.

Additionally, SEM was performed to evaluate marginal sealing and identify potential micro-gaps at the enamel–sealant interface. This dual approach allowed for comprehensive visualization of both the internal interfacial integrity and the surface morphology at high resolution.

Statistical analyses

All obtained data were subjected to statistical analysis using OriginPro 2025 (OriginLab Corporation, Northampton, USA) and Microsoft Excel 2013 (Microsoft Corporation, Redmond, USA). For each parameter, including mechanical properties, surface characteristics and fluoride release, mean values and standard deviations (SDs) were calculated to summarize the central tendency and variability of the data. The distribution of the datasets was evaluated, and because some datasets deviated from normality ($p < 0.05$), nonparametric statistical testing was performed. Statistical significance was assessed at a threshold of $p < 0.05$ using the Mann–Whitney U post hoc test. For cumulative fluoride release data, error values were calculated as the square root of the sum of the squares of the individual SDs, assuming that errors at each time point were independent. This approach allowed for a reliable assessment of differences between materials while accounting for variability across measurements.

Results

Morphological and physico-chemical characterization

Surface investigations of the sealants were conducted using SEM equipped with EDS, as well as ATR-FTIR.

Scanning electron microscopy observations performed at magnifications of ×280 and ×5,000 revealed that the analyzed surfaces were smooth and continuous, without the presence of microcracks within the polymerized material. At higher magnification (×5,000), particularly in AFS and FC sealants, the structure appeared fine-crystalline, containing particles of approx. 0.5–1 µm in size. Spectroscopic analysis identified these particles as silicate phases. The presence of silicon and aluminum in the sealants is most likely derived from silica (SiO_2), which is a commonly applied inorganic filler in dental composite.[26] In addition, AFS and FC materials demonstrated minor amounts of titanium and barium, suggesting the incorporation of additives aimed at enhancing radiopacity of the dental materials. In contrast, FIA sealant exhibited the highest carbon content (42.9%) and simultaneously the lowest oxygen content (48.8%), with significantly lower silicon content (6.87%) compared to the other tested materials (Fig. 3). The more diversified elemental composition observed in AFS and FC relative to FIA may account for differences in their physico-chemical performance.

All evaluated fissure sealants contained various methacrylate derivatives forming their resin matrix (Table 1). The primary differences among the materials relate to their filler type and additional components, which are responsible for variations in clinical performance. FTIR spectra of all specimens (Fig. 4) exhibited a characteristic band at ~1,700 cm^{-1}, corresponding to the C=O stretching vibration of the methacrylate carbonyl group. Minor shifts in this band reflect the use of different methacrylate derivatives. The spectral region between 2,750 and 3,000 cm^{-1} displayed overlapping C–H stretching vibrations from alkane and aldehyde groups, confirming the aliphatic nature of the polymer matrix.

The fingerprint region below 1,500 cm^{-1} is distinct for each sealant and depends on the specific composition and relative amounts of fillers and additives. Due to the complexity of the formulations, a detailed quantitative analysis of all peaks was not performed.

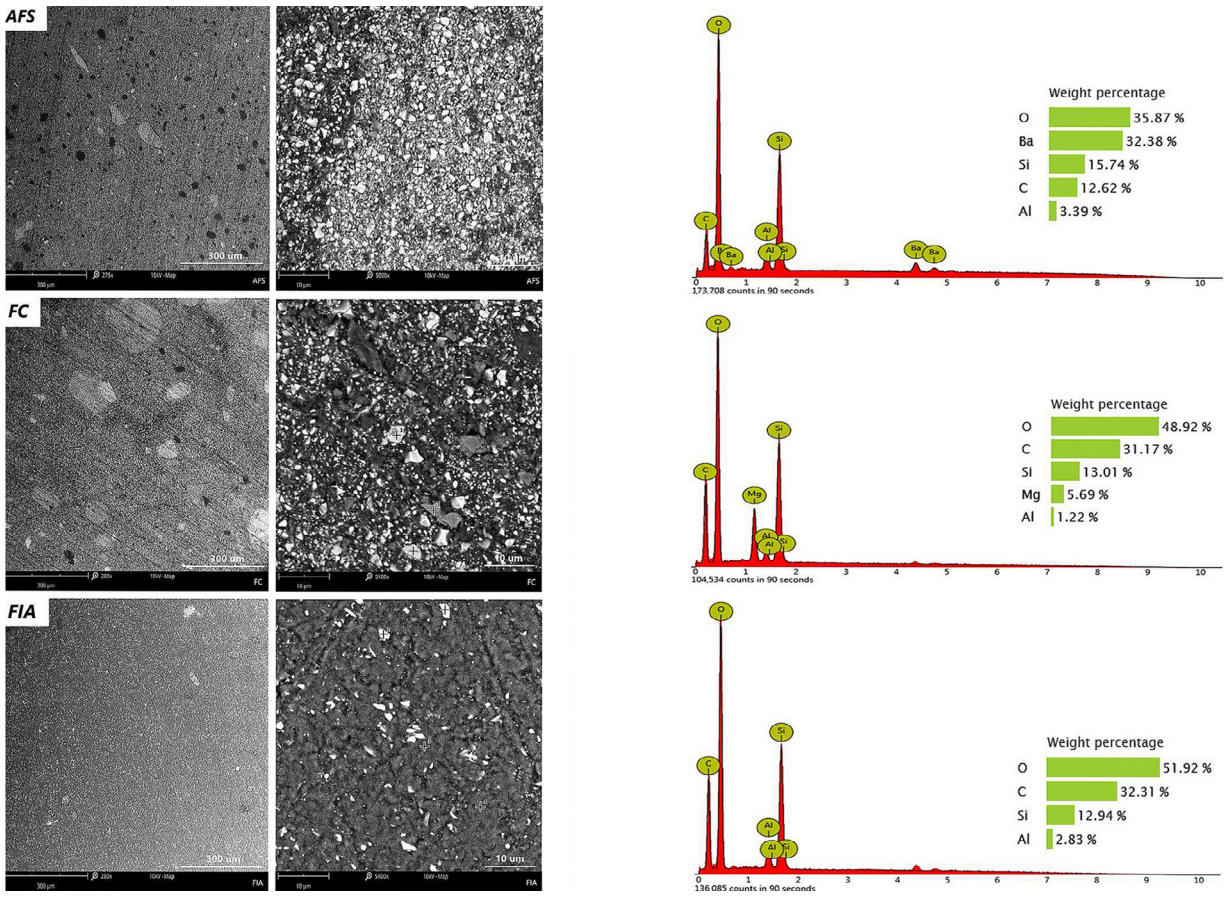

Fig. 3. Comparative morphological scanning electron microscopy (SEM) images and corresponding energy-dispersive spectroscopy (EDS) spectra of the investigated fissure sealants. Micrographs were acquired at magnifications of ×280 (left column) and ×5000 (middle row) for AFS, FC, and FIA materials, illustrating surface topography and filler distribution. The right column presents representative EDS spectra confirming elemental composition

AFS – Arkona Fissure Sealant (Arkona, Nasutów, Poland); FC – Flow-Color (Arkona); FIA – Flow-It ALC (Pentron, Orange, USA).

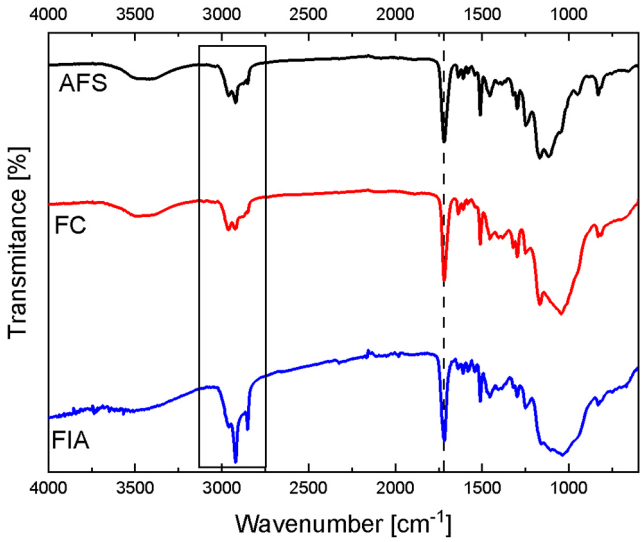

Fig. 4. Attenuated total reflectance Fourier-transform infrared spectroscopy (ATR-FTIR) spectra of AFS, FC, and FIA fissure sealants, showing characteristic absorption bands of methacrylate-based resin matrices. The ~1700 cm^{-1} band corresponds to C=O stretching vibrations, while the 2750–3000 cm^{-1} region indicates overlapping C–H stretching from aliphatic groups. The fingerprint region (<1500 cm^{-1}) reflects variations in filler and additive composition

AFS – Arkona Fissure Sealant (Arkona, Nasutów, Poland); FC – Flow-Color (Arkona); FIA – Flow-It ALC (Pentron, Orange, USA).

Surface wettability and surface free energy

Contact angle measurements provided valuable information regarding the hydrophilicity of the tested fissure sealants (Table 3). According to standard interpretation, a contact angle below 90° indicates a hydrophilic surface with affinity for water, whereas a contact angle above 90° suggests a hydrophobic surface that tends to repel water. Based on the measured contact angles, the surface free energy components were calculated using the Owens–Wendt method,[21] including the dispersive component (γ_S^d), polar component (γ_S^p) and total surface free energy (γ_S).

AFS sealant exhibited the lowest contact angles, indicating relatively higher wettability. In contrast, FC and FIA showed higher contact angles, particularly with distilled water, suggesting a larger contribution of the dispersive component and consequently lower hydrophilicity. Analysis of the surface energy components confirmed these observations. The total surface energy of AFS was the highest at 55.1 mJ/m², while FC showed the lowest value of 50.7 mJ/m². The higher wettability and adhesive potential of AFS may be important for interactions with

Table 3. Mean contact angle values (for water and diiodomethane) and calculated surface energy components (γ_S^d – dispersive component, γ_S^p – polar component, γ_S – total surface energy) for the 3 tested fissure sealants (AFS, FC, FIA)

Sample	Contact angle [°]		Surface energy [mJ/m^2]			Polar ratio (P_S)
	water	diiodomethane	γ_S	γ_S^p	γ_S^d	
AFS	57.7 ±3.8^b	42.3 ±1.8^b	55.1 ±1.9	14.2 ±2.3^{a,b}	38.4 ±0.9^b	0.269 ±0.03^{a,b}
FC	63.9 ±6.9	38.0 ±3.5	50.7 ±4.6	10.2 ±3.1^a	40.5 ±1.7	0.198 ±0.04^a
FIA	62.8 ±2.7^b	35.6 ±2.7^b	52.0 ±1.8	10.3 ±1.3^b	41.7 ±1.2^b	0.198 ±0.02^b

Superscript letters (a,b,c) indicate statistically significant differences between groups ($p < 0.05$, Mann–Whitney U test); a – relation AFS/FC; b – relation AFS/FIA; c – relation FC/FIA; AFS – Arkona Fissure Sealant (Arkona, Nasutów, Poland); FC – Flow-Color (Arkona); FIA – Flow-It ALC (Pentron, Orange, USA).

dental tissues. Differences between FC and FIA were less pronounced, but may reflect variations in the surface structure of the tested materials. The FIA sealant exhibited the highest polar ratio (Ps) values, which are associated with its fine-crystalline and homogeneous structure. This finding also indicates that FIA possesses the greatest ability to attract polar molecules, such as water.

Mechanical properties

The mechanical performance of 3 commercially available fissure sealants (AFS, FC and FIA) was evaluated using instrumented indentation tests (Table 4). Parameters assessed included indentation depth (h_r), Martens hardness (HM and H_{IT}), indentation modulus (E_{IT}), and work ratio (η_{IT}). These tests allowed quantification of each sealant's resistance to mechanical deformation and its elastic response under load.

The mechanical and indentation tests showed clear differences among the 3 fissure sealants. AFS exhibited the lowest indentation depth 5.14 µm and the highest hardness (HM: 396.74 N/mm^2; H_{IT} = 545.55 N/mm^2), indentation modulus (E_{IT} = 11.93 kN/mm^2) and work ratio (η_{IT} = 37.44%), indicating superior mechanical resistance. FC showed intermediate values across all parameters (h = 7.78 µm; HM = 183.05 N/mm^2; H_{IT} = 246.50 N/mm^2; E_{IT} = 5.97 kN/mm^2; η_{IT} = 30.69%), while FIA presented the highest indentation depth (h_r = 10.00 µm) and the lowest hardness and modulus values (HM = 111.32 N/mm^2; H_{IT} = 149.70 N/mm^2; E_{IT} = 3.83 kN/mm^2; η_{IT} = 29.46%), indicating the weakest mechanical performance. In our study, mechanical characterization was carried out using both traditional indentation (yielding HV and H_{IT} values) and instrumented indentation testing, which additionally provided Martens hardness (HM). Unlike conventional Vickers hardness, HM is derived from the continuous recording of applied force and indentation depth, making it less sensitive to the selected test load and thereby more reproducible. For dental materials with a composite structure of resin matrix and inorganic fillers, HM offers a more comprehensive assessment of mechanical performance, as it accounts for both elastic and plastic responses of the material.

Statistical analysis (Mann–Whitney test) confirmed that most differences between sealant types were significant ($p < 0.05$), with superscript letters in Table 4 denoting pairwise significant differences. Overall, these results suggest that AFS has the highest mechanical resistance, FC is intermediate, and FIA shows the lowest mechanical performance among the tested fissure sealants.

Fluoride release

The release of fluoride was evaluated in artificial saliva (pH = 4.5, 5.5, 7.0, 7.5) and deionized water for all the sealants that were analyzed. The evaluation was conducted over a period of 3, 24, 48, 72, 96 h, and then once a week for a period of 7 weeks. The values of the CFRI are presented in Fig. 5 for the artificial saliva solution and in Fig. 6 for the deionized water.

The cumulative fluoride release index (CFRI) value demonstrated an upward trend over time for every solution and every evaluated sealant. Results indicate highest fluoride release in the 1st week of incubation. After 7 weeks of incubation, AFS possessed the highest CFRI in artificial saliva with pH = 7.5 (0.772 ppm) and pH = 7.0 (0.516 ppm). The pH of 5.5 highest CFRI value was comparable for AFS (0.373 ppm) and FC (0.378 ppm). As per artificial saliva

Table 4. Mechanical and indentation properties of fissure sealants specimens used in dentistry. Values are presented as mean ± standard deviation (SD)

Sample	h_r [µm]	HV	HM [N/mm^2]	H_{IT} [N/mm^2]	E_{IT} [kN/mm^2]	η_{IT} [%]
AFS	5.14 ±0.1^{a,b,c}	51.93 ±1.66^{a,b}	396.74 ±9.5^{a,b,c}	545.55 ±16.6^{a,b,c}	11.93 ±0.6^{a,b,c}	37.44 ±2.1^{a,b}
FC	7.78 ±0.5^{a,b,c}	23.27 ±2.88^a	183.05 ±21.0^{a,b,c}	246.50 ±30.0^{a,b,c}	5.97 ±0.7^{a,b,c}	30.69 ±0.8^{a,b}
FIA	10.00 ±0.1^{a,b,c}	14.07 ±0.38^b	111.32 ±6.1^{a,b,c}	149.70 ±3.1^{a,b,c}	3.83 ±0.7^{a,b,c}	29.46 ±4.2^{a,b}

FS – fissure sealants; Superscript letters (a,b,c) indicate statistically significant differences between groups ($p < 0.05$, Mann–Whitney test); a – relation AFS/FC; b – relation AFS/FIA; c – relation FC/FIA; h_r – indentation depth; HM and H_{IT} – Martens hardness; E_{IT} – indentation modulus; η_{IT} – work ratio; AFS – Arkona Fissure Sealant (Arkona, Nasutów, Poland); FC – Flow-Color (Arkona); FIA – Flow-It ALC (Pentron, Orange, USA).

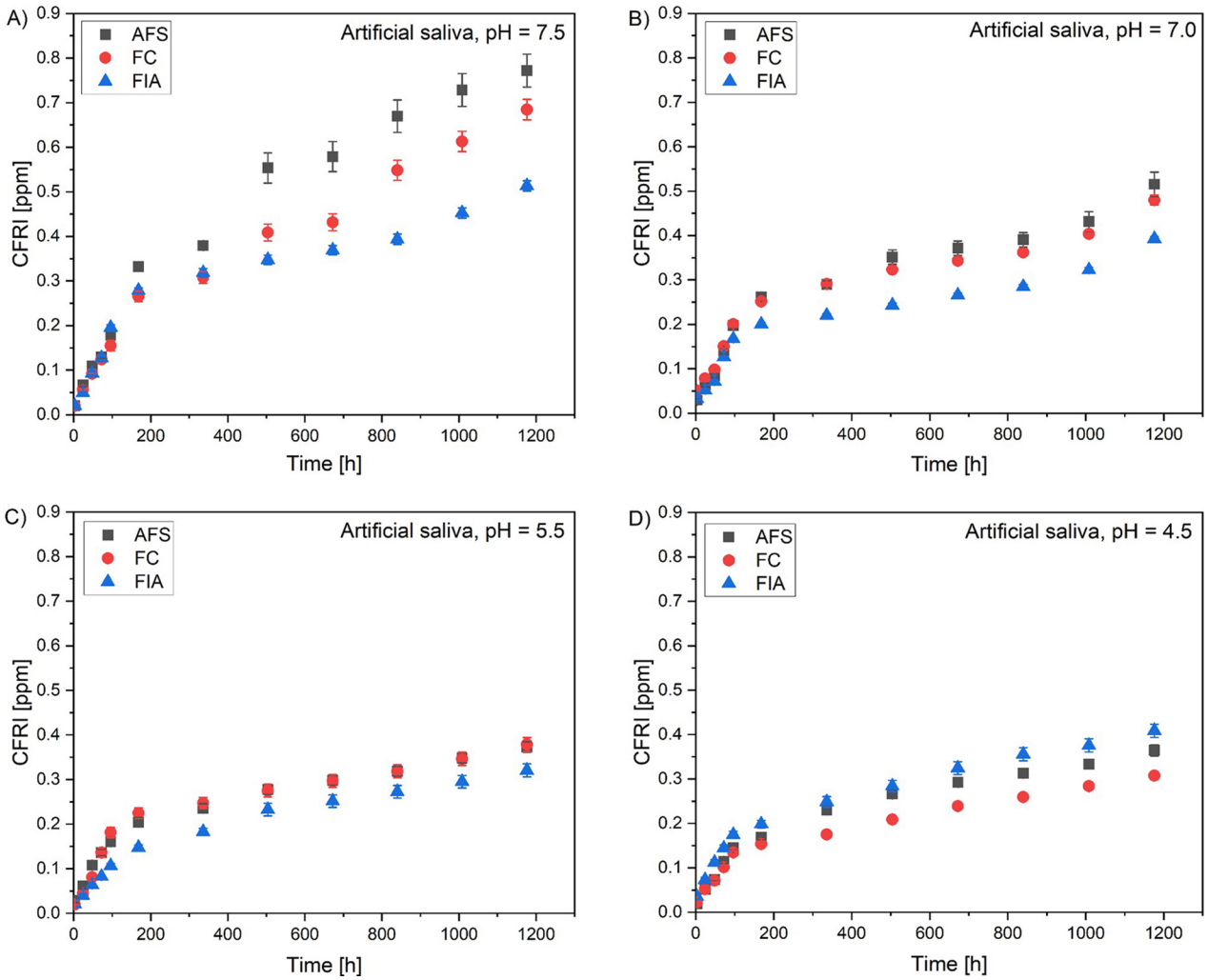

Fig. 5. CFRI of AFS, FC and FIA in artificial saliva in pH = 4.5 (A), 5.5 (B), 7.0 (C) and 7.5 (D) in measurement points ranging from 3 h to 7 weeks. Results are presented as cumulative medians with MAD as a measure of dispersion

AFS – Arkona Fissure Sealant (Arkona, Nasutów, Poland); FC – Flow-Color (Arkona); FIA – Flow-It ALC (Pentron, Orange, USA).

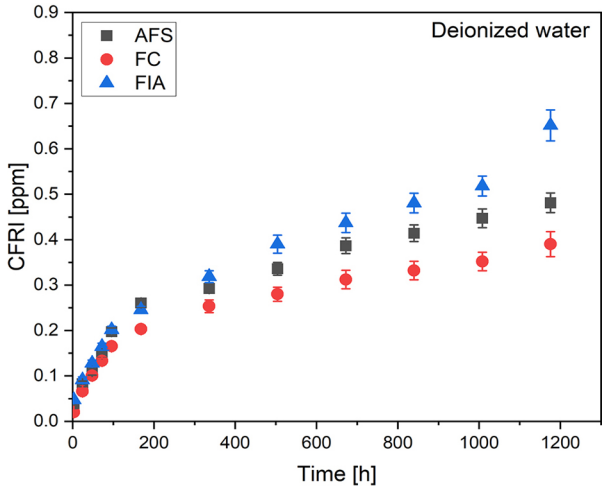

Fig. 6. Cumulative fluoride release index (CFRI) of AFS, FC and FIA in deionized water in measurement points ranging from 3 h to 7 weeks. Results are presented as cumulative medians with median absolute deviation (MAD) as a measure of dispersion

AFS – Arkona Fissure Sealant (Arkona, Nasutów, Poland); FC – Flow-Color (Arkona); FIA – Flow-It ALC (Pentron, Orange, USA).

with pH = 4.5 and deionized water, highest CFRI was assessed for FIA – 0.408 ppm and 0.651 ppm, respectively.

Fluoride release rate (FRR) profiles were derived from the 1st derivative of the CFRI with respect to time for all tested solutions and materials (Fig. 7). For the purpose of comparative evaluation, the following parameters were extracted: IBR, maximum FRR, time at maximum FRR, $t_{1/2}$, and cumulative release values at 7 weeks (Table 5).

The IBR after 24 h exhibited variation across evaluated solutions and sample types (AFS, FC, FIA), ranging from 8.2% to 17.9%. The maximum FRR observed ranged from 0.0010 to 0.0025 ppm/h, with the time to reach maximum release occurring primarily at either 3 h or 72 h. The $t_{1/2}$ occurred at 96–168 h, 1–2 and 1–3 weeks' time ranges, while the CFRI at 7 weeks ranged between 0.308 and 0.772 ppm.

Specifically, in artificial saliva with a pH of 7.5, the IBR values were lowest (8.2–9.5%), with maximum release mostly occurring after 3 h, and a half-life of 2–3 weeks for AFS and FC, and 96–168 h for FIA. The CFRI values after 7 weeks were the highest, reaching 0.772 ppm for AFS. In artificial

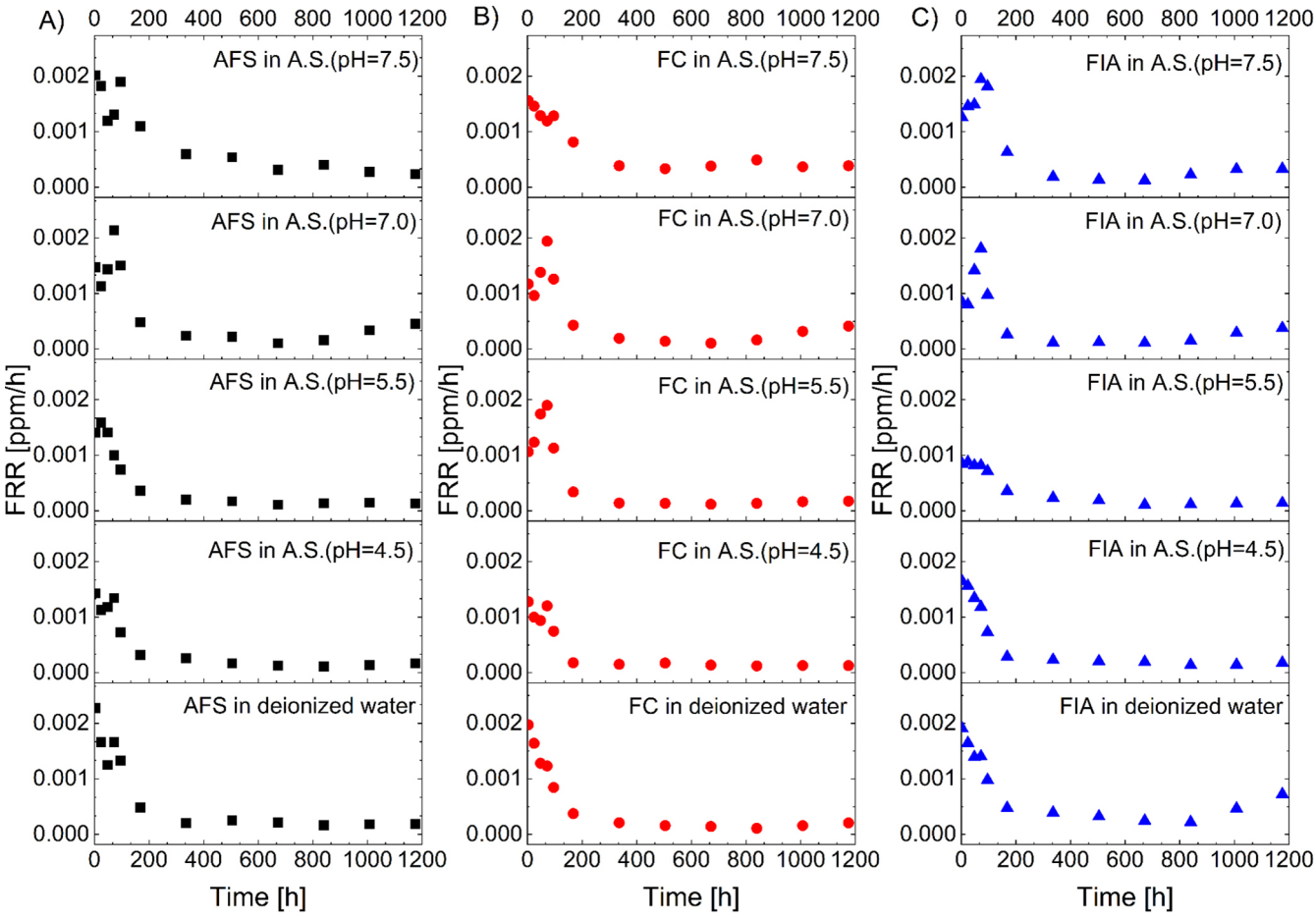

Fig. 7. Derivative of cumulative fluoride release index (CFRI) over time, showing the fluoride release r ate (FRR) in each time interval for AFS (A), FC (B), and FIA (C) in all evaluated solutions. Artificial saliva is denoted as A.S.

AFS – Arkona Fissure Sealant (Arkona, Nasutów, Poland); FC – Flow-Color (Arkona); FIA – Flow-It ALC (Pentron, Orange, USA).

Table 5. Initial burst release (IBR), maximum fluoride release rate (FRR), time at maximum release, $t_{1/2}$ and cumulative fluoride release index (CFRI) at 7 weeks for the 3 tested fissure sealants (AFS, FC, FIA) in all evaluated solutions. Artificial saliva is denoted as A.S.

Parameter	IBR [%]			Maximum FRR [ppm/h]			Time at maximum FRR [h]			$t_{1/2}$			CFRI at 7 weeks [ppm]		
Solution	AFS	FC	FIA	AFS	FC	FIA	AFS	FC	FIA	AFS	FC	FIA	AFS	FC	FIA
A.S. (pH = 7.5)	8.6	8.2	9.5	0.0022	0.0017	0.0021	3	3	72	2–3 weeks	2–3 weeks	96–168 h	0.772	0.685	0.514
A.S. (pH = 7.0)	12.3	16.3	13.1	0.0024	0.0021	0.0020	72	72	72	96–168 h	96–168 h	96–168 h	0.516	0.480	0.393
A.S. (pH = 5.5)	16.5	11.6	12.3	0.0017	0.0021	0.0010	24	72	24	96–168 h	96–168h	1–2 weeks	0.373	0.379	0.321
A.S. (pH = 4.5)	14.3	16.9	17.9	0.0016	0.0013	0.0013	3	72	72	1–2 weeks	1–2 weeks	1–2 weeks	0.365	0.308	0.409
Deionized water	17.2	16.9	14.0	0.0025	0.0022	0.0021	3	3	3	96–168 h	96–168 h	2–3 weeks	0.481	0.390	0.652

AFS – Arkona Fissure Sealant (Arkona, Nasutów, Poland); FC – Flow-Color (Arkona); FIA – Flow-It ALC (Pentron, Orange, USA).

saliva with pH = 7.0, the IBR increased to 12.3–16.3%, with maximal release at 72 h and a half-life of 96–168 h. However, the maximum CFRI decreased. At lower pH values (5.5 and 4.5), the IBR remained elevated (11.6–17.9%) with variable timing of maximum release and shorter half-lives, mostly between 1 and 2 weeks. In deionized water, the IBR was in the upper range (14.0–17.2%), with a rapid maximum FRR at 3 h, while the half-lives were similar to those at higher pH values. Overall, the results demonstrate that the IBR, release kinetics, and half-life are influenced by both the pH and the surrounding medium. The highest initial burst and highest FRR were observed in artificial saliva and deionized

water at lower pH values, while cumulative release after 7 weeks tended to decline under these conditions.

Adhesion of fissure sealants to enamel surfaces

Polymerization shrinkage represents a critical limitation of dental restorative materials, as it can induce microcracks and interfacial gaps due to both intrinsic polymerization and thermal stresses. The material's microstructure, in combination with its elastic properties, facilitates optimal adaptation and intimate contact with the enamel surface, promoting effective adhesion. Figures 8–10 present micro-computed tomography (micro-CT) reconstructions alongside SEM images of premolars filled with AFS, FC and FIA sealants. Sagittal and frontal cross-sections reveal the internal structure of the materials, while magnified views highlight the interface between the sealant and enamel. Examination of these sections clearly demonstrates the presence of cracks, pores and marginal gaps, which arise from polymerization-induced shrinkage and thermal stresses.

Figure 11 provides a top-down view of the sealant–enamel interface, showing an overlay-type connection characterized by structural discontinuities. These discontinuities are likely associated with local variations in wear properties. Given the higher stiffness and hardness of enamel relative to the sealant, the resin layer is expected to undergo initial wear during occlusal loading. From a mechanical perspective, the formation of such an interface, particularly during polymerization, can create localized stress concentrations, potentially promoting crack initiation associated with shrinkage.[27] Effective adaptation to the enamel surface in pit and fissure sealants also relies on micromechanical interlocking with acid-etched enamel, which creates

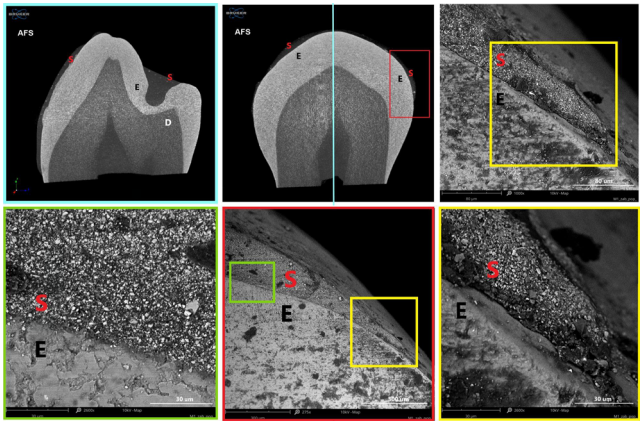

Fig. 8. Examples of sagittal and frontal cross-sections of a premolar filled with AFS fissure sealant, obtained using micro-computed tomography (micro-CT). Magnified views show the sealant–enamel interface in selected regions, captured with a scanning electron microscope. Additional labels in the images: S (red) – fissure sealant; E (black) – enamel; D (white) – dentin

AFS – Arkona Fissure Sealant (Arkona, Nasutów, Poland).

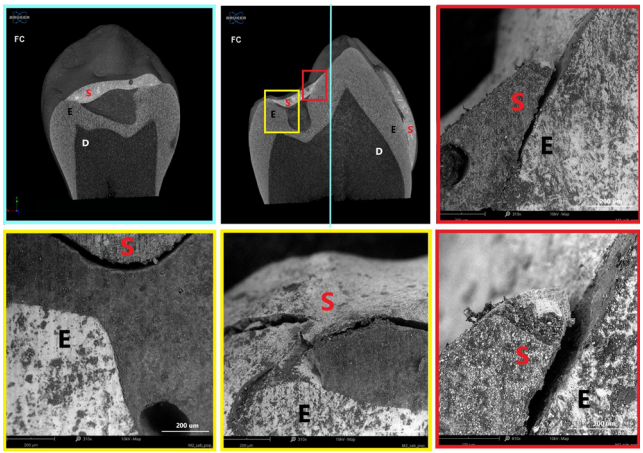

Fig. 9. Examples of sagittal and frontal cross-sections of a premolar tooth filled with FC fissure sealant, obtained via micro-computed tomography, along with magnified views of sealant–enamel adhesion in selected regions of the preparation, captured using a scanning electron microscope. Additional labels in the images: S (red) – fissure sealant; E (black) – enamel; D (white) – dentin

FC – Flow-Color (Arkona, Nasutów, Poland).

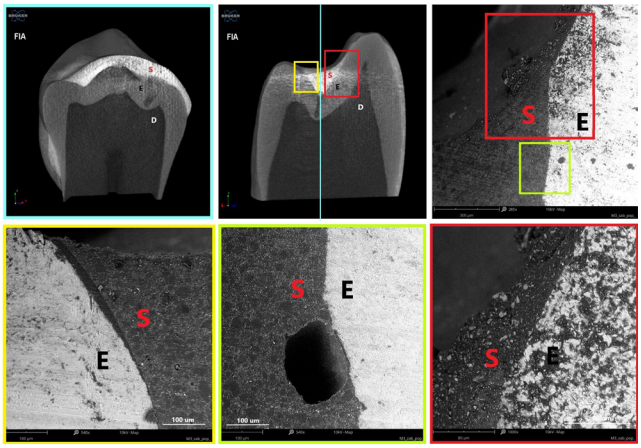

Fig. 10. Examples of cross-sections (sagittal and frontal) of a premolar tooth filled with FIA fissure sealant obtained using a micro-computed tomography (micro-CT), and enlargements of areas of sealant adhesion to enamel in selected locations of the preparation obtained using a scanning electronmicroscope

FIA – Flow-It ALC (Pentron, Orange, USA).

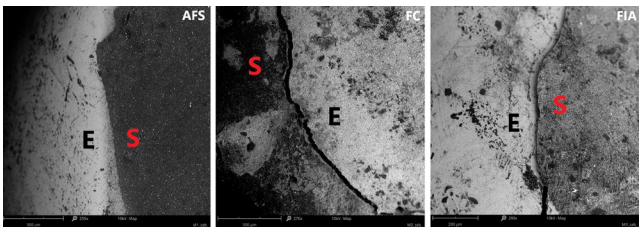

Fig. 11. Comparison of top views of the fissure sealant–enamel interface, images acquired using a scanning electron microscope (SEM; ×250 magnification)

AFS – Arkona Fissure Sealant (Arkona, Nasutów, Poland); FC – Flow-Color (Arkona, Nasutów, Poland); FIA – Flow-It ALC (Pentron, Orange, USA).

microscopic porosities on the tooth surface. The resin penetrates these micropores, forming a stable physical bond between the enamel and the sealant.[26] This micromechanical connection is crucial for enhancing sealant retention and minimizing microleakage.

According to the manufacturer, the polymerization shrinkage of AFS ranges from 3% to 7%. In contrast, flowable materials,[28] despite their higher viscosity and flowability, may exhibit polymerization shrinkage 1–2% greater than conventional Bis-GMA-based dental resins.[29] This increased shrinkage contributes to wider interfacial gaps, which can act as microleakage pathways.

These microenvironments facilitate the accumulation of microorganisms, particularly in areas that are difficult to clean, potentially leading to subsurface carious lesions beneath the sealant. Such findings underscore the influence of the material's elastic properties, filler content and microstructure on its ability to adapt to enamel surfaces and achieve effective adhesion. Consequently, the formation of interfacial gaps not only compromises marginal integrity but also increases the risk of secondary caries, underscoring the importance of optimizing material composition, filler architecture and application techniques to minimize polymerization shrinkage, thermal stress and related clinical complications.

Discussion

The present study provides a comprehensive evaluation of the physico-chemical, morphological, mechanical, and fluoride-release properties of 3 commercially available dental sealants (AFS, FC, FIA), highlighting how these characteristics directly influence clinical performance. The long-term effectiveness of pit and fissure sealants is strongly determined by their surface properties, mechanical behavior and fluoride release, which collectively govern adhesion, retention and caries-preventive potential.

The quality of marginal sealing is critically influenced by both intrinsic material properties and enamel preparation methods. Polymerization shrinkage, for instance, plays a major role in marginal adaptation. Kucukyilmaz et al.[30] reported that sealants with higher filler content, such as Helioseal F, exhibited lower volumetric shrinkage (~3.3%), whereas materials with lower filler load, such as Teethmate F-1, reached ~7.4%. These findings emphasize the importance of filler fraction in minimizing interfacial gaps and preserving long-term adhesion. Surface conditioning is equally crucial; Amend et al.[28] demonstrated that enamel etching with 37% phosphoric acid or using Clearfil SE Bond produced tighter marginal sealing and lower microleakage than self-etching primer systems, as confirmed by dye penetration and SEM imaging. Procedural variations also affect sealant retention. Chaitra et al.[31] compared conventional preparation, enameloplasty, and fissurotomy, showing that enameloplasty significantly reduced microleakage and generated longer resin tags (~12 μm vs ~6 μm for other methods). Adhesive performance under suboptimal conditions is another determinant; Memarpour et al.[32] observed that saliva contamination disrupted mechanical interlocking and increased gaps at the enamel–sealant interface, highlighting the importance of contamination-free application or corrective adhesive protocols. Together, these studies support our observation that AFS systems, by design, provide superior adhesion and marginal sealing.

Excessive polymerization shrinkage and thermal stresses are well-known contributors to interfacial gap formation.[33] Our study, employing high-resolution micro-CT combined with SEM, allowed detailed visualization of cracks and interfacial gaps induced by polymerization. These defects are not merely structural artifacts; they may serve as pathways for microleakage, facilitating microbial infiltration into the fissure system. Once microorganisms penetrate these gaps, they can proliferate, forming biofilms that are difficult to remove during routine oral hygiene. Such colonization compromises sealant integrity and increases the risk of secondary caries, underscoring the clinical importance of minimizing shrinkage and thermal stress through material selection and optimized application techniques. Correlating micro-CT and SEM data enabled precise mapping of the spatial distribution and dimensions of these defects, providing mechanistic insight into how polymerization-related stresses translate into functional vulnerabilities. Therefore, the internal structure and filler architecture of sealants appear to be key determinants in mitigating such effects.

Elemental analysis using EDS revealed that AFS and FC contained higher concentrations of silicon and aluminum, indicative of a greater inorganic filler content. Scanning electron microscopy imaging confirmed a granular, rough surface morphology with visible filler agglomerates for these materials, correlating with enhanced mechanical properties, potentially increasing susceptibility to biofilm formation.[34,35] FIA, in contrast, exhibited fewer inorganic components, lacked detectable aluminum and titanium, and presented a smoother, more homogeneous surface with loosely packed filler particles and void spaces. These morphological characteristics explain the lower mechanical resistance and higher indenter penetration observed for FIA.

The mechanical performance of resin composites is largely dictated by filler content, size and geometry.[36] Early studies by Li et al.[37] established that both filler fraction and particle size critically determine hardness, elastic modulus and wear resistance, with higher loadings and smaller particles conferring superior properties. Subsequent investigations confirmed that filler geometry further modulates mechanical behavior. Turssi et al.[38] demonstrated that particle shape and dispersion significantly affect wear resistance and monomer conversion, impacting long-term stability. At the nanoscale, El-Safty et al.[39] showed that incorporation of nanosized fillers enhances hardness and modulus relative to bulk-fill composites. Rodríguez et al.[36] and Okamoto et al.[40] further confirmed that well-dispersed small fillers improve

microstructure and mechanical strength, whereas oversized or agglomerated particles reduce these benefits. These findings provide a mechanistic rationale for AFS formulations, which employ controlled filler architectures to optimize hardness, stiffness and wear resistance. Mechanical testing confirmed the observed compositional and morphological trends. AFS demonstrated the highest hardness and stiffness (HV = 51.9; HM = 396.74 N/mm^2), indicating superior resistance to deformation and wear. FC showed intermediate values (HV = 42.7; HM = 183.05 N/mm^2), whereas FIA was the softest and weakest (HV = 28.3; HM = 111.32 N/mm^2), consistent with its higher organic matrix fraction. These findings highlight the strong interplay between filler composition, surface morphology and mechanical behavior in determining overall sealant performance. Literature reports hardness values for commercial sealants ranging within 19–99 HV[4] and 21–75 HV,[41] placing our measurements within expected ranges. In our study, indentation tests were performed using both traditional methods (yielding HV and H_{IT} values) and instrumented indentation testing, which additionally provided Martens hardness (HM) and work ratio (η_{IT}).

Martens hardness, based on the continuous recording of force and penetration depth, is less sensitive to the choice of test load and captures both elastic and plastic contributions to material deformation, offering a more reliable characterization of composite materials than conventional Vickers hardness.[42] Work ratio (η_{IT}), in turn, quantifies the proportion of elastic to total work during indentation, thereby reflecting the material's resilience and ability to recover from occlusal stresses.[43] Notably, AFS exhibited the highest η_{IT} values among the tested sealants, confirming its superior elastic recovery and mechanical durability compared with FC and FIA.

Surface energy and wettability are critical determinants of adhesion in restorative dentistry, governing the ability of materials to form intimate contact with etched enamel and dentin. Experimental evidence demonstrates that decreased contact angles, e.g., from 58.8° ±4.1° to 49.1° ±5.7° upon exposure to acidic media, enhance wettability and adhesive potential.[44] Materials with critical surface energy above 40 mJ/m^2, such as acrylic resins, generally exhibit strong adhesion, whereas BIS-GMA–based composites with lower energies show inferior bonding. High-energy substrates favor lower contact angles, promoting stronger adhesion through thermodynamically favorable interactions as described by the Young–Dupre equation.[45] Optimal adhesion requires that the adhesive's surface tension be lower than the substrate's surface energy to achieve effective bonding.

Our measurements revealed moderate hydrophilicity for all tested sealants, with water contact angles of 57.7° (AFS), 63.9° (FC) and 60.5° (FIA). Angles below 90° indicate hydrophilicity, enhancing wetting and adhesion in moist environments.[46] FC was the most hydrophilic, potentially improving its ability to seal pits and fissures in clinical conditions. Conversely, AFS and FIA, being relatively more hydrophobic, may resist moisture contamination during application, supporting long-term durability. Total surface free energy ranged from 50.7 mJ/m^2 (FC) to 55.1 mJ/m^2 (AFS), with the polar component highest for AFS (γSp = 14.2 mJ/m^2), indicating superior potential for adhesion to enamel surfaces. Elevated surface energy and polar fraction facilitate intimate contact with hydrophilic tooth structures, improving wetting, retention and adhesive performance.

Fluoride release was evaluated in deionized water and artificial saliva at pH 4.5, 5.5, 7.0, and 7.5. AFS released the highest amounts under neutral and basic conditions (CFRI = 0.772 ppm at pH 7.5), whereas FIA released more in acidic conditions (pH 4.5) and deionized water. The initial burst release ranged within 8.2–17.9%, with maximum release times between 3–72 h and half-life values of 4–7 days to 2–3 weeks. Over 1,200 h, all materials acted as fluoride reservoirs, supporting remineralization and caries prevention. Differences in fluoride kinetics reflect variations in composition, filler type and excipients, consistent with previous studies.[20,47,48] Tailored compositions, such as in AFS, provide prolonged fluoride availability under varying pH, enhancing anti-caries efficacy.

It has been reported that excipients in dentifrice can significantly influence the retention of fluoride in the oral cavity.[49,50] This concept may also extend to dental sealants, where the composition and excipients of the material could impact fluoride release and retention, thereby influencing their caries-preventive efficacy.

Clinical evidence corroborates these material characteristics. Systematic reviews report that resin-based sealants reduce caries incidence by 11–51% over 24 months, with benefits persisting up to 48 months.[51] Hydrophilic sealants show superior short-term retention (odds ratio (OR) = 3.00 at 3 months; OR = 2.00 at 12 months), while long-term caries prevention is comparable to hydrophobic systems. Auto- and light-cured resin sealants achieve the highest long-term retention (up to 70% at 5 years), whereas glass ionomer and primer-modified sealants show lower retention (14–43% at 2–3 years). Performance is generally consistent across tooth types, though premolars may have slightly better outcomes. Comparisons of resin-based sealants and flowable composites indicate similar retention, though long-term data are limited.

In summary, the combination of higher filler content, optimized particle architecture, superior mechanical properties, favorable surface energy, and controlled fluoride release renders AFS a particularly promising sealant system. It exhibits the most favorable overall profile, with high mechanical strength, surface energy, polar fraction, and sustained fluoride release, supporting adhesion, wetting and resistance to occlusal forces. Moderate hydrophilicity ensures effective wetting in clinical conditions, while relative hydrophobicity during application reduces moisture sensitivity, promoting long-term retention.[35] FC demonstrates intermediate performance, whereas FIA is mechanically

weaker, but exhibits higher fluoride release under acidic conditions.

Strategies to enhance the performance of resin-based pit and fissure sealants focus on optimizing filler content and incorporating bioactive or appropriately selected nanofillers,[52,53] which can simultaneously improve mechanical, surface and antibacterial properties, as well as enhance physico-mechanical characteristics, thereby increasing their effectiveness in preventing dental caries.

Overall, these findings emphasize the importance of integrating physico-chemical, morphological, mechanical, and bioactive assessments when selecting pit and fissure sealants. AFS demonstrates superior clinical potential and longevity compared with FC and FIA, providing a mechanistic and clinical rationale for its preferential use in preventive dentistry.

Limitation

It is imperative that long-term in vitro studies are necessary to comprehensively evaluate the clinical performance of the tested sealants. Furthermore, it is imperative to take into account the feedback provided by clinicians to optimize the application procedures and its conditions. This will ensure that the prevention of caries is improved and that the sealant is retained in the long term.

Conclusions

The present study provides a comprehensive evaluation of the physico-chemical, morphological, mechanical, and fluoride-release properties of 3 commercially available dental sealants (AFS, FC, FIA), highlighting their direct impact on clinical performance. Among the tested materials, AFS exhibited the most favorable overall profile, combining high filler content, optimized particle architecture, superior mechanical strength, elevated surface energy, and sustained fluoride release, which together support robust adhesion, resistance to occlusal forces, and effective caries prevention. Its moderate hydrophilicity ensures efficient wetting and retention in moist clinical conditions, enhancing short-term performance, while its mechanical robustness and surface energetics, comparable to high-durability auto- and light-cured resin systems, indicate potential for superior long-term retention. AFS demonstrated superior effectiveness during evaluation, supporting its universal applicability in clinical practice, and its retention properties are comparable to flowable composites while providing additional advantages, such as improved hydrophilicity. Overall, these findings underscore the mechanistic and clinical rationale for the adhesive superiority, functional reliability, and long-term durability of AFS sealants, making them a particularly promising choice for preventive dentistry.

ORCID iDs

Paweł J. Piszko https://orcid.org/0000-0002-7577-8509
Aleksandra Piszko https://orcid.org/0000-0003-0386-216X
Justyna Marcula https://orcid.org/0009-0003-6600-715X
Anna Nikodem https://orcid.org/0000-0002-1418-247X
Maria Szymonowicz https://orcid.org/0000-0003-4251-6841
Maciej Dobrzyński https://orcid.org/0000-0003-2368-1534

References

1. Balaji S. Dental caries: Research perspective. *Indian J Dent Res*. 2018; 29(1):3. doi:10.4103/ijdr.IJDR_61_18
2. Fejerskov O, ed. *Dental Caries: The Disease and Its Clinical Management*. 3rd ed. Oxford, UK: Wiley Blackwell; 2015. ISBN:978-1-118-93582-8.
3. Kassebaum NJ, Bernabé E, Dahiya M, Bhandari B, Murray CJL, Marcenes W. Global burden of untreated caries: A systematic review and metaregression. *J Dent Res*. 2015;94(5):650–658. doi:10.1177/0022034515573272
4. Piszko A, Piszko PJ, Lubojański A, Grzebieluch W, Szymonowicz M, Dobrzyński M. Brief narrative review on commercial dental sealants: Comparison with respect to their composition and potential modifications. *Material s (Basel)*. 2023;16(19):6453. doi:10.3390/ma16196453
5. Pollick H. The role of fluoride in the prevention of tooth decay. *Pediatr Clin North Am*. 2018;65(5):923–940. doi:10.1016/j.pcl.2018.05.014
6. Xu J, Shi H, Luo J, et al. Advanced materials for enamel remineralization. *Front Bioeng Biotechnol*. 2022;10:985881. doi:10.3389/fbioe.2022.985881
7. Chestnutt IG, Playle R, Hutchings S, et al. Fissure seal or fluoride varnish? A randomized trial of relative effectiveness. *J Dent Res*. 2017;96(7):754–761. doi:10.1177/0022034517702094
8. Azarpazhooh A, Main PA. Pit and fissure sealants in the prevention of dental caries in children and adolescents: A systematic review. *J Can Dent Assoc*. 2008;74(2):171–177. PMID:18353204.
9. Juntavee A, Juntavee N, Chaisuntitrakoon A, Millstein PL, Abedian B. Microleakage and penetration capability of various pit and fissure sealants upon different sealant application techniques. *J Clin Exp Dent*. 2023;15(10):e810–e820. doi:10.4317/jced.60577
10. Faria M, Guedes A, Rompante P, et al. Wear pathways of tooth occlusal fissure sealants: An integrative review. *Biotribology*. 2021;27:100190. doi:10.1016/j.biotri.2021.100190
11. Jeevanandan G, Kengadaran S, Prabakar J. In vitro evaluation of viscosity, depth of penetration, microleakage, and shear bond strength of conventional and hydrophilic sealants. *Int J Clin Pediatr Dent*. 2023;16(5):745–750. doi:10.5005/jp-journals-10005-2684
12. Nam SM, Ku HM, Lee ES, Kim BI. Detection of pit and fissure sealant microleakage using quantitative light-induced fluorescence technology: An in vitro study. *Sci Rep*. 2024;14(1):9066. doi:10.1038/s41598-024-59651-x
13. Beauchamp J, Caufield PW, Crall JJ, et al. Evidence-based clinical recommendations for the use of pit-and-fissure sealants: A report of the American Dental Association Council on Scientific Affairs. *J Am Dent Assoc*. 2008;139(3):257–268. doi:10.14219/jada.archive.2008.0155
14. Cîrdei MV, Margan MM, Margan R, et al. Surface and mineral changes of primary enamel after laser diode irradiation and application of remineralization agents: A comparative in vitro study. *Children (Basel)*. 2024;11(9):1069. doi:10.3390/children11091069
15. Ferracane J. Developing a more complete understanding of stresses produced in dental composites during polymerization. *Dent Mater*. 2005;21(1):36–42. doi:10.1016/j.dental.2004.10.004
16. Bao Z, Sun H, Fan D, Wang X, Wang Q. Shear bond strength and microleakage of pit and fissure sealants placed after saliva-contaminated etched enamel. *Coatings*. 2022;12(4):441. doi:10.3390/coatings12040441
17. Piszko A, Nikodem A, Piszko P, Dobrzyński M. Fluoride release and selected chemo mechanical characteristics of three different commercially available dental materials for sealing. *Acta Biomech Bioeng*. 2023;25(Suppl 1):112–113. https://actabio.pwr.edu.pl/fcp/eGBUKOQtTKlQhbx08SlkTUARAUWRuHQwFDBoIVURNWH9SFVZpCFghUHcKVigEQUw/302/public/publikacje/v25-s1-2023/1.pdf. Accessed August 15, 2025.

18. Arkona. Flow-Color: Kompozycja typu flow. Niemce, Poland: Arkona; 2025. https://arkonadent.com/wp-content/uploads/2024/12/PL_FlowColor_KOMPENDIUM_23_07_2025_WEB.pdf.
19. Pentron Clinical. Flow-It® ALCTM Flowable Composite: Safety Data Sheet (SDS). Orange, USA: Peltron Clinical; 2015. https://www.skydentalsupply.com/files/products/1flow%20it.pdf.
20. Kosior P, Klimas S, Nikodem A, et al. An in vitro examination of fluoride ions release from selected materials: Resin-modified glass-ionomer cement (Vitremer) and nanohybrid composite material (Tetric EvoCeram). *Acta Bioeng Biomech*. 2023;25(1):101–115. PMID:38314640.
21. Owens DK, Wendt RC. Estimation of the surface free energy of polymers. *J Appl Polym Sci*. 1969;13(8):1741–1747. doi:10.1002/app.1969.070130815
22. Song K, Lee J, Choi SO, Kim J. Interaction of surface energy components between solid and liquid on wettability, and its application to textile anti-wetting finish. *Polymers (Basel)*. 2019;11(3):498. doi:10.3390/polym11030498
23. Dziarski P, Makuch N. Effect of indentation load on nanomechanical properties measured in a multiphase boride layer. *Materials (Basel)*. 2021;14(21):6727. doi:10.3390/ma14216727
24. Dobrzyński W, Nikodem A, Diakowska D, et al. Comparison of the fluoride ion release from nanofluoroapatite-modified orthodontic cement under different pH conditions: An in vitro study. *Acta Bioeng Biomech*. 2023;25(3):159–176. doi:10.37190/ABB-02321-2023-02
25. Piszko PJ, Kulus M, Piszko A, et al. The influence of calcium ions and pH on fluoride release from commercial fluoride gels in an in vitro study. *Gels*. 2025;11(7):486. doi:10.3390/gels11070486
26. Zhang S, Wang X, Yang J, Chen H, Jiang X. Micromechanical interlocking structure at the filler/resin interface for dental composites: A review. *Int J Oral Sci*. 2023;15(1):21. doi:10.1038/s41368-023-00226-3
27. Kleverlaan CJ, Feilzer AJ. Polymerization shrinkage and contraction stress of dental resin composites. *Dent Mater*. 2005;21(12):1150–1157. doi:10.1016/j.dental.2005.02.004
28. Amend S, Frankenberger R, Boutsiouki C, Scharrelmann V, Winter J, Krämer N. Microleakage of pit and fissure sealings placed after enamel conditioning with phosphoric acid or with self-etching primers/adhesives. *Clin Exp Dent Res*. 2021;7(5):763–771. doi:10.1002/cre2.420
29. Ilie N, Hickel R. Resin composite restorative materials. *Aust Dent J*. 2011;56(s1):59–66. doi:10.1111/j.1834-7819.2010.01296.x
30. Kucukyilmaz E, Savas S, Sener Y, Tosun G, Botsali M. Polymerization shrinkage of six different fissure sealants. *J Res Dent*. 2014;2(2):88. doi:10.4103/2321-4619.136645
31. Chaitra T, Subba Reddy V, Devarasa G, Ravishankar T. Microleakage and SEM analysis of flowable resin used as a sealant following three fissure preparation techniques: An in vitro study. *J Clin Pediatr Dent*. 2011;35(3):277–282. doi:10.17796/jcpd.35.3.7x217772q7146288
32. Memarpour M, Rafiee A, Shafiei F, Dorudizadeh T, Kamran S. Adhesion of three types of fissure sealant in saliva-contaminated and non-contaminated conditions: An in vitro study. *Eur Arch Paediatr Dent*. 2021;22(5):813–821. doi:10.1007/s40368-021-00626-1
33. Abbasi M, Moradi Z, Mirzaei M, Kharazifard MJ, Rezaei S. Polymerization shrinkage of five bulk-fill composite resins in comparison with a conventional composite resin. *J Dent (Tehran)*. 2019;15(6):355–364. doi:10.18502/jdt.v15i6.330
34. Zheng S, Bawazir M, Dhall A, et al. Implication of surface properties, bacterial motility, and hydrodynamic conditions on bacterial surface sensing and their initial adhesion. *Front Bioeng Biotechnol*. 2021;9:643722. doi:10.3389/fbioe.2021.643722
35. Ng TCH, Chu CH, Yu OY. A concise review of dental sealants in caries management. *Front Oral Health*. 2023;4:1180405. doi:10.3389/froh.2023.1180405
36. Rodríguez HA, Kriven WM, Casanova H. Development of mechanical properties in dental resin composite: Effect of filler size and filler aggregation state. *Mater Sci Eng C Mater Biol Appl*. 2019;101:274–282. doi:10.1016/j.msec.2019.03.090
37. Li Y, Swartz ML, Phillips RW, Moore BK, Roberts TA. Materials science effect of filler content and size on properties of composites. *J Dent Res*. 1985;64(12):1396–1403. doi:10.1177/00220345850640121501
38. Turssi C, Ferracane J, Vogel K. Filler features and their effects on wear and degree of conversion of particulate dental resin composites. *Biomaterials*. 2005;26(24):4932–4937. doi:10.1016/j.biomaterials.2005.01.026
39. El-Safty S, Akhtar R, Silikas N, Watts DC. Nanomechanical properties of dental resin-composites. *Dent Mater*. 2012;28(12):1292–1300. doi:10.1016/j.dental.2012.09.007
40. Okamoto A, Sekiya K, Fukushima M, Iwaku M. In vivo wear pattern of experimental light-cured hybrid composite resins. *Dent Mater J*. 1993;12(2):225–232,276. doi:10.4012/dmj.12.225
41. Kuşgöz A, Tüzüner T, Ülker M, Kemer B, Saray O. Conversion degree, microhardness, microleakage and fluoride release of different fissure sealants. *J Mech Behav Biomed Mater*. 2010;3(8):594–599. doi:10.1016/j.jmbbm.2010.07.008
42. Shahdad SA, McCabe JF, Bull S, Rusby S, Wassell RW. Hardness measured with traditional Vickers and Martens hardness methods. *Dent Mater*. 2007;23(9):1079–1085. doi:10.1016/j.dental.2006.10.001
43. Alexandropoulos A, Al Jabbari YS, Zinelis S, Eliades T. Chemical and mechanical characteristics of contemporary thermoplastic orthodontic materials. *Australas Orthod J*. 2015;31(2):165–170. doi:10.21307/aoj-2020-151
44. Liber-Kneć A, Łagan S. Surface testing of dental biomaterials: Determination of contact angle and surface free energy. *Materials (Basel)*. 2021;14(11):2716. doi:10.3390/ma14112716
45. Jiang H, Müller-Plathe F, Panagiotopoulos AZ. Contact angles from Young's equation in molecular dynamics simulations. *J Chem Phys*. 2017;147(8):084708. doi:10.1063/1.4994088
46. Law KY. Definitions for hydrophilicity, hydrophobicity, and superhydrophobicity: Getting the basics right. *J Phys Chem Lett*. 2014;5(4):686–688. doi:10.1021/jz402762h
47. De Moor RJG, Verbeeck RMH, De Maeyer EAP. Fluoride release profiles of restorative glass ionomer formulations. *Dent Mater*. 1996;12(2):88–95. doi:10.1016/S0109-5641(96)80074-1
48. Shen C, Shokry TE, Anusavice KJ. Influence of pH and oxygen-inhibited layer on fluoride release properties of fluoride sealant. *J Dent*. 2007;35(4):275–281. doi:10.1016/j.jdent.2006.09.005
49. Parkinson CR, Burnett GR, Thomas GV, Davies L, Payne D. Randomised study of intra-oral kinetics of fluoride-containing toothpastes. *J Dent*. 2021;106:103587. doi:10.1016/j.jdent.2021.103587
50. Burnett G, Nehme M, Parkinson C, et al. A randomised oral fluoride retention study comparing intra-oral kinetics of fluoride-containing dentifrices before and after dietary acid exposure. *Arch Oral Biol*. 2020;119:104891. doi:10.1016/j.archoralbio.2020.104891
51. Ahovuo-Saloranta A, Forss H, Walsh T, Nordblad A, Mäkelä M, Worthington HV. Pit and fissure sealants for preventing dental decay in permanent teeth. *Cochrane Database Syst Rev*. 2017;2017(7):CD001830. doi:10.1002/14651858.CD001830.pub5
52. Bourgi R, Doumandji Z, Cuevas-Suárez CE, et al. Exploring the role of nanoparticles in dental materials: A comprehensive review. *Coatings*. 2025;15(1):33. doi:10.3390/coatings15010033
53. Yassin SM, Mohamad D, Togoo RA, Sanusi SY, Johari Y. Do nanofillers provide better physicomechanical properties to resin-based pit and fissure sealants? A systematic review. *J Mech Behav Biomed Mater*. 2023;145:106037. doi:10.1016/j.jmbbm.2023.106037

Propolis-infused heat-polymerized acrylic denture bases: Enhanced mechanical properties in vitro study

Rasha Mehdi[1,A–C], Intisar J. Ismail[1,D–F], Nabaa Al-Nawab[2,D–E], Ban M. Jassim[3,A,B]

[1] Department of Prosthodontics, College of Dentistry, Al-Esraa University, Baghdad, Iraq
[2] College of Medicine, Al Iraqia University, Baghdad, Iraq
[3] Department of Operative Dentistry, College of Dentistry, Al-Esraa University, Baghdad, Iraq

A – research concept and design; B – collection and/or assembly of data; C – data analysis and interpretation; D – writing the article; E – critical revision of the article; F – final approval of the article

Polymers in Medicine, ISSN 0370-0747 (print), ISSN 2451-2699 (online) *Polim Med*. 2025;55(2):105–111

Address for correspondence
Intisar J. Ismail
E-mail: dr.intesar.jameel@esraa.edu.iq

Funding sources
None declared

Conflict of interest
None declared

Acknowledgements
First and foremost, we thank God for His blessings and guidance in enabling us to complete this study. We would also like to express our sincere gratitude to the Scientific Committee of the College of Dentistry at Al-Esraa University for their encouragement and support throughout this research. Special thanks go to the research team for their dedication and collaboration in bringing this work to fruition. Finally, we extend our deepest appreciation to our families for their unwavering support and understanding during the course of this study and the writing process.

Received on January 4, 2025
Reviewed on April 14, 2025
Accepted on April 30, 2025

Published online on December 19, 2025

Cite as
Mehdi R, Ismail IJ, Al-Nawab N, Jassim BM. Propolis-infused heat-polymerized acrylic denture bases: Enhanced mechanical properties analysis. *Polim Med*. 2025;55(2):105–111. doi:10.17219/pim/204545

DOI
10.17219/pim/204545

Abstract

Background. Polymethyl methacrylate (PMMA) is widely used as a denture base material despite its limitations, which include low transverse strength, impact resistance, surface hardness, and relatively high water solubility and sorption. To enhance its mechanical and physical properties, PMMA has been modified by incorporating various metal powder fillers, such as aluminum and copper – despite their tendency to cause discoloration. These modifications aim to improve the overall quality and durability of dental prostheses.

Objectives. To evaluate the influence of incorporating microform propolis powder (known for its antifungal and antimicrobial properties and its rich composition of functional groups) into acrylic denture base material, and to assess its effect on selected physical and mechanical properties of the material.

Materials and methods. A total of 128 specimens were prepared to evaluate various mechanical properties. Four groups were tested: 1 control group containing acrylic resin without propolis, and 3 experimental groups with propolis powder added at concentrations of 1.0%, 2.0% and 3.0% by weight. Each group consisted of 8 specimens for each mechanical test. All specimens were cured using the conventional heat-curing method. The mechanical properties evaluated included transverse strength, impact strength, surface hardness, and surface roughness. The data were statistically analyzed using the IBM SPSS software.

Results. The group with 1.0% propolis addition showed the highest mean values in all tested mechanical properties: transverse strength (90.50 N/mm^2), impact strength (10.45 kJ/m^2) and surface hardness (84.39). These values were significantly higher than those of the control group, with statistical analysis revealing highly significant differences between groups ($p < 0.05$) using ANOVA. Regarding surface roughness, the 1.0% propolis group also recorded the lowest mean value (1.03 µm), compared to the control group (2.14 µm), with all experimental groups showing significantly reduced roughness.

Conclusions. The incorporation of 1.0% microform propolis powder into PMMA denture base material significantly improved its mechanical and surface properties. These promising results suggest that further studies are warranted – either to explore additional properties or to test different propolis concentrations, potentially combined with coupling agents such as silane to enhance bonding and performance.

Key words: mechanical properties, polymethyl methacrylate, propolis

Highlights

- Incorporating 1.0% propolis powder into PMMA significantly improved transverse strength, impact resistance, and surface hardness.
- Surface roughness was lowest in the 1.0% propolis group, indicating a smoother finish compared to control and higher concentrations.
- Propolis is a natural, color-neutral additive that enhances mechanical properties without affecting the appearance of the denture base.
- Results suggest 1.0% propolis is the optimal concentration for enhancing mechanical and surface properties of denture base materials.

Introduction

Poly (methyl methacrylate) (PMMA) has been widely used for dental prostheses due to its advantageous properties. However, it fails to meet several mechanical demands, such as exhibiting low transverse strength, low impact strength, low surface hardness and high water solubility and sorption.[1] Efforts to enhance PMMA include adding metal powder fillers like aluminum and copper, which improve properties but result in unacceptable color.[2] Another approach involves reinforcing PMMA with fibers such as nylon, carbon and glass.[3]

Propolis, a natural resin collected by bees from plant exudates and shoots, has been used in traditional medicine since ancient times.[4] In dentistry, propolis exhibits anti-inflammatory, antibacterial, antifungal, hemostatic, and tissue-rearrangement properties.[5] Propolis, at a 76% concentration, added to silicone soft liners for hot-cured denture base material, effectively inhibits *Candida albicans* growth and enhances tensile strength.[6] Research by Tobaldini-Valerio et al. demonstrated propolis's antifungal impact on *Candida albicans*,[7] preventing biofilm growth and eliminating mature biofilms. *Candida albicans* biofilms can reduce the mechanical properties of soft denture liners with heat-polymerized acrylic resin.[8]

Objectives

This study aims to investigate the effect of propolis micropowder on the mechanical and physical properties of PMMA denture base material at various concentrations, as well as its antifungal activity.

Materials and methods

The influence of propolis on heat-cured acrylic resin was analyzed by incorporating it into the acrylic powder at concentrations of 1%, 2% and 3%, while a propolis-free formulation served as the control. The additive, sieved to a fine 25-micron particle size, was mixed into the resin. Each concentration group consisted of 8 specimens, resulting in 32 samples per tested property. Altogether, 128 specimens were prepared and assessed to determine their mechanical characteristics.

Mold preparation

Molds were created using computer-measured plastic pattern blocks cut to precise dimensions. For transverse strength, hardness and surface roughness tests, specimens of 65 × 10 × 2.5 mm were manufactured. For impact strength tests, specimens of 80 × 10 × 4 mm were prepared.

The dental flask's lower half was filled with prepared stone slurry mixed according to the ratio. Plastic specimens were submerged in the slurry, which was allowed to set for 1 h before being coated with separating media (alginate solution). The typical curing process followed, including investing, removing the plastic mold and packing. Acrylic's power liquid (P/L) ratio was 2.5 g: 1.0 mL w/v per manufacturer's instructions. The mixture was left at room temperature in a covered jar for 45 s after mixing with the monomer; then, the appropriate amount of polymer and propolis was added. Once the dough stage was reached, each flask was filled with resin. The 2 halves of the flask were then joined and placed in a press (HYDROFIX press; BEGO, Bremen, Germany) with slow pressure application to allow the dough to flow evenly throughout the mold space. The press was then turned off after 5 min. The flasks were clamped and placed in a curing bath at 70°C for 30 min, then raised to 100°C for 2 h. After cooling, the flasks were opened, and acrylic specimens were carefully extracted, finished and polished. Only roughness test specimens were left unpolished.

Mechanical testing

Transverse strength was tested using an Instron universal testing machine (WDW-200 E; Instron, Norwood, USA; Fig. 1) Specimens were placed on a bending fixture with 2 parallel supports spaced 50 mm apart. The load was applied at a crosshead speed of 2 mm/min until fracture occurred.

Transverse strength (TS) was calculated using the following equation:

$$TS = 3LW/2bh^2$$

where L is the maximum load in newtons, W is the supporting width in mm, b is the width of the test specimen in mm, and h is the height of the test specimen in mm.

Impact strength was measured using the Charpy impact test for unnotched specimens. Specimens were struck by a free-swinging pendulum of 2 J, and impact energy was indicated by scale readings in joules. Impact strength (IS) was calculated using the equation:

$$IS = \frac{e}{db}10^3 \quad [\mathrm{kJ/m}]$$

where e is energy in joules, d is depth in mm and b is width in mm.

Surface hardness was measured using a Shore D durometer (Time Group Inc., Beijing, China), equipped with a 0.8 mm diameter spring-loaded indenter and a digital scale ranging from 0 to 100 units. The usual procedure is to press down swiftly and forcefully on the intender and then record the reading. Each specimen underwent 3 readings, 1 in the middle and 1 at each end, and the mean of the 3 readings was analyzed.

Specimens with dimensions of 65 × 10 × 2.5 ±0.1 mm were prepared. The effect of propolis particles on the surface microgeometry was assessed using a profilometer equipped with a sharp diamond-tipped stylus. This analyzer records the peaks and valleys that define the surface profile. The unpolished specimen was placed on a stable stage, and the test area was divided into 4 sections. The profilometer was moved across each section, and the average of the 4 readings was calculated.

Data analysis

Descriptive statistics, including mean and standard deviation (SD) values for each group, were processed using IBM SPSS v. 22 (IBM Corp., Armonk, USA). A one-way analysis of variance (ANOVA) test was conducted to determine the significance of propolis concentrations on the mechanical properties of heat-polymerized acrylic resin denture base material, with results from the least significant difference (LSD) analysis providing insights into the differences between the groups for each test.

Results

The following tables summarize the results of the 4 groups, defined by propolis concentration.

Transverse strength test

The highest mean transverse strength was observed in the group with 1% propolis (90.5 N/mm^2), which decreased as the propolis percentage increased (Table 1, Fig. 2). The ANOVA test results indicated highly significant differences between the groups (Table 2).

Surface roughness test

Experimental groups exhibited lower surface roughness values compared to the control group, which had a high

Fig. 1. Instron testing machine and the sample used

Table 1. Descriptive statistics of transverse strength test (N/mm^2) of all groups

Groups	n	Mean	SD	Minimum	Maximum
Control PMMA	8	76.299	2.787	72.51	79.38
1% propolis	8	90.5	5.382	84.21	97.27
2% propolis	8	73.539	9.138	52.37	79.69
3% propolis	8	68.136	1.142	66.55	69.92

SD – standard deviation; PMMA – polymethyl methacrylate.

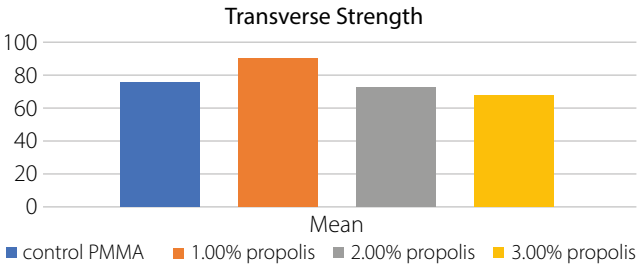

Fig. 2. Mean transverse strength test of specimens as a function of propolis addition percentage

PMMA – polymethyl methacrylate.

Table 2. Analysis of variance (ANOVA) test results of transverse strength test groups

ANOVA test		Sum of squares	df	Mean square	F	Sig.
Transverse strength (N/mm^2) * propolis %	between groups (combined)	2185.856	3	728.619	23.981	0.000
	within groups	850.746	28	30.384	–	–

df – degrees of freedom.

value of 2.138 µm. The lowest surface roughness was found in the 1.0 wt% propolis samples (1.027 µm) (Table 3, Fig. 3). The ANOVA test results revealed highly significant differences between the groups (Table 4).

Impact strength test

The highest mean impact strength was observed in the 1.0 wt% propolis group (10.454 KJ/m^2), with values decreasing but remaining close to the control group (Table 5, Fig. 4). The ANOVA test results indicated highly significant differences between the groups (Table 6).

Indentation hardness test

Surface hardness increased in the 1.0 wt% propolis group (84.538) and decreased with higher propolis percentages (Table 7, Fig. 5). The ANOVA test results showed highly significant differences between the groups (Table 8).

Least significant test

The results from the LSD analysis provide insights into the differences between the groups for each test. Here's what it implies:

Transverse strength test

- Significant differences:
  - Control PMMA vs 1% propolis;
  - Control PMMA vs 3% propolis;
  - 1% propolis vs 2% propolis;
  - 1% propolis vs 3% propolis.
- Nonsignificant differences:
  - Control PMMA vs 2% propolis;
  - 2% propolis vs 3% propolis.

Implication: The addition of 1% propolis significantly increases the transverse strength compared to the control and other concentrations. However, 2% and 3% propolis do not show significant differences from each other or the control.

Surface roughness test

- Significant differences:
  - Control PMMA vs all propolis concentrations (1%, 2%, 3%)
  - 1% propolis vs 2% propolis
  - 1% propolis vs 3% propolis
- Nonsignificant differences:
  - 2% propolis vs 3% propolis

Implication: All concentrations of propolis significantly reduce surface roughness compared to the control. The 1% propolis concentration shows the most significant reduction, while 2% and 3% propolis do not differ significantly from each other.

Impact strength test

- Significant differences:
  - Control PMMA vs 1% propolis;
  - Control PMMA vs 3% propolis;
  - 1% propolis vs 2% propolis;
  - 1% propolis vs 3% propolis;
  - 2% propolis vs 3% propolis.
- Nonsignificant differences:
  - Control PMMA vs 2% propolis.

Implication: The 1% propolis concentration significantly increases impact strength compared to the control and other concentrations. The 3% propolis concentration significantly decreases impact strength compared to the control and other concentrations.

Indentation hardness test

- Significant differences:
  - Control PMMA vs all propolis concentrations (1%, 2%, 3%);
  - 1% propolis vs 2% propolis;
  - 1% propolis vs 3% propolis.
- Nonsignificant differences:
  - 2% propolis vs 3% propolis

Implication: The addition of 1% propolis significantly increases indentation hardness compared to the control and other concentrations. The 2% and 3% propolis concentrations significantly decrease indentation hardness compared to the control.

Overall implications

- 1% propolis: Generally, improves transverse strength, reduces surface roughness, increases impact strength, and increases indentation hardness.
- 2% propolis: Does not significantly differ from the control in most tests, except for surface roughness.
- 3% propolis: Generally, decreases transverse strength and impact strength, while reducing surface roughness and indentation hardness.

These results suggest that the optimal concentration of propolis for improving material properties varies depending on the specific property being tested.

Discussion

Propolis is a natural substance known for its wide range of biological activities, including antioxidant, antibacterial, antifungal, anti-inflammatory, antiviral, and anticancer effects.[9–11] It is collected by bees from plant sources such as leaves and buds and mixed with pollen and wax to form a resinous material.[12,13] Chemically, propolis is complex, containing over 300 compounds such as phenolic acids, flavonoids, terpenes, amino acids, and various aromatic and

Table 3. Surface roughness [µm] test descriptive statistics

Groups	n	Mean	SD	Minimum	Maximum
Control PMMA	8	2.138	0.351	1.799	2.798
1% propolis	8	1.027	0.292	0.692	1.489
2% propolis	8	1.53	0.313	1.054	2.104
3% propolis	8	1.557	0.34	0.948	2.015

SD – standard deviation; PMMA – polymethyl methacrylate.

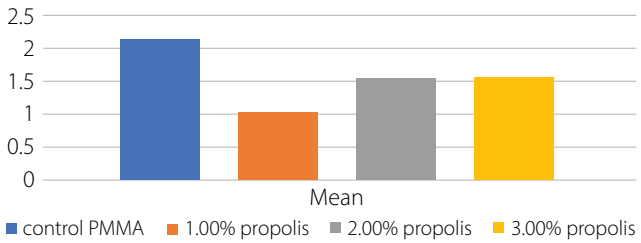

Fig 3. Mean of surface roughness test of specimens as a function of propolis addition percentage

PMMA – polymethyl methacrylate.

Table 4. Analysis of variance (ANOVA) test results of surface roughness test

ANOVA test		Sum of squares	df	Mean square	F	Sig.
Surface roughness [µm] * propolis %	between groups (combined)	4.946	3	1.649	15.634	0.000
	within groups	2.953	28	0.105	–	–

df – degrees of freedom.

Table 5. Impact strength test (Kj/m^2) test descriptive statistics

1% propolis	8	10.454	0.75	9.35	11.47
3% propolis	8	8.22	0.664	7.22	8.92

SD – standard deviation; PMMA – polymethyl methacrylate.

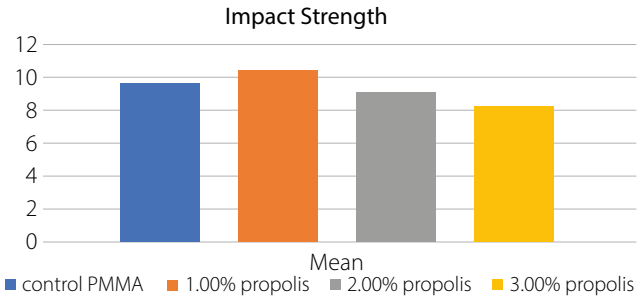

Fig 4. Mean of impact strength test of specimens as a function of propolis addition percentage

PMMA – polymethyl methacrylate.

Table 6. Analysis of variance (ANOVA) test results of impact strength test

	within groups	13.495	28	0.482	–	–

df – degrees of freedom.

Table 7. Indentation hardness test (No.) descriptive statistics

1% propolis	8	84.538	0.472	83.80	85.20
3% propolis	8	80.562	0.45336	80.00	81.30

SD – standard deviation.; PMMA – polymethyl methacrylate.

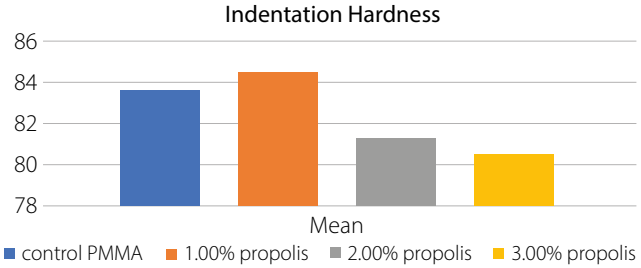

Fig. 5. Mean of indentation hardness test of specimens as a function of propolis addition percentage

PMMA – polymethyl methacrylate.

Table 8. Analysis of variance (ANOVA) indentation hardness test results of indentation hardness

	within groups	19.671	28	0.703	–	–

df – degrees of freedom

fatty substances.[14–16] This variability in composition can make standardization and quality control challenging.[17–19]

Typically, propolis consists of about 50% resin and vegetable balsam, 30% wax, 10% essential and aromatic oils, 5% pollen, and other minor components, including organic debris.[20] In this study, propolis was chosen for its antifungal properties and its neutral color, which does not alter the appearance of the denture base material. Its phenolic-rich composition[21] was incorporated into acrylic resin to explore its therapeutic potential and assess its influence on mechanical properties at different concentrations.[22]

The results showed that the highest transverse strength was achieved with 1% propolis. At higher concentrations, strength decreased compared to the control, with statistically significant differences confirmed with ANOVA. The reduction in strength at higher levels may be related to the wax content in propolis,[20] which could interfere with the resin matrix. In contrast, the 1% concentration may benefit from aromatic functional groups that enhance bonding within the polymer. The absence of coupling agents like silane, which typically improve adhesion, may also have contributed to the observed trends.

Surface roughness was lowest in the 1% propolis group, and all tested concentrations showed values below that of the control. These differences were statistically significant. A smoother surface is advantageous as it reduces bacterial adhesion and the risk of oral infections, consistent with findings by de Foggi et al.[23] This application of propolis appears to be novel, and the presence of wax and resinous components may have influenced the surface characteristics.

Propolis also offers several pharmacological benefits, including wound healing, anesthetic, hemostatic, anticariogenic, anti-inflammatory, and antibiotic effects,[24–26] and is considered non-cytotoxic to humans.[21] The increase in impact strength observed at 1% propolis suggests good dispersion and compatibility with the resin. Its plasticizing effect may contribute to improved flexibility, and the presence of functional groups could facilitate bonding with the polymer matrix.

Surface hardness increased slightly at 1% propolis but declined at higher concentrations. These differences were also statistically significant. The decrease in hardness at higher levels may be due to the absence of hard fillers in propolis and the influence of phenolic and antioxidant compounds, which can affect the structural integrity of the polymer.[27]

A study by Al-Khalifa et al.[28] reported similar findings, where 2.5% propolis in PMMA reduced *C. albicans* counts and increased surface roughness, while higher concentrations led to decreased hardness. These results support the current findings and highlight the potential of propolis as a bioactive additive. Incorporating 1% propolis into heat-cured acrylic resin appears to enhance transverse and impact strength, improve surface hardness, and reduce roughness, suggesting potential benefits for the performance and longevity of denture base materials.

Limitations

One challenge we encountered was related to the color of the material. Increasing the additive concentration beyond the level we used could affect the esthetic quality, making it less similar to the natural color of gum tissue. For this reason, we limited the concentration to 3% to maintain acceptable aesthetic properties. Additionally, since the material contains several active chemical groups, it is not yet clear which specific reactions are responsible for the results we observed. Further investigations are needed to identify the primary chemical reactions responsible for the observed effects.

Conclusions

This study highlights the significant potential of propolis as a new source of bioactive compounds and its ability to improve the mechanical properties of heat-cured acrylic resin denture bases. Incorporating 1% propolis powder may enhance the transverse and impact strength, as well as the hardness, while decreasing surface roughness. These improvements suggest that propolis incorporation could enhance the stability and shelf-life of commercial acrylic materials.

Use of AI and AI-assisted technologies

Not applicable.

References

1. Mohammed AA, Ismail IJ. In vitro performance of polymethyl-methacrylate with ultra-high density poly ethylene fiber and nano zirconium oxide particles composite. *J Bagh Coll Dent*. 2018;30(1):5–11. doi:10.12816/0046304
2. Sehajpal SB, Sood VK. Effect of metal fillers on some physical properties of acrylic resin. *J Prosthet Dent*. 1989;61(6):746–751. doi:10.1016/s0022-3913(89)80055-1
3. Yu SH, Lee Y, Oh S, Cho HW, Oda Y, Bae JM. Reinforcing effects of different fibers on denture base resin based on the fiber type, concentration, and combination. *Dent Mater J*. 2012;31(6):1039–1046. doi:10.4012/dmj.2012-020
4. Bankova V, Popova M, Bogdanov S, Sabatini AG. Chemical composition of European propolis: Expected and unexpected results. *Z Naturforsch C J Biosci*. 2002;57(5–6):530–533. doi:10.1515/znc-2002-5-622
5. Hartini. Test of antifungal activity of hive extract and North Luwu forest honey on Candida albicans [in Indonesian]. *Bioedukasi Jurnal Pendidikan Biologi*. 2017;10(2):44–46. https://jurnal.uns.ac.id/bioedukasi/article/view/15158/pdf. Accessed March 15, 2025.
6. Tarigan M, Nasution ID, Harahap U, Utami Ritonga PW. Effect of propolis addition to auto-polymerized silicone soft denture lining against inhibition zone of *Candida albicans* and tensile strength of heat-polymerized acrylic resin. *Nat Volatiles Essent Oils*. 2021;8(4):2348–2360. https://www.nveo.org/index.php/journal/article/view/445/411.
7. Tobaldini-Valerio FK, Bonfim-Mendonça PS, Rosseto HC, et al. Propolis: A potential natural product to fight *Candida* species infections. *Future Microbiol*. 2016;11(8):1035–1046. doi:10.2217/fmb-2015-0016
8. Perchyonok T. Bio-active denture soft liner materials from design to application: In vitro approach. *J Dent Health Oral Disord Ther*. 2017;6(4):101–105. doi:10.15406/jdhodt.2017.06.00206
9. Kujumgiev A, Tsvetkova I, Serkedjieva Y, Bankova V, Christov R, Popov S. Antibacterial, antifungal and antiviral activity of propolis of different geographic origin. *J Ethnopharmacol*. 1999;64(3):235–240. doi:10.1016/s0378-8741(98)00131-7

10. Valencia D, Alday E, Robles-Zepeda R, et al. Seasonal effect on chemical composition and biological activities of Sonoran propolis. *Food Chem*. 2012;131(2):645–651. doi:10.1016/j.foodchem.2011.08.086
11. Choi YM, Noh DO, Cho SY, Suh HJ, Kim KM, Kim JM. Antioxidant and antimicrobial activities of propolis from several regions of Korea. *LWT Food Sci Technol*. 2006;39(7):756–761. doi:10.1016/j.lwt.2005.05.015
12. Sanden M, Jørgensen S, Hemre GI, Ørnsrud R, Sissener NH. Zebrafish (*Danio rerio*) as a model for investigating dietary toxic effects of deoxynivalenol contamination in aquaculture feeds. *Food Chem Toxicol*. 2012;50(12):4441–4448. doi:10.1016/j.fct.2012.08.042
13. Bankova V. Chemical diversity of propolis and the problem of standardization. *J Ethnopharmacol*. 2005;100(1–2):114–117. doi:10.1016/j.jep.2005.05.004
14. Gregoris E, Stevanato R. Correlations between polyphenolic composition and antioxidant activity of Venetian propolis. *Food Chem Toxicol*. 2010;48(1):76–82. doi:10.1016/j.fct.2009.09.018
15. Erdogan S, Ates B, Durmaz G, Yilmaz I, Seckin T. Pressurized liquid extraction of phenolic compounds from Anatolia propolis and their radical scavenging capacities. *Food Chem Toxicol*. 2011;49(7):1592–1597. doi:10.1016/j.fct.2011.04.006
16. Sarikaya AO, Ulusoy E, Öztürk N, Tunçel M, Kolayli S. Antioxidant activity and phenolic acid constituents of chestnut *Castania sativa* Mill. *J Food Biochem*. 2009;33(4):470–481. doi:10.1111/j.1745-4514.2009.00231.x
17. Potkonjak NI, Veselinović DS, Novaković MM, Gorjanović SŽ, Pezo LL, Sužnjević DŽ. Antioxidant activity of propolis extracts from Serbia: A polarographic approach. *Food Chem Toxicol*. 2012;50(10):3614–3618. doi:10.1016/j.fct.2012.07.029
18. Sforcin JM, Bankova V. Propolis: Is there a potential for the development of new drugs? *J Ethnopharmacol*. 2011;133(2):253–260. doi:10.1016/j.jep.2010.10.032
19. Bankova V, Popova M, Trusheva B. New emerging fields of application of propolis. *Maced J Chem Chem Eng*. 2016;35(1):1. doi:10.20450/mjcce.2016.864
20. Kalogeropoulos N, Konteles SJ, Troullidou E, Mourtzinos I, Karathanos VT. Chemical composition, antioxidant activity and antimicrobial properties of propolis extracts from Greece and Cyprus. *Food Chem*. 2009;116(2):452–461. doi:10.1016/j.foodchem.2009.02.060
21. Ulloa PA, Vidal J, Ávila MI, Labbe M, Cohen S, Salazar FN. Effect of the addition of propolis extract on bioactive compounds and antioxidant activity of craft beer. *J Chem*. 2017;2017:716053. doi:10.1155/2017/6716053
22. Jaboinski LT, Miranda ME, Hofling RTB, Pereira EC, Pinto JRR, Vasconcellos AA. Effect of the addition of propolis on a soft denture liner on bond strength with an acrylic resin. *J Health Sci Inst*. 2015;33(3):223-227.
23. de Foggi CC, Machado AL, Zamperini CA, Fernandes D, Wady AF, Vergani CE. Effect of surface roughness on the hydrophobicity of a denture-base acrylic resin and *Candida albicans* colonization. *J Investig Clin Dent*. 2016;7(2):141–148. doi:10.1111/jicd.12125
24. Kang SH, Lee HJ, Hong SH, Kim KH, Kwon TY. Influence of surface characteristics on the adhesion of *Candida albicans* to various denture lining materials. *Acta Odontol Scand*. 2013;71(1):241–248. doi:10.3109/00016357.2012.671360
25. Salim N, Moore C, Silikas N, Satterthwaite JD, Rautemaa R. Fungicidal amounts of antifungals are released from impregnated denture lining material for up to 28 days. *J Dent*. 2012;40(6):506–512. doi:10.1016/j.jdent.2012.02.016
26. Vagish Kumar LS. Propolis in dentistry and oral cancer management. *N Am J Med Sci*. 2014;6(6):250–259. doi:10.4103/1947-2714.134369
27. AlBin-Ameer MA, Alsrheed MY, Aldukhi IA, et al. Effect of protective coating on surface properties and *Candida albicans* adhesion to denture base materials. *J Prosthodont*. 2020;29(1):80–86. doi:10.1111/jopr.13118
28. Al-Khalifa KS, Gad MM, Alshahrani FA, et al. Influence of propolis extract (caffeic acid phenethyl ester) addition on the *Candida albicans* adhesion and surface properties of autopolymerized acrylic resin. *Int J Dent*. 2022;2022:6118660. doi:10.1155/2022/6118660

Polymer matrix of biofilm in *Klebsiella pneumoniae* reduced by sub-MIC hydrogen peroxide enhances cefotaxime efficacy

Mohammed Talab Mohammed[A,B], Ayaid Khadem Zgair[A,C–F]

Department of Biology, College of Science, University of Baghdad, Iraq

A – research concept and design; B – collection and/or assembly of data; C – data analysis and interpretation;
D – writing the article; E – critical revision of the article; F – final approval of the article

Polymers in Medicine, ISSN 0370-0747 (print), ISSN 2451-2699 (online) *Polim Med*. 2025;55(2):113–122

Address for correspondence
Ayaid Khadem Zgair
E-mail: ayaid.zgair@sc.uobaghdad.edu.iq

Funding sources
None declared

Conflict of interest
None declared

Acknowledgements
The authors would like to thank all staff members of the Department of Biology, College of Science, University of Baghdad, Iraq, for their valuable support during the experimental work.

Received on June 20, 2025
Reviewed on July 3, 2025
Accepted on July 4, 2025

Published online on December 19, 2025

Abstract

Background. The polymer matrix of *Klebsiella pneumoniae* biofilm contributes to its resistance to a broad spectrum of antibiotics and poses a significant public health threat.

Objectives. The present study aims to use hydrogen peroxide (H_2O_2) sub-minimum inhibitory concentrations (sub-MICs) to improve cefotaxime efficiency against cefotaxime-resistant *K. pneumoniae* (CRKP) by disrupting the biofilm polymer matrix.

Objectives. The present study aims to determine whether sub-MICs of hydrogen peroxide (H_2O_2) can enhance the efficacy of cefotaxime against CRKP by disrupting the biofilm polymer matrix.

Materials and methods. *Klebsiella pneumoniae* was isolated from 140 burn wound samples. The effect of cefotaxime and sub-MICs of H_2O_2 on biofilm formation by pretreated *K. pneumoniae* was evaluated. A scanning electron microscope (SEM) was used to examine the effect of H_2O_2 sub-MICs on the biofilm matrix. The synergistic effect of H_2O_2 sub-MICs on the susceptibility of CRKP to cefotaxime and on the structure of the biofilm polymer matrix was also assessed.

Results. A moderately high incidence of wound infections caused by CRKP was observed. A statistically significant negative correlation was found between biofilm formation and bacterial susceptibility to cefotaxime ($r = -0.501$, $p = 0.024$). Treatment with various sub-MICs of H_2O_2 and cefotaxime reduced biofilm formation on polystyrene surfaces by the *K. pneumoniae* Kp10 isolate. Specifically, exposure to H_2O_2 at 1/8 MIC induced the formation of pores and channels within the biofilm matrix, resulting in a looser biofilm structure. A synergistic effect (fractional inhibitory concentration (FIC) index ≤ 0.5) was observed, where sub-MICs of H_2O_2 decreased the MIC of cefotaxime against Kp10 from 1,000 µg/mL to 250 µg/mL at ½ and ¼ MIC of H_2O_2, and produced a strong additive effect with a reduction to 500 µg/mL at other sub-MICs. The combination of H_2O_2 sub-MICs and cefotaxime was more effective in reducing biofilm formation than either agent used alone.

Conclusions. Sub-minimum inhibitory concentrations of H_2O_2 exhibited synergistic to strongly additive effects in enhancing the antibacterial activity of cefotaxime against CRKP and in reducing biofilm formation by the *K. pneumoniae* Kp10 isolate. This effect appears to be mediated by disruption of the biofilm polymer matrix, which may contribute to improved infection control.

Key words: biofilm polymer, cefotaxime, scanning electron microscope, sub-MICs, synergy

Cite as
Mohammed MT, Zgair AK. Polymer matrix of biofilm in *Klebsiella pneumoniae* reduced by sub-MIC hydrogen peroxide enhances cefotaxime efficacy. *Polim Med*. 2025;55(2):113–122. doi:10.17219/pim/207885

DOI
10.17219/pim/207885

Highlights

- Hydrogen peroxide enhances antibiotic efficacy by disrupting the biofilm matrix of cefotaxime-resistant *Klebsiella pneumoniae* at sub-minimum inhibitory concentrations (sub-MICs).
- Synergistic antimicrobial effect: hydrogen peroxide reduced the cefotaxime MIC from 1,000 µg/mL to 250 µg/mL in *K. pneumoniae* antibiotic-resistant isolates.
- Scanning electron microscopy analysis revealed hydrogen peroxide-induced pores and channels that weakened biofilm integrity and decreased biofilm formation.
- Combined hydrogen peroxide and cefotaxime therapy demonstrated significantly stronger biofilm inhibition than either treatment alone, suggesting a promising approach against antibiotic-resistant *K. pneumoniae* infections.

Background

The polymer matrix of bacterial biofilms is a highly organized extracellular environment composed of macromolecules such as polysaccharides, proteins, nucleic acids, and lipids. This matrix is fundamental to the biofilm's architecture and plays a key role in protecting bacterial cells.[1] The polymer matrix also contributes to the persistence of bacterial populations and their protection against external environmental factors, including antibiotics.[2] In clinical settings, the biofilm polymer matrix acts as a physical barrier that limits antibiotic penetration into bacterial cells, promotes chronic infection and significantly contributes to antibiotic resistance, particularly in Gram-negative bacteria such as *Klebsiella pneumoniae*.[3,4] The microenvironment within the deeper layers of the biofilm matrix is characterized by nutrient deprivation, hypoxia and altered pH, leading to metabolic adaptations in bacterial populations and the induction of a persistent state that further enhances antibiotic resistance.[5]

Klebsiella pneumoniae is an opportunistic pathogen responsible for a wide range of healthcare-associated infections, including pneumonia, urinary tract infections, wound infections, and, in some cases, sepsis. A major virulence factor of *K. pneumoniae* is its ability to form extensive polymeric biofilm masses on both biotic and abiotic surfaces.[6] This species exhibits resistance to a broad spectrum of antibiotics through multiple mechanisms, including β-lactamase production, efflux pump activity and biofilm formation, making such infections particularly difficult to treat.[7] It can colonize medical devices such as urinary catheters, endotracheal tubes and central venous catheters,[8] as well as hospital surfaces including bed rails, door handles and surgical instruments.[9] *Klebsiella pneumoniae* also forms biofilms on plastic and metal surfaces such as polyvinyl chloride (PVC), stainless steel and polystyrene.[10] Furthermore, it adheres to epithelial tissues, including the urinary tract epithelium.[11] On these surfaces, *K. pneumoniae* exhibits increased tolerance to antibiotics, largely mediated by its dense polymeric matrix, which restricts antibiotic diffusion.[12] The rising incidence of multidrug-resistant (MDR) *K. pneumoniae* strains in recent years underscores the urgent need for alternative therapeutic strategies aimed at enhancing antibiotic efficacy through biofilm modulation.[13]

One promising strategy involves the use of sub-minimum inhibitory concentrations (sub-MICs) of non-antibiotic agents to weaken the biofilm matrix and enhance antibiotic penetration into embedded bacteria. Hydrogen peroxide (H_2O_2), a reactive oxygen species (ROS) naturally produced by immune cells, has a well-documented impact on biofilm architecture.[14] While the bactericidal effects of high concentrations of H_2O_2 are well established, the influence of sub-MIC levels of H_2O_2 on the polymeric biofilm matrix of *K. pneumoniae* remains poorly characterized in the literature.

This study focuses on the effects of sub-MICs of H_2O_2 on the biofilm polymer matrix of *K. pneumoniae* and its potential influence on antibiotic interaction. Investigating biofilm modulation through oxidative stress may provide a better understanding of approaches to improve the effectiveness of existing antibiotics.

Previous studies have shown that hydroxyl radical formation induced by bactericidal antibiotics represents the final stage of an oxidative damage pathway leading to bacterial cell death.[15] In combination with antibiotics, H_2O_2 has demonstrated the potential to reverse antibiotic resistance by disrupting bacterial defense mechanisms, thereby enhancing antibiotic efficacy. A previous study by Alkawareek et al. reported the synergistic antibacterial effect of silver nanoparticles and H_2O_2 against *Staphylococcus* and *Escherichia coli*. However, no prior research has investigated the synergistic effect of sub-MICs of H_2O_2 on the susceptibility of *K. pneumoniae* to antibiotics.[16]

Objectives

The objective of this study is to investigate the effects of sub-MIC concentrations of H_2O_2 on the structure and density of the biofilm polymer matrix in *K. pneumoniae* and to evaluate how these changes may influence the activity of cefotaxime.

Materials and methods

Isolation and identification of bacteria

Infected wound samples were collected aseptically from 140 inpatients with burn wound infections admitted to the Burns and Wounds Department at Baghdad Teaching Hospital (Baghdad, Iraq). Prior to sample collection, necrotic tissue and any residual ointments were carefully removed by a trained technician. None of the patients had received antibiotic treatment for at least 72 h before sampling, and all provided informed consent to participate in the study. Wound swabs were cultured on MacConkey agar (HiMedia, Mumbai, India) and incubated at 37°C for 24 h. Large, mucoid, pink colonies (lactose-fermenting) were collected and subjected to Gram staining, followed by standard biochemical tests, including oxidase, indole, urease, and citrate utilization assays. Identification of *K. pneumoniae* isolates was confirmed using the VITEK instrument (VITEK® DensiCHEK™; BioMérieux, Marcy-l'Étoile, France) and fluorescence system (bioMérieux) with the ID-GNB card. The bacterial isolates were preserved in 20% glycerol nutrient broth at –20 °C and subcultured weekly on nutrient agar.[17] The study was approved by the Human Ethics Committee of the Department of Biology, College of Science, University of Baghdad, Iraq (approval No. CSEC/1124/0113, issued on November 27, 2023).

Kirby-Bauer method

The Kirby–Bauer disk diffusion method was used to identify cefotaxime-resistant *K. pneumoniae* (CRKP). A bacterial suspension adjusted to the turbidity of a 0.5 McFarland standard was spread onto Mueller–Hinton agar (MHA; HiMedia). Cefotaxime disks (30 µg; Bioanalyse, Ankara, Turkey) were placed on the MHA plates and incubated at 37°C for 24 h. Following incubation, the diameters of the inhibition zones around the cefotaxime disks were measured and interpreted according to the Clinical and Laboratory Standards Institute (CLSI) breakpoint guidelines to classify isolates as susceptible (S), intermediate (I) or resistant (R) to cefotaxime.[18]

Minimum inhibitory concentration

The microdilution method described by Al-Mutalib and Zgair was used to determine the MICs of cefotaxime (AdvaCare Pharma, Durham, USA) and H_2O_2 (Merck Millipore, St. Louis, USA) against the CRKP isolate (Kp10). The minimum inhibitory concentration (MIC) was defined as the lowest concentration of the antimicrobial agent that completely inhibited visible bacterial growth.[19,20]

Biofilm formation

The microdilution method combined with a spectrophotometric assay using crystal violet was employed to assess biofilm formation in 20 *K. pneumoniae* isolates.[15–17] The method has been described in detail in previous studies.[19–21] Briefly, 100 µL of sterile tryptic soy broth (TSB; HiMedia) was added to the wells of a flat-bottom polystyrene tissue culture plate. Then, 5 µL of CRKP suspension (0.1 OD_{600} of an overnight bacterial culture, washed 3 times with sterile TSB) was added to each well, and the plates were incubated at 37°C for 24 h. After incubation, the TSB was discarded and the plates were washed 3 times with distilled water. The plates were then air-dried and stained with 100 µL of 0.4% Hucker crystal violet for 15 min, followed by 5 washes with distilled water. After drying, 100 µL of anhydrous ethanol was added to each well to solubilize the bound dye. The absorbance was measured at 570 nm using a microplate reader (BioTek 800 TS; BioTek, Winooski, USA). The experiment was repeated 3 times.

Effect of sub-MICs on biofilm formation

In this experiment, the effect of different sub-MICs of H_2O_2 or cefotaxime on biofilm formation by the CRKP isolate that exhibited the highest biofilm-producing capacity was evaluated. A similar biofilm formation assay was performed with slight modifications. Instead of using TSB alone, serial dilutions of sub-MICs of H_2O_2 or cefotaxime were prepared in TSB and added to the wells of a flat-bottom polystyrene microtiter plate. The plates were incubated at 37°C for 24 h and washed 3 times with distilled water. The wells were then stained with crystal violet, and after air drying, anhydrous ethanol was added to each well to solubilize the bound dye. The absorbance was measured at 570 nm using a microplate reader (BioTek 800 TS). The experiment was repeated 3 times.[21]

Scanning electron microscopy

The procedure described by Gomes and Mergulhão was followed to examine the biofilm of the CRKP isolate Kp10 using scanning electron microscopy (SEM) after treatment with a sub-MIC of cefotaxime.[22] Briefly, biofilm smears were prepared on sterile glass slides and treated with ⅛ MIC of cefotaxime to evaluate the effect of the sub-MIC on the biofilm polymer matrix. After staining, the slides were examined under a scanning electron microscope (Apreo 2 ChemiSEM; Thermo Fisher Scientific, Waltham, USA).

Effect of sub-MICs of H_2O_2 on cefotaxime MICs

The two-dimensional microdilution method (checkerboard assay) using a 96-well U-shaped polystyrene microtiter plate was employed to evaluate the effect of different

sub-MICs of H_2O_2 on the susceptibility of *K. pneumoniae* (CRKP isolate exhibiting the highest biofilm-forming ability) to cefotaxime, expressed in terms of MIC values. Briefly, 100 µL of sterile MHA was added to each well. A horizontal twofold serial dilution of cefotaxime, ranging from 2,000 µg/mL to 1.95 µg/mL, was prepared and applied across all wells in each row of the plate (wells 1–11). A vertical twofold serial dilution of hydrogen peroxide (H_2O_2; 30% stock solution: Merck Millipore) ranging from $^1/_{160}$ to $^1/_{10,240}$ was prepared in rows A–G of the microtiter plate. Subsequently, 5 µL of *K. pneumoniae* suspension (optical density (OD) of 0.1 at 600 nm) was added to each well. The plates were gently shaken and incubated at 37°C for 24 h.

The lowest antibiotic concentrations that completely inhibited bacterial growth were recorded as the MIC. Row H served as the first control, representing the MIC of cefotaxime in the absence of H_2O_2. Rows A–G demonstrated the effect of different H_2O_2 dilutions (sub-MICs) on the MIC of cefotaxime. Several control groups were included: 1) wells containing different H_2O_2 dilutions (sub-MICs in MHA) with the *K. pneumoniae* Kp10 isolate, 2) wells containing only MHA and bacteria, 3) wells containing only MHA, and 4) wells containing different cefotaxime dilutions (in MHA). The experiment was performed in triplicate. The fractional inhibitory concentration (FIC) index was calculated using the following equation:

$$\text{FIC index} = \text{FIC}_{\text{cefotaxime}} + \text{FIC}_{H_2O_2}$$

$$\text{FIC}_{\text{cefotaxime}} = \frac{\text{MIC of cefotaxime in combination}}{\text{MIC of cefotaxime alone}}$$

$$\text{FIC}_{H_2O_2} = \frac{\text{MIC of } H_2O_2 \text{ in combination}}{\text{MIC of } H_2O_2 \text{ alone}}$$

$$\text{FIC index} \leq 0.5\text{: Synergistic (strong combined effect)}$$

$$\text{FIC index} > 0.5 \leq 1\text{: Additive (combined effect equals sum)}$$

$$\text{FIC index} > 1 \leq 4\text{: Indifferent (no interaction)}$$

$$\text{FIC index} > 4\text{: Antagonistic (combined effect less than individual)}$$

Effect of combination of sub-MICs of H_2O_2 and cefotaxime on biofilm formation

A similar procedure was followed to evaluate the effect of H_2O_2 on MICs of cefotaxime against the CRKP isolate exhibiting the highest level of biofilm formation, with minor modifications. Tryptic soy broth was used instead of MHA, and a 96-well flat-bottom polystyrene microtiter plate was used instead of a U-shaped plate. Following incubation, the plates were air-dried and stained with 100 µL of 0.4% Hucker crystal violet for 15 min, then washed 5 times with distilled water. After drying, 100 µL of anhydrous ethanol was added to each well to solubilize the bound dye. The absorbance was measured at 570 nm using a microplate reader (BioTek 800 TS). The experiment was performed in triplicate.[19–21]

Statistical analyses

Statistical analyses were performed and graphs were generated using Origin software v. 8.6 (OriginLab, Northampton, USA). Data are presented as means ± standard error (SE). Differences between groups were assessed using Student's t-test and one-way analysis of variance (ANOVA). Correlations were evaluated using Pearson's correlation coefficient. A $p < 0.05$ was considered statistically significant.

Results

Bacterial isolates

Twenty isolates of *K. pneumoniae* were obtained from 140 infected wound swabs collected from inpatients with severe wound infections. The bacterial species were identified using microscopic and biochemical tests, and further confirmed with the VITEK 2 system (bioMérieux). The incidence rate of wound infections caused by *K. pneumoniae* was 14.28%.

Antibiotic susceptibility and biofilm formation

The Kirby–Bauer disk diffusion method was used to determine the susceptibility of *K. pneumoniae* isolates to cefotaxime, thereby identifying CRKP, cefotaxime-susceptible (CSKP) and intermediate isolates. As shown in Table 1, 13 isolates were resistant to cefotaxime, 6 were susceptible and 1 exhibited intermediate susceptibility. Among the tested isolates, Kp10 produced the highest level of biofilm formation, followed by Kp1, whereas Kp18 showed the lowest biofilm formation on polystyrene microtiter plates.

The Kp10 isolate (CRKP), which produced the most robust biofilm and exhibited the smallest zone of inhibition in the cefotaxime disk diffusion assay, was selected for further experiments. In this study, the MIC of cefotaxime against Kp10 was 1,000 µg/mL, while the MIC of hydrogen peroxide (H_2O_2) was 0.046% (equivalent to 0.468 mg/mL), corresponding to a $^1/_{640}$ dilution of the 30% H_2O_2 stock solution.

Figure 1 illustrates the relationship between biofilm formation and the inhibition zone diameter of cefotaxime against 20 clinical isolates of *K. pneumoniae*. A statistically

Table 1. The diameter of the inhibitory zone of 20 isolates of *Klebsiella pneumoniae* and their corresponding levels of biofilm formation. The Clinical and Laboratory Standards Institute (CLSI) guidelines were followed to determine the cefotaxime breakpoints

Isolate No.	*Klebsiella pneumoniae*	Cefotaxime diameter of inhibitory zone	Interpretation	Biofilm formation OD^{570nm}
1	Kp1	17.5 ±1.2	R	0.24 ±0.013
2	Kp2	30 ±1.4	S	0.204 ±0.08
3	Kp3	27.1 ±1.05	S	0.124 ±0.04
4	Kp4	22.3 ±1.1	R	0.17 ±0.09
5	Kp5	22.2 ±1.5	R	0.13 ±0.008
6	Kp6	18.9 ±1.4	R	0.16 ±0.02
7	Kp7	10 ±1.14	R	0.19 ±0.06
8	Kp8	23.1 ±1.1	I	0.112 ±0.049
9	Kp9	28.1 ±2.9	S	0.08 ±0.0014
10	Kp10	9 ±0.9	R	0.323 ±0.0169
11	Kp11	19.1 ±1.5	R	0.14 ±0.007
12	Kp12	29 ±0.9	S	0.191 ±0.005
13	Kp13	8.3 ±0.7	R	0.218 ±0.03
14	Kp14	28.4 ±2.9	S	0.101 ±0.0096
15	Kp15	16.7 ±3.9	R	0.179 ±0.09
16	Kp16	20.15 ±2.7	R	0.145 ±0.0056
17	Kp17	17.2 ±1.3	R	0.183 ±0.01
18	Kp18	33.6 ±3.1	S	0.06 ±0.001
19	Kp19	17 ±1.24	R	0.179 ±0.006
20	Kp20	19.2 ±2.7	R	0.143 ±0.006

S (sensitive): ≥26 mm; I (intermediate): 23–25 mm and R (resistant): ≤22 mm. Optical density (OD) ≤ 0.1: weak biofilm producer, 0.1 < OD ≤ 0.2: moderate biofilm producer, and OD > 0.2: strong biofilm producer.

significant negative correlation was observed between biofilm formation and the susceptibility of *K. pneumoniae* to cefotaxime, as indicated by the inhibition zone diameter ($r = -0.501$, $p < 0.05$).

Effect of sub-MICs of cefotaxime or H_2O_2 on biofilm formation

The effect of sub-MICs of H_2O_2 and cefotaxime on biofilm formation by the *K. pneumoniae* Kp10 isolate was evaluated. The results showed that both cefotaxime and H_2O_2 significantly reduced biofilm formation at higher sub-MIC levels (½ to 1/16 MIC) ($p < 0.05$). The reduction was minimal at lower sub-MICs (1/32 and 1/64 MIC) compared with the control (biofilm formation of Kp10 without treatment). At ½, ⅛, 1/16, 1/32, and 1/64 MIC, cefotaxime appeared to be more effective than H_2O_2 in reducing biofilm formation; however, no statistically significant differences were observed between the effects of H_2O_2 and cefotaxime at corresponding sub-MIC levels ($p > 0.05$).

Furthermore, at 1/32 and 1/64 MIC, neither treatment showed a significant effect on biofilm formation compared with the control levels (Fig. 2). The results demonstrated that both cefotaxime and H_2O_2 reduced biofilm formation by *K. pneumoniae* Kp10 in a concentration-dependent manner at sub-MIC levels. The most pronounced effects were observed at ½ to ⅛ MIC, with cefotaxime exhibiting slightly greater biofilm inhibition than H_2O_2. These findings support the potential anti-biofilm activity of both agents at sub-MIC levels.

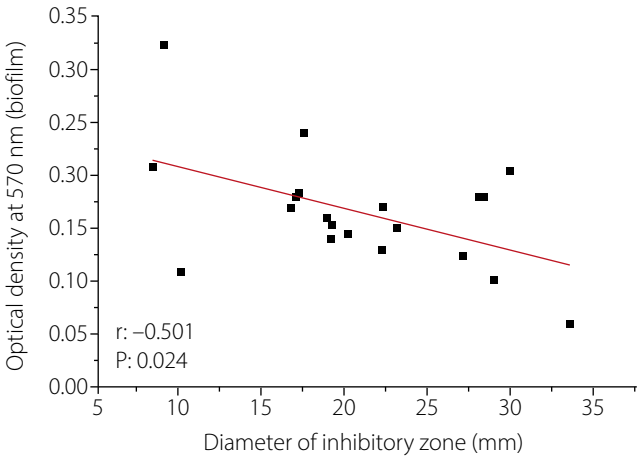

Fig. 1. Correlation between biofilm formation, measured by crystal violet absorbance at 570 nm, and the inhibition zone diameter of cefotaxime against 20 *Klebsiella pneumoniae* isolates (measured in millimeters)

r – Pearson correlation coefficient; $p < 0.05$.

Effect of sub-MIC H_2O_2 on the biofilm polymer structure

To examine the effect of sub-MICs of H_2O_2 on the polymer structure of the biofilm, smears of *K. pneumoniae* (Kp10) biofilm were prepared under ⅛ MIC H_2O_2 stress (Fig. 3). The SEM images revealed a disrupted and porous biofilm architecture, indicating that sub-MIC levels of H_2O_2 (⅛ MIC) compromise the integrity of the biofilm matrix. Arrows in the images highlight distinct pores and cavities, suggesting disruption and partial degradation of the exopolysaccharide (EPS), a key component responsible for the structural stability of the biofilm polymer matrix.

Figure 3A shows the biofilm surface exhibiting numerous perforations and EPS regions. Some bacterial cells appear embedded within or surrounded by partially degraded matrix material. The presence of pores indicates a loss of structural compactness and possible formation of water channels resulting from oxidative stress. Figure 3B, which depicts the biofilm under the same stress conditions at lower magnification, provides a broader view of the overall biofilm structure. Similar to Fig. 3A, pores and surface irregularities are evident. The matrix appears less dense and loosely organized, with fragmented regions and disrupted continuity.

The SEM images confirm that H_2O_2 at ⅛ MIC induces structural weakening of the biofilm matrix without complete eradication. The formation of pores likely increases biofilm permeability, facilitates greater penetration of antimicrobial agents and reduces the mechanical stability of the biofilm. Thus, the SEM observations demonstrate that pretreatment with ⅛ MIC H_2O_2 leads to marked porosity and disruption of the *K. pneumoniae* biofilm EPS matrix.

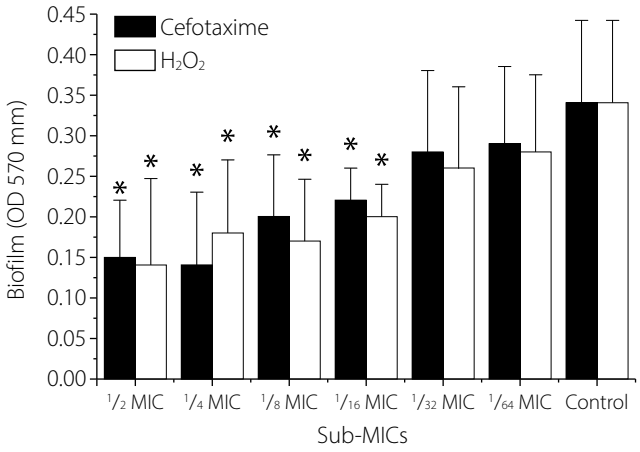

Fig. 2. Effect of sub-minimum inhibitory concentrations (sub-MICs; ½ MIC, ¼ MIC, ⅛ MIC, 1/16 MIC, and 1/32 MIC) of cefotaxime (black bars) and hydrogen peroxide (H_2O_2; white bars) on biofilm formation by *Klebsiella pneumoniae* Kp10. Results are presented as mean ± standard deviation (SD). Asterisks indicate a statistically significant difference ($p < 0.05$) compared with the control (biofilm level measured as optical density (OD) at 570 nm without exposure to H_2O_2 or cefotaxime)

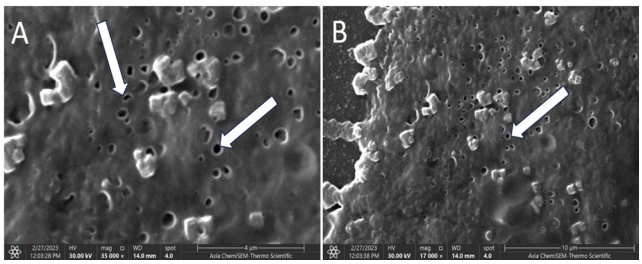

Fig. 3. Scanning electron microscopy (SEM) images of the *Klebsiella pneumoniae* Kp10 biofilm after treatment with 1/8 minimum inhibitory concentration (MIC) of hydrogen peroxide (H_2O_2). Arrows indicate pores formed within the biofilm polymer matrix

1st control – biofilm formation of Kp10 under the stress of different concentrations of cefotaxime; 2nd control – biofilm formation of Kp10 under the stress of different percentages of H_2O_2; 3rd control – biofilm formation of Kp10 without stress of both agents.

Effect of H_2O_2 on cefotaxime MICs

The effect of various sub-MICs of H_2O_2 on the susceptibility of the *K. pneumoniae* isolate Kp10 to cefotaxime is presented in Table 2. The results show that all tested sub-MICs of H_2O_2 reduced the cefotaxime MIC required to completely inhibit Kp10 growth compared with the control (cefotaxime MIC without H_2O_2). The greatest reduction was observed at ½ and ¼ MIC of H_2O_2, which decreased the cefotaxime MIC from 1,000 µg/mL to 250 µg/mL. Furthermore, sub-MICs of H_2O_2 at ⅛, 1/16, 1/32, and 1/64 lowered the cefotaxime MIC against Kp10 from 1,000 µg/mL to 500 µg/mL.

This study presents a novel observation that the anti-biofilm agent H_2O_2 enhances the susceptibility of the *K. pneumoniae* isolate Kp10 to cefotaxime. However, Kp10 remains classified as resistant to cefotaxime, as the MIC values remain above the susceptibility threshold defined by the CLSI guidelines for *K. pneumoniae*. The FIC index was calculated to determine the nature of the interaction between H_2O_2 and cefotaxime. The FIC indices for combinations of cefotaxime with ½, ¼, ⅛, 1/16, 1/32, and 1/64 MIC of H_2O_2 were 0.5, 0.5, 0.625, 0.526, 0.514, and 0.515, respectively. These results indicate a low synergistic effect at ½ and ¼ MIC levels and a strong additive effect at ⅛, 1/16, 1/32, and 1/64 MIC levels of H_2O_2 on the cefotaxime MIC. Overall, the present study demonstrates that sub-MIC levels of H_2O_2 exhibit an additive to mildly synergistic effect on the susceptibility of *K. pneumoniae* Kp10 to cefotaxime.

Effect of combination of H_2O_2 and cefotaxime on biofilm formation

Table 3 illustrates the effect of sub-MICs of H_2O_2 and cefotaxime on biofilm formation by the *K. pneumoniae* Kp10 isolate. The results show that the greatest inhibition of biofilm formation occurred when Kp10 was simultaneously exposed to higher sub-MICs of H_2O_2 (½ and ¼ MIC) and cefotaxime (½ and ¼ MIC), producing results comparable

Table 2. Checkboard assay: combined effect of cefotaxime and H_2O_2 on *Klebsiella pneumoniae* Kp10 growth

H_2O_2 (%)	Cefotaxime concentration [µg/mL]											2nd control no cefotaxime
	2000	1000	500	250	125	62.5	31.25	15.63	7.8	3.9	1.95	
0.187	–	–	–	–	–	–	–	–	–	–	–	–
0.093	–	–	–	–	–	–	–	–	–	–	–	–
0.046 (MIC)	–	–	–	–	–	–	–	–	–	–	–	–
0.023 (½)	–	–	–	FIC: 0.5	+	+	+	+	+	+	+	+
0.011 (¼)	–	–	–	FIC: 0.5	+	+	+	+	+	+	+	+
0.0058 (⅛)	–	–	FIC: 0.63	+	+	+	+	+	+	+	+	+
0.0029 (1/16)	–	–	FIC: 0.56	+	+	+	+	+	+	+	+	+
0.0014 (1/32)	–	–	FIC: 0.514	+	+	+	+	+	+	+	+	+
0.0007 (1/64)	–	–	FIC: 0.515	+	+	+	+	+	+	+	+	+
1st control (0)	–	–	+	+	+	+	+	+	+	+	+	+

1st control – biofilm formation of Kp10 under the stress of different concentrations of cefotaxime; 2nd control – biofilm formation of Kp10 under the stress of different percentages of H_2O_2; 3rd control – biofilm formation of Kp10 without stress of both agents; MIC – minimum inhibitory concentration; FIC – fractional inhibitory concentration.

to those observed in MIC wells. In contrast, minimal inhibition of biofilm formation was observed when Kp10 was exposed to the lowest sub-MIC levels of both cefotaxime and H_2O_2 (1/64 MIC).

The results were compared with control 1, control 2 and control 3. This study is the first to demonstrate that the combined effect of sub-MICs of cefotaxime and H_2O_2 significantly reduced biofilm formation in the *K. pneumoniae* Kp10 isolate compared with exposure to sub-MICs of either agent alone (controls 1 and 2; $p < 0.05$). This observation provides insight into a potential mechanism by which sub-MIC levels of H_2O_2 and cefotaxime enhance the susceptibility of Kp10 to cefotaxime.

Discussion

The principal structural component of the biofilm biomass is its polymeric matrix, which is primarily composed of EPS, proteins and extracellular DNA. This matrix provides both mechanical stability and protective shielding against antibiotics.[1] It functions as a physical and biochemical barrier, limiting antibiotic diffusion and facilitating horizontal gene transfer, thereby enhancing bacterial resistance to antimicrobial agents.[3,4,22] In *K. pneumoniae*, the capsular polysaccharide contributes significantly to antibiotic resistance and plays a crucial role in biofilm formation.[23]

Table 3. Biofilm formation in terms of optical density at 570 nm of *Klebsiella pneumoniae* Kp10 isolate incubated for 18 h at 37°C under stress of H_2O_2, cefotaxime, and a combination of H_2O_2 and cefotaxime

H_2O (%)	Concentrations of cefotaxime [µg/mL]											2nd control only H_2O_2
	2000	1000	500 (½ MIC)	250 (¼ MIC)	125 (⅛ MIC)	62.5 (1/16 MIC)	31.2 (1/32 MIC)	15.6 (1/64 MIC)	7.8 (1/128 MIC)	3.9 (1/256 MIC)	1.95 (1/512 MIC)	
0.187	0.04	0.039	0.04	0.041	0.041	0.043	0.042	0.041	0.037	0.043	0.041	0.04
0.093	0.039	0.037	0.042	0.038	0.037	0.042	0.041	0.039	0.038	0.037	0.042	0.035
0.046 (MIC)	0.041	0.038	0.043	0.037	0.041	0.044	0.042	0.043	0.039	0.038	0.041	0.037
0.023 (½ MIC)	0.042	0.041	0.041	0.05	0.089	0.088	0.09	0.11	0.13	0.12	0.15	0.14
0.011 (¼ MIC)	0.04	0.04	0.04	0.048	0.096	0.12	0.1	0.13	0.15	0.148	0.16	0.18
0.0058 (⅛ MIC)	0.039	0.042	0.044	0.078	0.1	0.11	0.14	0.13	0.16	0.16	0.165	0.17
0.0029 (1/16 MIC)	0.037	0.04	0.06	0.09	0.13	0.12	0.12	0.135	0.17	0.156	0.21	0.2
0.0014 (1/32 MIC)	0.0384	0.039	0.052	0.1	0.14	0.15	0.2	0.22	0.23	0.24	0.25	0.26
0.0007 (1/64 MIC)	0.043	0.042	0.057	0.11	0.154	0.146	0.25	0.24	0.23	0.234	0.26	0.28
1st control	0.041	0.039	0.15	0.14	0.2	0.22	0.28	0.29	0.31	0.32	0.325	0.34 3rd control

1st control – biofilm formation of Kp10 under the stress of different concentrations of cefotaxime; 2nd control – biofilm formation of Kp10 under the stress of different percentages of H_2O_2; 3rd control – biofilm formation of Kp10 without stress of both agents; MIC – minimum inhibitory concentration.

In *K. pneumoniae*, the biofilm polymer represents a significant clinical challenge, particularly in nosocomial infections and chronic conditions where antibiotic therapy often fails.[2] The emergence and spread of multidrug-resistant (MDR) and extensively drug-resistant (XDR) *K. pneumoniae* strains have markedly increased morbidity and mortality among infected patients.[2]

In the present study, we demonstrated that exposure of *K. pneumoniae* biofilms to sub-MICs of H_2O_2 resulted in a marked reduction in the production of the biofilm polymer matrix. Scanning electron microscopy revealed that exposure to sub-MIC levels of H_2O_2 induced the formation of distinct pores within the biofilm structure, potentially facilitating antibiotic penetration. This effect significantly enhanced the antibacterial activity of cefotaxime, a third-generation cephalosporin. The primary finding of this study is that sub-MICs of H_2O_2 can disrupt the synthesis or stability of the extracellular biofilm polymer matrix. Our results indicate a significant decrease in total biofilm biomass and polymeric content following H_2O_2 exposure, as evidenced by reduced crystal violet staining intensity and diminished carbohydrate content within the EPS fraction.

This finding is consistent with previous reports indicating that oxidative stress can interfere with biofilm regulatory pathways,[24] including quorum sensing and cyclic di-GMP signaling, both of which play central roles in biofilm matrix production and maintenance.[25] It is plausible that H_2O_2 alters redox-sensitive regulatory networks in *K. pneumoniae*, leading to the downregulation of matrix-associated genes such as *mrkA* (fimbriae-related), *wza* (capsular polysaccharide export) and other genes involved in EPS biosynthesis.[26]

Previous studies have shown that sub-MICs of antibiotics such as rifampicin, ceftriaxone and ofloxacin can reduce biofilm formation, which is particularly relevant to the present study.[19–21] However, other reports have indicated that sub-MIC levels of certain antibiotics may instead induce biofilm formation,[27] highlighting the need for further investigation to clarify this phenomenon. While previous research has examined the bactericidal and anti-biofilm effects of H_2O_2 against various bacterial isolates,[28,29] no prior studies have specifically investigated the impact of sub-MIC levels of H_2O_2 on the antibiotic susceptibility of pathogenic bacteria. Therefore, the present study fills an important knowledge gap in this critical area of research.

The disruption of the solidity and integrity of the biofilm polymer matrix facilitates antibiotic penetration through the bacterial membrane, ultimately increasing antibiotic efficacy. Under normal conditions, the polysaccharide meshwork of the biofilm can markedly hinder the diffusion of β-lactam antibiotics such as cefotaxime, thereby reducing their local concentration and allowing bacteria embedded in deeper biofilm layers to survive.[30]

However, when the biofilm polymer matrix is weakened by H_2O_2 pretreatment, a marked increase in antibiotic susceptibility can be observed, as evidenced by reduced viable cell counts and enhanced killing kinetics.[31] This mechanism may help restore the bactericidal activity of cefotaxime.[31] Importantly, these findings do not reflect a direct synergistic interaction between hydrogen peroxide and cefotaxime in planktonic cells, but rather a biofilm-specific phenomenon, further confirming the critical role of the biofilm polymer matrix in antibiotic tolerance. This observation aligns well with the results obtained in the present study.

The present study also supports the hypothesis that the biofilm polymer matrix plays an active role in the dynamic and metabolic response of *K. pneumoniae* to environmental stress, such as exposure to H_2O_2. Thus, sub-MICs of H_2O_2 may trigger oxidative stress responses that redirect bacterial energy and resources from polysaccharide synthesis toward essential survival processes, including macromolecular repair pathways.[32] This shift reduces the production of the biofilm polymer matrix, thereby increasing bacterial susceptibility to antibiotics.

Thus, the present study supports an innovative strategy for the treatment of wound infections caused by broad-spectrum resistant bacteria through the use of anti-biofilm agents, such as enzymes or oxidative compounds like H_2O_2 (at low concentrations). This approach offers a complementary therapeutic avenue by weakening the protective biofilm barrier and enabling existing antibiotics to act more effectively. However, it is important to note that the clinical application of H_2O_2 should be approached with caution, given its potential cytotoxic effects at higher concentrations.

While sub-MICs of H_2O_2 were effective in vitro, their in vivo application must take into account host tissue compatibility, potential cytotoxicity and the risk of selecting for bacterial strains resistant to oxidative stress, as multiple physiological mechanisms may interfere with antimicrobial efficacy.[33] In the present study, the concentrations of H_2O_2 used ranged from ½ to $^1/_{64}$ MIC, corresponding to 0.023% to 0.000719%. According to previous reports, these concentrations are considered safe for topical use, as studies have demonstrated that 0.5% H_2O_2 can be safely applied to the skin,[34] and others have shown that 0.3%, 1% and even 3% H_2O_2 solutions are safe when used topically.[35–37]

Several nanotechnology-based delivery systems, such as H_2O_2-loaded nanocarriers, have been developed to enable controlled release and reduce toxicity, thereby making H_2O_2 safer for in vivo applications.[38] Based on the present findings, it can be proposed that low concentrations of H_2O_2 be used in combination with antibiotics such as cefotaxime for the topical treatment of wound infections (e.g., skin injuries), rather than for systemic in vivo administration, due to potential toxicity-related complications. However, further research is required to validate this approach and assess its clinical efficacy and safety.

Limitations of the study

The present data focused on enhancing cefotaxime efficacy against a single clinical isolate of *K. pneumoniae*. The wider perspective may be developed in further studies, including investigations of multiple isolates, additional antibiotics and in vivo models to assess clinical applicability. Thus, the data present our perspective on sub-MIC H_2O_2 effects; however, in the future, the interactions between oxidative stress, biofilm dynamics and antibiotic efficacy may be studied and analyzed in more detail.

Conclusions

The present study demonstrated that sub-MICs of H_2O_2 effectively disrupt the biofilm polymer matrix of *K. pneumoniae* by inducing pore formation within the biofilm structure. These concentrations significantly enhanced the efficacy of cefotaxime by reducing its MIC values. The findings underscore the critical role of the biofilm matrix in antibiotic tolerance and support the concept of combining matrix-targeting agents with conventional antibiotics as a promising therapeutic strategy against biofilm-associated infections. By weakening the physical barrier of the biofilm, it may be possible to overcome one of the major challenges in the treatment of persistent bacterial infections.

Data availability

The datasets generated and/or analyzed during the current study are available from the corresponding author on reasonable request.

Consent for publication

Not applicable.

Use of AI and AI-assisted technologies

Not applicable.

ORCID iDs

Mohamed Talab Mohamed https://orcid.org/0009-0005-0549-0234
Ayaid Khadem Zgair https://orcid.org/0000-0002-2356-3338

References

1. Jakubovics NS, Goodman SD, Mashburn-Warren L, Stafford GP, Cieplik F. The dental plaque biofilm matrix. *Periodontology 2000*. 2021;86(1):32–56. doi:10.1111/prd.12361
2. Xu F, Jiang M, Li D, Yu P, Ma H, Lu H. Protective effects of antibiotic resistant bacteria on susceptibles in biofilm: Influential factors, mechanism, and modeling. *Sci Total Environ*. 2024;930:172668. doi:10.1016/j.scitotenv.2024.172668
3. Rotello VM. Nanomaterials for fighting multidrug-resistant biofilm infections. *BME Front*. 2023;4:0017. doi:10.34133/bmef.0017
4. Ramakrishnan R, Nair AV, Parmar K, Rajmani RS, Chakravortty D, Das D. Combating biofilm-associated *Klebsiella pneumoniae* infections using a bovine microbial enzyme. *NPJ Biofilms Microbiomes*. 2024;10(1):119. doi:10.1038/s41522-024-00593-7
5. Sønderholm M, Bjarnsholt T, Alhede M, et al. The consequences of being in an infectious biofilm: Microenvironmental conditions governing antibiotic tolerance. *Int J Mol Sci*. 2017;18(12):2688. doi:10.3390/ijms18122688
6. Chang D, Sharma L, Dela Cruz CS, Zhang D. Clinical epidemiology, risk factors, and control strategies of *Klebsiella pneumoniae* infection. *Front Microbiol*. 2021;12:750662. doi:10.3389/fmicb.2021.750662
7. Martin RM, Bachman MA. Colonization, infection, and the accessory genome of *Klebsiella pneumoniae*. *Front Cell Infect Microbiol*. 2018;8:4. doi:10.3389/fcimb.2018.00004
8. Wolcott R. Biofilm and catheter-related bloodstream infections. *Br J Nurs*. 2021;30(8):S4–S9. doi:10.12968/bjon.2021.30.8.S4
9. Pati D, Valipoor S, Lorusso L, et al. The impact of the built environment on patient falls in hospital rooms: An integrative review. *J Patient Saf*. 2021;17(4):273–281. doi:10.1097/PTS.0000000000000613
10. Hu S, Johnson DM, Jiang M, et al. The effect of polyvinyl chloride (PVC) color on biofilm development and biofilm-heavy metal chemodynamics in the aquatic environment. *Sci Total Environ*. 2023;905:166924. doi:10.1016/j.scitotenv.2023.166924
11. Hu R, Wan L, Liu X, et al. *K. pneumoniae* and *M. smegmatis* infect epithelial cells via different strategies. *J Thorac Dis*. 2023;15(8):4396–4412. doi:10.21037/jtd-23-493
12. Liu W, Tang JW, Lyu JW, et al. Discrimination between carbapenem-resistant and carbapenem-sensitive *Klebsiella pneumoniae* strains through computational analysis of surface-enhanced Raman spectra: A pilot study. *Microbiol Spectr*. 2022;10(1):e02409-21. doi:10.1128/spectrum.02409-21
13. Awoke T, Teka B, Seman A, et al. High prevalence of multidrug-resistant *Klebsiella pneumoniae* in a tertiary care hospital in Ethiopia. *Antibiotics (Basel)*. 2021;10(8):1007. doi:10.3390/antibiotics10081007
14. Hahn MM, González JF, Gunn JS. *Salmonella* biofilms tolerate hydrogen peroxide by a combination of extracellular polymeric substance barrier function and catalase enzymes. *Front Cell Infect Microbiol*. 2021;11:683081. doi:10.3389/fcimb.2021.683081
15. Kohanski MA, Dwyer DJ, Hayete B, Lawrence CA, Collins JJ. A common mechanism of cellular death induced by bactericidal antibiotics. *Cell*. 2007;130(5):797–810. doi:10.1016/j.cell.2007.06.049
16. Alkawareek MY, Bahlool A, Abulateefeh SR, Alkilany AM. Synergistic antibacterial activity of silver nanoparticles and hydrogen peroxide. *PLoS One*. 2019;14(8):e0220575. doi:10.1371/journal.pone.0220575
17. Yang Y, Peng Y, Jiang J, et al. Isolation and characterization of multidrug-resistant *Klebsiella pneumoniae* from raw cow milk in Jiangsu and Shandong provinces, China. *Transbound Emerg Dis*. 2021;68(3):1033–1039. doi:10.1111/tbed.13787
18. Weinstein MP, ed. *Performance Standards for Antimicrobial Susceptibility Testing*. 31st ed. Malvern, USA: Clinical and Laboratory Standards Institute; 2021. ISBN:978-1-68440-105-5
19. Al-Mutalib LAA, Zgair A. Effect of subinhibitory doses of rifaximin on in vitro *Pseudomonas aeruginosa* adherence and biofilm formation to biotic and abiotic surface models. *Polim Med*. 2023;53(2):97–103. doi:10.17219/pim/166584
20. Al-Mutalib LAA, Zgair A. Sub-inhibitory doses of ofloxacin reduce adhesion and biofilm formation of *Pseudomonas aeruginosa* to biotic and abiotic surfaces. *Pharm Sci Asia*. 2023;50(3):196–203. doi:10.29090/psa.2023.03.23.377
21. Talib MM, Ghafil JA. Effect of sub-minimum inhibitory concentrations of ceftriaxone on the *Pseudomonas aeruginosa* adhesion to human oral mucosal epithelial cells and biofilm formation to polystyrene in vitro. *Pharm Sci Asia*. 2024;51(2):180–189. doi:10.29090/psa.2024.02.24.1752
22. Gomes LC, Mergulhão FJ. SEM analysis of surface impact on biofilm antibiotic treatment. *Scanning*. 2017;2017:2960194. doi:10.1155/2017/2960194
23. Paczosa MK, Mecsas J. *Klebsiella pneumoniae*: Going on the offense with a strong defense. *Microbiol Mol Biol Rev*. 2016;80(3):629–661. doi:10.1128/MMBR.00078-15
24. Da Cruz Nizer WS, Adams ME, Allison KN, et al. Oxidative stress responses in biofilms. *Biofilm*. 2024;7:100203. doi:10.1016/j.bioflm.2024.100203
25. Waters CM, Lu W, Rabinowitz JD, Bassler BL. Quorum sensing controls biofilm formation in *Vibrio cholerae* through modulation of cyclic Di-GMP levels and repression of *vpsT*. *J Bacteriol*. 2008;190(7):2527–2536. doi:10.1128/JB.01756-07

26. Li L, Ma J, Cheng P, et al. Roles of two-component regulatory systems in *Klebsiella pneumoniae*: Regulation of virulence, antibiotic resistance, and stress responses. *Microbiol Res*. 2023;272:127374. doi:10.1016/j.micres.2023.127374
27. Elawady R, Aboulela AG, Gaballah A, Ghazal AA, Amer AN. Antimicrobial sub-MIC induces *Staphylococcus aureus* biofilm formation without affecting the bacterial count. *BMC Infect Dis*. 2024;24(1):1065. doi:10.1186/s12879-024-09790-3
28. Shirato M, Ikai H, Nakamura K, et al. Synergistic effect of thermal energy on bactericidal action of photolysis of H_2O_2 in relation to acceleration of hydroxyl radical generation. *Antimicrob Agents Chemother*. 2012;56(1):295–301. doi:10.1128/AAC.05158-11
29. Shirato M, Nakamura K, Tenkumo T, et al. Inhibition of tooth demineralization caused by *Streptococcus mutans* biofilm via antimicrobial treatment using hydrogen peroxide photolysis. *Clin Oral Invest*. 2022;27(2):739–750. doi:10.1007/s00784-022-04821-2
30. Ma H, Liu D, Song C, Fan H, Zhou W, Zhao H. Cefoxitin inhibits the formation of biofilm involved in antimicrobial resistance MDR *Escherichia coli*. *Anim Biotechnol*. 2025;36(1):2480176. doi:10.1080/10495398.2025.2480176
31. Shnyoor HA, Zgair AK. Exploring the effects of hydrogen peroxide on biofilm development and antibiotic susceptibility. *World J Exp Biosci*. 2024;12(2):26–31. doi:10.65329/wjeb.v12.02.001
32. Wang J, Li G, Yin H, An T. Bacterial response mechanism during biofilm growth on different metal material substrates: EPS characteristics, oxidative stress and molecular regulatory network analysis. *Environ Res*. 2020;185:109451. doi:10.1016/j.envres.2020.109451
33. Hayashi E, Mokudai T, Yamada Y, et al. In vitro and in vivo anti-*Staphylococcus aureus* activities of a new disinfection system utilizing photolysis of hydrogen peroxide. *J Biosci Bioeng*. 2012;114(2):193–197. doi:10.1016/j.jbiosc.2012.03.020
34. Mohanan PV, Sangeetha V, Sabareeswaran A, et al. Safety of 0.5% hydrogen peroxide mist used in the disinfection gateway for COVID-19. *Environ Sci Pollut Res*. 2021;28(47):66602–66612. doi:10.1007/s11356-021-15164-y
35. Mut M, Yemisci M, Gursoy-Ozdemir Y, Ture U. Hydrogen peroxide–induced stroke: Elucidation of the mechanism in vivo. Laboratory investigation. *J Neurosurg*. 2009;110(1):94–100. doi:10.3171/2008.3.17434
36. Roy S, Khanna S, Nallu K, Hunt TK, Sen CK. Dermal wound healing is subject to redox control. *Mol Ther*. 2006;13(1):211–220. doi:10.1016/j.ymthe.2005.07.684
37. Stone JR, Yang S. Hydrogen peroxide: A signaling messenger. *Antioxid Redox Signal*. 2006;8(3–4):243–270. doi:10.1089/ars.2006.8.243
38. Khorshidi S, Younesi S, Karkhaneh A. Peroxide mediated oxygen delivery in cancer therapy. *Colloids Surf B Biointerfaces*. 2022;219:112832. doi:10.1016/j.colsurfb.2022.112832

Physicochemical, compressional, mechanical, and dissolution properties of metronidazole tablets prepared with cocoa pod gum

Olutayo Ademola Adeleye[1,A,C–F], Aishat Olalekan[2,B–D,F], Emmanuel Adelaja Bamigbola[1,C,E,F], Adepero Olubukola Awolesi[3,B–D,F], Oluwatobi Oladayo Olakojo[4,C,D,F], Olufunke Esther Olorunsola[3,B–D,F], Bernard Opatimidi Patani[5,C,E,F], Musiliu Oluseun Adedokun[1,C,E,F]

[1] Department of Pharmaceutics and Pharmaceutical Technology, Federal University Oye-Ekiti, Nigeria
[2] Department of Pharmaceutics and Pharmaceutical Technology, Olabisi Onabanjo University, Ago-Iwoye, Nigeria
[3] Department of Pharmacognosy and Herbal Medicine, Federal University Oye-Ekiti, Nigeria
[4] Department of Pharmaceutical and Medicinal Chemistry, Federal University Oye-Ekiti, Nigeria
[5] Medical Department, Oando Energy Resources Ltd., Port Harcourt, Nigeria

A – research concept and design; B – collection and/or assembly of data; C – data analysis and interpretation;
D – writing the article; E – critical revision of the article; F – final approval of the article

Polymers in Medicine, ISSN 0370-0747 (print), ISSN 2451-2699 (online) *Polim Med*. 2025;55(2):123–134

Address for correspondence
Olutayo Ademola Adeleye
Email: olutayo.adeleye@fuoye.edu.ng

Funding sources
None declared

Conflict of interest
None declared

Acknowledgements
The authors express their gratitude to Exus Pharmaceuticals, Ejirin, Lagos, Nigeria, for their generous support in providing metronidazole powder as a gift.

Received on August 7, 2025
Reviewed on August 19, 2025
Accepted on September 26, 2025

Published online on December 19, 2025

Cite as
Adeleye OA, Olalekan A, Bamigbola EA, et al. Physicochemical, compressional, mechanical and dissolution properties of metronidazole tablets prepared with cocoa pod gum. *Polim Med*. 2025;55(2):123–134. doi:10.17219/pim/211375

DOI
10.17219/pim/211375

Abstract

Background. Natural gums offer environmentally friendly, biodegradable and non-toxic alternatives to synthetic binders in pharmaceutical formulations. Cocoa pod gum (CPG), derived from cocoa pod husk (CPH), presents a sustainable and underexplored source for pharmaceutical application.

Objectives. This study investigates the potential of CPG as a natural binder in metronidazole tablet formulations, evaluating its physicochemical and compressional properties, mechanical strength, drug release behavior, and compatibility with the active pharmaceutical ingredient.

Materials and methods. The CPG was extracted from CPH and characterized alongside xanthan gum (XNG), a standard natural binder. Physicochemical analyses included pH, flow properties, viscosity, particle size, crystallinity, and thermal behavior. Compaction behavior was assessed using Heckel and Kawakita equations. Metronidazole tablets were formulated with varying concentrations (10–20% w/w) of both gums and evaluated for hardness, friability, disintegration time, and in vitro drug release. Compatibility was examined using Fourier transform infrared spectroscopy (FTIR).

Results. Cocoa pod gum demonstrated better flow properties and swelling capacity, while XNG showed higher viscosity and plastic deformation, yield pressure (Py) and PK values. Tablets formulated with XNG had greater hardness and slower disintegration, resulting in more delayed drug release. Cocoa pod gum-based tablets disintegrated faster and showed rapid drug release, making them more suitable for immediate release formulations. Fourier transform infrared spectroscopy confirmed no drug-excipient incompatibilities.

Conclusions. Cocoa pod gum exhibits promising binder properties comparable to XNG and may serve as a cost-effective, sustainable and biocompatible alternative to conventional excipients in tablet formulations.

Key words: drug release, cocoa pod gum, natural binder, tablet formulation, compaction behavior

Highlights

- Cocoa pod gum (CPG) offers a biodegradable and sustainable alternative to synthetic binders in pharmaceutical tablets.
- CPG-based metronidazole tablets show faster disintegration and drug release, ideal for immediate release formulations.
- Compared to xanthan gum, CPG demonstrates superior flow properties and swelling capacity with no drug incompatibility.
- CPG is a cost-effective, eco-friendly binder with physicochemical properties suitable for tablet formulation.

Background

Natural gums and mucilages are biopolymers that provide eco-friendly, biocompatible, biodegradable, and cost-effective alternatives to synthetic excipients in pharmaceutical formulations.[1–3] These plant-derived polymers serve multiple functional roles – including binders, disintegrants, stabilizers, and release modifiers – across various dosage forms.[1,4]

Unlike synthetic polymers, which may have challenges regarding toxicity, biocompatibility, biodegradability, and environmental concerns, natural gums are non-toxic and non-irritant, making them ideal for sustainable drug delivery systems.[2,4] The polysaccharide structures of natural gums allow for chemical modifications to enhance their performance in modified drug delivery systems applications.[5–7]

Agricultural by-products are increasingly explored as sustainable sources of functional polymers.[8–10] The large quantities of agro-industrial waste generated worldwide contribute substantially to environmental pollution and greenhouse gas emissions.[11] Valorizing such waste through its conversion into useful bioproducts not only mitigates environmental impacts but also enhances its economic value.

Cocoa pod husk (CPH), a major by-product of Theobroma cacao, is rich in polysaccharides and represents a promising raw material for gum extraction.[12,13] Cocoa pod gum (CPG), derived from CPH, has demonstrated potential as a binder in tablet formulations, offering an innovative and sustainable approach to excipient development.[14] Metronidazole is a widely used nitroimidazole antimicrobial that is effective against anaerobic bacteria and protozoa. It is commonly formulated in tablet dosage forms, where the binder plays a crucial role in ensuring adequate mechanical strength, disintegration, and dissolution efficiency.

Objectives

Traditional binders such as starch and synthetic polymers have long been used in tablet formulations; however, they may pose challenges related to cost, potential toxicity and limited sustainability.[4] Consequently, the search for novel, plant-based binders has become increasingly important. Cocoa pod gum represents a promising alternative, offering a sustainable, eco-friendly and cost-effective option compared with conventional synthetic polymers. The present study explores the applicability of CPG as a binding agent in metronidazole tablet formulations. The study aims to evaluate the compressional behavior, mechanical properties, drug release profile, and compatibility of CPG with metronidazole, using xanthan gum (XNG) as a standard binder for comparison.

Materials and methods

The materials used in this study included metronidazole (a gift from Exus Pharmaceuticals, Ejirin, Nigeria), xanthan gum (Jungbunzlauer, Germany), lactose monohydrate (Ind-Swift Labs Ltd., Parwanoo, India), corn starch (S.D. Fine Chemicals, Mumbai, India), magnesium stearate (Loba Chemie Ltd., Mumbai, India), and CPH (locally sourced). All other solvents and reagents used were of analytical grade.

Collection and extraction of cocoa pod gum from *Theobroma cacao*

Dried CPHs were locally sourced in Ago-Iwoye, Nigeria. The husks were sun-dried for approx. 2 weeks, ground into a fine powder, sieved and further dried in a hot-air oven. Briefly, 500 g of CPH powder were subjected to aqueous extraction by boiling in 3 L of distilled water at 80°C for 2 h with continuous stirring. The resulting mixture was filtered through white muslin cloth, and the filtrate was treated with acetone in a 3 : 1 (v/v) ratio to precipitate the gum. The precipitate was collected by filtration and dried in a desiccator. The dried product, referred to as CPG, was then ground and passed through a fine sieve.

Phytochemical screening

Cocoa pod husk and the CPG were subjected to phytochemical screening using well-established procedures

to detect the major classes of secondary metabolites.[14] The frothing test was used for the detection of saponins, while Molisch's test confirmed the presence of carbohydrates. Alkaloids were identified using Mayer's, Dragendorff's and Wagner's reagents. Proteins were detected by the Biuret and Ninhydrin tests. Additional phytochemical constituents screened included lignin, tannins, flavonoids, and triterpenoids.

Physicochemical properties

pH determination

A dispersion of each gum was prepared by dissolving 1 g of CPG or XNG in 50 mL of distilled water and allowed to stand. The supernatant pH was then measured with a Jenway pH meter model 3510 (Jenway, Great Dunmow, UK). Each measurement was performed 3 times, and the mean value was calculated.

Density and flow properties determination

The bulk density, tapped density and true density of both gums were determined using standard procedures as described by Adeleye et al.[14] Flow properties – including the angle of repose, Hausner's ratio and Carr's index – were also evaluated following the methods outlined in the same reference.[14]

Mean particle size distribution determination

The mean particle size distribution of each gum was determined by sieving 20 g of sample through a series of sieves arranged in descending mesh sizes (1.0 mm to 90 µm). The sieve stack was mounted on a mechanical shaker (Endecotts, London, UK) and operated for 15 min at room temperature to facilitate particle separation according to size. The material retained on each sieve was weighed, the percentage retained was calculated, and these values were used to compute the mean particle size for each gum.[15]

Moisture content

The loss on drying method was employed to determine the moisture content. A 5 g portion of gum was weighed and placed into a pre-tarred glass petri dish and dried in an oven at 105°C to constant weight. The percentage of moisture loss was calculated by subtracting the weight after drying from the initial weight, divided by the weight after drying and multiplying by 100.

Swelling capacity

Three grams each of gum were transferred into separate 50 mL measuring cylinders, followed by the addition of 20 mL of distilled water. The cylinder was agitated at 10-min intervals for 1 h at room temperature, then it was left undisturbed at room temperature for 5 h. Swelling capacity (%) was calculated as the difference between the hydrated and initial tapped volumes of the gum, divided by the initial tapped volume and multiplied by 100.

Viscosity of gum

The viscosity of each gum was determined using 2% w/v aqueous dispersions, which were allowed to hydrate for 2 h before measurement. Viscosity was measured at room temperature using a Brookfield DV-II+ Pro viscometer (AMETEK Brookfield, Middleboro, USA) fitted with spindle No. 2, operating at a shear rate of 50 rpm.

Physicochemical characterizations of the gums

The physicochemical characteristics of the gums were evaluated using scanning electron microscopy (SEM), Fourier-transform infrared (FTIR) spectroscopy, X-ray diffraction (XRD), and differential scanning calorimetry (DSC), following the procedures described by Adeleye et al.[14] Scanning electron microscopy was employed to examine the shape and surface morphology of the gums. A focused electron beam was directed onto the sample surface to obtain high-resolution images at various magnifications. Fourier-transform infrared spectroscopy was performed using an FTIR spectrophotometer, with the samples prepared as potassium bromide (KBr) pellets. The crystallinity of the gum samples was determined using XRD to evaluate their amorphous or crystalline nature. The thermal behavior of the gums was analyzed using DSC, which measures differences in heat flow associated with physical and chemical transitions within the samples.

Preparation of gum compacts

Tablet compression was carried out using a Carver hydraulic manual hand press (Model C; Carver Inc., Menomonee Falls, USA). Briefly, 500 mg portions of CPG and XNG powders were individually compressed into tablets using a 10 mm diameter die fitted with flat-faced punches. A 1% w/v solution of magnesium stearate in ethanol was applied to the die surfaces as a lubricant prior to compression.

Tablets were compressed at 6 different pressure values – 28.82, 56.64, 84.96, 113.28, 141.60, and 169.92 MPa – with a dwell time of 30 s. After ejection, the tablets were stored

over silica gel for 24 h to allow for elastic recovery. Tablet weight, thickness and diameter were then measured using standard procedures.

Compaction properties

Heckel plot

The Heckel equation, proposed by Heckel,[16] is commonly used to study the compaction behavior of powders. It relates the relative density of a powder bed (D) to the applied compression pressure (P).

The Heckel equation is expressed as:

$$\ln \frac{1}{1-D} = KP + A$$

where: D – relative density of the compact at pressure P, K – slope of the linear portion of the plot and A – intercept of the extrapolated linear region. The reciprocal slope K = mean yield pressure (P_y) of the material. The intercept A is related to the original compact volume and reflects 2 stages of consolidation – densification due to the initial relative density of the powder and densification by particle rearrangement before deformation.

The relative density of powder bed at the onset of plastic deformation (D_A) is calculated using

$$D_A = 1 - e^{-A}$$

The relative density (D_0) – the density at zero pressure – describes the initial rearrangement phase of densification immediately after die filling, before compression. While the relative density of powder at low pressure (D_B) describes the extent of particle rearrangement at low pressures during initial stages of compression before plastic deformation is defined as

$$D_B = D_A - D_0$$

Kawakita equation

The Kawakita equation describes the relationship between the volume reduction of a powder bed and the applied pressure during compression.[17] It is expressed as follows:

$$C = \frac{V_0 - V_P}{V_0} = \frac{abP}{1+bp}$$

The equation can be simplified to yield:

$$\frac{P}{C} = \frac{P}{a} + \frac{1}{ab}$$

where: C – degree of volume reduction, V_0 – initial volume of the powder bed, V_P – volume under applied pressure P, and a and b are constants characteristic of the powder material. A plot of P/C vs P is used to obtain the constants a and b. Constant "a" is the minimum porosity before pressure is applied, while the reciprocal of the constant "b" is designated as PK, which represents the pressure required to reduce the powder bed volume by 50%.

Determination of mechanical properties of compact

Tablet hardness test

Tablet hardness was determined using a Monsanto hardness tester (Campbell Electronics, Mumbai, India). Each tablet was placed between the spindle and the anvil of the tester, and the knob was gently turned until the tablet was held firmly in position. The pointer was then set to 0, and pressure was gradually applied until the tablet fractured diametrically. The pressure at the point of fracture was recorded as the hardness value. This procedure was repeated 3 times for each tablet batch.

Tablet friability test

Tablet friability was determined using a Veego tablet friability apparatus (Veego Scientific Devices, Mumbai, India). Ten tablets were collectively weighed (W_1) and placed in the friabilator, which was operated at 25 rpm for 4 min. The tablets were then removed, dedusted and reweighed (W_2). The percentage friability was calculated using the following equation:

$$\left(\frac{W_1 - W_2}{W_1}\right) \times 100$$

This determination was carried out in triplicate, and the mean value was recorded..

Formulation of metronidazole tablet

Briefly, 200 mg of metronidazole powder was blended with 5 different concentrations (10.0% w/w, 12.5% w/w, 15.0% w/w, 17.5% w/w, and 20.0% w/w) of CPG and XNG, respectively, to yield a total of 10 formulations, as presented in Table 1. Each formulation also contained 50 mg of corn starch as a disintegrant, and the total tablet weight was adjusted to 100% using lactose monohydrate as a filler. The powder blend was mixed in a planetary mixer for 5 min. Then, 400 mg of the blend from each formulation batch was directly compressed using a Carver hydraulic manual hand press (Model 38510E; Carver Inc.) fitted with flat-faced 10 mm diameter punches. A 1% w/v solution of magnesium stearate in ethanol was applied to the die surfaces as a lubricant prior to compression. Tablets were compressed at a pressure of 113.28 MPa with a dwell time of 30 s.

Table 1. Tablet formulation composition

Ingredients	MCP1	MCP2	MCP3	MCP4	MCP5	MXN1	MXN2	MXN3	MXN4	MXN5
Metronidazole (% w/w)	50.0	50. 0	50.0	50.0	50.0	50.0	50.0	50.0	50.0	50.0
Cocoa pod gum (% w/w)	10.0	12.5	15.0	17.5	20.0	–	–	–	–	–
Xanthan gum (% w/w)	–	–	–	–	–	10.0	12.5	15.0	17.5	20.0
Corn starch (% w/w)	12.5	12.5	12.5	12.5	12.5	12.5	12.5	12.5	12.5	12.5
Lactose (% w/w)	27.5	25.0	22.5	20.0	17.5	27.5	25.0	22.5	20.0	17.5

MCP1, MCP2, MCP3, MCP4 and MCP5 – metronidazole tablets containing 10.0% w/w, 12.5% w/w, 15.0% w/w, 17.5% w/w, and 20.0% w/w cocoa pod gum, respectively; MXN1, MXN2, MXN3, MXN4 and MXN5 – metronidazole tablets containing 10.0% w/w, 12.5% w/w, 15.0% w/w, 17.5% w/w, and 20.0% w/w xanthan gum, respectively.

Metronidazole tablet evaluation

Tablet hardness and friability were determined following the procedure used for evaluating the mechanical properties of compacts.

Assessment of disintegration time of metronidazole tablet

The disintegration test was performed using a DBK tablet disintegration apparatus (DBK Instruments, Mumbai, India), with distilled water maintained at 37 ±0.5°C as the disintegration medium. The time required for each tablet to completely disintegrate and pass through the mesh was recorded. All measurements were carried out in triplicate, and the mean disintegration time was calculated.

Calibration curve of metronidazole

A calibration curve for metronidazole was constructed by preparing standard solutions in 0.1 N hydrochloric acid (HCl) at concentrations ranging from 1 to 6 µg/mL. The absorbance of each solution was measured at 278 nm using a Jenway UV-7305 UV–Visible spectrophotometer (Jenway), and the resulting data were used to generate a linear equation.

Dissolution profile of metronidazole tablet

Drug release was evaluated using a USP rotating basket dissolution apparatus (Biobase Model BK-RC1; Biobase Biodustry Co., Ltd., Jinan, China) operated at 50 rpm in 900 mL of 0.1 N hydrochloric acid (HCl) as the dissolution medium, maintained at 37 ±0.5°C. At predetermined time intervals, 5 mL samples were withdrawn and immediately replaced with an equal volume of fresh dissolution medium. The withdrawn samples were analyzed spectrophotometrically at 278 nm using a Jenway UV-7305 UV–Visible spectrophotometer (Jenway). All tests were performed in triplicate, and the mean values ± standard deviation (SD) were recorded. The percentage of drug released at each time point was calculated from the calibration curve (Fig. 1).

Statistical analyses

All statistical analyses were performed using Microsoft Excel 2013 (Microsoft Corp., Redmond, USA) and GraphPad Prism v. 5.01 (GraphPad Software, San Diego, USA). Results are expressed as mean ± SD from at least 3 replicates for each analysis. Student's t-test and one-way analysis of variance (ANOVA) were employed to evaluate significant differences among the tablet formulations. A $p < 0.05$ was considered statistically significant in all cases.

Results

Physicochemical properties the gums

The physicochemical properties of CPG and XNG, including color, odor, particle size, true and bulk densities, and flow indices (Hausner's ratio, Carr's index, and angle of repose),

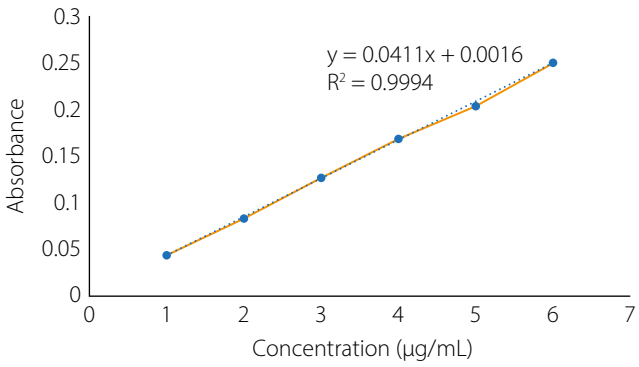

Fig. 1. Calibration curve of metronidazole at 278 nm

are summarized in Table 2. Additional parameters evaluated included swelling capacity, moisture content, viscosity, pH, and crystallinity index to assess their suitability for tablet formulation.

Cocoa pod gum appeared as a dark brown powder with a characteristic coffee-like odor, whereas XNG was white and odorless. The mean particle diameter of CPG (118.61 µm) was larger than that of XNG (83.08 µm). Regarding densities, the true density of XNG (1.352 g/cm^3) was higher than that of CPG (1.198 g/cm^3). The bulk and tapped densities of both gums were relatively similar; however, XNG exhibited a slightly higher tapped density (0.769 g/cm^3) compared with CPG (0.690 g/cm^3).

Regarding flow properties, XNG exhibited a higher Hausner's ratio (1.44) and compressibility index (30.66%) compared with CPG, which showed a Hausner's ratio of 1.30 and a compressibility index of 23.20%. The angle of repose was significantly higher for XNG (23.96°) than for CPG (20.53°) ($p < 0.001$), indicating poorer flowability of XNG. In contrast, CPG exhibited a significantly higher moisture content (18.20%) compared with XNG (11.20%) ($p < 0.001$).

A similar trend was observed for swelling capacity, where CPG demonstrated a significantly greater swelling capacity (60.45%) compared with XNG (51.53%) ($p < 0.001$). The pH values of both gums were near neutral, with CPG exhibiting a pH of 7.2 and XNG a pH of 6.8, indicating good compatibility for oral formulations. Interestingly, CPG showed a markedly higher crystallinity index (84.14%) than XNG (44.74%).

Table 2. Physicochemical properties of the gums

Parameters	CPG	XNG
Color	dark brown	white
Odor	coffee	odorless
Mean particle diameter [µm]	118.61	83.08
True density [g/cm^3]	1.198 ±0.21	1.352 ±0.09
Bulk density [g/cm^3]	0.534 ±0.11	0.533 ±0.21
Tapped density [g/cm^3]	0.690 ±0.15	0.769 ±0.18
Hausner's ratio	1.30	1.44
Carr's index [%]	23.20	30.66
Angle of repose [°]	20.53 ±0.63	23.96 ±0.52
Moisture content [%]	18.20 ±0.41	11.20 ±0.48
Swelling capacity [%]	60.45 ±0.05	51.53 ±0.01
Viscosity [cP]	870	3,620
pH	7.2 ±0.37	6.8 ±0.18
Crystallinity index [%]	84.14	44.74

CPG – cocoa pod gum; XNG – xanthan gum.

Phytochemical properties of the gums

The phytochemical constituents of CPH and CPG were evaluated, and the results are presented in Table 3. The CPH extract contained a wide range of phytochemicals, including saponins, tannins, alkaloids, carbohydrates, flavonoids, proteins, lignin, and triterpenoids, whereas these constituents were absent in the purified gum (CPG).

Table 3. Phytochemical screening of CPH and CPG

Constituent	CPH	CPG
Saponin	+	–
Tannins	+	–
Alkaloids	+	–
Carbohydrate	+	–
Flavonoids	+	–
Protein	+	–
Lignin	+	–
Triterpenoids	+	–

+ present; – absent; CPG – cocoa pod gum; CPH – cocoa pod husk.

Compressional properties of the gums

The compressional behavior of CPG and XNG was evaluated using the Heckel and Kawakita equations, and the results are presented in Table 4. The Heckel model describes the relationship between applied compression pressure and powder bed porosity, providing parameters such as the mean yield pressure (P_Y) and initial relative density (D_0). Xanthan gum exhibited a lower P_Y value (74.41 MPa) compared with CPG (138.52 MPa), indicating that XNG deforms more readily under pressure. In contrast, CPG showed a higher D_0 (0.445) than XNG (0.394).

The Kawakita model, which assesses volume reduction under pressure, provided values for total compressibility (a) and PK (pressure to reduce volume by 50%). Xanthan gum demonstrated a higher Di (0.420) than CPG (0.388), with a lower PK value (6.57) compared to CPG (7.88).

Table 4. Heckel's and Kawakita's plots parameters

Sample	Heckel				Kawakita	
	D_A	D_B	D_0	P_y	Di(1-a)	PK
CPG	0.752	0.307	0.445	138.52	0.388	7.88
XNG	0.763	0.369	0.394	74.41	0.420	6.57

CPG – cocoa pod gum; XNG – xanthan gum, DA – relative density of powder bed at the onset of plastic deformation, DB – relative density of powder at low pressure, D0 – relative density of powder at zero pressure, Py – mean yield pressure, Di – initial relative density, PK – pressure required to reduce powder bed by 50%

Mechanical properties of compacts

The results of hardness and percentage friability of tablets compressed at varying pressures (28.82–169.92 MPa) are presented in Table 5. Both gums exhibited increased hardness and reduced friability with increasing compression pressure. However, XNG produced tablets with significantly higher hardness and lower friability than those formulated with CPG at all pressure levels ($p < 0.001$).

SEM analysis of the gums

The scanning electron micrographs of CPG and XNG are shown in Fig. 2. The surface morphology of CPG displayed irregular, coarse and aggregated particles with rough surfaces and non-uniform edges, whereas XNG exhibited a finer and more fibrous morphology characterized by fragmented and elongated particles.

FTIR spectroscopy of the gums

The FTIR spectra of CPG and XNG are shown in Fig. 3. Both gums exhibited characteristic absorption bands typical of polysaccharides, including a broad O–H stretching vibration in the region of 3,750–3,925 cm^{-1} and a distinct C–H or secondary O–H stretching band around 2,645–2,650 cm^{-1}. No new peaks or significant peak shifts were observed in either spectrum. However, CPG displayed consistently higher peak intensities across all major absorption regions.

XRD analysis of the gums

The structural characteristics of CPG and XNG were further examined using XRD, and the resulting diffractograms are presented in Fig. 4. The XRD patterns of both gums revealed distinct diffraction profiles, reflecting differences in their molecular organization and degree

Table 5. Percent friability and hardness of compact

Sample code	Applied pressure [MPa]	Friability [%]	Crushing strength [N]
CPG	28.82	0.51 ±0.03	95.50 ±0.20
	56.64	0.36 ±0.01	108.83 ±0.16
	84.96	0.28 ±0.04	125.80 ±0.38
	113.28	0.15 ±0.06	182.85 ±0.28
	141.60	0.09 ±0.04	196.17 ±0.12
	169.92	0.00 ±0.03	211.90 ±0.31
XNG	28.82	0.18 ±0.12	109.83 ±0.17
	56.64	0.14 ±0.02	171.30 ±0.53
	84.96	0.08 ±0.05	213.00 ±0.25
	113.28	0.02 ±0.01	299.50 ±0.32
	141.60	0.00 ±0.15	374.00 ±0.44
	169.92	0.00 ±0.10	345.30 ±0.20

CPG – cocoa pod gum; XNG – xanthan gum.

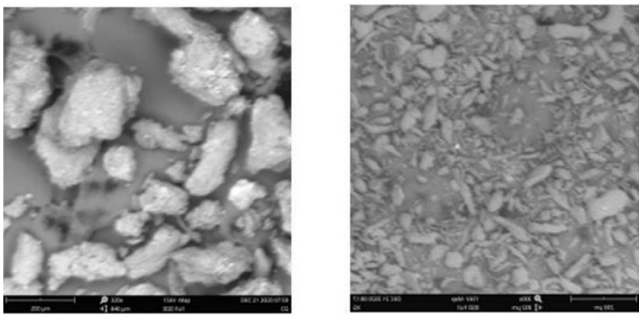

cocoa pod gum xanthan gum

Fig. 2. Scanning electron micrographs of cocoa pod gum and xanthan gum

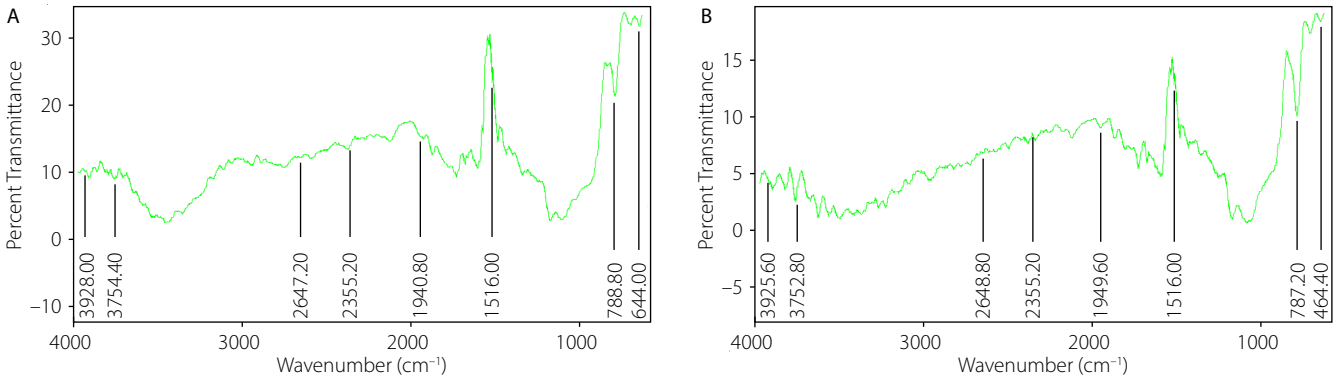

Fig. 3. Fourier transform infrared spectroscopy (FTIR) of cocoa pod gum (A) and xanthan gum (B)

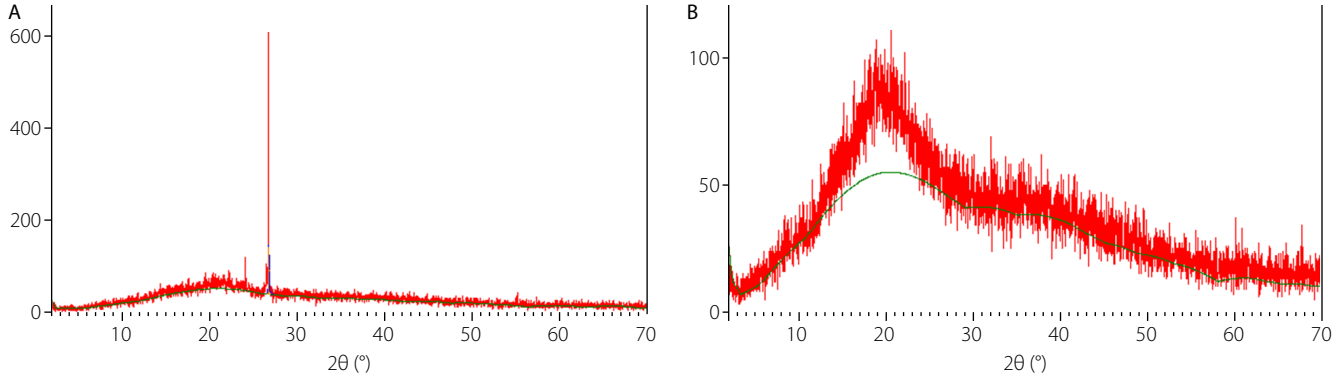

Fig. 4. Diffractograms of cocoa pod gum (A) and xanthan gum (B)

of crystallinity. Cocoa pod gum displayed a sharp and well-defined diffraction peak at 2θ ≈ 26.7°, indicating a higher level of crystallinity, whereas XNG showed a broad peak with maximum intensity in the 2θ region of 16–22°, characteristic of amorphous materials.

Thermal analysis of the gums

The thermal behavior of the isolated gums was analyzed using DSC to evaluate their thermal stability, and the resulting thermograms are presented in Fig. 5. Cocoa pod gum exhibited a broad endothermic transition with an onset temperature of 30.16°C, a peak at 115.86°C, and an endset at 145.32°C. In contrast, XNG displayed a thermal transition beginning at 73.09°C, peaking at 81.00°C and ending at 243.65°C.

Compatibility studies

To ensure the safe and effective use of CPG as a binder in metronidazole tablet formulations, drug–excipient compatibility studies were performed using FTIR spectroscopy to evaluate potential interactions between metronidazole and CPG. The FTIR spectra of pure metronidazole, CPG and their physical mixture are presented in Fig. 6.

Mechanical properties and disintegration time of metronidazole tablet formulations

The mechanical properties (hardness and friability) and disintegration times of metronidazole tablets formulated with CPG and XNG as binders are presented in Table 6. A statistically significant progressive increase in tablet hardness ($p < 0.001$) was observed with increasing binder concentration for both formulations. Tablet hardness ranged from 3.82 kgf (MCP1) to 6.05 kgf (MCP5) for the CPG-based tablets and from 5.08 kgf (MXN1) to 8.17 kgf (MXN5) for the XNG-based tablets. A corresponding decrease in friability was observed with increasing binder

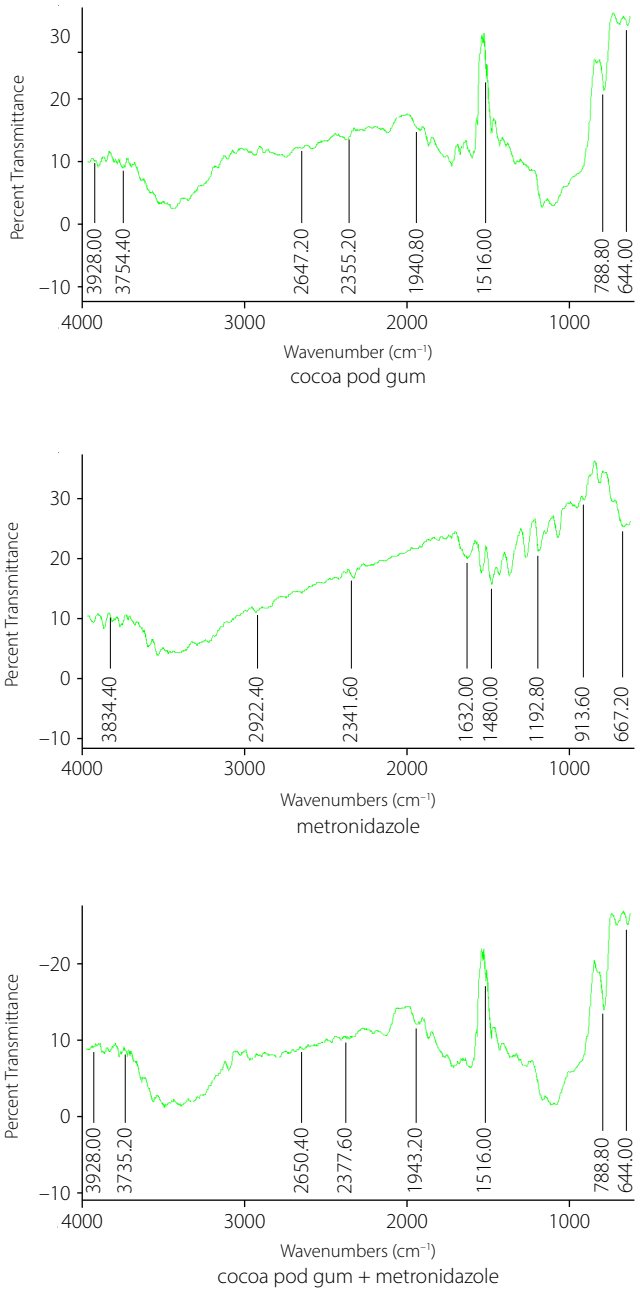

Fig. 6. Drug-excipient compatibility

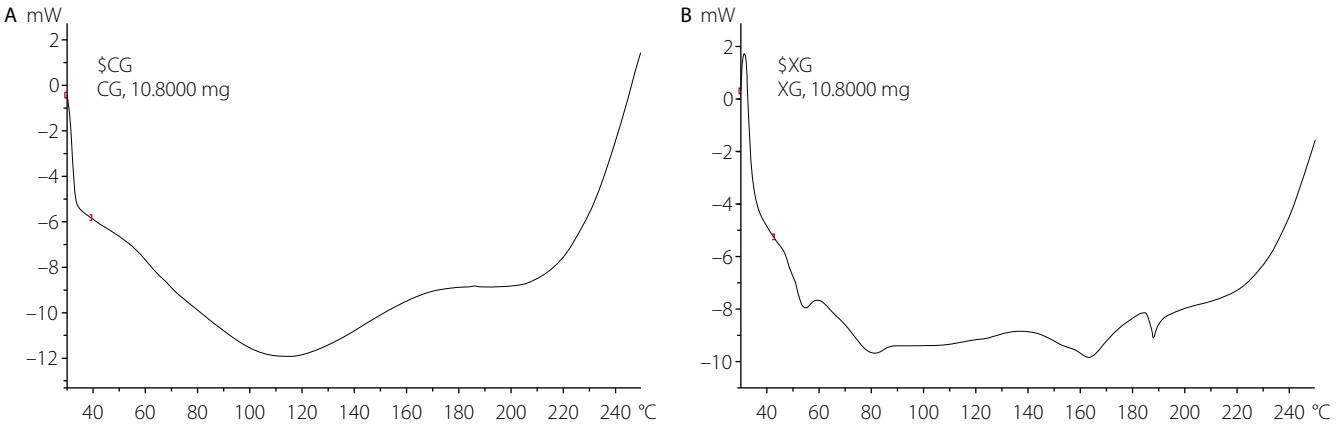

Fig. 5. Differential scanning calorimetry (DSC) thermograms of cocoa pod gum (A) and xanthan gum (B)

Table 6. Mechanical properties and disintegration time of metronidazole tablet formulations

Formulation	Hardness [kgf]	Friability [%]	Disintegration time [min]
MCP1	3.82 ±1.32	2.32 ±0.04	4.54 ±0.82
MCP2	4.65 ±0.71	1.95 ±0.12	5.33 ±0.68
MCP3	5.12 ±1.05	1.01 ±0.26	6.82 ±0.22
MCP4	5.28 ±1.52	0.86 ±0.08	7.37 ±1.04
MCP5	6.05 ±0.77	0.81 ±0.10	9.42 ±0.28
MXN1	5.08 ±0.26	1.09 ±0.02	6.81 ±0.39
MXN2	5.67 ±0.50	0.86 ±0.21	8.34 ±0.63
MXN3	6.52 ±0.41	0.69 ±0.45	11.51 ±0.92
MXN4	7.24 ±0.63	0.52 ±0.05	12.34 ±0.23
MXN5	8.17 ±1.21	0.35 ±0.01	15.86 ±0.67

MCP1, MCP2, MCP3, MCP4 and MCP5 – metronidazole tablets containing 10.0%w/w, 12.5%w/w, 15.0%w/w, 17.5%w/w and 20.0%w/w cocoa pod gum respectively; MXN1, MXN2, MXN3, MXN4 and MXN5 – metronidazole tablets containing 10.0% w/w, 12.5% w/w, 15.0% w/w, 17.5% w/w and 20.0% w/w xanthan gum respectively.

concentration, ranging from 2.32% to 0.81% for the CPG formulations (MCP1–MCP5) and from 1.09% to 0.35% for the XNG formulations (MXN1–MXN5). Tablets containing xanthan gum exhibited significantly lower friability ($p < 0.003$) compared with those containing CPG. Disintegration time increased with higher binder concentration, ranging from 4.54 min (MCP1) to 9.42 min (MCP5) for the CPG tablets, and from 6.81 min (MXN1) to 15.86 min (MXN5) for the XNG tablets. Xanthan gum-based tablets exhibited significantly longer disintegration times ($p < 0.001$) compared with CPG-based tablets at corresponding binder concentrations. However, all formulations generally complied with the United States Pharmacopeia (USP) disintegration limit of not more than 15 min, except for MXN5, which marginally exceeded this specification.

In vitro drug release profiles of metronidazole tablet formulations

The in vitro release profiles of metronidazole tablet formulations containing CPG and XNG as binders are shown in Fig. 7. Drug release was monitored over a 60-min period to evaluate the effect of binder type and concentration on the release profile. All formulations exhibited a time-dependent release pattern, with the percentage of drug released increasing progressively with time.

Cocoa pod gum formulations demonstrated faster drug release, achieving more than 85% release within 30 min across all batches and reaching up to 99.4% at 60 min. In contrast, XNG formulations exhibited a slower release profile, with cumulative drug release ranging from 79.1% to 92.8% at 60 min, and only the lower-concentration batches achieving ≥85% release within the first 30 min. Tablets formulated with lower binder concentrations exhibited faster drug release, whereas those containing higher binder levels showed

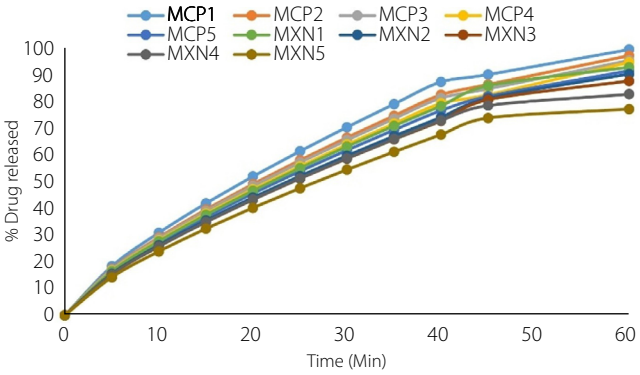

Fig. 7. Drug release profiles of metronidazole

a more sustained release profile. In general, CPG formulations complied with the USP dissolution requirement of not less than 85% drug release within 30 min. By contrast, formulations containing higher concentrations of XNG displayed a slower release profile, with partial deviation from the USP specification for immediate-release tablets.

Discussion

The physicochemical properties of CPG and XNG, as presented in Table 2, are essential for evaluating their suitability and acceptability as pharmaceutical excipients – particularly with respect to appearance, flow behavior, swelling capacity, viscosity, and structural integrity. The observed physicochemical characteristics of both gums indicate distinct differences that may influence their functional performance in pharmaceutical formulations.

Cocoa pod gum exhibited a darker color and a characteristic coffee-like odor, whereas XNG was white and odorless, reflecting differences in their botanical source and purity profiles. The mean particle size of CPG was larger than that of XNG, which may influence powder flow and compressibility. According to standard pharmacopeial classification, angle of repose values below 30° indicate good flow, values above 40° suggest irregular flow, and those exceeding 50° denote poor flow.

Similarly, a Carr's index of 5–15% indicates excellent flow, 16–18% good, 19–25% fair, 26–35% poor, and values above 40% denote cohesive powders with very poor flow. Similarly, Hausner's ratio values below 1.25 reflect good flow, whereas values above 1.25 indicate poor flow characteristics. The flowability indicators, including Carr's index and Hausner's ratio, suggested better flow for CPG compared with XNG, a trend further supported by the lower angle of repose observed for CPG.

Specifically, the angle of repose was significantly higher for XNG (23.96°) than for CPG (20.53°) ($p < 0.001$), although both values fall within the range indicative of good flow. However, XNG exhibited a higher Carr's index (30.66%) and Hausner's ratio (1.44), corresponding to poor

flow, compared with CPG, which showed a Carr's index of 23.20% (fair flow) and a Hausner's ratio of 1.30 (poor flow). These differences may influence blend uniformity and tablet die filling during formulation. Xanthan gum exhibited markedly higher viscosity than CPG, suggesting superior gelling and thickening properties. The crystallinity index of XNG was lower than that of CPG, indicating its predominantly amorphous nature. This lower degree of crystallinity contributes to the higher viscosity of XNG, as previously reported by Yahoum et al.[18] and supported by additional findings.[19] Phytochemical screening was conducted to determine the presence of bioactive compounds that may influence the functional and therapeutic properties of the materials. Cocoa pod husk contains a wide range of phytochemicals, whereas these constituents are absent in CPG, as presented in Table 3. This confirms that the purification process effectively removed the bioactive components, yielding a chemically inert polysaccharide matrix desirable for pharmaceutical use, as it enhances the biocompatibility, chemical stability and safety of the gum in drug formulations, minimizing the risk of drug–excipient interactions.

The compressional behavior of CPG and XNG as pharmaceutical excipients was evaluated using the Heckel and Kawakita equations, which provide insight into the mechanism of powder densification under applied pressure – an important factor that determines the tabletability and compaction ability of powders during direct compression. These models enable a comparative assessment of the compressibility and deformation characteristics of the gums, supporting their potential use as functional tablet binders or matrix-forming agents. The Py value obtained from the Heckel analysis was significantly lower for XNG than for CPG, indicating that XNG undergoes plastic deformation more readily under applied pressure. Similarly, the PK value obtained from the Kawakita analysis, which represents the pressure required to achieve a 50% volume reduction, was lower for XNG than for CPG. This further confirms that XNG exhibits greater plasticity and better packing ability, making it more favorable for direct compression processes. The mechanical strength of compacts prepared using both gums, as evaluated by crushing strength and friability, revealed significant differences in compaction behavior and binding efficiency across increasing compression pressures. Hardness provides a measure of the mechanical integrity of a tablet, while friability assesses its tendency to crumble under abrasion.[20] For both gums, an increase in applied pressure led to a corresponding increase in hardness and a decrease in friability, demonstrating improved compact consolidation and mechanical resistance to abrasion.

However, XNG produced compacts with higher hardness at all pressure levels compared to CPG. This suggests that XNG exhibits greater plastic deformation and interparticle bonding,[21] which aligns with its lower Py and PK values observed in the Heckel and Kawakita analyses. These findings are consistent with literature reports indicating that XNG imparts excellent mechanical strength to materials.[22] The large, aggregated structures with rough surfaces and non-uniform edges observed in CPG suggest a limited surface area, which may contribute to slower hydration rates and prolonged swelling in aqueous environments. In contrast, the finer, more fibrous morphology of XNG, characterized by fragmented and elongated particles, indicates greater surface area exposure, potentially facilitating faster water uptake and more rapid hydration dynamics.

Fourier transform infrared spectroscopy was used to identify and compare the functional groups present in CPG and XNG. The spectra provided insight into their compatibility and chemical composition. Both gums exhibited characteristic polysaccharide functional groups typically associated with natural gums.[23,24] However, CPG showed higher peak intensities across all major regions, implying a greater concentration of active functional groups that may influence its performance as a pharmaceutical excipient. Cocoa pod gum exhibits greater thermal sensitivity and is more suitable for low-temperature processing; therefore, its use requires careful handling to prevent degradation. In contrast, XNG demonstrates higher thermal stability, making it ideal for thermally intensive applications. The potential physicochemical interactions between metronidazole and CPG, evaluated with FTIR, confirmed the absence of new absorption bands or significant peak shifts, indicating that metronidazole and XNG are chemically compatible.

The mechanical properties of tablet formulations are important factors in determining their ability to withstand stresses during manufacturing, packaging, transportation, and administration without compromising tablet integrity.[25] As shown in Table 6, increasing the concentrations of both CPG and XNG led to greater tablet hardness and reduced friability, indicating enhanced mechanical strength and cohesive integrity. This trend is consistent with the expected behavior of binders, where higher polymer content promotes interparticulate bonding, adhesion and cohesion during compression, resulting in stronger tablets. It also aligns with the results of the mechanical strength of compacts reported in Table 5.[25,26] The differences observed in the mechanical properties of these gums may be attributed to the inherent physicochemical characteristics and smaller particle size of XNG, which facilitate more efficient particle packing and binding during compression. Literature indicates that smaller particle sizes enhance interparticulate contact, promoting stronger bonding and increased tensile strength in tablets.[27] Moreover, the prolonged disintegration time observed in XNG-based tablets could be a direct consequence of stronger interparticulate bonding. This is further supported by the Py and PK values obtained in this study, which align with the superior compressional behavior and binding efficiency of XNG. The in vitro drug release study of metronidazole tablets was conducted to evaluate the influence of binder type and concentration on the drug's release

profile. The results revealed that drug release was both time- and concentration-dependent, with the percentage of drug released increasing over time but decreasing with increasing binder concentration. Tablets formulated with XNG exhibited a more pronounced retardation in drug release compared with those containing CPG. This observation may be attributed to the higher viscosity and mechanical strength of XNG, as evidenced by the data presented in Tables 2 and 6.

The elevated viscosity of XNG contributes to the formation of a dense hydration layer and gel matrix upon contact with the dissolution medium, thereby extending the diffusional path length and impeding drug diffusion through the gel layer.[28] Furthermore, the enhanced mechanical strength resulting from XNG's plastic deformation characteristics produces tablets with greater compact density and lower porosity. This structural compactness limits the penetration of the dissolution medium, reduces surface area exposure, and ultimately delays the drug dissolution process.[29]

Conclusions

The study demonstrates that both CPG and XNG are effective natural binders in metronidazole tablet formulations. An increase in binder concentration resulted in improved mechanical properties and slower disintegration and drug release. Xanthan gum produced compacts with higher hardness and slower drug release, attributed to its higher viscosity, greater plastic deformation capacity, and stronger interparticulate bonding. On the other hand, CPG produced tablets with faster disintegration and higher drug release, indicating its potential suitability for immediate-release formulations. Fourier transform infrared spectroscopy results confirmed no incompatibility between the gums and metronidazole. These findings affirm the applicability of CPG as a promising, sustainable and biocompatible alternative to conventional binders.

Data availability

The datasets generated and/or analyzed during the current study are available from the corresponding author on reasonable request.

Consent for publication

Not applicable.

Use of AI and AI-assisted technologies

Not applicable.

ORCID iDs

Olutayo Ademola Adeleye https://orcid.org/0000-0001-8716-4064
Emmanuel Adelaja Bamigbola https://orcid.org/0000-0002-0686-8906
Adepero Olubukola Awolesi https://orcid.org/0000-0003-1441-3095
Oluwatobi Oladayo Olakojo https://orcid.org/0000-0002-6619-5838
Musiliu Oluseun Adedokun https://orcid.org/0000-0002-8269-7133

References

1. Adeleye OA, Femi-Oyewo MN, Odeniyi MA. The effect of processing variables on the mechanical and release properties of tramadol matrix tablets incorporating *Cissus populnea* gum as controlled release excipient. *Polim Med*. 2014;44(4):209–220. PMID:25932902.
2. Amiri MS, Mohammadzadeh V, Yazdi MET, Barani M, Rahdar A, Kyzas GZ. Plant-based gums and mucilages applications in oharmacology and nanomedicine: A review. *Molecules*. 2021;26(6):1770. doi:10.3390/molecules26061770
3. Shiam MdAH, Islam MS, Ahmad I, Haque SS. A review of plant-derived gums and mucilages: Structural chemistry, film forming properties and application. *J Plastic Film Sheeting*. 2025;41(2):195–237. doi:10.1177/87560879251316553
4. Jadav M, Pooja D, Adams DJ, Kulhari H. Advances in xanthan gum-based systems for the delivery of therapeutic agents. *Pharmaceutics*. 2023;15(2):402. doi:10.3390/pharmaceutics15020402
5. Prajapati VD, Jani GK, Moradiya NG, Randeria NP. Pharmaceutical applications of various natural gums, mucilages and their modified forms. *Carbohydr Polym*. 2013;92(2):1685–1699. doi:10.1016/j.carbpol.2012.11.021
6. Malviya R, Tyagi V, Singh D. Techniques of mucilage and gum modification and their effect on hydrophilicity and drug release. *Recent Pat Drug Deliv Formul*. 2021;14(3):214–222. doi:10.2174/1872211314666201204160641
7. Mahajan HS, Deore UV, Suryawanshi M, Sarode R. Polysaccharides based gums and mucilage: As potential biomaterial. In: Faiyazuddin Md, Suryawanshi M, eds. *Design and Processing of Green Materials*. Vol. 4. Biomaterials, Bioengineering and Sustainability. Cham, Switzerland: Springer Nature Switzerland; 2025:315–328. doi:10.1007/978-3-031-91790-5_12
8. Panda J, Mishra AK, Mohanta YK, Patowary K, Rauta PR, Mishra B. Exploring biopolymer for food and pharmaceuticals application in the circular bioeconomy: An agro-food waste-to-wealth approach. *Waste Biomass Valor*. 2024;15(10):5607–5637. doi:10.1007/s12649-024-02452-0
9. Tanwar M, Gupta RK, Rani A. Natural gums and their derivatives based hydrogels: In biomedical, environment, agriculture, and food industry. *Crit Rev Biotechnol*. 2024;44(2):275–301. doi:10.1080/07388551.2022.2157702
10. Benalaya I, Alves G, Lopes J, Silva LR. A review of natural polysaccharides: Sources, characteristics, properties, food, and pharmaceutical applications. *Int J Mol Sci*. 2024;25(2):1322. doi:10.3390/ijms25021322
11. Siddiqua A, Hahladakis JN, Al-Attiya WAKA. An overview of the environmental pollution and health effects associated with waste landfilling and open dumping. *Environ Sci Pollut Res*. 2022;29(39):58514–58536. doi:10.1007/s11356-022-21578-z
12. Younes A, Karboune S, Liu L, Andreani ES, Dahman S. Extraction and characterization of cocoa bean shell cell wall polysaccharides. *Polymers (Basel)*. 2023;15(3):745. doi:10.3390/polym15030745
13. Anoraga SB, Shamsudin R, Hamzah MH, Sharif S, Saputro AD. Cocoa by-products: A comprehensive review on potential uses, waste management, and emerging green technologies for cocoa pod husk utilization. *Heliyon*. 2024;10(16):e35537. doi:10.1016/j.heliyon.2024.e35537
14. Adeleye OA, Bamiro OA, Albalawi DA, et al. Characterizations of alpha-cellulose and microcrystalline cellulose isolated from cocoa pod husk as a potential pharmaceutical excipient. *Materials (Basel)*. 2022;15(17):5992. doi:10.3390/ma15175992
15. Latreille PL, Pazhayattil AB, Turner S, Talwar N. A novel image processing technique for weighted particle size distribution assessment. *Drug Dev Ind Pharm*. 2024;50(6):550–560. doi:10.1080/03639045.2024.2358366
16. Heckel W. Density-pressure relationship in powder compaction. *Trans Metall Soc AIME*. 1961;221:671–675.
17. Kawakita K, Lüdde KH. Some considerations on powder compression equations. *Powder Technol*. 1971;4(2):61–68. doi:10.1016/0032-5910(71)80001-3

18. Yahoum MM, Toumi S, Tahraoui H, et al. Evaluation of physicochemical and amphiphilic properties of new xanthan gum hydrophobically functionalized derivatives. *Sustainability*. 2023;15(8):6345. doi:10.3390/su15086345
19. Bhardwaj BY, Vihal S, Pahwa R, et al. Recent advancements in xanthan gum-based gastroretentive floating formulations: Chemical modification, production and applications. *Carbohydr Polym*. 2025;348:122809. doi:10.1016/j.carbpol.2024.122809
20. Çomoğlu T. Evaluation of the impact of different superdisintegrants on the in vitro characterization parameters of orally disintegrating tablets containing ketoprofen. *Ankara Ecz Fak Derg*. 2024;48(2):10. doi:10.33483/jfpau.1425266
21. Jiang T, Zhao JD, Zhang JR. Splitting tensile strength and microstructure of xanthan gum-treated loess. *Sci Rep*. 2022;12(1):9921. doi:10.1038/s41598-022-14058-4
22. Muhamad H, Mawla N, Dereiah S, Ward A, Williamson J, Asare-Addo K. Comparative analysis of drug release kinetics in polyethylene oxide and xanthan gum matrices with various excipients. *RSC Pharm*. 2025;2(2):303–317. doi:10.1039/D4PM00296B
23. Faria S, De Oliveira Petkowicz CL, De Morais SAL, et al. Characterization of xanthan gum produced from sugar cane broth. *Carbohydr Polym*. 2011;86(2):469–476. doi:10.1016/j.carbpol.2011.04.063
24. Sharma V, Kumar R, Arora N, et al. Effect of heat treatment on thermal and mechanical stability of NaOH-doped xanthan gum-based hydrogels. *J Solid State Electrochem*. 2020;24(6):1337–1347. doi:10.1007/s10008-020-04641-y
25. Okunlola A. Optimization of formulations of chloroquine phosphate tablets containing Ofada rice (Oryza glaberrina) starch as a binder: A Taguchi based grey-relational design. *J Excip Food Chem*. 2020;11(3):62–75. https://jefc.scholasticahq.com/article/17444-optimization-of-formulations-of-chloroquine-phosphate-tablets-containing-ofada-rice-oryza-glaberrina-starch-as-a-binder-a-taguchi-based-grey-relational-design.pdf.
26. Apeji YE, Olayemi OJ, Anyebe SN, et al. Impact of binder as a formulation variable on the material and tableting properties of developed co-processed excipients. *SN Appl Sci*. 2019;1(6):561. doi:10.1007/s42452-019-0585-2
27. Zhang Y, Law Y, Chakrabarti S. Physical properties and compact analysis of commonly used direct compression binders. *AAPS PharmSciTech*. 2003;4(4):489–499. doi:10.1208/pt040462
28. Hassan DS, Hasary HJ. The impact of viscosity on the dissolution of naproxen immediate-release tablets. *J Taibah Univ Med Sci*. 2023;18(4):687–695. doi:10.1016/j.jtumed.2022.12.009
29. Adeleye OA. Relationship between compression pressure, mechanical strength and release properties of tablets. *Polim Med*. 2019;49(1):27–33. doi:10.17219/pim/111888

Application of polymeric surfactants in research and development of drugs applied topically to the skin and mucous membranes

Zastosowanie surfaktantów polimerowych w badaniach i rozwoju leków stosowanych miejscowo na skórę i błony śluzowe

Remigiusz Zapolski[B–F], Witold Musiał[A–F]

Department of Physical Chemistry and Biophysics, Faculty of Pharmacy, Wroclaw Medical University, Poland

A – research concept and design; B – collection and/or assembly of data; C – data analysis and interpretation;
D – writing the article; E – critical revision of the article; F – final approval of the article

Polymers in Medicine, ISSN 0370-0747 (print), ISSN 2451-2699 (online) *Polim Med*. 2025;55(2):135–144

Address for correspondence
Witold Musiał
E-mail: witold.musial@umw.edu.pl

Funding sources
This work was supported by Wroclaw Medical University grant No. SUBK.D060.22.078.

Conflict of interest
None declared

Received on March 6, 2025
Reviewed on June 8, 2025
Accepted on June 9, 2025

Published online on December 19, 2025

Abstract

Polymeric surfactants play an important role in the research and development of drugs applied topically to the skin and mucous membranes. Their versatile properties include the ability to lower surface tension, thereby favorably contributing to the energetic balance of the emulsification process during the preparation of various dosage forms. In addition, they offer important structural advantages that enhance the stability of the resulting pharmaceutical or cosmetic products through electrostatic repulsion and steric effects. The influence of viscosity and density should also be taken into account when polymeric surfactants are considered as additives, as these are crucial components of various drug formulations. Emulsions used in ointments and creams are among the most relevant dosage forms affected by surface and interfacial tension phenomena. However, other dosage forms also require the use of surfactants, which may belong to the group of polymeric compounds.

Streszczenie

Polimerowe surfaktanty odgrywają ważną rolę w badaniach i rozwoju leków stosowanych miejscowo na skórę i błony śluzowe. Ich wszechstronne właściwości obejmują obniżanie napięcia powierzchniowego, a tym samym korzystnie wpływają na równowagę energetyczną procesu emulsyfikacji podczas przygotowywania różnych form leków. Z drugiej strony polimerowe surfaktanty posiadają ważne i cenne zalety strukturalne, które zwiększają stabilność otrzymanego produktu farmaceutycznego lub kosmetycznego poprzez odpychanie elektrostatyczne, a także efekty steryczne. Należy również wziąć pod uwagę wpływ lepkości i gęstości, gdyż polimerowe surfaktanty są uważane za dodatki, które są kluczowymi składnikami różnych form leków. Emulsje stosowane jako maści i kremy są najbardziej interesującymi formami leków, na które może wpływać zjawiska napięcia granicznego powierzchni. Jednak również inne formy leków wymagają stosowania surfaktantów, które mogą pochodzić z grupy polimerów.

Key words: surface tension, van der Waals forces, polymeric surfactants, steric effect, electrostatic repulsion

Słowa kluczowe: napięcie powierzchniowe, surfaktanty polimerowe, efekt steryczny, odpychanie elektrostatyczne, siły van der Waalsa

Cite as
Zapolski R, Musiał W. Application of polymeric surfactants in research and development of drugs applied topically to the skin and mucous membranes. *Polim Med*. 2025;55(2):135–144. doi:10.17219/pim/206092

DOI
10.17219/pim/206092

Introduction: General remarks on surfactants

The skin is a complex, predominantly lipophilic barrier to substances with prophylactic and therapeutic effects. Moreover, when targeting the deeper layers of the skin or subcutaneous tissue, the thickness and diffusion resistance of the hydrophilic layers also play an important role. Therefore, surfactants, by reducing surface tension at interfaces, can positively influence both the skin–blood barrier and the ointment base–skin interface. As chemical compounds that lower surface tension, surfactants play a crucial role in the formulation of numerous drug products, particularly those in which the modification of surface tension at the phase boundary is a key factor. A good example of such formulations are emulsions (Fig. 1), in which reducing surface tension at the phase boundary decreases the energy required to achieve the desired level of dispersion. Lowering surface tension is also important for maintaining the emulsion as a stable dispersion over time and for ensuring a favorable re-dispersion profile when low energy is applied – e.g., by simply shaking the container before use. The essence of the functional definition of surfactants lies in their ability to reduce surface tension – a property first observed and applied in research by early 20th-century scientists such as Szyszkowski and Langmuir, building upon Gibbs' foundational work.[1–3]

Objectives

In this review, the authors aim to present the fundamental mechanisms and examples of the application of polymeric surfactants as components of pharmaceutical and cosmetic preparations intended for topical use on the skin. Selected equations that may facilitate understanding of formulation processes and the stability of pharmaceutical emulsions are also included.

Mechanisms of action of surfactants

A surfactant, by positioning itself at the interface between 2 phases, hydrophilic and hydrophobic, reduces the cohesive forces between the molecules of these phases and lowers the energy required to disperse one phase within the other. The orientation of the corresponding structural groups of the amphiphilic surfactant molecule within the hydrophilic or hydrophobic phase also serves to stabilize the droplets of the dispersed phase.

Both electrostatic effects, arising from the electric charges of the surfactant's functional groups, and steric effects, resulting from the spatial arrangement of these groups within the dispersed and dispersing phases, contribute to this stabilization. The mechanisms through which surfactants interact to stabilize emulsions are schematically illustrated in Fig. 2.

A key aspect in considering systems containing surfactants at interfaces is the relationship between surface tension and the degree of surfactant coverage at the interface.[4,5] Within an emulsion droplet, there is a certain pressure, called capillary pressure, described by the Laplace equation, in which the pressure difference between the interior of the emulsion droplet and the continuous phase (ΔP) depends on the surface tension (γ) and the radius of the dispersed particle (r). A decrease in surface tension positively influences the size of the formed emulsion droplets (Eq. (1)).

$$r = 2\frac{2\gamma}{\Delta P} \quad \text{Eq. (1)}$$

The illustrative equation (Eq. (2)) demonstrates the effect of reducing the surface tension (γ) on the surface area (A) obtained using a specific energy input (E) to produce an emulsion.[6,7]

$$E = \gamma a \quad \text{Eq. (2)}$$

However, surfactants with a macromolecular structure can also interact with the environment through polymer chains anchored in the dispersed phase. It is easy to infer that the structure of these chains, along with their size and amphiphilic properties, can significantly influence the stability of the resulting emulsions. In the simplest

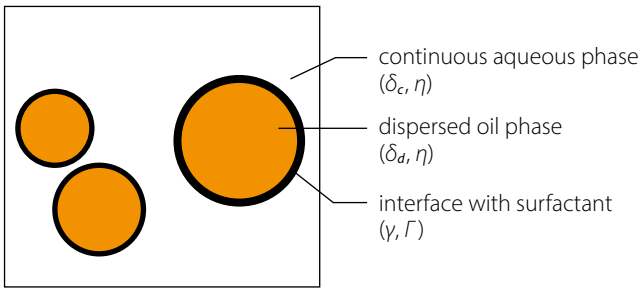

Fig. 1. Schematic representation of a surfactant-stabilized oil-in-water emulsion

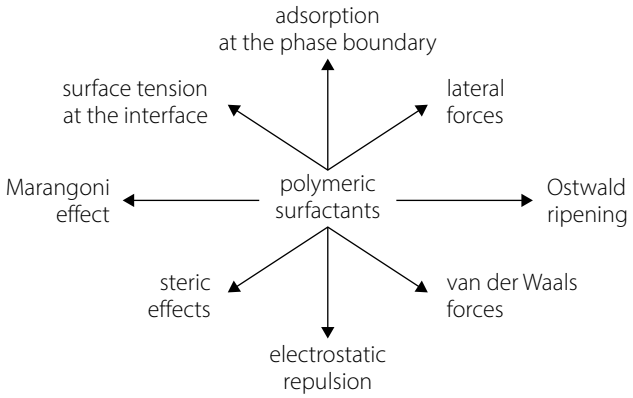

Fig. 2. Selected phenomena related to the action of polymeric surfactants at the phase boundary

terms, this occurs through their effect on parameters such as particle radius (r), medium viscosity (η), and the densities of the continuous and dispersed phases (ϱ_c, ϱ_d), as described by Stokes' equation, which defines the sedimentation velocity (u) of dispersed particles under gravitational acceleration (g), as shown in Eq. (3).[8]

$$u = \frac{2r^2(\varrho_c - \varrho_d)g}{9\eta} \quad \text{Eq. (3)}$$

Other factors also influence the stability of these dispersions, as described by the Derjaguin–Landau–Verwey–Overbeek (DLVO) theory.[9,10] Furthermore, 2 well-known phenomena – the Ostwald effect and the Marangoni effect – also impact the stability of pharmaceutical emulsions, including those intended for topical application.[11–14]

The Ostwald effect involves the growth of larger emulsion droplets at the expense of smaller surrounding droplets. In this phenomenon (Eq. (4)), the basic relationship between the radius of particles dispersed over time ($r_{(t)}$) and the initial radius ($r_{(o)}$), as described by Lifshitz and Slyozov for solid particles, depends on the surface tension (γ), the solubility of the dispersed particle material (c_ss), its molar volume (V_m), and the diffusion coefficient (D), with the universal gas constant (R) and absolute temperature (T) appearing in the equation.[15]

$$r_{(t)}{}^3 - r_{(t)}{}^3 = \frac{8\gamma c_s {V_m}^2 D}{9RT} \quad \text{Eq. (4)}$$

The Marangoni effect can contribute to emulsion stabilization; however, an inappropriately selected surfactant or changes in temperature can alter the Marangoni force, as described in Eq. 5 (F_M). This force arises from local differences in concentration (dC) and temperature (dT) across different regions (dx) of the stabilized emulsion particle surface.[16] The resulting flow of the surrounding medium between emulsion particles influences the tendency of opposing surfaces to aggregate.

$$F_M = \frac{d\gamma}{dT}\frac{dT}{dx} + \frac{d\gamma}{dC}\frac{dC}{dx} \quad \text{Eq. (5)}$$

Adsorption at the phase boundary

In studies of adsorbate adsorption on an adsorbent, a key concept is the degree of interfacial surface coverage by the adsorbate (θ). By lowering surface tension, the surfactant accumulates at the interface. This process is interpreted as adsorption and is described by Eq. (6), which introduces the concepts of surface excess (Γ) and maximum surface excess (Γ_∞). The ratio of these 2 quantities represents the degree of surfactant coverage at the phase boundary.

$$\theta = \frac{\Gamma}{\Gamma_\infty} \quad \text{Eq. (6)}$$

In isotherm equations and the corresponding surface tension equations, the concept of the minimum surface area per molecule – or per mole of molecules – accumulated at the surface (ω) is often used instead of the maximum surface excess. The latter is therefore the inverse of the maximum surface excess.[17] Adsorption at the interface can be described by the Gibbs isotherm (Eq. (7)), which relates the surfactant concentration (C) to the surface tension of the solution (γ) and the surface excess (Γ).

$$\Gamma = -\frac{1}{nRT}\left(\frac{d\gamma}{d\ln C}\right)_T \quad \text{Eq. (7)}$$

In the case of the Langmuir isotherm (Eq. (8)), the surface excess equation takes a slightly different form, incorporating a characteristic adsorption constant of the surfactant at the interface (K).

$$\Gamma = \Gamma_\infty \frac{C}{1+KC} \quad \text{Eq. (8)}$$

In some cases, strong lateral interactions affect the behavior described by the previously mentioned equations. The Frumkin isotherm (Eq. (9)) accounts for the influence of these interactions, represented by the lateral interaction coefficient (a).[18,19]

$$KC = \frac{\theta}{1-\theta}e^{-2a\theta} \quad \text{Eq. (9)}$$

The influence of surfactants on surface tension at the phase boundary

With surfactant adsorption at the interface, the interactions between solvent molecules at the solution surface are reduced, resulting in a decrease in surface tension. In studies using a Langmuir balance, authors often employ Eq. (10) for the equilibrium surface pressure (Π), defined as the difference between the surface tension of the pure solvent (γ_0) and that of the solution (γ).[20,21]

$$\Pi = \gamma_0 - \gamma \quad \text{Eq. (10)}$$

When lateral interactions are taken into account, the Frumkin isotherm (Eq. (11)) yields the corresponding expression for surface pressure.[22]

$$-\frac{\Pi\omega}{RT} = \ln(1-\theta) + a\theta^2 \quad \text{Eq. (11)}$$

Surface tension is explicitly expressed in the Gibbs isotherm equation. Other equations, such as the Langmuir and Frumkin isotherms, use the relationship described by the Gibbs isotherm, allowing surface tension to be determined from these respective models. The Szyszkowski equation (Eq. (12)), derived from the Langmuir isotherm, is among the most widely used in studies examining the effects of various substances on the surface tension of their solutions. It includes system-specific constants (a, b), which can be further interpreted.[23–25]

$$\gamma - \gamma_0 = a\ln(1+bC) \quad \text{Eq. (12)}$$

By expanding the equation to include the adsorption constant (K), surfactant concentration (C) and saturated

surface excess (Γ_s) (Eq. (13)), a slightly modified but practically useful form is obtained.[26]

$$\gamma - \gamma_0 = nRT\Gamma_s \ln(1 + KC) \quad \text{Eq. (13)}$$

A modification of this equation, sometimes presented alongside the concept of the Langmuir–Szyszkowski distribution coefficient (Eq. (14)), can be used to examine changes in surface pressure (Π_t) in relation to variations in surface excess over time (Γ_t).[27]

$$\Pi_t = -RT\Gamma_\infty \ln\left(1 - \frac{\Gamma_t}{\Gamma_\infty}\right)\gamma_0 \quad \text{Eq. (14)}$$

Determining surface tension according to the Frumkin isotherm requires using an equation that incorporates lateral interactions between surfactant molecules, represented by the coefficient (A). Similar to the Szyszkowski equation, Eq. (15) also includes system-specific constants (a_f and b_f).[28]

$$\gamma - \gamma_0 = -b_f \ln\left(\frac{c}{a_f} + 1\right) - A\left(\frac{c}{c + a_f}\right)^2 \quad \text{Eq. (15)}$$

In mathematical modeling of interfacial phenomena, the effect of surfactant concentration on surface tension reduction is analyzed, allowing prediction of the formation and stabilization of emulsion-type dispersions.[29] In both the Gibbs isotherm (Eq. (7)) and the Szyszkowski equation, derived from the Langmuir isotherm (Eq. (13)), the term n appears in the expressions.

This term represents the number of species contributing to surface activity, which may arise from dissociation, even though the Langmuir isotherm describes a monolayer.[30,31] The equation linking the Langmuir isotherm to changes in surface tension, as described above, is sometimes referred to as the Langmuir–Szyszkowski equation (Eq. (13)).[32] In cases where adsorption and surface tension changes involve multicomponent mixtures, the Butler equation – a modification of the Szyszkowski equation – can be applied.[33]

The influence of surfactants on the interactions between emulsion particles

According to the generally accepted theory developed in the 2nd half of the 20th century, particles of the dispersed phase are subject to mutual interactions that depend on various factors. These interactions can lead to particle approach, aggregation and flocculation, which may ultimately result in the breakdown of the system, such as emulsion separation or suspension sedimentation.[34] This theory has broader applications, as it can also be used to describe interactions not only among inanimate particles but also in the context of microorganisms.[35]

The general consideration of particle interactions (Eq. (16)) includes the van der Waals attractive energy (E_a), repulsive energy due to the electric double layer (E_r) and steric repulsion (E_s).

$$E_t = E_a + E_r + E_s \quad \text{Eq. (16)}$$

Emulsion particles attract one another, with van der Waals forces playing the primary role in these interactions. These forces include dispersion forces – namely, London forces, dipole–dipole forces and induced dipole–dipole forces. According to the DLVO theory, the energy of these interactions governs the approach of emulsion droplets, which can ultimately lead to system destabilization. The van der Waals attractive energy (E_a) is approximately proportional to the square of the number of molecules packed into 1 cm^3 of the system (q) and the mutual interaction energy of 2 such molecules separated by 1 cm in vacuum (β), expressed as the Hamaker–London constant (A), as described in Eq. (17). The separation distance in the denominator (H) represents the difference between the distance between the centers of 2 emulsion particles (R) and twice the particle radius (a).[36]

$$E_a = -\frac{\pi^2 q^2 \beta a}{12(R-2a)} = -\frac{Aa}{12H} \quad \text{Eq. (17)}$$

The subsequent terms of the equation provide information on factors contributing to the stability of the dispersed system. An approximate solution of the equation (Eq. (18)) – for the electrostatic repulsion energy of the electric double layer according to the Debye–Hückel approximation (E_r) for spherical particles – describes the influence of the continuous phase properties, including its permittivity in the medium (ε) and in vacuum (ε_0), the ionic strength represented by the inverse Debye length (κ) and the electric potential at the surface of the emulsion particles (Ψ_0). This formulation allows estimation of the influence of the surface potential, in particular, on the stability of a liquid dispersion.[37]

$$E_r = \frac{2\pi \cdot 10^{-2}}{9} \varepsilon\varepsilon_0 r\Psi_0^2 \ln\left(1 + e^{-\kappa h}\right) \quad \text{Eq. (18)}$$

In addition to the attraction resulting from van der Waals forces (E_a) and electrostatic repulsion (E_r), the stability of the dispersion system is also influenced by the steric factor (E_s), which arises from the spatial configuration of the surface of a dispersed particle within a specific dispersing phase. This factor is sometimes interpreted as the enthalpic stabilization term (ΔG).

The approximate formula for this term (Eq. (19)) determines the repulsive potential based on the concentration of adsorbed surfactant in the adsorbed layer (C), the volume fraction of the solvent (v_1), the density of the adsorbed material (ρ), the entropic factor (ψ), the enthalpic factor (χ), the thickness of the adsorbed layer (δ), the distance between the surfaces of emulsion particles (H_0), and the radius of the dispersed particles (a).[38,39]

$$\Delta G = \frac{4\pi C^2}{3v_1\rho_2^2}(\psi_1 - \chi_1)\left(\delta - \frac{H_0}{2}\right)^2\left(3a + 2\delta + \frac{H_0}{2}\right)$$

Eq. (19)

According to Lazaridis et al. (Eq. (20)), steric repulsion (E_s) should be interpreted as the sum of terms arising from entropy changes due to the configuration of polymer chains – also referred to as volumetric confinement (E_{VR}) – and from the enthalpy changes of overlapping polymer surfactant regions, which contribute to system stabilization (E_H).[40] This energy is related to the enthalpy of mixing, i.e., the mutual interactions of polymer chains stabilizing the dispersed particles.

The 1st term, entropic in nature, is based on the cross-sectional area of the interacting layer between 2 particles (S_i), the fraction of interface coverage by surfactant (θ), the number of adsorbed molecules per unit area (N_s), the length of polymer chains (δ), and the distance between particle surfaces (h). It is further corrected by the ratio of the volume fraction of the adsorbed surfactant (ϕ) to the high-density fraction occurring at the contact point of the polymer shells (ϕ*), multiplied by Boltzmann's constant (k_B).

The 2nd term, enthalpic, is based on the volume of the interacting layer between 2 particles (V_i), the surfactant weight concentration in the adsorbed layer (C_i), and a coefficient derived from Flory and Krigbaum theory (B). This term is also adjusted to account for the relevant volume fractions of the adsorbed surfactant (ϕ, ϕ*).

$$E_S = \left(\frac{2\phi}{\phi^*}\right) k_B T S_i \theta N_s \ln\frac{2\delta}{h} + \left(1 - \frac{2\phi}{\phi^*}\right) 2RTV_i BC_i$$

Eq. (20)

In addition, the energy associated with elastic repulsive forces (E_e) and the energy resulting from the dissolution of surfactant molecules in the continuous and dispersed phases (E_d), which leads to differences in osmotic pressure, are also distinguished.[41] The formula for the energy of elastic repulsive forces (E_e), described as Eq. (21), takes into account parameters such as the minimum distance between particles (h_0), the contour length of polymer chains surrounding the stabilized emulsion particle (i.e., the thickness of the stabilizing barrier, l_e), the total number of attached chains per unit area (ν), and the radius of a spherical particle (r).[42]

$$E_e = k_B T \cdot 2\nu\pi r\left(h_0\left(\ln\frac{h_0}{l_e} - 1\right) + l_e\right) \quad \text{Eq. (21)}$$

The influence of osmotic pressure on the repulsive potential can be expressed, i.a., by Eq. (22), in which the osmotic pressure between the surfaces of macromolecules (Π) increases to a maximum value (Π_0). This pressure depends on the ratio of the distance between the surfaces (h) to the minimum separation distance (λ), which may be determined, e.g., by the gyration radius.[43]

$$\Pi = \Pi_0^{-\frac{h}{\lambda}} \quad \text{Eq. (22)}$$

General overview of polymeric surfactants

Among amphiphilic chemical compounds used in pharmaceutical formulations, macromolecular compounds – polymers containing both hydrophilic and lipophilic components – deserve special attention. The combination of amphiphilic properties with features inherent to the macromolecular structure significantly enhances their potential applications in semi-solid drug forms, such as ointments, creams and hydrophilic gels. Numerous methods exist for the systematic classification of polymers affecting surface tension. One approach considers the structure of the polymer chain, including the arrangement of interwoven hydrophilic and lipophilic segments and the presence or absence of branching in the main linear chain. Table 1[44–68] presents an example of the systematic classification of polymeric surfactants.

One of the oldest and most widely used groups of polymers influencing phase-boundary properties in dispersed systems are amphiphilic polymers – homopolymers and copolymers obtained through random polymerization. These polymers are characterized by the random distribution of hydrophobic and hydrophilic groups.[69] Among them, nonionic polymers can form weak micelles but primarily adsorb at interfaces. Adsorption at the interface alters the interactions between molecules in both phases. These polymers find applications in cosmetics as hydrophilic coatings and emulsion stabilizers.[70]

Ionic polymers of this type contain hydrophilic ionic groups, such as carboxyl or sulfonic groups, along with corresponding randomly distributed hydrophobic segments. In the presence of oppositely charged ions or other surfactants, these polymers can form aggregates. They reduce surface tension through electrostatic interactions and are used as thickening agents, emulsion stabilizers and drug carriers, e.g., to control the release of active substances from formulations.[71]

Amphiphilic block copolymers are a particularly interesting and widely used class of polymers.[72] In these polymers, hydrophilic and hydrophobic segments are systematically arranged in blocks, with a defined content of mer units in each segment, as illustrated by poloxamers. Block copolymers form micelles in aqueous solutions and stabilize oil-in-water emulsions by forming a hydrophobic core surrounded by a hydrophilic shell. Their applications include drug carriers, bases for dermatological and cosmetic creams and gels, solubilizers, and stabilizers of emulsions and foams.

Polymers with comb-like side chains possess characteristic long hydrophobic side chains that adsorb at interfaces and reduce surface tension. These polymers stabilize emulsions in practice via steric effects and surface tension reduction.[73]

Advances in polymer synthesis have enabled the production of hyperbranched and dendrimeric polymer surfactants.[74,75] These macromolecules form aggregates and encapsulate hydrophobic molecules within a three-dimensional branched structure, facilitating the solubilization

Table 1. Examples of amphiphilic block copolymers that affect surface tension and can be used as polymeric surfactants

Polymer surfactant group		Examples	Reference
Amphiphilic polymers – homopolymers and copolymers	non-ionic	polyoxazolines (POx)	44
		polyethylene glycol (PEG)	45
		polyvinyl pyrrolidone (PVP)	46
		polyacrylamide (PAM)	47
	ionic	polyacrylates (PAA-Na)	48
		polystyrene sulfonates (PSS)	49
		modified polysaccharides	50,51
Amphiphilic block copolymers		poloxamers	52
		PEG-PLA copolymers	53,54
		PEG-PCL copolymers	55
		PEG-PGA copolymers	56
		PEG-PHPMA copolymers	57
Polymers with combing side chains		poly(acrylic acid) with alkyl chains (PAA-Cn)	58
		polyoxazolines with alkyl groups (POx-Cn)	59
		alkyl-modified cellulose (eg. cetylcellulose)	60
		polysiloxanes with PEG and alkyl groups (PDMS-g-PEG-Cn)	61,62
Hyperbranched and dendrimeric polymeric surfactants		polyamidoamine dendrimers (PAMAM)	63,64
		pyperbranched polyesters (Boltorn)	65,66
		dendrimers poly(propyleneimine) (PPI)	67
		PEG dendrimers (PEG-Dendr)	68

of hydrophobic substances. A hydrophobic, nonpolar molecule is surrounded by branched hydrophobic fragments of the macromolecule, allowing the creation of diverse nanostructures and drug carriers, and effective solubilization of hydrophobic compounds.

Selected examples of polymeric surfactants

The use of an appropriate surfactant or surfactant mixture is particularly important for the efficacy of topically administered drugs and has been the subject of detailed research for many years.[76] Table 2[77–96] presents examples of applications of polymeric surfactants in selected formulations with therapeutic, prophylactic or cosmetic effects.

Among polymeric emulsifiers commonly used in topical preparations, poloxamer 407 and poloxamer 188 are noteworthy. Poloxamer 407 is a block copolymer consisting of 3 sequential blocks – hydrophilic, lipophilic and hydrophilic – with the hydrophilic blocks composed of 101 mer units and the lipophilic block containing 56 mer units. Its molar mass is approx. 12,600 g/mol. Poloxamer 188 contains 75, 30 and 75 corresponding mer units in its hydrophilic–lipophilic–hydrophilic blocks, with a molar mass of approx. 8,400 g/mol.

Alternatives to conventional block copolymers containing oxyethylene and oxypropylene groups include polymers with sequences based on polyoxybutylene, polyoxyethylene and polyoxybutylene units, proposed for applications such as anticancer drug carriers.[97,98] As shown in Table 2, many applications of polymeric surfactants involve the production of emulsions or nanoemulsions.

The potential of PEG-400 as a co-surfactant in microemulsions for drug delivery was evaluated using carvedilol as a model compound. The authors suggest that such systems may be applied to enhance various drug delivery routes.[99] Polyvinylpyrrolidone (PVP) has also been successfully used in systems requiring surface tension reduction, such as self-emulsifying systems for enhanced delivery of cyclosporine A.[100]

Poloxamers and poloxamine surfactants are frequently considered suitable for designing transdermal drug delivery systems, with their activity appearing to be reversible – an important advantage over traditional surfactants, which may irreversibly alter the structure of the skin layers.[101] Among polysiloxane surfactants, solvation activity has been exploited, with nystatin used as a model drug to demonstrate the beneficial effects of these polymeric surfactants.[102]

Polymeric surfactants also play a significant role in cosmetic science, improving the design of numerous cosmeceutical products through film formation, modification of viscous properties, thickening, and stabilization or destabilization of foams.[103] Another notable application of polymeric surfactants is the stabilization of liposomal structures. They can be applied as ready-to-use materials or may undergo polymerization during the application process.[104,105]

Table 2. Selected examples of the use of polymeric surfactants in the production of drugs and other preparations used topically

Evaluated type of composition	Medicinal/active substance	Surfactant	Reference
Aggregates	17-beta-estradiol	poloxamer 407	77
Emulsion	green tea extract	cetyl PEG/PPG-10/1 dimethicone	78
Emulsion	model emulsion	poloxamer 407	79
Emulsion	α-hydroxy acids	PEG 55 PGO and PEG 80 SL	80
Film	ketoprofen	polyoxyethylene-20 oleyl ether	81
Foam	silver sulfadiazine	polyethylene glycol	82
Hydrogel	miconazole	poloxamer 407, poloxamer 188	83
Hydrogel	(+)-l-ascorbic acid	polymer surfactant PMDP (NIPA-PMDP gel)	84
Micelar solution	bisabolol	poloxamer 407	85
Multiple emulsion	model emulsion	poloxamer 407	86
Nanoemulsion	rapanea ferruginea extract	PEG-40 hydrogenated castor oil	87
Nanoemulsion	itraconazole	pectin	88
Nanoemulsion	tocopherol	poloxamer 188	89
Nanoemulsion	minoxidil	poloxamer 188	90
Nanoemulsion	piperine	poloxamer 188	91
Nanoemulsion	piroxicam	poloxamer 188	92
Nanoparticles	terbinafine	polyvinyl alcohol	93
Nanospheres	lidocaine	dextran derivatives containing various grafted hydrophobic group	94
Nanostructures	griseofulvin or fluconazole	poly(butylene oxide)-poly(ethylene oxide)-poly(butylene oxide)	95
Solution	griseofulvin	poloxamer 407	96

Limitations of the study

Polymeric surfactants are widely used in dermatological drug formulations, but their impact on rheology cannot be neglected. Both the impact on rheological parameters and the chemical nature of their functional groups in selected cases can complicate their use in topically administered drug formulations. In the case rheological complications, an unfavorable increase or decrease in the formulation's viscosity cannot be ruled out, even during use. On the other hand, surfactant functional groups can interact physically or chemically with their counterparts in the molecules of other excipients, as well as in the molecules of the drug. Consequently, in some cases, a modification of the biological activity of the formulation can be expected. The limitations mentioned above are eliminated through careful analysis and selection of formulation components, as well as proper technological procedures.

Conclusions

The production of nanostructures, nanoparticles and nanospheres represents another important area of application for polymeric surfactants. Many researchers emphasize their potential to form specific aggregates that can function as independent drug delivery systems. In addition, polymeric surfactants are used in advanced formulations such as films, foams, multiple emulsions, and hydrogels. In some cases, their primary role lies in the ability to create a stable solution, a micellar drug solution or a complex of various substances.

Use of AI and AI-assisted technologies

Not applicable.

ORCIDs

Remigiusz Zapolski https://orcid.org/0000-0002-9255-0418
Witold Musiał https://orcid.org/0000-0001-5695-5998

References

1. Langmuir I. The adsorption of gases on plane surface of glass, mica and olatinum. *J Am Chem Soc*. 1918;40(9):1361–1403. doi:10.1021/ja02242a004
2. Langmuir I. Surface chemistry. *Chem Rev*. 1933;13(2):147–191. doi:10.1021/cr60045a001
3. Gibbs JW. On the equilibrium of heterogeneous substances. *Am J Sci*. 1878;s3-16(96):441–458. doi:10.2475/ajs.s3-16.96.441
4. Menger FM, Rizvi SAA. Relationship between surface tension and surface coverage. *Langmuir*. 2011;27(23):13975–13977. doi:10.1021/la203009m
5. Prosser AJ, Franses EI. Adsorption and surface tension of ionic surfactants at the air–water interface: Review and evaluation of equilibrium models. *Colloids Surf A Physicochem Eng Aspects*. 2001;178(1–3):1–40. doi:10.1016/S0927-7757(00)00706-8
6. Joyner HS, Pernell CW, Daubert CR. Impact of oil-in-water emulsion composition and preparation method on emulsion physical properties and friction behaviors. *Tribol Lett*. 2014;56(1):143–160. doi:10.1007/s11249-014-0393-1
7. Bos MA, Van Vliet T. Interfacial rheological properties of adsorbed protein layers and surfactants: A review. *Adv Coll Interface Sci*. 2001;91(3):437–471. doi:10.1016/S0001-8686(00)00077-4

8. Derkach SR. Rheology of emulsions. *Adv Coll Interface Sci*. 2009;151(1–2):1–23. doi:10.1016/j.cis.2009.07.001
9. Eccleston GM, Florence AT. Application of emulsion theory to complex and real systems. *Int J Cosmet Sci*. 1985;7(5):195–212. doi:10.1111/j.1467-2494.1985.tb00414.x
10. Ninham BW. On progress in forces since the DLVO theory. *Adv Coll Interface Sci*. 1999;83(1–3):1–17. doi:10.1016/S0001-8686(99)00008-1
11. Khedr A, Striolo A. Quantification of Ostwald ripening in emulsions via coarse-grained simulations. *J Chem Theory Comput*. 2019;15(9):5058–5068. doi:10.1021/acs.jctc.9b00296
12. Taylor P. Ostwald ripening in emulsions. *Adv Coll Interface Sci*. 1998;75(2):107–163. doi:10.1016/S0001-8686(98)00035-9
13. Sternling CV, Scriven LE. Interfacial turbulence: Hydrodynamic instability and the Marangoni effect. *AIChE J*. 1959;5(4):514–523. doi:10.1002/aic.690050421
14. Ebrahimi A, Kazemzadeh Y, Akbari A. Impact of the Marangoni phenomenon on the different Enhanced Oil Recovery methods. *Heliyon*. 2024;10(21):e39919. doi:10.1016/j.heliyon.2024.e39919
15. Lifshitz IM, Slyozov VV. The kinetics of precipitation from supersaturated solid solutions. *J Phys Chem Solids*. 1961;19(1–2):35–50. doi:10.1016/0022-3697(61)90054-3
16. Scriven LE, Sternling CV. The Marangoni effects. *Nature*. 1960;187(4733):186–188. doi:10.1038/187186a0
17. Bresler MR, Hagen JP. Surfactant adsorption: A revised physical chemistry lab. *J Chem Educ*. 2008;85(2):269. doi:10.1021/ed085p269
18. Kutner W, Behr B, Kemula W. Detection of cholanoic acids in high-performance liquid chromatography based on effects of double layer capacity changes at the dropping mercury electrode. *Fresenius' Zeitschrift für Analytische Chemie*. 1982;312(2):121–125. doi:10.1007/BF00467725
19. Broadhead DE, Baikerikar KG, Hansen RS. Application of the Frumkin equation to electrocapillary and capacity data of some aliphatic compounds. *J Phys Chem*. 1976;80(4):370–375. doi:10.1021/j100545a007
20. Azizian S, Kashimoto K, Matsuda T, Matsubara H, Takiue T, Aratono M. Interfacial tension studies of crown ethers at air/water and hexane/water interfaces. *J Colloid Interface Sci*. 2007;316(1):25–30. doi:10.1016/j.jcis.2007.07.068
21. Tripathi S, Tan SN, Bhattacharya A, Tabor RF. Measuring and modelling the adsorption kinetics of polydisperse PiBSA-based emulsifiers using dynamic interfacial tension measurements. *Colloids Surf A Physicochem Eng Aspects*. 2021;624:126728. doi:10.1016/j.colsurfa.2021.126728
22. Hildmann A, Kairaliyeva T, Danker K, Shmanai V, Fainerman VB, Miller R. Adsorption characteristics of the alkyl phospholipid Inositol-C2-PAF at the solution/air interface. *Colloids Surf A Physicochem Eng Aspects*. 2017;532:578–582. doi:10.1016/j.colsurfa.2017.03.028
23. Habrdová K, Hovorka Š, Bartovská L. Concentration dependence of surface tension for very dilute aqueous solutions of organic nonelectrolytes. *J Chem Eng Data*. 2004;49(4):1003–1007. doi:10.1021/je049955d
24. Wołowicz A, Staszak K. Study of surface properties of aqueous solutions of sodium dodecyl sulfate in the presence of hydrochloric acid and heavy metal ions. *J Mol Liq*. 2020;299:112170. doi:10.1016/j.molliq.2019.112170
25. Jańczuk B, Zdziennicka A, Wójcik W. Adsorption of sodium dodecyl sulphate and propanol mixtures at aqueous solution–air interface. *Colloids Surf A Physicochem Eng Aspects*. 2004;244(1–3):1–7. doi:10.1016/j.colsurfa.2004.05.007
26. Phan CM, Le TN, Yusa SI. A new and consistent model for dynamic adsorption of CTAB at air/water interface. *Colloids Surf A Physicochem Eng Aspects*. 2012;406:24–30. doi:10.1016/j.colsurfa.2012.04.044
27. Neys B, Joos P. Equilibrium surface tensions and surface potentials of some fatty acids. *Colloids Surf A Physicochem Eng Aspects*. 1998;143(2–3):467–475. doi:10.1016/S0927-7757(98)00610-4
28. Staszak K, Wieczorek D, Michocka K. Effect of sodium chloride on the surface and wetting properties of aqueous solutions of cocamidopropyl betaine. *J Surfact Detergents*. 2015;18(2):321–328. doi:10.1007/s11743-014-1644-8
29. Kaptay G. Partial surface tension of components of a solution. *Langmuir*. 2015;31(21):5796–5804. doi:10.1021/acs.langmuir.5b00217
30. Domínguez-Arca V, Sabín J, Taboada P, García-Río L, Prieto G. Micellization thermodynamic behavior of gemini cationic surfactants: Modeling its adsorption at air/water interface. *J Mol Liq*. 2020;308:113100. doi:10.1016/j.molliq.2020.113100
31. Zhu BY, Gu T. Surfactant adsorption at solid-liquid interfaces. *Adv Coll Interface Sci*. 1991;37(1–2):1–32. doi:10.1016/0001-8686(91)80037-K
32. Siddiqui FA, Franses EI. Equilibrium adsorption and tension of binary surfactant mixtures at the air/water interface. *Langmuir*. 1996;12(2):354–362. doi:10.1021/la9506032
33. Hey MJ, Kippax PG. Surface tensions of mixed aqueous solutions of tert-butanol and n-pentanol. *Colloids Surf A Physicochem Eng Aspects*. 2005;262(1–3):198–203. doi:10.1016/j.colsurfa.2005.04.036
34. Tajima K, Koshinuma M, Nakamura A. Steric repulsion of polyoxyethylene groups for emulsion stability. *Colloid Polym Sci*. 1992;270(8):759–767. doi:10.1007/BF00776147
35. Hermansson M. The DLVO theory in microbial adhesion. *Colloids Surf B Biointerfaces*. 1999;14(1–4):105–119. doi:10.1016/S0927-7765(99)00029-6
36. Napper DH. Colloid stability. *Product R&D*. 1970;9(4):467–477. doi:10.1021/i360036a005
37. Ottewill RH. Direct measurements of a particle-particle interactions. In: Rupprecht H, Bonart R, Müller FH, Weiss A, eds. *Mechanisches Verhalten von Polymeren Wechselwirkung in Polymeren Bzw. Kolloiden Systemen*. Vol 67. Progress in Colloid & Polymer Science. Darmstadt, West Germany: Steinkopff; 1980:71–83. doi:10.1007/BFb0117387
38. Ottewill RH, Walker T. The influence of non-ionic surface active agents on the stability of polystyrene latex dispersions. *Kolloid-Zeitschrift & Zeitschrift für Polymere*. 1968;227(1–2):108–116. doi:10.1007/BF02085284
39. Ono H, Jidai E, Fujii A. Stability of polymer latexes prepared using mixtures of anionic and nonionic surfactants. *J Phys Chem*. 1975;79(19):2020–2024. doi:10.1021/j100586a008
40. Lazaridis N, Alexopoulos AH, Chatzi EG, Kiparissides C. Steric stabilization in emulsion polymerization using oligomeric nonionic surfactants. *Chem Eng Sci*. 1999;54(15–16):3251–3261. doi:10.1016/S0009-2509(98)00336-4
41. Kurihara K, Vincent B. The discovery of the depletion force. *J Chem Phys*. 2021;154(22):220401. doi:10.1063/5.0052306
42. Evans R, Smitham JB, Napper DH. Theoretical prediction of the elastic contribution to steric stabilization. *Coll Polym Sci*. 1977;255(2):161–167. doi:10.1007/BF01777275
43. Carrière D, Page M, Dubois M, et al. Osmotic pressure in colloid science: Clay dispersions, catanionics, polyelectrolyte complexes and polyelectrolyte multilayers. *Colloids Surf A Physicochem Eng Aspects*. 2007;303(1–2):137–143. doi:10.1016/j.colsurfa.2007.02.050
44. Korchia L, Bouilhac C, Aubert A, Robin JJ, Lapinte V. Light-switchable nanoparticles based on amphiphilic diblock, triblock and heterograft polyoxazoline. *RSC Adv*. 2017;7(68):42690–42698. doi:10.1039/C7RA07094B
45. D'Souza AA, Shegokar R. Polyethylene glycol (PEG): A versatile polymer for pharmaceutical applications. *Exp Opin Drug Deliv*. 2016;13(9):1257–1275. doi:10.1080/17425247.2016.1182485
46. Kamli M, Guettari M, Tajouri T. Structure of polyvinylpyrrolidone aqueous solution in semi-dilute regime: Roles of polymer-surfactant complexation. *J Mol Struct*. 2019;1196:176–185. doi:10.1016/j.molstruc.2019.06.069
47. Wu S, Shanks RA, Bryant G. Properties of hydrophobically modified polyacrylamide with low molecular weight and interaction with surfactant in aqueous solution. *J Appl Polym Sci*. 2006;100(6):4348–4360. doi:10.1002/app.23282
48. Hu RYZ, Wang ATA, Hartnett JP. Surface tension measurement of aqueous polymer solutions. *Exp Therm Fluid Sci*. 1991;4(6):723–729. doi:10.1016/0894-1777(91)90079-7
49. Sen AK, Roy S, Juvekar VA. Effect of structure on solution and interfacial properties of sodium polystyrene sulfonate (NaPSS). *Polym Int*. 2007;56(2):167–174. doi:10.1002/pi.2154
50. Demé B, Lee LT. Adsorption of a hydrophobically modified polysaccharide at the air–water interface: Kinetics and structure. *J Phys Chem B*. 1997;101(41):8250–8258. doi:10.1021/jp9714328
51. Wei Y, Xie Y, Cai Z, et al. Interfacial and emulsion characterisation of chemically modified polysaccharides through a multiscale approach. *J Colloid Interface Sci*. 2020;580:480–492. doi:10.1016/j.jcis.2020.07.048
52. Buckton G, Machiste EO. Differences between dynamic and equilibrium surface tension of poly(oxyethylene)–poly(oxypropylene)–poly(oxyethylene) block copolymer surfactants (poloxamers P407, P237, and P338) in aqueous solution. *J Pharm Sci*. 1997;86(2):163–166. doi:10.1021/js960343o

53. Rabanel JM, Faivre J, Tehrani SF, Lalloz A, Hildgen P, Banquy X. Effect of the polymer architecture on the structural and biophysical properties of PEG–PLA nanoparticles. *ACS Appl Mater Interfaces*. 2015;7(19):10374–10385. doi:10.1021/acsami.5b01423
54. Garofalo C, Capuano G, Sottile R, et al. Different insight into amphiphilic PEG–PLA copolymers: Influence of macromolecular architecture on the micelle formation and cellular uptake. *Biomacromolecules*. 2014;15(1):403–415. doi:10.1021/bm401812r
55. You JH, Choi SW, Kim JH, Kwak YT. Synthesis and microphase separation of biodegradable poly(ε-caprolactone)-poly(ethylene glycol)-poly(ε-caprolactone) multiblock copolymer films. *Macromol Res*. 2008;16(7):609–613. doi:10.1007/BF03218568
56. Gu D, O'Connor AJ, G.H. Qiao G, Ladewig K. Hydrogels with smart systems for delivery of hydrophobic drugs. *Exp Opin Drug Deliv*. 2017;14(7):879–895. doi:10.1080/17425247.2017.1245290
57. Hatton FL. Mixing dendron and PEG initiators for the polymerisation of branched pHPMA and aqueous nanoparticle formation. In: *Hyperbranched Polydendrons*. Springer Theses. Cham, Switzerland: Springer International Publishing; 2015:79–116. doi:10.1007/978-3-319-18753-2_3
58. Perrin P, Lafuma F. Low hydrophobically modified poly(acrylic acid) stabilizing macroemulsions: Relationship between copolymer structure and emulsions properties. *J Colloid Interface Sci*. 1998;197(2):317–326. doi:10.1006/jcis.1997.5224
59. Giardi C, Lapinte V, Charnay C, Robin JJ. Nonionic polyoxazoline surfactants based on renewable source: Synthesis, surface and bulk properties. *React Funct Polym*. 2009;69(9):643–649. doi:10.1016/j.reactfunctpolym.2009.04.008
60. McMullen RL, Ozkan S, Gillece T. Physicochemical properties of cellulose ethers. *Cosmetics*. 2022;9(3):52. doi:10.3390/cosmetics9030052
61. Jo S, Park K. Surface modification using silanated poly(ethylene glycol)s. *Biomaterials*. 2000;21(6):605–616. doi:10.1016/S0142-9612(99)00224-0
62. Petroff LJ, Snow SA. Silicone Surfactants. In: Owen MJ, Dvornic PR, eds. *Silicone Surface Science*. Vol. 4. Advances in Silicon Science. Dordrecht, the Netherlands: Springer Netherlands; 2012:243–280. doi:10.1007/978-94-007-3876-8_9
63. Esumi K, Kuwabara K, Chiba T, Kobayashi F, Mizutani H, Torigoe K. Interactions between a hydrophobically modified poly(amidoamine) dendrimer and surfactants in aqueous solutions. *Colloids Surf A Physicochem Eng Aspects*. 2002;197(1–3):141–146. doi:10.1016/S0927-7757(01)00873-1
64. Yoshimura T, Abe S, Esumi K. Unique solution properties of quaternized oligomeric surfactants derived from ethylenediamine or G0 poly (amidoamine) dendrimers. *J Oleo Sci*. 2012;61(12):699–706. doi:10.5650/jos.61.699
65. Voit B. Hyperbranched polymers: All problems solved after 15 years of research? *J Polym Sci A Polym Chem*. 2005;43(13):2679–2699. doi:10.1002/pola.20821
66. Jaisingh A, Leena N. Dendrimers and hyperbranched polymers as promising and versatile additives in polyolefins. *ACS Appl Eng Mater*. 2024;2(2):236–261. doi:10.1021/acsaenm.3c00675
67. Dendrimers and their applications as novel drug delivery carriers. *J Appl Pharm Sci*. 2013;3(9):142–149. doi:10.7324/JAPS.2013.3924
68. Desai PN, Yuan Q, Yang H. Synthesis and characterization of photocurable polyamidoamine dendrimer hydrogels as a versatile platform for tissue engineering and drug delivery. *Biomacromolecules*. 2010;11(3):666–673. doi:10.1021/bm901240g
69. Chowdhury S, Rakshit A, Acharjee A, Saha B. Novel amphiphiles and their applications for different purposes with special emphasis on polymeric surfactants. *Chem Select*. 2019;4(23):6978–6995. doi:10.1002/slct.201901160
70. Coelho JF, Ferreira PC, Alves P, et al. Drug delivery systems: Advanced technologies potentially applicable in personalized treatments. *EPMA J*. 2010;1(1):164–209. doi:10.1007/s13167-010-0001-x
71. Peng F, Ke Y, Lu S, Zhao Y, Hu X, Deng Q. Anion amphiphilic random copolymers and their performance as stabilizers for O/W nanoemulsions. *RSC Adv*. 2019;9(26):14692–14700. doi:10.1039/C9RA01383K
72. Bodratti AM, Alexandridis P. Amphiphilic block copolymers in drug delivery: Advances in formulation structure and performance. *Exp Opin Drug Deliv*. 2018;15(11):1085–1104. doi:10.1080/17425247.2018.1529756
73. Raduan NH, Horozov TS, Georgiou TK. "Comb-like" non-ionic polymeric macrosurfactants. *Soft Matter*. 2010;6(10):2321. doi:10.1039/b926822g
74. Abdelhafiz FM, Mohamed DE, Khattab A, Mohamed AS, Soliman ESA, Kassem TM. Designing of quaternized hyperbranched polyamidoamines dendrimers: Surface activity, pharmaceutical efficacy, and safety approach. *J Drug Deliv Sci Technol*. 2022;67:102929. doi:10.1016/j.jddst.2021.102929
75. Svenson S, Chauhan AS. Dendrimers for enhanced drug solubilization. *Nanomedicine*. 2008;3(5):679–702. doi:10.2217/17435889.3.5.679
76. Shelmire JB. Factors affecting the diffusion of drugs from vehicles to the skin surface. *J Invest Dermatol*. 1956;27(6):383–387. doi:10.1038/jid.1956.112
77. Barreiro-Iglesias R, Alvarez-Lorenzo C, Concheiro A. Controlled release of estradiol solubilized in carbopol/surfactant aggregates. *J Control Release*. 2003;93(3):319–330. doi:10.1016/j.jconrel.2003.08.015
78. Mahmood T. Formulation and characterization of a green tea extract containing emulsion prepared with AbilEM90 as a lipophilic surfactant. *Afr J Pharm Pharmacol*. 2012;6(19):1395–1399. doi:10.5897/AJPP10.172
79. Vasiljevic D, Vuleta G, Primorac M. The characterization of the semisolid W/O/W emulsions with low concentrations of the primary polymeric emulsifier. *Int J Cosmet Sci*. 2005;27(2):81–87. doi:10.1111/j.1467-2494.2004.00247.x
80. Ertan G, Özer Ö, Sarcin ZB. Pre-formulation and some stability studies on cosmetic emulsions prepared with alpha-hydroxy acids. *Acta Pharm Turc*. 1999;41(2):86–92. https://www.actapharmsci.com/uploads/pdf/pdf_411.pdf
81. Suksaeree J, Charoenchai L, Monton C, et al. Preparation of a pseudolatex-membrane for ketoprofen transdermal drug delivery systems. *Ind Eng Chem Res*. 2013;52(45):15847–15854. doi:10.1021/ie402345a
82. Cho YS, Lee JW, Lee JS, et al. Hyaluronic acid and silver sulfadiazine-impregnated polyurethane foams for wound dressing application. *J Mater Sci Mater Med*. 2002;13(9):861–865. doi:10.1023/A:1016500429225
83. Kumar M. Development of miconazole nitrate loaded micellar gel for improved topical delivery. *Thai J Pharm Sci*. 2016;40(2):87–94. doi:10.56808/3027-7922.1930
84. Yan H, Tsujii K. Potential application of poly(N-isopropylacrylamide) gel containing polymeric micelles to drug delivery systems. *Colloids Surf B Biointerfaces*. 2005;46(3):142–146. doi:10.1016/j.colsurfb.2005.10.007
85. Ivanova N, Ermenlieva N, Andonova V. Alpha-bisabolol-loaded cosmetic micellar solution with cleansing and antimicrobial action for facial skin hygiene. *Cosmetics*. 2024;11(5):173. doi:10.3390/cosmetics11050173
86. Schmidts T, Dobler D, Nissing C, Runkel F. Influence of hydrophilic surfactants on the properties of multiple W/O/W emulsions. *J Colloid Interface Sci*. 2009;338(1):184–192. doi:10.1016/j.jcis.2009.06.033
87. Bresolin TMB, Dal Mas J, Zermiani T, et al. Nanoemulsion as a carrier to improve the topical anti-inflammatory activity of stem bark extract of *Rapanea ferruginea*. *Int J Nanomed*. 2016;11:4495–4507. doi:10.2147/IJN.S110486
88. Burapapadh K, Kumpugdee-Vollrath M, Chantasart D, Sriamornsak P. Fabrication of pectin-based nanoemulsions loaded with itraconazole for pharmaceutical application. *Carbohydrate Polym*. 2010;82(2):384–393. doi:10.1016/j.carbpol.2010.04.071
89. Teo BSX, Basri M, Zakaria MRS, Salleh AB, Rahman RNZRA, Rahman MBA. A potential tocopherol acetate loaded palm oil esters-in-water nanoemulsions for nanocosmeceuticals. *J Nanobiotechnol*. 2010;8(1):4. doi:10.1186/1477-3155-8-4
90. Cardoso SA, Barradas TN. Developing formulations for drug follicular targeting: Nanoemulsions loaded with minoxidil and clove oil. *J Drug Deliv Sci Technol*. 2020;59:101908. doi:10.1016/j.jddst.2020.101908
91. Ozkan B, Altuntas E, Cakir Koc R, Budama-Kilinc Y. Development of piperine nanoemulsions: An alternative topical application for hypopigmentation. *Drug Dev Ind Pharm*. 2022;48(3):117–127. doi:10.1080/03639045.2022.2100901
92. Mat Hadzir N, Basri M, Abdul Rahman MB, Salleh AB, Raja Abdul Rahman RNZ, Basri H. Phase behaviour and formation of fatty acid esters nanoemulsions containing piroxicam. *AAPS PharmSciTech*. 2013;14(1):456–463. doi:10.1208/s12249-013-9929-1
93. Rencber S, Tuncay Tanrıverdi S. Terbinafine hydrochloride loaded PLGA nanoparticles for topical administration. In: Budapest, Hungary: The 3rd World Congress on Recent Advances in Nanotechnology; Scientific Collegium: 2018. doi:10.11159/nddte18.112
94. Rouzes C, Leonard M, Durand A, Dellacherie E. Influence of polymeric surfactants on the properties of drug-loaded PLA nanospheres. *Colloids Surf B Biointerfaces*. 2003;32(2):125–135. doi:10.1016/S0927-7765(03)00152-8

95. Figueroa-Ochoa EB, Villar-Alvarez EM, Cambón A, et al. Lenghty reverse poly(butylene oxide)-poly(ethylene oxide)-poly(butylene oxide) polymeric micelles and gels for sustained release of antifungal drugs. *Int J Pharm*. 2016;510(1):17–29. doi:10.1016/j.ijpharm.2016.06.013
96. Pittol V, Veras KS, Kaiser S, Danielli LJ, Fuentefria AM, Ortega GG. Poloxamer-enhanced solubility of griseofulvin and its related antifungal activity against *Trichophyton* spp. *Braz J Pharm Sci*. 2022;58:e19731. doi:10.1590/s2175-97902022e19731
97. Villar-Alvarez E, Cambón A, Blanco M, et al. Surface self-assembly and properties of monolayers formed by reverse poly(butylene oxide)-poly(ethylene oxide)-poly(butylene oxide) triblock copolymers with lengthy hydrophilic blocks. *J Phys Chem C*. 2017;121(23):12684–12695. doi:10.1021/acs.jpcc.7b00728
98. Cambón A, Rey-Rico A, Mistry D, et al. Doxorubicin-loaded micelles of reverse poly(butylene oxide)–poly(ethylene oxide)–poly(butylene oxide) block copolymers as efficient "active" chemotherapeutic agents. *Int J Pharm*. 2013;445(1–2):47–57. doi:10.1016/j.ijpharm.2013.01.056
99. Taher SS, Al-Kinani KK, Hammoudi ZM, Ghareeb MM. Co-surfactant effect of polyethylene glycol 400 on microemulsion using BCS class II model drug. *J Adv Pharm Educ Res*. 2022;12(1):63–69. doi:10.51847/1h17TZqgyI
100. Lee DR, Ho MJ, Choi YW, Kang MJ. A polyvinylpyrrolidone-based supersaturable self-emulsifying drug delivery system for enhanced dissolution of cyclosporine A. *Polymers (Basel)*. 2017;9(4):124. doi:10.3390/polym9040124
101. Cappel MJ, Kreuter J. Effect of nonionic surfactants on transdermal drug delivery: II. Poloxamer and poloxamine surfactants. *Int J Pharm*. 1991;69(2):155–167. doi:10.1016/0378-5173(91)90220-I
102. Racles C, Mares M, Sacarescu L. A polysiloxane surfactant dissolves a poorly soluble drug (nystatin) in water. *Colloids Surf A Physicochem Eng Aspects*. 2014;443:233–239. doi:10.1016/j.colsurfa.2013.11.010
103. Torchilin VP. Structure and design of polymeric surfactant-based drug delivery systems. *J Control Release*. 2001;73(2–3):137–172. doi:10.1016/S0168-3659(01)00299-1
104. Morgan SE, Havelka KO, Lochhead RY, eds. *Cosmetic Nanotechnology: Polymers and Colloids in Cosmetics*. ACS Symposium Series. Vol. 961. Washington, D.C, USA: American Chemical Society; 2007. doi:10.1021/bk-2007-0961
105. Fendler JH, Tundo P. Polymerized surfactant aggregates: Characterization and utilization. *Acc Chem Res*. 1984;17(1):3–8. doi:10.1021/ar00097a001

Photodynamic therapy: Basics and new directions for clinical applications

Aneta Popiel-Kopaczyk[1,A,B,E,F], Tomasz Stanisław Kręcicki[2,B,D], Roksana Kozieł[3,C]

[1] Division of Histology and Embryology, Department of Human Morphology and Embryology, Wroclaw Medical University, Poland
[2] Department of Otolaryngology, Head and Neck Surgery, Wroclaw Medical University, Poland
[3] Institute of Internal Medicine, Wroclaw Medical University, Poland

A – research concept and design; B – collection and/or assembly of data; C – data analysis and interpretation;
D – writing the article; E – critical revision of the article; F – final approval of the article

Polymers in Medicine, ISSN 0370-0747 (print), ISSN 2451-2699 (online) *Polim Med.* 2025;55(2):145–151

Address for correspondence
Aneta Popiel-Kopaczyk
E-mail: aneta.popiel-kopaczyk@umw.edu.pl

Funding sources
None declared

Conflict of interest
None declared

Received on May 30, 2025
Reviewed on June 27, 2025
Accepted on June 10, 2025

Published online on December 19,2025

Abstract

Photodynamic therapy (PDT) remains a developing modality in cancer treatment. It is a minimally invasive approach that employs a photosensitizing drug, activated by light, to induce localized cytotoxic effects. Initially introduced in oncology, PDT has proven effective for cancers such as skin malignancies and head and neck tumors, while sparing surrounding healthy tissue. Beyond oncology, its use has expanded to dermatology, ophthalmology and dentistry, and it shows promise in the management of chronic inflammatory conditions, pediatric nephrology and emerging applications in cardiovascular and neurodegenerative diseases. Despite persistent challenges such as limited light penetration, advances in photosensitizers and integration with technologies including immunotherapy and polymeric nanocarriers underscore PDT's potential as a versatile tool in precision medicine. Recent studies suggest that PDT can also modulate the tumor microenvironment (TME) and stimulate anti-tumor immune responses, thereby enhancing its therapeutic impact. Consequently, it is increasingly being investigated in combination with other treatment modalities to overcome resistance and improve patient outcomes.

Key words: photodynamic therapy, polymers, photosensitizing effect

Cite as
Popiel-Kopaczyk A, Kręcicki TS, Kozieł R. Photodynamic therapy: Basics and new directions for clinical applications. *Polim Med.* 2025;55(2):145–151. doi:10.17219/pim/208132

DOI
10.17219/pim/208132

Highlights

- Photodynamic therapy (PDT) provides targeted, minimally invasive cancer treatment, achieving tumor control while sparing surrounding healthy tissues.
- Applications of PDT extend beyond oncology, with growing evidence supporting its use in dermatology, ophthalmology and neurodegenerative disorders.
- Next-generation photosensitizers and nanocarriers improve PDT efficacy, enabling deeper light penetration and advancing its role in precision medicine.
- PDT reshapes the tumor microenvironment and enhances immune response, increasing effectiveness when combined with immunotherapies and other treatment modalities.

Introduction

Photodynamic therapy (PDT) is a contemporary, localized approach for treating tumors and precancerous conditions. The technique selectively targets diseased tissues while sparing adjacent healthy structures, often resulting in superior cosmetic outcomes compared with conventional therapies. It involves administering a photosensitizer that preferentially accumulates in tumor cells; upon activation by light, it triggers cytotoxic reactions that lead to cell death. A major advantage of PDT is its selectivity: photosensitizers accumulate preferentially in tumor cells, thereby increasing safety for patients.[1,2] In clinical practice, PDT is primarily employed in dermatology,[3] urology,[4] ophthalmology,[5] and gynecology,[6] for both oncological and non-oncological conditions. Its applications in cardiology, neurosurgery and orthopedics are less frequent. It is also used in the management of age-related macular degeneration (AMD) and other ocular diseases.[7] Research into its potential for treating coronary diseases, leukemias and transplant rejection prevention is ongoing. The forgotten approach of PDT, i.e., photodynamic antimicrobial chemotherapy (PACT), has been intensively developed in recent years.[8] Similarly to PDT, PACT involves phototoxic reactions activated by visible or ultraviolet light, activating photosensitizers, primarily porphyrin-based. It is often recently used to neutralize viruses, drug-resistant bacteria, yeasts, and parasites. Moreover, PACT is successfully applied in dentistry, e.g., in treating caries and gingivitis, as well as for plaque removal. Thus, PDT procedures find a broad application in various neoplastic and non-neoplastic diseases, with relatively good patient comfort.

In recent years, the versatility and precision of PDT have attracted growing interest in the context of personalized medicine. Ongoing research explores the combination of PDT with nanotechnology and immunotherapy, enhancing both its specificity and therapeutic efficacy. Moreover, new generations of photosensitizers are being developed to optimize light absorption, improve tumor selectivity and reduce systemic toxicity. These advances could help overcome current limitations, such as poor light penetration into deep tissues. As such, PDT continues to evolve as a promising, multi-faceted modality in modern clinical practice, with the potential to reshape treatment paradigms across diverse medical disciplines.

Photosensitizers

Photosensitizers are dyes that initiate physicochemical reactions when exposed to light of a specific wavelength. In PDT, the radiation used falls within the visible spectrum (400–700 nm). Tissue penetration depends on both wavelength and energy, increasing with longer wavelengths at a constant intensity. Blue and green light, with shorter wavelengths, penetrate up to approx. 2 mm, whereas red light (>600 nm) can reach depths beyond 3.5 mm.[9,10] However, light energy decreases substantially in deeper tissue layers, limiting the photodynamic effect. For this reason, photosensitizers that absorb light at longer wavelengths are preferred to improve penetration into deeper structures. Most currently available photosensitizers absorb at approx. 630–650 nm, a range often referred to as the "therapeutic window." Natural pigments such as hemoglobin also absorb light and thereby restrict penetration. To be effective, an ideal photosensitizer must satisfy several criteria[9,11,12]:

- Retention in tissue for at least several hours;
- An absorption spectrum distinct from naturally occurring pigments in the body;
- Minimal side effects;
- High efficiency in generating singlet oxygen or radical oxygen species.

Hematoporphyrin derivatives (HpDs) are the most widely used first-generation photosensitizers and only partially fulfill the criteria for an ideal agent. Hematoporphyrin, first described by Lipson et al. in 1961, was the earliest photosensitizer applied in PDT and later received U.S. Food and Drug Administration (FDA) approval. When administered intravenously at a dose of 2 mg/kg body weight, HpD accumulates in tumor tissue within 48–72 h but persists in the body for 6–8 weeks, leading to prolonged photosensitivity. Hematoporphyrin derivatives are activated by red light at 630 ±3 nm.[13] The purified form of this compound was commercialized as Photofrin and has been

widely used in clinical practice (https://photofrin.com/).[13] Other groups of photosensitizing agents include cyanines and phthalocyanines,[14,15] chlorins[16] and bacteriochlorins, as well as naturally derived compounds such as curcumin, hypericin and riboflavin.[9]

Procedure and basic mechanisms of PDT

Photodynamic therapy involves several stages: photosensitizer administration, cellular accumulation, irradiation, induction of cytotoxic reactions, and subsequent wound formation. The first step is administration, during which the patient receives a photosensitizer that penetrates tumor cells. Over the next several hours, the photosensitizer accumulates selectively within tumor cells, preparing the tissue for light activation. The tumor site is then irradiated with light at a wavelength corresponding to the absorption spectrum of the photosensitizer, typically applied for about 10 min per site. This irradiation triggers cytotoxic reactions in which reactive oxygen species (ROS) and free radicals are generated within tumor cells. The treatment is followed by localized wound formation and subsequent healing, with the affected area typically resolving over several weeks and leaving minimal scarring.[2]

Photodynamic reactions can proceed through distinct mechanisms, and 3 principal pathways of PDT-induced effects on tumor tissue have been described. In the Type I mechanism, photosensitizers react with acceptor molecules to generate radical species. In the Type II mechanism, triplet-state photosensitizers interact directly with molecular oxygen, producing singlet oxygen.[17] The Type III mechanism is associated with stimulation of the immune response against cancer cells.[18] Following PDT, tumor cells may undergo cell death – through apoptosis, necrosis or other regulated pathways – triggered by photodamage to intracellular compartments such as mitochondria, lysosomes or the endoplasmic reticulum.[19]

Clinical applications of PDT

Photodynamic therapy has evolved into a versatile treatment modality with applications extending well beyond its original focus on oncology. Its expanding clinical utility – from inflammatory conditions to pediatric nephrology – offers an increasingly attractive area of investigation for both clinicians and researchers. Recent advances in PDT have focused on improving photosensitizer delivery and combining the technique with chemotherapeutics, antibodies or other adjuvant agents.[6,20] Importantly, PDT can be applied in 2 main directions: the treatment of oncological and non-oncological diseases.

Oncological applications

Photodynamic therapy is well established in the treatment of a variety of cancers, including skin malignancies (e.g., basal cell carcinoma (BCC), squamous cell carcinoma (SCC) and actinic keratosis), as well as head and neck cancers, esophageal cancer, bladder cancer, and lung cancer.[13,17] In oncological protocols, PDT primarily employs broad-spectrum red light, with typical therapeutic doses ranging within 100–150 J/cm^2 at an intensity of 100–200 mW/cm^2.[19] The mechanisms of PDT involve the selective accumulation of photosensitizers in malignant tissues, followed by light activation that triggers cytotoxic reactions leading to cell death, vascular damage and local inflammation, while sparing surrounding healthy tissue. This selectivity not only reduces treatment-related morbidity but also improves cosmetic outcomes, reinforcing confidence in PDT's clinical efficacy.[19] Selectivity can be further enhanced through the use of nanocarriers to optimize photosensitizer delivery or by conjugating photosensitizers with antibodies that target specific cell populations.[17,18]

Non-oncological dermatological and inflammatory conditions

In dermatology, PDT has been employed to manage[21,22]:

- Psoriasis: PDT modulates immune responses and reduces keratinocyte proliferation.[23]
- Acne vulgaris: PDT with 5-aminolaevulinic acid (ALA) or methyl aminolevulinate targets sebaceous glands and reduces *Cutibacterium acnes* load.[24]
- Vitiligo: PDT procedure promotes melanocyte regeneration through photomodulation.[25]
- Chronic ulcers: photodynamic therapy enhances wound healing by reducing microbial load and stimulating angiogenesis.
- Recurrent palmar and plantar warts caused by human papillomavirus (HPV) infection.[26]

It is also used in several non-oncological disorders, with lower PDT doses in the range of 10–40 J/cm^2 and intensity of 50–70 mW/cm^2.[21] Similar PDT doses have shown promise in treating inflammatory diseases due to their ability to reduce pro-inflammatory cytokines and modulate immune responses.[27] This procedure can be effectively used in:

- Rheumatoid arthritis: Experimental studies suggest that PDT can reduce joint inflammation and synovial hyperplasia.
- Periodontitis and gingivitis, where this method is applied in dental settings: PDT targets biofilms and resistant bacteria, improving oral health outcomes.
- Inflammatory bowel disease (IBD): Early-stage research indicates its potential in managing localized intestinal inflammation.

Applications in pediatric diseases

In pediatrics, PDT is emerging as a potential therapeutic approach to address conditions involving inflammation, infections or dental disorders[28]:

- Nephrology and urinary tract infections (UTIs): PDT can serve as an adjunct to antibiotics, targeting multidrug-resistant bacterial strains and reducing recurrent infections in children.[29,30]
- Renal fibrosis: Studies indicate that PDT may inhibit fibroblast proliferation and collagen deposition, which are central to chronic kidney disease (CKD) progression. The potential of PDT in managing CKD offers a ray of hope for future therapeutic approaches.[30]
- Dentistry: PDT's immunomodulatory effects could potentially attenuate systemic inflammation associated with glomerular diseases.[31]

Ophthalmological disorders

Photodynamic therapy, as a highly precise technique, has also found important applications in ophthalmology, where it is commonly employed for[5,7]:

- Age-related macular degeneration: PDT slows the progression of neovascularization and is primarily indicated for the wet form of the disease, which is characterized by abnormal blood vessel growth and may lead to vision loss.
- Non-AMD choroidal neovascularization: PDT is also used to manage neovascularization unrelated to AMD.
- Central serous chorioretinopathy (CSCR): PDT reduces retinal detachment and fluid accumulation.
- Choroidal hemangioma: PDT with verteporfin has been applied as a targeted treatment option.
- Diabetic retinopathy: PDT minimizes angiogenesis and preserves visual acuity.

Photodynamic therapy is widely used in ophthalmology, most commonly with verteporfin as the photosensitizer. It selectively targets choroidal vascular abnormalities, inducing occlusion of affected vessels. Initially, it was extensively applied at full-dose verteporfin for the treatment of neovascular age-related macular degeneration (nAMD). However, when vascular endothelial growth factor (VEGF) receptor inhibitors were detected, the clinical approach has shifted toward other chorioretinal disorders, including central serous chorioretinopathy, polypoidal choroidal vasculopathy and choroidal hemangioma.[32]

Emerging applications in cardiovascular and neurological diseases

Research on PDT is also expanding into novel fields. In atherosclerosis, photodynamic activation of porphyrins has been investigated for targeting atherosclerotic plaques and improving vascular health.[33,34] In neurodegenerative diseases, PDT-mediated clearance of amyloid plaques is being explored as a potential therapeutic approach for Alzheimer's disease.[35]

It was noted that cardiovascular disorders are among the leading causes of death worldwide. Photodynamic therapy can be used to treat atherosclerotic cardiovascular disease (ACD), and the photosensitizing agent should have a specific affinity for macrophages, which are crucial in the development of atherosclerosis.[33] Available studies indicate that PDT using indocyanine green (ICG) is a promising approach for the prevention of restenosis[36] and the treatment of atherosclerosis.[37]

Photodynamic therapy has also shown potential in the field of neurodegenerative diseases. Studies have demonstrated that nano-photosensitizers, such as core–shell azobenzene–spiropyran structures on gold nanoparticles, can inhibit tau protein aggregation in neural cells and promote dendritic growth in neuronal cells.[38]

Advantages of PDT in multisystem diseases

The localized action of PDT, which spares surrounding healthy tissues and produces minimal systemic effects, makes it particularly suitable for delicate pediatric populations and chronic inflammatory conditions. Furthermore, its adaptability to different photosensitizers and light sources broadens its potential for application across diverse pathologies. Table 1[21–24,30,32,34,39–47] provides a structured overview of PDT applications and their clinical relevance. Porfimer sodium, a first-generation photosensitizer, is extensively used in oncology. In contrast, ALA and methyl aminolevulinate (MAL), both second-generation photosensitizers, are more commonly applied in dermatology.[39] Verteporfin is predominantly used in ophthalmology for conditions such as AMD.[5] Additionally, emerging applications in inflammatory and pediatric conditions remain under experimental investigation, with ongoing efforts focused on developing optimized photosensitizers.

Photodynamic procedures with polymeric nanocarriers

Recently, PDT protocols have preferably used encapsulated photosensitizers to target cancer cells more precisely.[47] One of the most applied types is polymeric nanocarriers,[48] such as PEGylated micelles (PEG – polyethylene glycol micelles), poly(lactic-co-glycolic acid) (PLGA) or chitosan nanoparticles, dendrimers, and stimuli-responsive polymerosomes, which are increasingly explored to overcome the pharmacokinetic and selectivity barriers that still limit classical PDT.[49] When we encapsulate hydrophobic photosensitizers, these biodegradable carriers protect them from early degradation, prolong systemic circulation, and favor passive accumulation within cancer tissue by the enhanced-permeation-and-retention effect, and simultaneously enhancing photo-dependent cytotoxicity.

Table 1. Diseases treated with photodynamic therapy (PDT) and commonly used photosensitizers

Disease/condition	Clinical application	Photosensitizers	Light wavelength	Reference
Oncological applications				
Skin cancers (BCC, SCC)	treatment of localized tumors with excellent cosmetic outcomes	Photofrin, Metvixia (MAL), ALA	630–650 nm (red light)	21, 22, 39
Head and neck cancers	ablation of tumors in hard-to-reach areas	Photofrin	630 nm	40
Esophageal cancer	localized destruction of malignant tissues	Photofrin	630 nm	41
Lung cancer	treatment of early-stage or non-resectable tumors	Photofrin	630 nm	42, 43
Non-oncological applications				
Psoriasis	modulation of immune response and keratinocyte proliferation	MAL, ALA	630–650 nm	23
Acne vulgaris	targeting sebaceous glands and *Cutibacterium acnes*	ALA	400–450 nm (blue light)	24
Age-related macular degeneration	neovascularization inhibition	Verteporfin	689 nm (infrared)	34
Central serous chorioretinopathy	fluid accumulation reduction	Verteporfin	689 nm (infrared)	32
Periodontitis and gingivitis	bacterial biofilm reduction in dental applications	Toluidine blue, Methylene blue	630–700 nm	44
Inflammatory conditions				
Rheumatoid arthritis	reducing joint inflammation	photosensitizers under development	experimental range	45
IBD	reducing localized intestinal inflammation	photosensitizers under development	experimental range	46
Pediatric nephrology				
Urinary tract infection	targeting multidrug-resistant bacteria	photosensitizers under development	experimental range	47
Renal fibrosis	mitigation of fibroblast proliferation	photosensitizers under development	experimental range	30

UTIs – urinary tract infections; IBD – inflammatory bowel disease; BCC – basal cell carcinoma; SCC – squamous cell carcinoma; MAL – methyl aminolevulinate; ALA – aminolevulinic acid.

Available studies highlight additional advantages when nanocarrier surfaces are functionalized with antibodies, peptides or small-molecule ligands that actively direct the photosensitizer toward overexpressed cancer biomarkers.[50] At the same time, pH-, redox- or light-cleavable polymer shells allow on-demand release precisely at the tumor target site. Beyond effective drug transport, polymeric platforms provide space to co-load oxygen carriers, immune adjuvants or chemotherapeutics, creating multifunctional "all-in-one" nanoreactors that synergize PDT with diagnostics, immuno- or chemotherapy.[51,52] Early pre-clinical studies already report superior tumor regression and reduced skin phototoxicity compared with free photosensitizers, underlining the clinical promise of polymer-based nanotechnology in both oncological and inflammatory indications.

Limitations

Despite its wide-ranging clinical potential, PDT is limited by shallow light penetration, lack of standardized treatment protocols and the prolonged photosensitivity caused by some photosensitizers. Additionally, many of its emerging applications remain experimental and require further clinical validation to confirm their safety and efficacy.

Conclusions

Photodynamic therapy has evolved into a highly versatile and innovative treatment modality, extending beyond its oncological origins. This technique utilizes the selective activation of photosensitizers through light exposure to induce cytotoxic effects, exhibiting significant efficacy in targeting malignancies while preserving adjacent healthy tissue. Over time, the selectivity and minimally invasive characteristics of PDT have established it as a valuable asset in various clinical fields.

Initially a foundational approach in the management of conditions such as skin cancers, head and neck tumors and internal organ malignancies, PDT has broadened its applications to include dermatological conditions, such as acne and psoriasis, as well as ophthalmological disorders, particularly AMD and diabetic retinopathy. Additionally,

its immunomodulatory properties facilitate the treatment of chronic inflammatory diseases, including rheumatoid arthritis, periodontitis and IBD. There is emerging potential for PDT in pediatric nephrology, addressing UTIs, alleviating inflammation in nephrotic syndrome and mitigating renal fibrosis.

Recent research also highlights the promise of PDT in treating cardiovascular diseases, particularly atherosclerosis, and neurodegenerative conditions, including Alzheimer's disease, thereby expanding its clinical applications. The localized application of PDT minimizes collateral damage to healthy tissues, enhancing its value in sensitive areas such as the eyes or specific areas in pediatric disorders. Its low systemic toxicity ensures patient safety, while its adaptability allows for integration across diverse medical disciplines ranging from oncology to dentistry.

However, PDT is not without challenges. Limited light penetration restricts its efficacy to surface or near-surface lesions, necessitating the development of advanced photosensitizers with improved selectivity and deeper tissue penetration. Additionally, standardized treatment protocols are required to optimize outcomes across a wide range of diseases. Future research should prioritize next-generation photosensitizers and explore combinations with other therapies, such as immunotherapy or nanotechnology, to overcome current limitations and extend PDT's potential.

In conclusion, PDT represents a cutting-edge, minimally invasive treatment that connects traditional methods and modern precision medicine. Its success in oncology and other fields has paved the way for diverse applications, including inflammation management and pediatric nephrology, underscoring its multidisciplinary potential. With advancements in photosensitizer technology and light delivery systems, PDT is poised to play an increasingly significant role in medical practice. By addressing its current challenges and fostering interdisciplinary collaborations, PDT holds the promise of unlocking new therapeutic possibilities and improving patient outcomes across a wide spectrum of diseases.

Use of AI and AI-assisted technologies

Not applicable.

ORCID iDs

Aneta Popiel-Kopaczyk https://orcid.org/0000-0001-5746-4824
Tomasz Stanisław Kręcicki https://orcid.org/0000-0001-9934-5794

References

1. Castano AP, Demidova TN, Hamblin MR. Mechanisms in photodynamic therapy. Part one: Photosensitizers, photochemistry and cellular localization. *Photodiagnosis Photodyn Ther.* 2004;1(4):279–293. doi:10.1016/S1572-1000(05)00007-4
2. Kwiatkowski S, Knap B, Przystupski D, et al. Photodynamic therapy: Mechanisms, photosensitizers and combinations. *Biomed Pharmacother.* 2018;106:1098–1107. doi:10.1016/j.biopha.2018.07.049
3. Zwiebel S, Baron E. PDT in squamous cell carcinoma of the skin. *G Ital Dermatol Venereol.* 2011;146(6):431–444. PMID:22095175.
4. Pinthus JH, Bogaards A, Weersink R, Wilson BC, Trachtenberg J. Photodynamic therapy for urological malignancies: Past to current approaches. *J Urol.* 2006;175(4):1201–1207. doi:10.1016/s0022-5347(05)00701-9
5. Raizada K, Naik M. Photodynamic therapy for the eye. In: *StatPearls*. Treasure Island, USA: StatPearls Publishing; 2025:Bookshelf ID: NBK560686. http://www.ncbi.nlm.nih.gov/books/NBK560686/. Accessed July 17, 2025.
6. Allison RR, Cuenca R, Downie GH, Randall ME, Bagnato VS, Sibata CH. PD/PDT for gynecological disease: A clinical review. *Photodiagnosis Photodyn Ther.* 2005;2(1):51–63. doi:10.1016/S1572-1000(05)00033-5
7. Wormald R, Evans J, Smeeth L, Henshaw K. Photodynamic therapy for neovascular age-related macular degeneration. *Cochrane Database Syst Rev.* 2005;(4):CD002030. doi:10.1002/14651858.CD002030.pub2
8. Hampden-Martin A, Fothergill J, El Mohtadi M, et al. Photodynamic antimicrobial chemotherapy coupled with the use of the photosensitizers methylene blue and temoporfin as a potential novel treatment for *Staphylococcus aureus* in burn infections. *Access Microbiol.* 2021;3(10):000273. doi:10.1099/acmi.0.000273
9. Abrahamse H, Hamblin MR. New photosensitizers for photodynamic therapy. *Biochem J.* 2016;473(4):347–364. doi:10.1042/bj20150942
10. Vázquez-Hernández F, Granada-Ramírez DA, Arias-Cerón JS, et al. Use of nanostructured materials in drug delivery. In: Narayan R, ed. *Nanobiomaterials*. Sawston, UK: Woodhead Publishing; 2018:503–549. doi:10.1016/b978-0-08-100716-7.00020-9
11. Dougherty TJ, Gomer CJ, Henderson BW, et al. Photodynamic therapy. *J Natl Cancer Inst.* 1998;90(12):889–905. doi:10.1093/jnci/90.12.889
12. Agostinis P, Berg K, Cengel KA, et al. Photodynamic therapy of cancer: An update. *CA Cancer J Clin.* 2011;61(4):250–281. doi:10.3322/caac.20114
13. Sun H, Yang W, Ong Y, Busch TM, Zhu TC. Fractionated photofrin-mediated photodynamic therapy significantly improves long-term survival. *Cancers (Basel).* 2023;15(23):5682. doi:10.3390/cancers15235682
14. Kassab K. Photophysical and photosensitizing properties of selected cyanines. *J Photochem Photobiol B.* 2002;68(1):15–22. doi:10.1016/s1011-1344(02)00325-1
15. Lange N, Szlasa W, Saczko J, Chwiłkowska A. Potential of cyanine derived dyes in photodynamic therapy. *Pharmaceutics.* 2021;13(6):818. doi:10.3390/pharmaceutics13060818
16. Allison RR, Downie GH, Cuenca R, Hu XH, Childs CJ, Sibata CH. Photosensitizers in clinical PDT. *Photodiagnosis Photodyn Ther.* 2004;1(1):27–42. doi:10.1016/s1572-1000(04)00007-9
17. Zhao W, Wang L, Zhang M, et al. Photodynamic therapy for cancer: Mechanisms, photosensitizers, nanocarriers, and clinical studies. *MedComm (2020).* 2024;5(7):e603. doi:10.1002/mco2.603
18. Wang X, Luo D, Basilion JP. Photodynamic therapy: Targeting cancer biomarkers for the treatment of cancers. *Cancers (Basel).* 2021;13(12):2992. doi:10.3390/cancers13122992
19. Mali SB, Dahivelkar S. Photodynamic therapy for cancer. *Oral Oncol Rep.* 2024;9:100129. doi:10.1016/j.oor.2023.100129
20. Choromańska A, Kulbacka J, Saczko J. Terapia fotodynamiczna – założenia, mechanizm, aplikacje kliniczne. *Nowa Medycyna.* 2013;1:26–30. https://www.nowamedycyna.pl/wp-content/uploads/2014/10/nm_2013_026-030.pdf.
21. Darlenski R, Fluhr JW. Photodynamic therapy in dermatology: Past, present, and future. *J Biomed Opt.* 2012;18(6):061208. doi:10.1117/1.jbo.18.6.061208
22. Mitra A, Stables GI. Topical photodynamic therapy for non-cancerous skin conditions. *Photodiagnosis Photodyn Ther.* 2006;3(2):116–127. doi:10.1016/S1572-1000(06)00035-4
23. Makuch S, Dróżdż M, Makarec A, Ziółkowski P, Woźniak M. An update on photodynamic therapy of psoriasis: Current strategies and nanotechnology as a future perspective. *Int J Mol Sci.* 2022;23(17):9845. doi:10.3390/ijms23179845
24. Taylor MN, Gonzalez ML. The practicalities of photodynamic therapy in acne vulgaris. *Br J Dermatol.* 2009;160(6):1140–1148. doi:10.1111/j.1365-2133.2009.09054.x
25. Rahimi H, Zeinali R, Tehranchinia Z. Photodynamic therapy of vitiligo: A pilot study. *Photodiagnosis Photodyn Ther.* 2021;36:102439. doi:10.1016/j.pdpdt.2021.102439

26. Shen S, Feng J, Song X, Xiang W. Efficacy of photodynamic therapy for warts induced by human papilloma virus infection: A systematic review and meta-analysis. *Photodiagnosis Photodyn Ther*. 2022;39:102913. doi:10.1016/j.pdpdt.2022.102913
27. Ratkay LG, Waterfield JD, Hunt DWC. Photodynamic therapy in immune (non-oncological) disorders: Focus on benzoporphyrin derivatives. *BioDrugs*. 2000;14(2):127–135. doi:10.2165/00063030-200014020-00006
28. Mazur A, Koziorowska K, Dynarowicz K, Aebisher D, Bartusik-Aebisher D. Photodynamic therapy for treatment of disease in children: A review of the literature. *Children (Basel)*. 2022;9(5):695. doi:10.3390/children9050695
29. Kunisue T, Chen Z, Buck Louis GM, et al. Urinary concentrations of benzophenone-type UV filters in U.S. women and their association with endometriosis. *Environ Sci Technol*. 2012;46(8):4624–4632. doi:10.1021/es204415a
30. Matin SF, Tinkey PT, Borne AT, Stephens LC, Sherz A, Swanson DA. A pilot trial of vascular targeted photodynamic therapy for renal tissue. *J Urol*. 2008;180(1):338–342. doi:10.1016/j.juro.2008.02.042
31. Silva T, Lunardi A, Barros A, et al. Application of photodynamic therapy in pediatric dentistry: Literature review. *Pharmaceutics*. 2023;15(9):2335. doi:10.3390/pharmaceutics15092335
32. Van Dijk EHC, Van Rijssen TJ, Subhi Y, Boon CJF. Photodynamic therapy for chorioretinal diseases: A practical approach. *Ophthalmol Ther*. 2020;9(2):329–342. doi:10.1007/s40123-020-00250-0
33. Oskroba A, Bartusik-Aebisher D, Myśliwiec A, et al. Photodynamic therapy and cardiovascular diseases. *Int J Mol Sci*. 2024;25(5):2974. doi:10.3390/ijms25052974
34. Wańczura P, Aebisher D, Kłosowicz M, Myśliwiec A, Dynarowicz K, Bartusik-Aebisher D. Application of photodynamic therapy in cardiology. *Int J Mol Sci*. 2024;25(6):3206. doi:10.3390/ijms25063206
35. Ding L, Gu Z, Chen H, et al. Phototherapy for age-related brain diseases: Challenges, successes and future. *Ageing Res Rev*. 2024;94:102183. doi:10.1016/j.arr.2024.102183
36. Lin JS, Wang CJ, Li WT. Photodynamic therapy of balloon-injured rat carotid arteries using indocyanine green. *Lasers Med Sci*. 2018;33(5):1123–1130. doi:10.1007/s10103-018-2488-7
37. Houthoofd S, Vuylsteke M, Mordon S, Fourneau I. Photodynamic therapy for atherosclerosis: The potential of indocyanine green. *Photodiagnosis Photodyn Ther*. 2020;29:101568. doi:10.1016/j.pdpdt.2019.10.003
38. Hau-Ting Wei J, Cai-Syaun Wu M, Chiang C, et al. Enhanced photodynamic therapy for neurodegenerative diseases: Development of Azobenzene-Spiropyran@Gold Nanoparticles for controlled singlet oxygen generation. *Chemistry*. 2024;30(62):e202402479. doi:10.1002/chem.202402479
39. Tarstedt M, Gillstedt M, Wennberg Larkö AM, Paoli J. Aminolevulinic acid and methyl aminolevulinate equally effective in topical photodynamic therapy for non-melanoma skin cancers. *Acad Dermatol Venereol*. 2016;30(3):420–423. doi:10.1111/jdv.13558
40. Biel MA. Photodynamic therapy of head and neck cancers. *Methods Mol Biol*. 2010;635:281–293. doi:10.1007/978-1-60761-697-9_18
41. Inoue T, Ishihara R. Photodynamic therapy for esophageal cancer. *Clin Endosc*. 2021;54(4):494–498. doi:10.5946/ce.2020.073
42. Saczko J, Kulbacka J, Chwiłkowska A, Lugowski M, Banaś T. Levels of lipid peroxidation in A549 cells after PDT in vitro. *Rocz Akad Med Bialymst*. 2004;49(Suppl 1):82–84. PMID:15638383.
43. Shafirstein G, Battoo A, Harris K, et al. Photodynamic therapy of non-small cell lung cancer: Narrative review and future directions. *Ann Am Thorac Soc*. 2016;13(2):265–275. doi:10.1513/annalsats.201509-650fr
44. Gallardo-Villagrán M, Leger DY, Liagre B, Therrien B. Photosensitizers used in the photodynamic therapy of rheumatoid arthritis. *Int J Mol Sci*. 2019;20(13):3339. doi:10.3390/ijms20133339
45. Deng B, Wang K, Zhang L, Qiu Z, Dong W, Wang W. Photodynamic therapy for inflammatory and cancerous diseases of the intestines: Molecular mechanisms and prospects for application. *Int J Biol Sci*. 2023;19(15):4793–4810. doi:10.7150/ijbs.87492
46. Huang YY, Wintner A, Seed PC, Brauns T, Gelfand JA, Hamblin MR. Antimicrobial photodynamic therapy mediated by methylene blue and potassium iodide to treat urinary tract infection in a female rat model. *Sci Rep*. 2018;8(1):7257. doi:10.1038/s41598-018-25365-0
47. Li L, Huh KM. Polymeric nanocarrier systems for photodynamic therapy. *Biomater Res*. 2014;18:19. doi:10.1186/2055-7124-18-19
48. Kulbacka J, Choromańska A, Łapińska Z, Saczko J. Natural polymers in photodynamic therapy and diagnosis. *Polim Med*. 2021;51(1):33–41. doi:10.17219/pim/139587
49. Bazylińska U, Kulbacka J, Chodaczek G. Nanoemulsion structural design in co-encapsulation of hybrid multifunctional agents: Influence of the smart PLGA polymers on the nanosystem-enhanced delivery and electro-photodynamic treatment. *Pharmaceutics*. 2019;11(8):405. doi:10.3390/pharmaceutics11080405
50. Bajracharya R, Song JG, Patil BR, et al. Functional ligands for improving anticancer drug therapy: Current status and applications to drug delivery systems. *Drug Deliv*. 2022;29(1):1959–1970. doi:10.1080/10717544.2022.2089296
51. Wang X, Li C, Wang Y, et al. Smart drug delivery systems for precise cancer therapy. *Acta Pharm Sin B*. 2022;12(11):4098–4121. doi:10.1016/j.apsb.2022.08.013
52. Chu S, Shi X, Tian Y, Gao F. pH-responsive polymer nanomaterials for tumor therapy. *Front Oncol*. 2022;12:855019. doi:10.3389/fonc.2022.855019

The historic development of plant virus-like particles as nanocarrier systems for bioactive molecules: Perspective and future opportunities

Milton Naranjo[1,2,A–F], Kyoshi Akimita[3,B–D]

[1] Department of Bionanotechnology, Center for Nanoscience and Nanotechnology, National Autonomous University of Mexico, Mexico City, Mexico
[2] Ensenada Center for Scientific Research and Higher Education, Mexico
[3] Department of Biotechnology, Technological University of Morelia, Mexico

A – research concept and design; B – collection and/or assembly of data; C – data analysis and interpretation;
D – writing the article; E – critical revision of the article; F – final approval of the article

Polymers in Medicine, ISSN 0370-0747 (print), ISSN 2451-2699 (online) *Polim Med*. 2025;55(2):153–164

Address for correspondence
Milton Naranjo
E-mail: milthonnm@outlook.com

Funding sources
None declared

Conflict of interest
None declared

Received on September 22, 2025
Reviewed on September 25, 2025
Accepted on October 13, 2025

Published online on December 19, 2025

Abstract

For several decades, conventional treatments for chronic and degenerative diseases have been constrained by technological limitations, particularly those related to the physicochemical properties, stability and bioavailability of therapeutic molecules, as well as the efficiency of their delivery systems. Medical polymers are widely used in drug delivery to enhance the solubility, stability and controlled release of therapeutic agents, and they can be engineered into nanoparticles (NPs) derived from either natural or synthetic materials. Toward the end of the 20th century, the use of plant viral capsids as supramolecular structures for the packaging and controlled release of therapeutic compounds emerged, introducing a versatile, sustainable and cost-effective strategy that has progressively gained scientific and clinical relevance. Capsid proteins (CPs) derived from plant viruses can act as nanocages for drug encapsulation and delivery, and they can be surface-modified or functionalized with a wide range of biomolecules, including peptides, carbohydrates, functional groups, proteins, and oligonucleotides, through either chemical conjugation or genetic engineering approaches. This review explores the historical development, current biomedical applications, inherent challenges, and future prospects of plant-derived virus-like particles (pVLPs).

Key words: biopolymers, nanomedicine, drug delivery systems, plant viruses, nanocapsules

Cite as
Naranjo M, Akimita K. The historic development of plant virus-like particles as nanocarrier systems for bioactive molecules: Perspective and future opportunities. *Polim Med*. 2025;55(2):153–164. doi:10.17219/pim/211981

DOI
10.17219/pim/211981

Highlights

- Plant-derived virus-like particles (pVLPs) provide a sustainable and multifunctional nanoplatform for drug delivery, enhancing drug solubility, bioavailability and controlled therapeutic release.
- Plant virus capsid proteins act as natural nanocages that enable efficient drug encapsulation, surface modification and targeted delivery through chemical or genetic engineering.
- pVLPs integrate biotechnology and materials science, offering a biocompatible, cost-effective and eco-friendly alternative to synthetic polymer nanoparticles (NPs) in nanomedicine.
- This review article explores the development, biomedical applications, challenges and future prospects of plant virus-based nanostructures in controlled drug delivery and therapeutic innovation.

Introduction

One of the main challenges in the therapeutic management of a wide range of human diseases is maintaining the structural integrity and biological activity of drugs while ensuring their specific, efficient and controlled delivery to target cells and tissues. Nanomedicine, an emerging interdisciplinary field, focuses on the design and development of nanoscale structures for therapeutic, diagnostic and theranostic applications, thereby enhancing the stability, efficacy and overall performance of therapeutic agents. These nanostructures, commonly referred to as nanoparticles (NPs), are typically produced through chemical or physical synthesis methods that require considerable technical expertise, specialized equipment and high-purity chemical reagents. Consequently, their production is often associated with high costs and substantial generation of hazardous waste.[1] In contrast, naturally derived NPs are assembled from polymers of biomolecules such as sugars, lipids, nucleic acids, and proteins, offering lower production costs and greater environmental sustainability.

Among these, virus-like particles (VLPs) are noninfectious, protein-based supramolecular structures that can be produced in various organisms or host cells.[2,3] Virus-like particles produced in plants (pVLPs) provide safe and cost-effective platforms for biomedical applications. In contrast to the production of animal pathogenic viruses, the generation of plant pathogenic viruses for pVLP production does not require high-level biosafety facilities or specialized containment measures and, in most cases, is exempt from strict bioethical regulations.

Moreover, large-scale production in plants is relatively simple, scalable and economically viable, supported by well-established agroinfiltration and transgenic expression strategies. These advantages make pVLPs highly attractive candidates for the development of vaccines, drug delivery systems and diagnostic tools, combining biosafety, high yield and structural fidelity.[3] Since the beginning of the 21st century, pVLPs have attracted growing interest as drug delivery systems due to their biocompatibility, monodispersity and ability to encapsulate or display therapeutic molecules. Numerous comprehensive reviews have been published, showcasing the broad range of applications for pVLPs.[2–7] However, these studies have not addressed the historical challenges and development of these supramolecular structures in nanomedicine. The present review aims to highlight the historical evolution of pVLPs as nanocarriers of bioactive molecules.

Materials and methods

The literature analyzed for this work was retrieved from the PubMed, Google Scholar, Web of Science, and Scopus databases. To maximize the scope of relevant sources, no temporal restrictions were applied to the articles and studies reviewed. The search strategy included terms such as "plant virus," "virus-like particle," "plant virus-like particle," "plant virus capsid," and "plant virus protein nanocages." Nevertheless, the most significant contributions considered in this review are derived from original studies published from the 20th century to the present.

A total of 111 references were selected after applying inclusion criteria that considered only peer-reviewed publications presenting relevant and original contributions (excluding replications of previous studies or works with minor variations). The selected articles were carefully evaluated and mapped along a timeline, with 11 identified as representative historical milestones. In addition, other selected works were analyzed in relation to key concepts that have guided the evolution of medical perspectives, as well as current applications and future prospects.

Early development of the concept of viruses as potentially therapeutic tools

With the advancement of medical knowledge during the 18th and 19th century, bacteria, fungi, protozoa, and viruses were exclusively considered infectious agents capable of affecting both animals and plants. This view persisted for

almost 3 centuries, until the introduction of concepts such as microbiota – though mentioned since the 20th century, it was widely popularized in the 21st century – which redefines the relationships between host and pathogen. It is now recognized that some microorganisms that are pathogenic to certain species can be harmless, or even beneficial, to others, establishing cooperative consortia resulting from long evolution process.[8,9] During the past century this new paradigm allowed for a revival and expansion of Félix d'Herelle's vision, who in the early 20th century proposed the use of bacteriophages (viruses that infect bacteria) as specific antimicrobial therapeutic agents, without affecting human health.[10,11] Although his proposals initially did not succeed, by the end of the last century and up to the present day, phage therapy has a broad research focus[12] resulting in the commercial use of phages approved by the U.S. Food and Drug Administration (FDA) in 2006.[13] With this new approach, the idea of using viruses as polymeric systems for therapeutic purposes has increased in recent years.

Another important concept that contributed to the development of VLPs for drug delivery was the use of viral particles in vaccine generation. From the smallpox vaccine developed by Edward Jenner in the late 18th century to the end of the 20th century, viruses were utilized in vaccine production, broadening the understanding of viral particles as therapeutic tools.[14]

By the 1980s, novel strategies emerged based on the encapsulation of genetic material and the use of VLPs for vaccine development, establishing one of the earliest precedents for employing viruses as carriers of therapeutic agents.[15,16] In particular, plant pathogenic viruses have demonstrated remarkable potential in biomedical applications, and with ongoing advances in nanotechnology and molecular biology, their capacity for therapeutic delivery continues to expand.[3,10,17,18]

What is nanotechnology and where was it born?

Although it is difficult to precisely define the boundaries of the "nano" classification, the term "nano" is generally used to describe structures or molecules ranging in size from 1 to 200 nanometers (nm), whereas nanotechnology refers to the application of such materials in various scientific and industrial contexts. Nanoscience, in turn, focuses on the study, design and generation of structures at the nanoscale.[1,19–21]

When these findings are applied to address specific problems, the field of nanotechnology emerges. The term 'nanotechnology' was first introduced in 1959 by physicist Richard Feynman during the annual meeting of the American Physical Society.[22] However, it was in 1974 that Norio Taniguchi formally defined it as a set of tools and techniques for the separation, consolidation and formation of materials at the atomic or molecular level.[23]

Building on these principles, nanotechnology has advanced toward the development of nanostructures through 2 main approaches: the "top-down" and "bottom-up" methods, each with distinct implications for quality, precision and production costs. Although historical records indicate the use of NPs as early as the 4th century in the Roman Empire, true mastery of nanotechnology – including its synthesis, modeling, modification, and application – has emerged only within the past few decades.

A major turning point was the development of the scanning tunneling microscopy (STM), a technique that enabled the visualization and manipulation of individual atoms. In 1983, the STM was used to reconstruct the surface of silicon (111)-7×7, and in 1990, a team led by Don Eigler at IBM manipulated 35 xenon atoms on a nickel surface to form the company's logo.

These milestones demonstrated, for the first time, the ability to control matter at the atomic level, sparking global scientific interest in the manipulation of NPs.[24–26] Both nanoscience and nanotechnology are relatively recent disciplines, as work at the nanoscale requires techniques that have only become available in the past few decades. Both fields are expanding rapidly and have revealed enormous potential for the development of future technological applications.[5,27]

Bio-nanomedicine

Initially, nanotechnology focused on addressing challenges in the chemical sciences, such as the development of new materials for industrial applications. However, its uses and applications soon expanded across multiple disciplines. In particular, nanomaterials began to offer solutions to long-standing problems in medicine, serving as strategies for the transport of poorly soluble drugs and for targeted delivery to hard-to-reach sites such as the brain and tumors.[5,25,28]

From the applications of classical nanotechnology across various scientific fields, modern nanotechnology emerged, integrating principles from chemistry, electronics, physics, and biology.[29–34] In the biological sciences, advances in biomaterials and biomolecular research have been particularly beneficial, enabling the development of biologically derived NPs with strong potential for medical and therapeutic applications.[19] One of the most important properties of biomaterials is their biocompatibility, i.e., their ability to avoid activating the immune system, which makes many nanosystems ideal for therapeutic applications.[35–39] This is particularly relevant for NPs that structurally resemble viruses.[18,40–42]

The term 'nanomedicine' was first coined in the 1990s by Eric Drexler and collaborators in the book *Unbounding the Future: The Nanotechnology Revolution*,[43] and was later formally defined in 1999 in the book *Nanomedicine*.[44] Since then, the discipline was consolidated as a science

with the incorporation of nanomaterials into therapeutic strategies.

Despite its relatively recent origin, nanomedicine has undergone rapid expansion driven by technological advances. One of its most promising branches is bionanomedicine, which applies nanotechnological methods and biomaterials for the diagnosis, monitoring and treatment of diseases at the cellular level. This approach focuses on the interaction and modification of biomolecules such as extracellular vesicles, proteins, mRNA, and viral particles.[1,41,45–47]

Virus-like particles

Virus-like particles are natural nanosystems derived from native viral structures that lack infectious capability. These NPs can be produced using a variety of methods and expression systems, including cultivation in plant, mammalian, insect, or bacterial hosts. They can also be generated recombinantly through genetic engineering and molecular biology techniques (Fig. 1).

The capsid proteins (CPs) that make up the VLPs are quite resilient, measuring only a few nanometers, have the ability to self-assemble and are biocompatible. The self-assembly capability of the CP allows for the trapping and transport of drugs in VLPs to prevent premature degradation and facilitate their delivery while improving bioavailability in the system.[6,48,49] Since the early 21st century, a wide variety of drugs and other therapeutic agents have been encapsulated using the proteins that form the capsid of viruses as nanocages.[50–53]

One of the first viral particle systems for the delivery of molecules was developed by Zhou et al. using papillomavirus to activate the immune response against tumor models with defined epitopes.[51] Subsequently, Braun et al. used polyoma VP1 to encapsulate oligonucleotides and DNA plasmids,[54] and in 2000, a system based on the capsid of the papillomavirus was used to transport epitopes and activate the cytotoxic response of T lymphocytes, inducing an improvement in the immune response against the tumor.[55] In the following years, VLPs began to be used for the packaging of therapeutic molecules targeting cancer by various research groups with distinct approaches, primarily focusing on disease contexts in which dosage, solubility and specificity represented the greatest challenges.[2,6,7,30,56–58]

The loading of VLPs can occur through electrochemical processes that promote the assembly of the CP around the therapeutic cargo or through pH-induced pore opening, which allows the cargo to be adsorbed. However, one limitation of VLPs is that the cargo must be compatible with the electrostatic charge and internal cavity diameter of the particle, restricting the number and size of molecules that can be encapsulated.[59–61]

Virus-like particles based on plant viruses

Currently, much of the research on VLPs focuses on obtaining capsids from plant pathogenic viruses, as their manipulation and inoculation are simpler than those of animal viruses and they do not pose biological risks. Plant viruses generally exhibit 2 main structural types: rod-like forms, such as the tobacco mosaic virus (TMV), and icosahedral forms, such as the cowpea chlorotic mottle virus (CCMV) of the Bromovirus genus – both of which are widely used as nanocarriers (Fig. 2). Regardless of their structure, viruses possess functional groups on their surfaces that can be used to anchor molecules such as antibodies or peptides, thereby improving targeting and enhancing therapeutic efficacy.[59,60,62,63]

Plant virus-like particle platforms for drug delivery emerged in the early 21st century, with several key studies

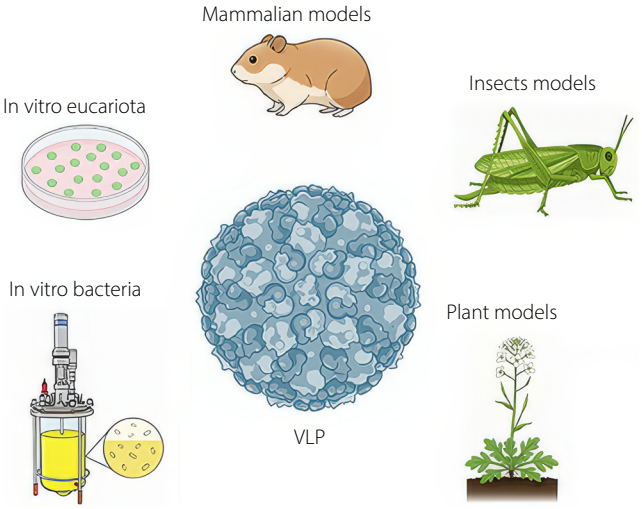

Fig. 1. Graphical representation of the production host systems for virus-like particles (VLPs).

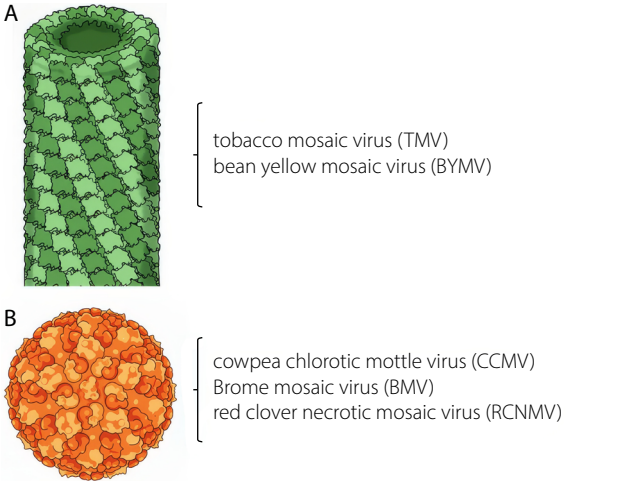

Fig. 2. Main structural types of plant virus-like particles (pVLPs) commonly used for pVLP production. A. Cylindrical or filamentous structure; B. Icosahedral structure

demonstrating the ability of these viruses to transport cargos other than their genetic material and, subsequently, to deliver poorly water-soluble chemotherapeutic agents such as doxorubicin (Table 1).[15,17,29,42,50,59,60,62,64–80] However, one of the main advantages of using plant viruses as nanocarriers resulted in relatively simple production, low resource demand, high yield of virus per gram of infected leaf, and rapid purification of these.[3,18]

These characteristics, combined with the ease of production, storage and manipulation of this type of virus, are rarely found in other types of infectious viruses for humans, giving pVLPs an almost unbeatable advantage as biomaterials.

Encapsulation techniques

There are 2 main methods for loading the internal cavity of a VLP with cargo: reassembly of the CP around a negatively charged core, or infusion through pore opening. To induce pore expansion, the native virus and the cargo are incubated together under mildly alkaline conditions.[42,59,65,81] Under acidic conditions, VLPs maintain their native conformation, whereas under alkaline pH conditions, their pores open, allowing the entry of cargo molecules in contact with them (Fig. 3A).[82–84] However, it should be clarified that this method is limited by the pore size of the virus, so larger particles than that size will not be able to enter the internal cavity of the virus; for those purposes, encapsulation protocols through CP self-assembly

Table 1. Biomedical applications of plant virus-like particles (pVLPs) as nanocarrier systems

pVLP platform	Cargo	Application	Reference
Tobacco mosaic virus (TMV)	epitope	vaccine generation	Haynes et al., 1986[15]
Papaya mosaic virus (PapMV)	epitope	vaccine generation / Immunomodulation	Lacasse et al., 2008[17]
Brome mosaic virus (BMV) and cowpea chlorotic mottle cirus (CCMV)	chemotherapeutic drugs	cancer	Tejeda-Rodríguez et al., 2019[29]
Hibiscus chlorotic ringspot virus (HCRV)	polyacids	exploratory / possible drug delivery	Ren et al., 2006[42]
Physalis mottle virus (PhMV)	several fluorescent agents and chemotherapeutic drugs	theranostic for cancer	Masarapu et al., 2017[50]
Brome mosaic virus (BMV)	metallic nanoparticles	exploratory	Xie et al., 2021[59]
Cowpea chlorotic mottle virus (CCMV)	RNA	exploratory / gene therapy	Cadena-Nava et al., 2012[60]
Cowpea chlorotic mottle virus (CCMV)	RNA and ssRNA	exploratory / gene therapy	Comas-Garcia et al., 2012[62]
Brome mosaic virus (BMV)	metallic nanoparticles	imagining	Dragnea et al., 2003[64]
Red clover necrotic mosaic virus (RCNMV)	chemotherapeutic drugs	cancer therapy	Cao et al., 2014[65]
Cowpea chlorotic mottle virus (CCMV)	anionic polymer	exploratory / general drug delivery	Douglas and Young, 1998[66]
Johnson grass chlorotic stripe mosaic virus (JgCSMV)	chemotherapeutic drugs	cancer therapy	Alemzadeh et al., 2019[67]
Tomato bushy stunt virus (TBSV)	peptide	cancer therapy	Marchetti et al., 2023[68]
Bamboo mosaic virus (BaMV)	fluorescent antibody	imagining	Kuo et al., 2018[69]
Potato virus X (PVX)	tumor antigen	immunomodulation / cancer vaccine generation	Jobsri et al., 2015[70]
Cowpea mosaic virus (CPMV)	protein	immunomodulation / cancer therapy	Chatterji et al., 2004[71]
Cowpea mosaic virus Capsid	carbohydrates	immunomodulation / cancer therapy	Miermont et al., 2008[72]
CPMV, PVX, TMV, and BMV	several fluorescent agents	imagining	Wen et al., 2012[73]
Cowpea mosaic virus (CPMV)	fluorescent agent and antibodies	imagining	Sapsford et al, 2006[74]
Tobacco mosaic virus (TMV)	antibodies, peptides and several therapeutic molecules	exploratory/ general drug delivery / vaccine generation	Kriwaczek et al., 1978[75]
Tobacco mosaic virus (TMV)	peptides	vaccine generation	Fearney et al., 1971[76]
Physalis mottle virus (PhMV)	chemotherapeutic drugs	cancer therapy	Hu and Steinmetz, 2020[77]
Tobacco mosaic virus (TMV)	fluorescent agent	imagining	Qiu et al., 2022[78]
Tobacco mosaic virus (TMV)	peptides	vaccine generation	Sugiyama et al.,1995[79]
Cowpea chlorotic mottle virus (CCMV)	peptides	cancer therapy	Wu et al., 2017[80]

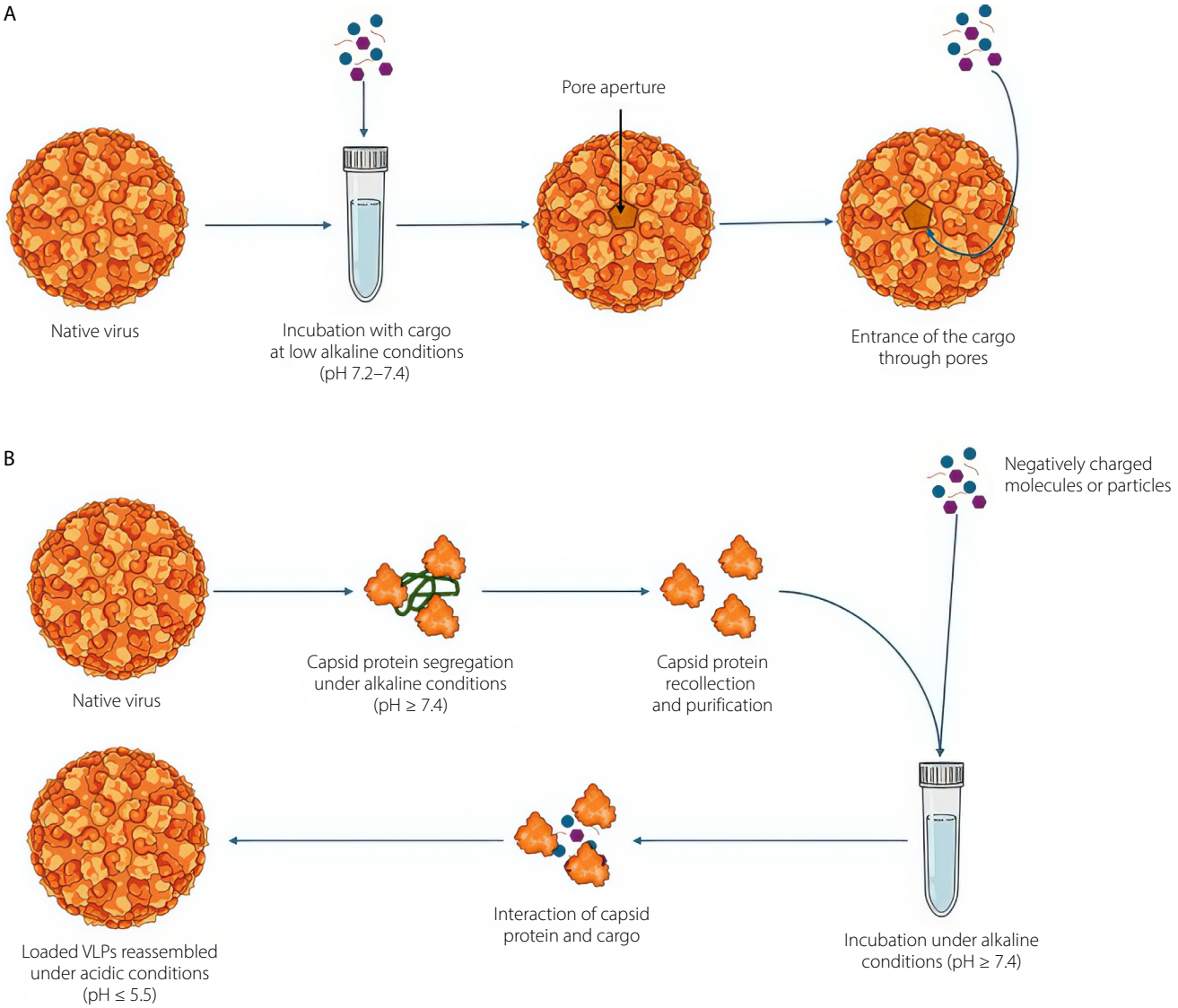

Fig. 3. Loading methods in virus-like particles (VLPs). A. Schematic representation of diffusion through pore apertures; B. Schematic representation of loading via the disassembly–reassembly method

are suggested. The self-assembly capability of viruses was first explored in 1955 through successful reconstruction of TMV in vitro.[85] By the end of the 1960s, the assembly mechanisms of TMV were well known,[86,87] and during the following decade, the self-assembly mechanisms of icosahedral plant viruses were studied and described.[63] The reconstruction of the particles is first achieved by purifying the CP, generally subjecting the viruses to high ionic strength conditions, resulting in the disassembly of the virions into proteins and nucleic acids. At that point, the proteins are recovered and the nucleic acids are removed. The protein must be purified before attempting to assemble the cargo. To achieve assembly, the CP is incubated in cycles with the cargo under high ionic strength conditions, followed by incubation or dialysis against an acidic pH buffer solution (Fig. 3B). These changes in electrostatic forces promote the binding of positively charged amino residues inside the capsid to the core, which must have a negative electrostatic charge.[53,60,64,66] Since then, this field of research has developed significantly.

Recently, a strategy based in the infusion using metal ions and pH-dependent reversible mechanisms has been developed.[65,67] This approach relies on the opening of capsid pores induced by abrupt pH changes: At acidic values, the particles retain their native conformation, whereas under basic conditions, the pores open and permit the incorporation of molecules of interest.

Structural modifications

Almost half of the virus families have icosahedral geometry, with CPs that facilitate assembly and disassembly to introduce the cargo. The proteins that form the surface, called “coat proteins”, contain lysine, cysteine and aspartic/glutamic acid residues that can be modified or used

as an anchoring platform for other molecules. The main types of functionalization are based on the conjugation of biomolecules (bioconjugation) such as antibodies, peptides, oligonucleotides, or carbohydrates[68–72]; however, fuctionalization can be also achieved with organic and inorganic molecules, such as drugs (Fig. 4), various chemical agents, such as N-hydroxysuccinimide (NHS), polyethylene glycol (PEG), biotin, or carbodiimide, as well as through genetic modification methods.[71,73,74]

The first approach of the conjugation of a VLPs was made by Frank et al. in 1971; They conjugated a decapeptide representing a fraction of the TMV CP to a succinylated bovine serum albumin and observed an immunization effect in rabbits. Years before, Kriwaczek et al. conjugated molecules of α-melanotropin to TMV virus like particles, creating the first conjugated plant VLP.[75,76] First spherical fitovirus to be functionalized was the CCMV, by Wang et al.[3,88] Hydrazone conjugation is a relatively recent chemoselective strategy that enables the sequential and controlled introduction of multiple peptides by regulating the reaction conditions. This technique demonstrates high chemoselectivity, with the resulting products exhibiting absorbance around 350 nm. The method is based on the reaction between a terminal hydrazine group on the substrate and benzaldehyde-functionalized VLPs. Hydrazone chemistry is particularly valuable for conjugating VLPs with ligands that are unstable under click chemistry conditions.[10,77,78]

Biomedical applications

The use of VLPs has considerably expanded across the spectrum of biological and medical sciences, having outstanding applications for both areas. With VLPs, it is possible to perform gene therapy, diagnostic utility testing, targeted delivery systems, and vaccine development.[2,5,6,89–91] These applications have supported the development of therapeutic strategies for the treatment of cancer, neuropathological disorders and other diseases of genetic origin.

Targeted delivery

The proper administration of therapeutic drugs has 2 challenges: correct dose delivery and the reduction of side effects through targeted delivery.[27,48,92] The ideal drug dose is determined by balancing bioavailability and concentration to achieve therapeutic efficacy. However, this balance is often disrupted by physiological processes that degrade the active compound before it reaches its target site. To compensate, drug concentrations are frequently increased, which can lead to adverse side effects resulting from excessive exposure of healthy tissues to the drug.[93–95] As other NPs, the application of VLPs ensures the integrity of the dose until it is delivered specifically. It is achieved through bioconjugation techniques, but in contrast with other NPs, the VLPs and pVLPs exhibit chemical groups allowing to be conjugated with molecules of different natures that respond to indicated situations without previous modifications; e.g., in conjugation with antibodies, the particle recognizes a receptor on the cell and triggers a response. Other molecules such as peptides, carbohydrates and nucleic acids are also used to direct therapy to specific cells and they can be anchored directly to the VLP or pVLP on the surface.[6,96] Meanwhile, other classes of NPs, such as metallic NPs or mesoporous silica NPs, require the addition of chemical groups to which other molecules can be anchored through chemical modifications performed

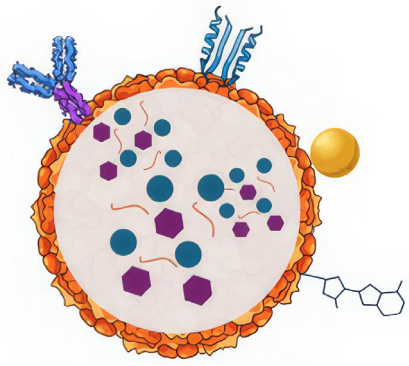

Functionalization	Method	Possible application
Antibodies	**Genetic/Chemical**	Improving selectivity Immune stimulation
Peptides	**Genetic/Chemical**	Improving selectivity Cytotoxic effect Immune stimulation Antimicrobial activity
Nanoparticles	**Chemical**	Biomedical imaging Phototherapy Thermal therapy Antimicrobial activity
Chemical compounds (antigens, drugs, metabolites)	**Chemical**	Improving selectivity Immune stimulation Cytotoxic effect

Fig. 4. Surface modifications in virus-like particles (VLPs): methods and potential applications

either during or after synthesis. Similarly, various mechanisms employ strategies that exploit disease-specific conditions – e.g., the acidic environment of the tumor microenvironment (TME), where pH changes are utilized to trigger the release of chemotherapeutic agents.[97–99] Other NPs have exhibited toxic effects and failed to induce the desired pro-inflammatory response. These side effects are associated with factors such as surface charge and size polydispersity of the NPs.[100] Monodispersity has been identified as an important characteristic for efficient cellular uptake.[101] Through evolutionary processes, viruses achieved monodisperse size – a feature that can be exploited to minimize unwanted activation of the inflammatory response. Consequently, VLPs and pVLPs can function as targeted delivery systems that help reduce undesirable toxic or proinflammatory effects.[3,18,102]

Immunomodulation

The immunomodulatory activity of VLPs is related to the mimicry they can have with wild viruses. Like a wild virus, VLPs are capable of activating the immune response at the humoral or innate level. The size and structure of VLPs alert antigen-presenting dendritic cells, which will subsequently initiate the action chain of the adaptive response, but they can also be recognized by toll-like receptors (TLR) of the innate system.[103] Some clinical studies have used viral particles from pathogenic viruses such as influenza and have reported the induction of an effective immune response (both humoral and cellular), which has allowed the development of vaccines, findings in immunotherapy and the fight against immunodeficiency.[103–105] Through recombinant DNA and genetic engineering methods, chimeric VLPs can be synthesized that express short sequences of peptides or proteins, which allows for the maintenance of peptide integrity and achieving optimal therapeutic activity.[68,79] This strategy has been used both for vaccine development and recruitment of immune system cells in tumors.

Vaccine production

There is a wide variety of approved vaccines based on VLPs, and many more are in development or clinical trial phases. Some of the VLP-based vaccines on the market include CervarixVR (HPV), Gardasil, Gardasil 9, and Merck and Co., Inc.'s Recombivax HBVR.[106] The immune response to these vaccines focuses on the recombination of the particle with specific antigens that generate immunity, the delivery of RNA transcripts that will be translated to produce the immunogenic response, or the delivery of specific antigens.[56,107,108] The transport of specific epitopes in VLPs for vaccines has demonstrated the ability to generate memory in immunity, leaving the immune system prepared for an infection event, in addition to being able to fully transport the epitopes.[7,58] Complementarily, VLPs offer a solid and well-designed alternative platform for the development of cancer vaccines. Various working groups have created cancer vaccines using VLPs for different types of cancer.[51,52,99] In addition to strategies that display epitopes on the surface of the VLP, other strategies use VLPs to transport mRNA transcripts to induce immunity against certain types of cancer.[58] Vaccines based on pVLPs began to be developed in the previous century. The first pVLP vaccine candidates were generated using TMV as a platform.[15,76] Plant viruses such as TMV and CCMV have shown promising characteristics for vaccine development, including biocompatibility, efficient and selective immune activation, and well-described genetic and phenotypic profiles that make them highly amenable to modification. Additionally, the production costs of these vaccine platforms are comparatively low. Despite having great utility and good results in this field, the greatest benefit that VLPs provide to vaccine development is the broad potential for improvement they present.

Discussion

Historically, viruses have been regarded as agents of disease and epidemics, a perception that has long shaped the public consciousness. However, with the technological and scientific advances of the contemporary era, it is now recognized that viruses can also function as bio-nanoparticles (bio-NPs) with a wide range of biotechnological and medical applications (Fig. 5).

The self-assembly capability allows for effective encapsulation of therapeutic and theranostic molecules, such as antigens, fluorescent markers, metals, and drugs, facilitating targeted delivery to tissues or organs.[66,95,98,109] Given their capacities, CP proteins can be used, designed and modified to produce natural, safe, stable and biodegradable nanocages for therapeutic purposes.

On the other hand, VLPs have also positioned themselves in the fields of vaccine generation. Compared to traditional vaccines, which are often produced from an attenuated or inactivated viral strain, genome-free VLPs allow for the transport of RNA transcripts or isolated antigens that enable the activation of the immune response, offering innovative alternatives that are safe.[7,72,106,107] The variety of VLPs makes them structurally attractive and functionally diverse, allowing them to be designed to carry antigenic molecules to specific target tissues. Nevertheless, most of commercial VLP based vaccines use mammalian viruses as platform.[106] Consequently, the production methods, storage and transportation requires more resources, and bioethical considerations that significantly influence the costs and availability of these vaccines. In contrast, plant viruses can be easily propagated, facilitating the large-scale production of p-VLPs and potentially reducing

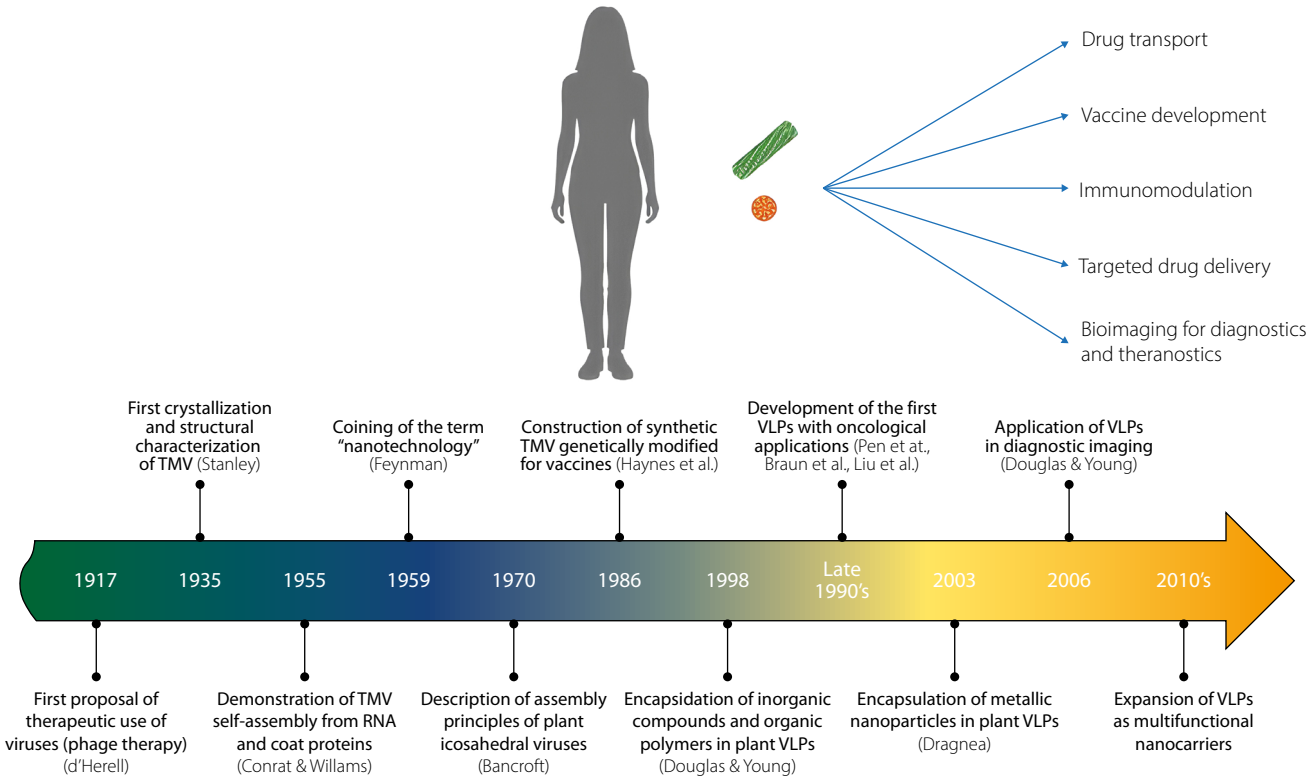

Fig. 5. Historical milestones in the development and application of plant virus-like particles (pVLPs)

costs. Furthermore, viruses such as TMV and its mutants exhibit significant temperature resistance,[110,111] eliminating the need for preserving a cold chain.

Although the development of VLPs is relatively recent, it has been demonstrated that they have enormous potential to resolve therapeutic problems.[3,6,49]

Limitations

This study provides a comprehensive analysis of key works that have contributed to the development of pVLPs for biomedical applications, from their initial conceptualization in the past century till now. It is important to emphasize that although some of the studies discussed here describe the physicochemical properties of pVLPs and fundamental proof-of-concept experiments (e.g., CP reassembly and NP encapsidation), the primary focus was on those that demonstrated biotherapeutic applications or represented pioneering exploratory efforts that have driven the advancement of pVLPs in biomedical research.

Conclusions

This work has explored the development of pVLPs as nanocarriers in the emerging era of nanomedicine, encompassing their use in the delivery of novel therapeutic agents, antigen presentation, and the enhancement of existing drugs through improved bioavailability, solubility and stability.

The comprehensive compilation of the most relevant findings and historical studies is important for understanding the development of pVLPs, as well as recent advances that demonstrate their current applications, relevance and future potential. Furthermore, this review highlights the inherent advantages of pVLP production methods and the mechanisms by which drug loading is achieved, providing an overview of their therapeutic promise.

Finally, new technologies and methodologies may further enhance pVLP production, loading strategies and biomedical applications. Future studies should also focus on evaluating key characteristics such as structural integrity, safety and potential toxicity during the preclinical stage.

Use of AI and AI-assisted technologies

Not applicable.

ORCID iDs

Milton Naranjo https://orcid.org/0000-0003-1397-0017

References

1. Satalkar P, Elger BS, Shaw DM. Defining nano, nanotechnology and nanomedicine: Why should it matter? *Sci Eng Ethics*. 2016;22(5):1255–1276. doi:10.1007/s11948-015-9705-6
2. Chroboczek J, Szurgot I, Szolajska E. Virus-like particles as vaccine. *Acta Biochim Pol*. 2014;61(3):531–539. PMID:25273564.

3. Alemzadeh E, Dehshahri A, Izadpanah K, Ahmadi F. Plant virus nanoparticles: Novel and robust nanocarriers for drug delivery and imaging. *Coll Surf B Biointerfaces*. 2018;167:20–27. doi:10.1016/j.colsurfb.2018.03.026
4. Mejía-Méndez JL, Vazquez-Duhalt R, Hernández LR, Sánchez-Arreola E, Bach H. Virus-like particles: Fundamentals and biomedical applications. *Int J Mol Sci*. 2022;23(15):8579. doi:10.3390/ijms23158579
5. Boisgérault F, Morón G, Leclerc C. Virus-like particles: A new family of delivery systems. *Exp Rev Vaccines*. 2002;1(1):101–109. doi:10.1586/14760584.1.1.101
6. He J, Yu L, Lin X, et al. Virus-like particles as nanocarriers for intracellular delivery of biomolecules and compounds. *Viruses*. 2022;14(9):1905. doi:10.3390/v14091905
7. Tissot AC, Renhofa R, Schmitz N, et al. Versatile virus-like particle carrier for epitope based vaccines. *PLoS One*. 2010;5(3):e9809. doi:10.1371/journal.pone.0009809
8. Hayes W, Sahu S. The human microbiome: History and future. *J Pharm Pharm Sci*. 2020;23:406–411. doi:10.18433/jpps31525
9. Prescott SL. History of medicine: Origin of the term microbiome and why it matters. *Hum Microb J*. 2017;4:24–25. doi:10.1016/j.humic.2017.05.004
10. Sokullu E, Soleymani Abyaneh H, Gauthier MA. Plant/bacterial virus-based drug discovery, drug delivery, and therapeutics. *Pharmaceutics*. 2019;11(5):211. doi:10.3390/pharmaceutics11050211
11. d'Herelle F. Bacteriophage as a treatment in acute medical and surgical infections. *Bull N Y Acad Med*. 1931;7(5):329–348. PMID:19311785. PMCID:PMC2095997.
12. Soothill JS. Treatment of experimental infections of mice with bacteriophages. *J Med Microbiol*. 1992;37(4):258–261. doi:10.1099/00222615-37-4-258
13. Leverentz B, Conway WS, Camp MJ, et al. Biocontrol of *Listeria monocytogenes* on fresh-cut produce by treatment with lytic bacteriophages and a bacteriocin. *Appl Environ Microbiol*. 2003;69(8):4519–4526. doi:10.1128/AEM.69.8.4519-4526.2003
14. Jenner E. On the origin of the vaccine inoculation. *Med Phys J*. 1801;5(28):505–508.
15. Haynes JR, Cunningham J, Von Seefried A, Lennick M, Garvin RT, Shen SH. Development of a genetically-engineered, candidate polio vaccine employing the self-assembling properties of the tobacco mosaic virus coat protein. *Nat Biotechnol*. 1986;4(7):637–641. doi:10.1038/nbt0786-637
16. Karacostas V, Nagashima K, Gonda MA, Moss B. Human immunodeficiency virus-like particles produced by a vaccinia virus expression vector. *Proc Natl Acad Sci U S A*. 1989;86(22):8964–8967. doi:10.1073/pnas.86.22.8964
17. Lacasse P, Denis J, Lapointe R, Leclerc D, Lamarre A. Novel plant virus-based vaccine induces protective cytotoxic T-lymphocyte-mediated antiviral immunity through dendritic cell maturation. *J Virol*. 2008;82(2):785–794. doi:10.1128/JVI.01811-07
18. Blandino A, Lico C, Baschieri S, et al. In vitro and in vivo toxicity evaluation of plant virus nanocarriers. *Coll Surf B Biointerfaces*. 2015;129:130–136. doi:10.1016/j.colsurfb.2015.03.039
19. Hulla J, Sahu S, Hayes A. Nanotechnology: History and future. *Hum Exp Toxicol*. 2015;34(12):1318–1321. doi:10.1177/0960327115603588
20. Jones MG, Blonder R, Gardner GE, Albe V, Falvo M, Chevrier J. Nanotechnology and nanoscale science: Educational challenges. *Int J Sci Educ*. 2013;35(9):1490–1512. doi:10.1080/09500693.2013.771828
21. Whatmore RW. Nanotechnology: What is it? Should we be worried? *Occup Med (Lond)*. 2006;56(5):295–299. doi:10.1093/occmed/kql050
22. Feynman RP. There's plenty of room at the bottom [data storage]. *J Microelectromech Syst*. 1992;1(1):60–66. doi:10.1109/84.128057
23. Taniguchi N. On the basic concept of nanotechnology. In: *Proceedings of the International Conference on Production Engineering*. Tokyo, Japan: Tokyo Science University; 1974:18–23.
24. Binnig G, Rohrer H, Gerber Ch, Weibel E. 7 × 7 reconstruction on Si(111) resolved in real space. *Phys Rev Lett*. 1983;50(2):120–123. doi:10.1103/PhysRevLett.50.120
25. Bayda S, Adeel M, Tuccinardi T, Cordani M, Rizzolio F. The history of nanoscience and nanotechnology: From chemical–physical applications to nanomedicine. *Molecules*. 2019;25(1):112. doi:10.3390/molecules25010112
26. Eigler DM, Schweizer EK. Positioning single atoms with a scanning tunnelling microscope. *Nature*. 1990;344(6266):524–526. doi:10.1038/344524a0
27. Patra JK, Das G, Fraceto LF, et al. Nano based drug delivery systems: Recent developments and future prospects. *J Nanobiotechnol*. 2018;16(1):71. doi:10.1186/s12951-018-0392-8
28. Krukemeyer MG, Krenn V, Huebner F. History and possible uses of nanomedicine based on nanoparticles and nanotechnological progress. *J Nanomed Nanotechnol*. 2015;6(6):1–7. doi:10.4172/2157-7439.1000336
29. Tejeda-Rodríguez JA, Núñez A, Soto F, et al. Virus-based nanomotors for cargo delivery. *ChemNanoMat*. 2019;5(2):194–200. doi:10.1002/cnma.201800403
30. Mohan T, Kim J, Berman Z, Wang S, Compans RW, Wang BZ. Co-delivery of GPI-anchored CCL28 and influenza HA in chimeric virus-like particles induces cross-protective immunity against H3N2 viruses. *J Control Release*. 2016;233:208–219. doi:10.1016/j.jconrel.2016.05.021
31. Kankala RK, Han YH, Xia HY, Wang SB, Chen AZ. Nanoarchitectured prototypes of mesoporous silica nanoparticles for innovative biomedical applications. *J Nanobiotechnol*. 2022;20(1):126. doi:10.1186/s12951-022-01315-x
32. Rosenholm JM, Peuhu E, Bate-Eya LT, Eriksson JE, Sahlgren C, Lindén M. Cancer-cell-specific induction of apoptosis using mesoporous silica nanoparticles as drug-delivery vectors. *Small*. 2010;6(11):1234–1241. doi:10.1002/smll.200902355
33. Phillips E, Penate-Medina O, Zanzonico PB, et al. Clinical translation of an ultrasmall inorganic optical-PET imaging nanoparticle probe. *Sci Transl Med*. 2014;6(260):260ra149. doi:10.1126/scitranslmed.3009524
34. Anik MI, Mahmud N, Al Masud A, Hasan M. Gold nanoparticles (GNPs) in biomedical and clinical applications: A review. *Nano Select*. 2022;3(4):792–828. doi:10.1002/nano.202100255
35. Tarn D, Ashley CE, Xue M, Carnes EC, Zink JI, Brinker CJ. Mesoporous silica nanoparticle nanocarriers: Biofunctionality and biocompatibility. *Acc Chem Res*. 2013;46(3):792–801. doi:10.1021/ar3000986
36. Kyriakides TR, Raj A, Tseng TH, et al. Biocompatibility of nanomaterials and their immunological properties. *Biomed Mater*. 2021;16(4):042005. doi:10.1088/1748-605X/abe5fa
37. Merlo A, Mokkapati VRSS, Pandit S, Mijakovic I. Boron nitride nanomaterials: Biocompatibility and bio-applications. *Biomater Sci*. 2018;6(9):2298–2311. doi:10.1039/C8BM00516H
38. Patel V, Rajani C, Tambe V, et al. Nanomaterials assisted chemo-photothermal therapy for combating cancer drug resistance. *J Drug Deliv Sci Technol*. 2022;70:103164. doi:10.1016/j.jddst.2022.103164
39. Ramos AP, Cruz MAE, Tovani CB, Ciancaglini P. Biomedical applications of nanotechnology. *Biophys Rev*. 2017;9(2):79–89. doi:10.1007/s12551-016-0246-2
40. Ratner BD, Bryant SJ. Biomaterials: Where we have been and where we are going. *Annu Rev Biomed Eng*. 2004;6(1):41–75. doi:10.1146/annurev.bioeng.6.040803.140027
41. Banik BL, Brown JL. Polymeric biomaterials in nanomedicine. In: Kumbar SG, Laurencin CT, Deng M, eds. *Natural and Synthetic Biomedical Polymers*. Amsterdam, the Netherlands–New York, USA: Elsevier; 2014:387–395. doi:10.1016/B978-0-12-396983-5.00024-7
42. Ren Y, Wong SM, Lim LY. In vitro-reassembled plant virus-like particles for loading of polyacids. *J Gen Virol*. 2006;87(9):2749–2754. doi:10.1099/vir.0.81944-0
43. Drexler KE, Peterson C, Pergamit G. *Unbounding the Future: The Nanotechnology Revolution*. London, UK: Simon & Schuster; 1992. ISBN:978-0-671-71108-5.
44. Freitas RA. *Nanomedicine, Volume I: Basic Capabilities*. Boca Raton, USA: CRC Press; 2024. doi:10.1201/9781003579021
45. Yan Lee P, Wong KY.Nanomedicine: A new frontier in cancer therapeutics. *Curr Drug Deliv*. 2011;8(3):245–253. doi:10.2174/156720111795256110
46. He Q, Shi J. MSN anti-cancer nanomedicines: Chemotherapy enhancement, overcoming of drug resistance, and metastasis inhibition. *Adv Mater*. 2014;26(3):391–411. doi:10.1002/adma.201303123
47. Dawidczyk CM, Kim C, Park JH, et al. State-of-the-art in design rules for drug delivery platforms: Lessons learned from FDA-approved nanomedicines. *J Control Release*. 2014;187:133–144. doi:10.1016/j.jconrel.2014.05.036
48. Ghosh S, Banerjee M. A smart viral vector for targeted delivery of hydrophobic drugs. *Sci Rep*. 2021;11(1):7030. doi:10.1038/s41598-021-86198-y
49. Shahrivarkevishahi A, Hagge LM, Brohlin OR, et al. Virus-like particles: A self-assembled toolbox for cancer therapy. *Mater Today Chem*. 2022;24:100808. doi:10.1016/j.mtchem.2022.100808

50. Masarapu H, Patel BK, Chariou PL, et al. Physalis mottle virus-like particles as nanocarriers for imaging reagents and drugs. *Biomacromolecules*. 2017;18(12):4141–4153. doi:10.1021/acs.biomac.7b01196
51. Peng S, Frazer IH, Fernando GJ, Zhou J. Papillomavirus virus-like particles can deliver defined CTL epitopes to the MHC class I pathway. *Virology*. 1998;240(1):147–157. doi:10.1006/viro.1997.8912
52. Cheong WS, Reiseger J, Turner SJ, Boyd R, Netter HJ. Chimeric virus-like particles for the delivery of an inserted conserved influenza A-specific CTL epitope. *Antiviral Res*. 2009;81(2):113–122. doi:10.1016/j.antiviral.2008.10.003
53. Kao CC, Ni P, Hema M, Huang X, Dragnea B. The coat protein leads the way: An update on basic and applied studies with the Brome mosaic virus coat protein. *Mol Plant Pathol*. 2011;12(4):403–412. doi:10.1111/j.1364-3703.2010.00678.x
54. Braun H, Boller K, Löwer J, Bertling WM, Zimmer A. Oligonucleotide and plasmid DNA packaging into polyoma VP1 virus-like particles expressed in *Escherichia coli*. *Biotechnol Appl Biochem*. 1999;29(1):31–43. doi:10.1111/j.1470-8744.1999.tb01146.x
55. Liu WJ, Liu XS, Zhao KN, Leggatt GR, Frazer IH. Papillomavirus virus-like particles for the delivery of multiple cytotoxic T cell epitopes. *Virology*. 2000;273(2):374–382. doi:10.1006/viro.2000.0435
56. Roldão A, Mellado MCM, Castilho LR, Carrondo MJ, Alves PM. Virus-like particles in vaccine development. *Exp Rev Vaccines*. 2010;9(10):1149–1176. doi:10.1586/erv.10.115
57. Frietze KM, Peabody DS, Chackerian B. Engineering virus-like particles as vaccine platforms. *Curr Opin Virol*. 2016;18:44–49. doi:10.1016/j.coviro.2016.03.001
58. Bolli E, O'Rourke JP, Conti L, et al. A virus-like particle immunotherapy targeting epitope-specific anti-xCT expressed on cancer stem cell inhibits the progression of metastatic cancer in vivo. *OncoImmunology*. 2018;7(3):e1408746. doi:10.1080/2162402X.2017.1408746
59. Xie A, Tsvetkova I, Liu Y, et al. Hydrophobic cargo encapsulation into virus protein cages by self-assembly in an aprotic organic solvent. *Bioconjugate Chem*. 2021;32(11):2366–2376. doi:10.1021/acs.bioconjchem.1c00420
60. Cadena-Nava RD, Comas-Garcia M, Garmann RF, Rao ALN, Knobler CM, Gelbart WM. Self-assembly of viral capsid protein and RNA molecules of different sizes: Requirement for a specific high protein/RNA mass ratio. *J Virol*. 2012;86(6):3318–3326. doi:10.1128/JVI.06566-11
61. Lavelle L, Gingery M, Phillips M, et al. Phase diagram of self-assembled viral capsid protein polymorphs. *J Phys Chem B*. 2009;113(12):3813–3819. doi:10.1021/jp8079765
62. Comas-Garcia M, Cadena-Nava RD, Rao ALN, Knobler CM, Gelbart WM. In vitro quantification of the relative packaging efficiencies of single-stranded RNA molecules by viral capsid protein. *J Virol*. 2012;86(22):12271–12282. doi:10.1128/JVI.01695-12
63. Bancroft JB. The self-assembly of spherical plant viruses. In: Smith KM, Lauffer MA, Bang FB, eds. *Advances in Virus Research*. Vol. 16. Amsterdam, the Netherlands–New York, USA: Elsevier; 1970:99–134. doi:10.1016/S0065-3527(08)60022-6
64. Dragnea B, Chen C, Kwak ES, Stein B, Kao CC. Gold nanoparticles as spectroscopic enhancers for in vitro studies on single viruses. *J Am Chem Soc*. 2003;125(21):6374–6375. doi:10.1021/ja0343609
65. Cao J, Guenther RH, Sit TL, Opperman CH, Lommel SA, Willoughby JA. Loading and release mechanism of red clover necrotic mosaic virus derived plant viral nanoparticles for drug delivery of doxorubicin. *Small*. 2014;10(24):5126–5136. doi:10.1002/smll.201400558
66. Douglas T, Young M. Host–guest encapsulation of materials by assembled virus protein cages. *Nature*. 1998;393(6681):152–155. doi:10.1038/30211
67. Alemzadeh E, Dehshahri A, Dehghanian AR, et al. Enhanced antitumor efficacy and reduced cardiotoxicity of doxorubicin delivered in a novel plant virus nanoparticle. *Coll Surf B Biointerfaces*. 2019;174:80–86. doi:10.1016/j.colsurfb.2018.11.008
68. Marchetti L, Novelli F, Tanno B, et al. Peptide-functionalized and drug-loaded tomato bushy stunt virus nanoparticles counteract tumor growth in a mouse model of Shh-dependent medulloblastoma. *Int J Mol Sci*. 2023;24(10):8911. doi:10.3390/ijms24108911
69. Kuo SY, Lin YC, Lai YC, et al. Production of fluorescent antibody-labeling proteins in plants using a viral vector and the application in the detection of *Acidovorax citrulli* and bamboo mosaic virus. *PLoS One*. 2018;13(2):e0192455. doi:10.1371/journal.pone.0192455
70. Jobsri J, Allen A, Rajagopal D, et al. Plant virus particles carrying tumour antigen activate TLR7 and induce high levels of protective antibody. *PLoS One*. 2015;10(2):e0118096. doi:10.1371/journal.pone.0118096
71. Chatterji A, Ochoa W, Shamieh L, et al. Chemical conjugation of heterologous proteins on the surface of cowpea mosaic virus. *Bioconjugate Chem*. 2004;15(4):807–813. doi:10.1021/bc0402888
72. Miermont A, Barnhill H, Strable E, et al. Cowpea mosaic virus capsid: A promising carrier for the development of carbohydrate based antitumor vaccines. *Chemistry*. 2008;14(16):4939–4947. doi:10.1002/chem.200800203
73. Wen AM, Lee KL, Yildiz I, Bruckman MA, Shukla S, Steinmetz NF. Viral nanoparticles for in vivo tumor imaging. *J Vis Exp*. 2012;69:4352. doi:10.3791/4352
74. Sapsford KE, Soto CM, Blum AS, et al. A cowpea mosaic virus nanoscaffold for multiplexed antibody conjugation: Application as an immunoassay tracer. *Biosens Bioelectron*. 2006;21(8):1668–1673. doi:10.1016/j.bios.2005.09.003
75. Kriwaczek VM, Eberle AN, Müller M, Schwyzer R. Tobacco mosaic virus as a carrier for small molecules I: The preparation and characterization of a TMV/α-melanotropin conjugate. *Helvetica Chim Acta*. 1978;61(4):1232–1240. doi:10.1002/hlca.19780610405
76. Fearney FJ, Leung CY, Young JD, Benjamini E. The specificity of antibodies to a peptide determinant of the tobacco mosaic virus protein induced by immunization with the peptide conjugate. *Biochim Biophys Acta Protein Struct*. 1971;243(3):509–514. doi:10.1016/0005-2795(71)90024-9
77. Hu H, Steinmetz NF. Doxorubicin-loaded physalis mottle virus particles function as a pH-responsive prodrug enabling cancer therapy. *Biotechnol J*. 2020;15(12):2000077. doi:10.1002/biot.202000077
78. Qiu X, Kang X, Zhu J, Yi L. Chemical labeling and crosslinking of tobacco mosaic virus *via* multi-diazonium reagents: Examples, applications, and prospects. *Mater Adv*. 2022;3(13):5248–5259. doi:10.1039/D2MA00311B
79. Sugiyama Y, Hamamoto H, Takemoto S, Watanabe Y, Okada Y. Systemic production of foreign peptides on the particle surface of tobacco mosaic virus. *FEBS Lett*. 1995;359(2–3):247–250. doi:10.1016/0014-5793(95)00054-D
80. Wu Y, Li J, Yang H, et al. Targeted cowpea chlorotic mottle virus-based nanoparticles with tumor-homing peptide F3 for photothermal therapy. *Biotechnol Bioproc E*. 2017;22(6):700–708. doi:10.1007/s12257-017-0443-2
81. Zlotnick A, Aldrich R, Johnson JM, Ceres P, Young MJ. Mechanism of capsid assembly for an icosahedral plant virus. *Virology*. 2000;277(2):450–456. doi:10.1006/viro.2000.0619
82. Kasermann F, Kempf C. Low pH-induced pore formation by spike proteins of enveloped viruses. *J Gen Virol*. 1996;77(12):3025–3032. doi:10.1099/0022-1317-77-12-3025
83. Tama F, Brooks CL. The mechanism and pathway of pH induced swelling in cowpea chlorotic mottle virus. *J Mol Biol*. 2002;318(3):733–747. doi:10.1016/S0022-2836(02)00135-3
84. Bawden FC, Pirie NW. The effects of alkali and some simple organic substances on three plant viruses. *Biochem J*. 1940;34(8–9):1278–1292. doi:10.1042/bj0341278
85. Fraenkel-Conrat H, Williams RC. Reconstitution of active tobacco mosaic virus from its inactive protein and nucleic acid components. *Proc Natl Acad Sci U S A*. 1955;41(10):690–698. doi:10.1073/pnas.41.10.690
86. Caspar DLD. Assembly and stability of the tobacco mosaic virus particle. In: Anfinsen Jr CB, Anson ML, Edsall JT, eds. *Advances in Protein Chemistry*. Vol. 18. Amsterdam, the Netherlands–New York, USA: Elsevier; 1964:37–121. doi:10.1016/S0065-3233(08)60268-5
87. Lauffer MA, Stevens CL. Structure of the tobacco mosaic virus particle: Polymerization of tobacco mosaic virus protein. *Adv Virus Res*. 1968;13:1–63. doi:10.1016/s0065-3527(08)60250-x
88. Wang Q, Kaltgrad E, Lin T, Johnson JE, Finn MG. Natural supramolecular building blocks. *Chem Biol*. 2002;9(7):805–811. doi:10.1016/S1074-5521(02)00165-5
89. Shirbaghaee Z, Bolhassani A. Different applications of virus-like particles in biology and medicine: Vaccination and delivery systems. *Biopolymers*. 2016;105(3):113–132. doi:10.1002/bip.22759
90. Soliman H, Hogue D, Han H, et al. Oncolytic T-VEC virotherapy plus neoadjuvant chemotherapy in nonmetastatic triple-negative breast cancer: A phase 2 trial. *Nat Med*. 2023;29(2):450–457. doi:10.1038/s41591-023-02210-0

91. Lei W, Wang S, Xu N, et al. Enhancing therapeutic efficacy of oncolytic vaccinia virus armed with Beclin-1, an autophagic gene in leukemia and myeloma. *Biomed Pharmacother*. 2020;125:110030. doi:10.1016/j.biopha.2020.110030
92. Rohovie MJ, Nagasawa M, Swartz JR. Virus-like particles: Next-generation nanoparticles for targeted therapeutic delivery. *Bioeng Transl Med*. 2017;2(1):43–57. doi:10.1002/btm2.10049
93. Afzal O, Altamimi ASA, Nadeem MS, et al. Nanoparticles in drug delivery: From history to therapeutic applications. *Nanomaterials*. 2022;12(24):4494. doi:10.3390/nano12244494
94. Kundu M, Chatterjee S, Ghosh N, Manna P, Das J, Sil PC. Tumor targeted delivery of umbelliferone via a smart mesoporous silica nanoparticles controlled-release drug delivery system for increased anticancer efficiency. *Mater Sci Eng C Mater Biol Appl*. 2020;116:111239. doi:10.1016/j.msec.2020.111239
95. Biabanikhankahdani R, Ho K, Alitheen N, Tan W. A dual bioconjugated virus-like nanoparticle as a drug delivery system and comparison with a pH-responsive delivery system. *Nanomaterials*. 2018;8(4):236. doi:10.3390/nano8040236
96. Laomeephol C, Tawinwung S, Suppipat K, Arunmanee W, Wang Q, Amie Luckanagul J. Surface functionalization of virus-like particles via bioorthogonal click reactions for enhanced cell-specific targeting. *Int J Pharm*. 2024;660:124332. doi:10.1016/j.ijpharm.2024.124332
97. Thong QX, Biabanikhankahdani R, Ho KL, Alitheen NB, Tan WS. Thermally-responsive virus-like particle for targeted delivery of cancer drug. *Sci Rep*. 2019;9(1):3945. doi:10.1038/s41598-019-40388-x
98. Patel KG, Swartz JR. Surface functionalization of virus-like particles by direct conjugation using azide–alkyne click chemistry. *Bioconjugate Chem*. 2011;22(3):376–387. doi:10.1021/bc100367u
99. Salazar-González JA, Ruiz-Cruz AA, Bustos-Jaimes I, Moreno-Fierros L. Expression of breast cancer-related epitopes targeting the IGF-1 receptor in chimeric human parvovirus B19 virus-like particles. *Mol Biotechnol*. 2019;61(10):742–753. doi:10.1007/s12033-019-00198-y
100. Chou CC, Chen W, Hung Y, Mou CY. Molecular elucidation of biological response to mesoporous silica nanoparticles in vitro and in vivo. *ACS Appl Mater Interfaces*. 2017;9(27):22235–22251. doi:10.1021/acsami.7b05359
101. He C, Hu Y, Yin L, Tang C, Yin C. Effects of particle size and surface charge on cellular uptake and biodistribution of polymeric nanoparticles. *Biomaterials*. 2010;31(13):3657–3666. doi:10.1016/j.biomaterials.2010.01.065
102. Naupu PN, Van Zyl AR, Rybicki EP, Hitzeroth II. Immunogenicity of plant-produced human papillomavirus (HPV) virus-like particles (VLPs). *Vaccines*. 2020;8(4):740. doi:10.3390/vaccines8040740
103. Deml L, Speth C, Dierich MP, Wolf H, Wagner R. Recombinant HIV-1 Pr55gag virus-like particles: Potent stimulators of innate and acquired immune responses. *Mol Immunol*. 2005;42(2):259–277. doi:10.1016/j.molimm.2004.06.028
104. Ou J, Zhu M, Ju X, et al. One-dimensional rod-like tobacco mosaic virus promotes macrophage polarization for a tumor-suppressive microenvironment. *Nano Lett*. 2023;23(5):2056–2064. doi:10.1021/acs.nanolett.2c03809
105. Wang C, Beiss V, Steinmetz NF. Cowpea mosaic virus nanoparticles and empty virus-like particles show distinct but overlapping immunostimulatory properties. *J Virol*. 2019;93(21):e00129-19. doi:10.1128/JVI.00129-19
106. Mohsen MO, Zha L, Cabral-Miranda G, Bachmann MF. Major findings and recent advances in virus-like particle (VLP)-based vaccines. *Semin Immunol*. 2017;34:123–132. doi:10.1016/j.smim.2017.08.014
107. Meng C, Chen Z, Mai J, et al. Virus-mimic mRNA vaccine for cancer treatment. *Adv Ther*. 2021;4(11):2100144. doi:10.1002/adtp.202100144
108. Pan Y, Zhou Y, Wu H, et al. A therapeutic peptide vaccine against PCSK9. *Sci Rep*. 2017;7(1):12534. doi:10.1038/s41598-017-13069-w
109. Jolley C, Klem M, Harrington R, Parise J, Douglas T. Structure and photoelectrochemistry of a virus capsid–TiO_2 nanocomposite. *Nanoscale*. 2011;3(3):1004–1007. doi:10.1039/C0NR00378F
110. Cirulli M, Ciccarese F. Interactions between TMV isolates, temperature, allelic condition and combination of the Tm resistance genes in tomato. *Phytopathol Mediterr*. 1975;14(2/3):100–105. http://www.jstor.org/stable/42684268.
111. Hariharasubramanian V, Zaitlin M, Siegel A. A temperature-sensitive mutant of TMV with unstable coat protein. *Virology*. 1970;40(3):579–589. doi:10.1016/0042-6822(70)90202-3

Progress, prospect and explorations of polymeric nanoparticles for the treatment of ophthalmic complications

Pravin K. Pawar[F], Aishwarya Nerlekar[B], Nisha Jagtap[D], Ankita Vibhute[D]

Department of Pharmaceutics, Dr. Shivajirao Kadam College of Pharmacy (affiliated to Shivaji University, Kolhapur) Kasabe Digraj, Sangli, India

A – research concept and design; B – collection and/or assembly of data; C – data analysis and interpretation;
D – writing the article; E – critical revision of the article; F – final approval of the article

Polymers in Medicine, ISSN 0370-0747 (print), ISSN 2451-2699 (online) *Polim Med*. 2025;55(2):165–197

Address for correspondence
Pravin K. Pawar
E-mail: pkpawar80@yahoo.com

Funding sources
None declared

Conflict of interest
None declared

Acknowledgements
The authors express their sincere gratitude to Prof. D.D. Chougule, Director of Dr. Shivajirao Kadam College of Pharmacy, Kasabe Digraj, Sangli, for providing the necessary infrastructure and facilities for the successful completion of this review work.

Received on December 3, 2024
Reviewed on January 10, 2025
Accepted on January 15, 2025

Published online on December 19, 2025

Abstract

Due to physiological and anatomical barriers, optometrists and drug delivery specialists have long faced challenges in administering medications to the eyes. These ocular barriers – both permanent and temporary – limit the entry of foreign substances and reduce the effective absorption of therapeutic agents. Polymeric nanoparticles (NPs) provide advantages such as selective tissue targeting, improved drug bioavailability, stability, and controlled drug release. Their ability to overcome barriers like the precorneal film, cornea and intra-retinal regions depends on properties such as interfacial ligands, mucoadhesion, hydrophobicity, particle size, and surface charge. Careful design tailored to specific ocular tissues and diseases is essential. This study aims to explore the potential applications of polymeric NPs across various pharmaceutical categories in the treatment of ocular conditions.

Key words: stability, polymeric nanoparticles, ophthalmic application, challenges for vision

Cite as
Pawar PK, Nerlekar A, Jagtap N, Vibhute A. The progress, prospect and explorations of polymeric nanoparticles for the treatment of ophthalmic complications. *Polim Med*. 2025;55(2):165–179. doi:10.17219/pim/200146

DOI
10.17219/pim/200146

Introduction

Due to its complex anatomy and strong defense mechanisms against external substances, including therapeutic agents, the eye presents a significant challenge in drug delivery and medical treatment. While traditional topical formulations are commonly used for the anterior segment of the eye, the majority of the drug dose is lost due to ocular defense mechanisms. To improve drug retention, efforts have been made to minimize local and systemic side effects while enhancing therapeutic efficacy. For diseases affecting the posterior segment of the eye, intravitreal therapy or systemic administration of intravitreal implants and injections is often required. Developing ocular drug delivery methods that enhance therapeutic efficacy and enable targeted tissue absorption is essential. Since the cornea and conjunctiva are sensitive to penetration enhancers, careful selection of such agents and the design of compatible drug formulations are critical components of an effective delivery strategy.[1]

According to their intended purpose, nanoparticles (NPs) might or might not contain a therapeutic molecule. Drugs can be dissolved, adsorbed, entrapped, or chemically linked within nanoscale frameworks, resulting in various structures such as NPs, nanospheres or nanocapsules. All these terms share a common feature: they refer to NPs that encapsulate or carry drugs. Polymeric NPs offer remarkable flexibility as a drug delivery technology due to their ability to deliver medication to specific tissues or intracellular compartments by overcoming physiological barriers through both passive and ligand-mediated targeting mechanisms. When properly formulated, polymeric NPs require less frequent administration, exhibit prolonged retention in the extraocular area and can be as easy to use as topical solutions, while offering the added benefit of improved patient compliance.[2–4] To improve drug delivery and reduce harmful side effects, NPs have been extensively studied for their ability to carry a wide range of both small and large molecular entities, including drugs, peptides, amino acids, vaccines, and genetic material. Two fundamental requirements for polymeric NPs are that the polymers used in their fabrication must be both biocompatible and biodegradable, as the NPs remain within target cells and circulate for extended periods. A variety of polymers meeting these criteria have been employed, and evaluating their suitability, based on the resulting NP properties, represents a compelling area of research in the development of an optimal therapeutic platform for the treatment of various ocular conditions.[5]

Anatomy of the eye

The human eye is an extremely complex and delicate organ, composed of both anterior and posterior segments. The anterior segment includes the tear film, cornea, aqueous humor, pupil, lens, and ciliary body. The posterior segment consists of the vitreous humor, retina, optic nerve, and supporting structures. It should be noted that some elements, such as the conjunctiva and cornea, span both regions and play key roles in ocular protection and vision. The volume and composition of the tear film are regulated by the orbital glands and epithelial secretions. The cornea plays a crucial role in focusing light entering the visual field. It is composed of 3 distinct layers: the epithelium, stroma and endothelium. The corneal epithelium consists of 4–7 layers. The stroma is a dense layer composed primarily of water. The epithelium plays an important role in maintaining corneal transparency. The pigmented part of the eye is called the iris and it regulates the amount of light that enters the eye and reaches the retina. The structure of the ciliary body consists of ciliary muscles, stroma and both pigmented and non-pigmented epithelial layers.[6] Interaction between the anterior and posterior segments of the eye is facilitated by the capillary network within the ciliary body. The vitreous humor is a transparent, gel-like connective tissue located between the retina and the lens. It contains no blood vessels and is composed primarily of water (99.9%), along with hyaluronic acid (HA), collagen and electrolytes.[7] Conjunctiva is the fragile, translucent membrane covering the surface of the eye. The eyelids protect the anterior part of the sclera. The choroid is a vascular membrane located between the sclera and the retina. The retina is an extremely delicate structure composed of glial and neural tissues. It generates electric impulses, which are transmitted to the brain via the optic nerve.[8–12]

Barriers to ocular drug delivery

Ocular drug delivery is difficult due to various barriers that limit drug efficacy and absorption. These barriers include anatomical, physiological and metabolic factors.

Pre-corneal barriers

Capacity of the cul-de-sac

The human eye's conjunctival cul-de-sac is a small anatomical space with an approximate volume of 20–30 μL. It is formed where the bulbar and palpebral conjunctivae meet, including a deeper depression beneath the upper eyelid. When the lower eyelid returns to its normal position, the capacity of this space is reduced by approx. 70–80%.[13] Inflammation and allergic reactions of the eye can further reduce the capacity of the conjunctival cul-de-sac. Since a drug's residence time and concentration are closely correlated with its therapeutic efficacy, the limited capacity of the cul-de-sac may lead to a decrease in intraocular drug concentration, ultimately reducing the treatment's effectiveness (Fig. 1).

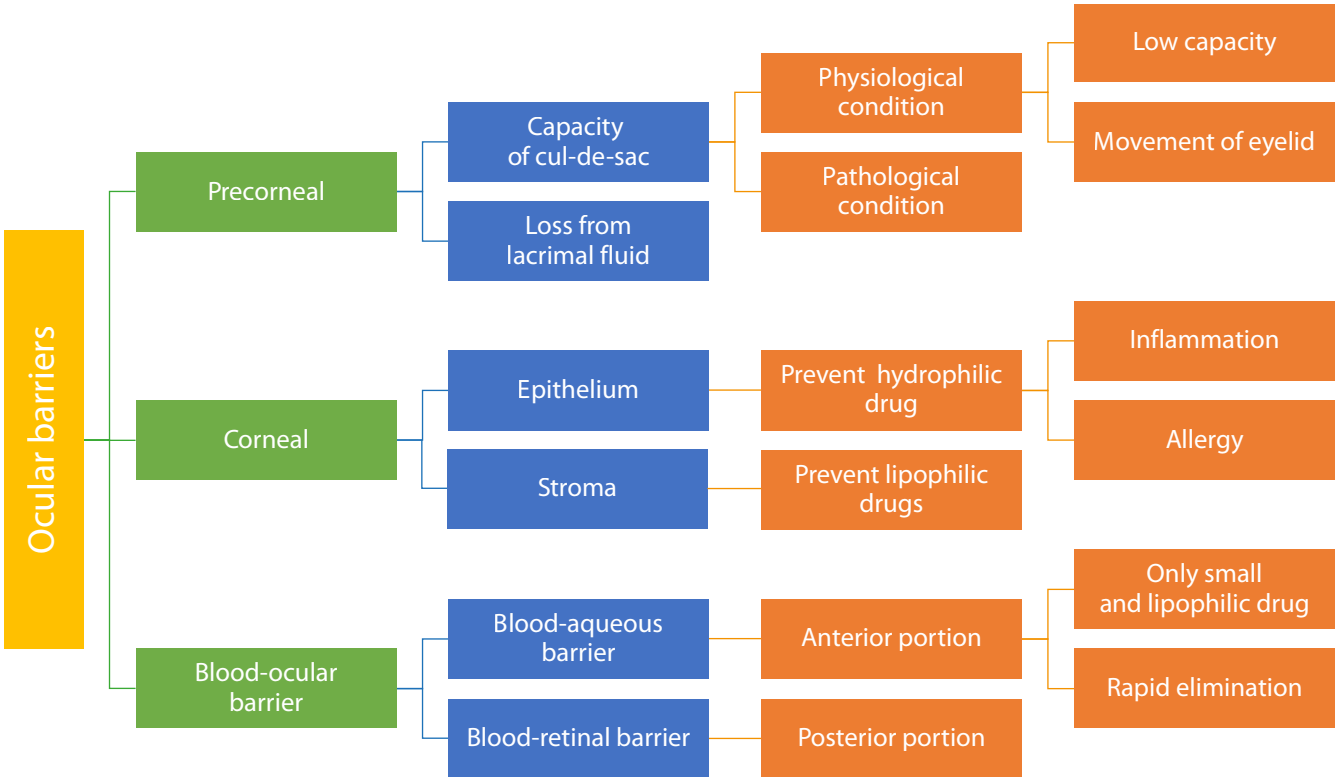

Fig. 1. Schematic representation of different barriers in ocular drug delivery system

Drug loss in lacrimal fluid

The management of ocular fluid drainage is one of the key challenges in the precorneal area. Drug loss from the lacrimal fluid can occur due to non-productive absorption through the conjunctiva, excessive lacrimation and nasolacrimal drainage. In addition, protein binding and metabolic processes within the ocular environment may further hinder drug uptake and reduce therapeutic efficacy.[14] The continuous replenishment of lacrimal fluid plays a vital role in keeping the eyes hydrated and protecting them from dust or pathogens that could reach deeper ocular structures. To ensure therapeutic efficacy, it is essential to prolong the residence time of the administered formulation. Various strategies can be employed to enhance retention time on the ocular surface.[15]

Corneal barriers

The cornea functions as a robust barrier, protecting the eye from various physiological and chemical insults. While the lens plays a key role in focusing light and filtering ultraviolet (UV) radiation, it is not involved in barrier functions at the ocular surface. It also plays a crucial role in focusing light onto the retina. The lens is composed of 3 parts: epithelium, stroma (cortex) and endothelium. The epithelium consists of tightly packed cells arranged in 5–7 layers. The stroma is a dense layer composed primarily of water. Lipophilic drugs penetrate more readily through the corneal epithelium, while hydrophilic drugs diffuse more efficiently through the stroma. The endothelium plays a key role in maintaining corneal transparency and facilitates the selective entry of hydrophilic drugs and macromolecules into the aqueous humor. Drug molecular weight, charge, degree of ionization, and hydrophobicity significantly influence corneal penetration. These factors collectively determine the rate-limiting step in the passage of drugs from the lacrimal fluid into the aqueous humor.[16]

Blood–retinal barriers

These barriers prevent foreign pathogens from entering the bloodstream. They are classified into 2 main types: blood–retinal barrier (BRB) and blood–aqueous barrier (BAB). The BAB, located in the anterior segment of the eye, restricts the entry of various substances into the intraocular environment. The BRB facilitates the passage of small, hydrophobic drugs. The clearance of medications from the anterior segment occurs more rapidly for such compounds than for larger, hydrophilic molecules. The BRB is located in the posterior segment of the eye and is formed by pigmented epithelial cells and vascular endothelial cells of the retina. It prevents from the entry of harmful substances, water and plasma components into the retinal tissue.[17]

Ocular diseases

Over 1 billion people worldwide suffer from vision impairment, with 36 million being blind. Anatomical barriers and frequent intravitreal injections make ocular drug delivery complex. Other factors, such as the need for intravitreal injections, further impede effective medication delivery to the inner structures of the eye. Therefore, addressing these challenges is crucial for effective treatment.[18] A promising strategy to enhance intraocular drug distribution involves the use of polymeric NPs with tailored surface properties and variable diameters, enabling targeted delivery to specific ocular tissues. These NPs may offer controlled release profiles, reducing the frequency of drug administration required.[19]

Glaucoma

Glaucoma, characterized by progressive vision loss, is the 2nd leading cause of blindness worldwide after cataracts. It is estimated that by 2040, the global number of glaucoma patients may reach 111.8 million. A key feature of glaucoma is elevated intraocular pressure (IOP).[20] Given that glaucoma is a complex disease, the primary goal of current treatment is to slow or prevent further vision loss caused by IOP.[21] In glaucoma management, brimonidine tartrate-loaded chitosan NPs, formulated using sodium tripolyphosphate, may help reduce dosing frequency and provide sustained drug release.[22] For the treatment of glaucoma, researchers developed HA-enhanced chitosan NPs loaded with hydroxychloroquine (DH) and timolol maleate (TM). Hyaluronic acid improves mucoadhesion, allowing the NPs to deliver the drugs locally and in a sustained manner to ocular tissues. The chitosan–HA NPs demonstrated a significant reduction in IOP, suggesting that HA may enhance both the efficacy and mucoadhesive properties of chitosan NPs.[23] Radwan et al. suggested that chitosan-coated bovine serum albumin NPs (CS-BSA-NPs) may serve as an effective platform for the topical delivery of tetrandrine (TET) in the treatment of glaucoma.[24] Shahab et al. aimed to develop chitosan-coated polycaprolactone (PCL) NPs loaded with dorzolamide to enhance ocular drug delivery. The NPs are optimized using a single-step emulsification method, guided by a 3-factor, 3-level Box–Behnken design. The optimized dorzolamide-loaded chitosan NPs showed a strong correlation between independent and dependent response variables. They exhibited biphasic release behavior and showed a 3.7-fold increase in mucoadhesion compared to the control formulation. Additionally, the NPs were found to be non-irritating and safe for ocular administration, indicating their safety and potential to enhance therapeutic efficacy.[25] Dubey et al. developed brinzolamide nanocapsules for glaucoma prevention using chitosan–pectin polymers. These nanocapsules offer improved bioavailability and better corneal penetration compared to conventional eye drops.[26] A recent study presented a safe, well-tolerated and neuroprotective topical formulation of poly(lactic-co-glycolic acid)–polyethylene glycol (PLGA–PEG) NPs loaded with memantine for glaucoma treatment. The formulation, containing 4 mg/mL of memantine, significantly reduced retinal ganglion cell damage in a murine model of ocular hypertension. Memantine-loaded NPs (MEM-NPs) were well tolerated in both in vivo and in vitro settings.[27] Another study developed nanoparticulate systems (NCs) containing acetazolamide (AZM) aimed at reducing IOP. The formulations had high encapsulation efficiency. They improved drug permeation, reduced IOP significantly and provided prolonged therapeutic effects.[28] Warsi et al. evaluated the encapsulation efficiency of dorzolamide-loaded PLGA NPs formulated with 2 different emulsifiers and vitamin E TPGS. The results showed that the NPs had high encapsulation efficiency, improved corneal permeability and were non-irritating. Additionally, drug concentration in ocular tissues was elevated. The formulation also showed therapeutic efficacy, with a significant reduction in IOP following a single topical administration.[29]

Uveitis

Autoimmune uveitis is an ocular disorder that affects the posterior segment of the eye. Studies have shown that NP-based drug delivery methods can offer more effective treatment with fewer adverse effects in managing immunological autoimmune uveitis.[30] Research on posterior segment disorders has explored the use of intravitreal injections of PLGA NPs loaded with dexamethasone (DEX). These systems have demonstrated the ability to sustain therapeutic DEX concentrations over an extended period and distribute the drug throughout various ocular layers.[31] Sakai et al. examined the therapeutic potential of betamethasone phosphate (BP) encapsulated in biocompatible and biodegradable NPs composed of poly(lactic acid) (PLA) homopolymers or PEG-block-PLA copolymers, referred to as stealth nanosteroids. This NP-based delivery system reduced pro-inflammatory cytokine levels in the retinas of rats with experimental autoimmune uveitis (EAU) and significantly lowered their clinical scores. These findings suggest that NP-mediated delivery may represent a promising strategy for managing intraocular inflammation.[32]

Cataract

Cataracts are one of the leading causes of visual impairment worldwide, accounting for approx. 40–60% of global blindness according to the National Program for Control of Blindness and Visual Impairment. A cataract is the opacification or progressive clouding of the ocular lens. Identified risk factors include prolonged exposure to UV radiation, diabetes, poor nutrition, genetic predisposition, and smoking.[33] Pranoprofen (PF) is an effective anti-inflammatory agent commonly used in the management

of blurred vision and during cataract surgery. The drug was formulated using PLGA NPs and evaluated for cytotoxicity, in vivo ocular penetration, ophthalmic tolerability, and anti-inflammatory efficacy. In vivo ocular penetration in New Zealand rabbits demonstrated comparable absorption levels across formulations, with PF-F2NPs showing the highest quantitative pupillometry (QP) value and a significant reduction in ocular edema. The PF-F1NPs formulation was well tolerated and non-irritating to ocular tissues, whereas PF-F2NPs exhibited higher Quick Response (QR) values (quantities of PF retained in the cornea) compared to other tested formulations.[34]

Fungal keratitis

Fungal keratitis is a serious ocular condition that primarily affects the cornea. It is caused by various fungal species, including *Candida albicans*, *Candida glabrata*, *Candida tropicalis*, *Candida krusei*, and *Candida parapsilosis*. Mycotic inflammation accounts for up to 40% of all cases of corneal inflammation in low-income countries.[35] Risk factors for fungal keratitis include ocular conditions such as trauma, contact lens use, topical corticosteroid application, and previous corneal surgery, as well as systemic conditions like leprosy.[36] Researchers developed voriconazole-loaded chitosan NPs using the ionic gelation method with sodium tripolyphosphate to establish an effective topical ocular delivery method. The NPs were characterized using X-ray diffraction (XRD), differential scanning calorimetry (DSC), scanning electron microscopy (SEM), and Fourier transform infrared spectroscopy (FTIR). A Box–Behnken design was employed and the formulation showed high drug loading capacity, absence of a burst release effect and sustained drug release over 48 h, making it a promising strategy for ocular antifungal therapy.[37]

Diabetic retinopathy

Diabetic retinopathy (DR) is one of the leading causes of vision loss and blindness worldwide and represents a permanent complication of diabetes. In severe cases, patients may experience progressive symptoms such as floaters, blurred or distorted vision and partial or complete vision loss due to retinal detachment. Clinically, timely laser therapy can improve ocular circulation, prevent vitreous hemorrhage and inhibit the formation of abnormal retinal blood vessels. Additionally, intravitreal anti-VEGF (vascular endothelial growth factor) injections are commonly required to reduce retinal inflammation and improve visual outcomes.[38] Unfortunately, some individuals respond effectively to intravitreal injections and repeated delivery may destroy optical cells.[39] Vitrectomy is commonly required in situations of vitreous hemorrhage or proliferative vitreoretinopathy. Many medications have poor ocular absorption, and the potential side effects or hazards associated with invasive treatments make there a rising need for novel drug delivery systems. These innovative techniques provide intriguing alternatives for the effective treatment of DR.[40]

Liu et al. investigated the effects of an intravitreal injection of bevacizumab-chitosan NPs on the expression of VEGF messenger ribonucleic acid (mRNA) and VEGF protein inside diabetic rat's corneas. The findings showed that bevacizumab could be continuously released from chitosan NPs and that this replacement was efficient in preventing choroidal neovascularization.[41] Furthermore, the anti-VEGF agent-containing NPs significantly reduced VEGF expression and had a long-lasting effect. Triamcinolone acetonide-loaded NPs were used in a mouse study for DR, with a PCL core and a hydrophilic poloxamer 188 shells made from PLGA and chitosan NPs.[42] Interleukin 12-encapsulated cytokines have been shown to prevent angiogenic tumors. Despite a moderate encapsulation efficiency of 34.7%, the formulation demonstrated prolonged drug release as well as a greater ability to reduce VEGF-A and matrix metalloproteinase 9 (MMP-9) production in mouse endothelial cells and DR mouse cornea. Increased retinal thickness and decreased new blood vessels following therapy show that the specific dosage significantly reduced retinal loss in DR rats.[43]

Age-related macular degeneration

Age-related macular degeneration (AMD) was the leading cause of visual loss in developed countries. People over the age of 50 are more likely to experience this disease, which accounts for around 8.7% of global blindness. In 2020, around 196 million people will be impacted by AMD.[44] Growing older, smoking, bad eating habits, hypertension, and physical inactivity are all risk factors. Although there are currently no therapies for AMD, appropriate care can slow its progression. Age-related macular degeneration is categorized as either dehydrated (atrophic or non-exudative) or wet (neovascular). The retinal epithelium shows unequal angiogenesis (the development of new blood vessels).[45] Varshochian et al. produced albumin-PLGA NPs to contain bevacizumab. The resultant NPs produced a bevacizumab formulation that allowed for extended release, with a vitreous concentration more than 500 ng mL^{-1} in a rabbit model for about 8 weeks.[46]

Dry eyes

Dry keratoconjunctivitis, or dry eye disease (DED), is a multifactorial ocular surface disease. Tear film instability, hypertonicity and inflammation are its distinguishing features. Dry eye disease has a substantial impact on a patient's quality of life, can cause mental health issues and imposes a significant financial cost on society. Dry eye disease is typically diagnosed and treated in 2 ways: aqueous tear-deficient dry eye and evaporative dry eye type. Artificial tears, local secretagogues, corticosteroids, and immunosuppressants are common pharmacological therapies, although they can have negative side effects

such as glaucoma, high IOP, poor patient adherence, and eye pain. Finding novel medication delivery strategies is critical for overcoming ocular obstacles and improving drug absorption.[47] Dry eye disease complicates problems by increasing tear membrane osmolarity and causing ocular surface irritation. Traditional corticosteroids may increase IOP. Tet-ATS@PLGA is a novel nanomedicine with excellent biocompatibility, long-term release and anti-inflammatory effects. Following 2 weeks of treatment, the nanomedicine considerably lowers tear production and tear film breakdown times in a dry eye illness model. Li et al. demonstrated that apoptosis of inflammatory corneal epithelial cells inhibits the release of inflammatory mediators, thereby preventing DED formation and enhancing tear production.[48] Poly(lactic-co-glycolic acid) NPs for ocular administration of cyclosporine A (CsA) to treat dry eye condition. The NPs were created using a solvent evaporation approach and their characteristics were evaluated using probe sonication. Wagh and Apar identified a 2-phase drug release mechanism, characterized by an initial rapid release followed by a sustained release. Enhancing the surface properties of NPs may improve drug absorption and retention in the eye, supporting the use of topical CsA as a safe and effective treatment for severe dry eye conditions.[49]

Retinoblastoma

The malignant tumor known as retinoblastoma usually affects youngsters under the age of 5. Untreated retinoblastoma leads to blindness and death (99%). It occurs in around one out of every 20,000 live births.[50] It occurs at an equal rate in both genders. The cause is a mutation in the cancer suppressor gene *RB1*, which encodes the retinal tumor protein. Bilateral (40%) or unilateral (60%) retinal tumor protein might be used. Radiation, cryotherapy, systemic chemotherapy, and surgery are all options for treating retinoblastomas. Current research suggests the release of compensatory proangiogenic factors in response to anti-angiogenic therapies used for retinoblastoma treatment. A critical aspect in the treatment of retinoblastoma involves targeting the angiogenic phase, during which the tumor establishes new blood vessels essential for its growth and progression.[51] Poly-lactic-co-glycolic acid NPs coated with curcumin or nutlin-3a are a unique approach to overcome the drug resistance of Y79 cells. Nutlin-3a is a potent medicine that acts as an antagonist of the murine double minute (MDM2), effectively inhibiting the interaction between p53 and MDM2. However, it acts as a substrate for Pgp and MRP-1, 2 multidrug-resistant proteins. It has relatively limited clinical use. Curcumin, a recognized regulator of multidrug resistance (MDR) proteins, may boost the anticancer activity of nutlin-3a in drug-resistant Y79 cells. The co-administration of folic acid functionalized targeted delivery system was discovered to improve its anticancer effects. The experiments on apoptosis, cell cycle analysis and in vitro cellular cytotoxicity confirmed the increased effectiveness of the folic acid functionalized NPs.[52]

The most popular and straightforward method of administering drugs to the eyes is the topical one (Table 1[53–58]). It offers the advantages of 1) being comparatively noninvasive; 2) reducing the drug's systemic adverse effects; and 3) being reasonably simple for patients to administer when compared to systemic administration. Ophthalmic solutions

Table 1. Comparison of several ocular medication administration routes

Reference	Delivery routes	Advantages	Disadvantage	Disease cured
[53]	topical	self-administration, noninvasive, high patient compliance	corneal barrier, dilution and efflux, limited bioavailability, excessive dosage	conjunctivitis, keratitis, uveitis, episcleritis, scleritis, blepharitis
[54]	sub-conjunctival and transscleral administration	anterior and posterior drug administration, suitable for depot development	subconjunctival hemorrhage is more harmful due to increased choroidal and conjunctival circulation	glaucoma, AMD cytomegalovirus retinitis
[55]	intracameral administration	directly deliver to the posterior segment; most efficient treatment for posterior segment	toxic endothelial cell death and toxic anterior segment syndrome	anesthesia, inflammation, endophthalmitis, pupil dilation
[56]	intravitreal injection	direct delivery to the vitreous humor and retina, BRB avoidance, high bioavailability and acute dosing	poor patient compliance, invasiveness, medication toxicity, retinal detachment, cataract endophthalmitis, hemorrhage	AMD, central/branched retinal vein occlusion, diabetic macular edema, cytomegalovirus retinitis
[57]	retrobulbar injection	selective delivery to both anterior and posterior segments, avoidance of corneal and conjunctival barriers, long duration of action, a site for depot formulations	poor patient compliance, invasiveness, drug deposition, complications such as discomfort, hemorrhages, infection, scarring, eyeball or optic nerve damage	anesthesia
[58]	systemic administration	high patient compliance	blood–ocular barrier, low bioavailability, systemic toxicity caused by high dosing	scleritis, episcleritis, cytomegalovirus retinitis

AMD – age-related macular degeneration; BRB – blood–retinal barrier.

are therefore the first choice for treating a variety of eye conditions, including glaucoma, DED, infection, inflammation, and allergies. Roughly 95% of the currently available products in the global market for ocular medications are thought to be topical ophthalmic solutions.[59] Subconjunctival administration is a minimally invasive and effective method for delivering drugs to the anterior eye chamber, avoiding corneal and BAB. However, it may result in drug loss due to drainage. Transscleral administration is simpler, less invasive and more suitable for patients, as it bypasses anterior obstacles and can deliver antioxidants, neuroprotective agents or antiangiogenic agents to targeted retina sites.[60] Intracameral administration injects drugs directly into the eye's anterior chamber, avoiding adverse effects and first-pass metabolism. It is used for prophylactic antibiotics or anesthetics in eye surgeries. However, it requires reorganization, dilution of the injected drug solution, sterility, special preparations, and appropriate concentrations and doses, which can lead to corneal endothelial cell toxicity and toxic anterior segment syndrome.[53] Intravitreal injections are a preferred method for treating eyeball diseases due to quick removal of free drugs. Frequent injections can cause side effects like retinal detachment and eyeball infection. The optimal protocol is a one-time injection without retracting the needle. Recent studies explore alternatives like NPs, implants, hydrogels, and minimally invasive techniques.[54] Amphotericin B and chlorpromazine-loaded retrobulbar injections showed effective concentrations of both active pharmaceutical ingredients (APIs).[55] Systemic administration is a drug delivery method for treating eye diseases like endophthalmitis, elevated IOP and uveitis, but frequent administration may cause side effects and poor patient compliance.[56]

Restrictions to use eye drops

Less than 5% of the amount of drugs applied topically penetrate the cornea and reach the ocular tissues, with a large percentage of the supplied dosage often being extensively absorbed by the nasal capillary channel and palpebral conjunctiva. Although many drugs have a short half-life and enter the systemic circulation quickly, ophthalmic solutions are extensively utilized because they are inexpensive, simple to create and manufacture, or have positive patient approval. Hypertension, bronchial asthma and tachycardia are examples of systemic adverse effects that could occur. Timolol eye drop has been shown to have such detrimental side effects.[57]

Colloidal system as a modified formulation for eye drops

The typical eye drops solution faces 3 major challenges: restricted bioavailability, non-targeted pharmacological effects and enzyme inactivation. Over the past 2 decades, substantial research has concentrated on colloidal carriers, including compact NPs, biodegradable polymeric NPs and liposomes, to overcome these limitations.[58] While they provided some benefits for extended drug delivery, alternative ophthalmic distribution methods such as ophthalmic inserts and in situ gelling techniques failed to address the issues of blurred vision as well as the 4 main challenges previously identified: visual disturbances, eyelid adhesion, poor systemic absorption, and insufficient patient compliance. Liquid eye drops confront various obstacles including sediment formation, settling, lack of homogeneity, and resuspension difficulties. Particles larger than 1,000 nm can cluster and cause ocular irritation. Glaucoma, DR, macular degeneration, and squamous cell carcinoma (SCC) all require continuous care.[61] It is impossible to maintain therapeutic concentration with a single eye drop for a lengthy period of time. The conventional replacement ophthalmic implant provide regular drug delivery but have limitations: They are challenging to implement, particularly in the elderly and people who are visually impaired, and are often used incorrectly; moreover, they can be released from the eye and patient adherence is poor. The main challenges of ocular formulations are: pain and eyesight impairment, insertion difficulty, and potential elimination during the conclusion of their effective lives.[62] The development of biodegradable and bio-erodible polymers, especially through aqueous-dependent colloidal nanotechniques, offers new potential for ocular medication delivery. Pharmaceutical scientists are increasingly interested in studying gene and protein alterations in eye drops, as well as medications containing NPs. These NPs may effectively target ocular tissues, are cost-effective and have great therapeutic efficiency.[63]

There are 2 ways to administer polymeric NPs: topically and intravenously. The injectable route is an invasive method for delivering therapeutic substances to ocular tissues since it contains colloidal drug-loaded NPs in a liquid medium with a viscosity similar to eye drop.[64] Furthermore, it extends the residence period on the ocular surface and improves penetration, making medication administration via ocular barriers easier. Biodegradable polymers' mucous adhesive characteristics lower the volume of fluid that drains from the outer layer of the eye by reacting with the existing mucus, therefore improving drug absorption and prolonging contact duration.[65]

Polymeric nanoparticles

Polymeric NPs are small, robust, colloidal molecules that range in size from 1 nm to 1,000 nm. Nanotechnologies create this innovative type of material to improve drug delivery and other therapeutic uses. Polymeric NPs could be modified for better selective distribution at the point of action or drugs bioavailability. They are widely used in drug delivery due to their high loading capacity, biodegradability and biocompatibility.[66,67]

Polymeric NPs are often used as drug delivery systems; they can transport both natural and synthetic molecules

like as proteins, peptides, growth hormones, and pharmaceuticals. There are 2 types of NPs that have distinct structures: nanospheres and nanocapsules. Medications can be absorbed onto the surface of nanospheres or kept inside their dense polymeric matrix. The drug, genetic material and other components are integrated into the nanocapsules' liquid/solid core, which is protected by a unique polymeric membrane.[68]

Types of polymeric nanoparticles

There are 2 types of polymeric NPs usually employed to create NPs: synthetic and natural. Polymeric NPs in ocular drug delivery systems are made from a variety of polymers (Table 2 [69–73]).

According to Kalam et al., tedizolid phosphate (TZP) can be administered ocularly using noninvasive chitosan NPs

Table 2. Various polymers used in the polymeric nanoparticles (NPs) in ocular drug delivery system

Reference	Polymer	Abbreviations	IUPAC name	Nature
69	chitosan	CS	5-amino-6-[(2R,4R,6S)-5-amino-6-[(2R)-5-amino-4,6-dihydroxy-2-(hydroxymethyl)oxan-3-yl]oxy-4-hydroxy-2-(hydroxymethyl)oxan-3-yl]oxy-2-(hydroxymethyl) oxane-3,4-diol	natural
70	poly (lactic-co-glycolic acid)	PLGA	2- hydroxyactic acid	synthetic
71	poly(ethyl acrylate-co-methyl methacrylate-co-trimethylammonioethyl methacrylate chloride	Eudragit RL-100	*N,N*-dimethylmethanamine;2-methylprop-2-enoic acid	synthetic
72	ammonio-methacrylate copolymer, type B	Eudragit RS-100	poly[(ethyl acrylate-co-methyl acrylate-co-methyl methacrylate)-co-[2-(trimethylammonio)ethyl methacrylate] chloride]	synthetic
73	ammonio-methacrylate copolymer, type A	Eudragit RLPO	poly(ethyl acrylate-methyl acrylate-methyl methacrylate-trimethylammonioethyl methacrylate chloride)	synthetic

CS – chitosan; PLGA – poly (lactic-co-glycolic acid).

(CSNPs) to treat Methicillin-resistant *Staphylococcus aureus* (MRSA) infections. The CSNPs demonstrated better drug loading and encapsulation and in rabbits, they caused no eye irritation indicating their potential for top-up application.[74] Polymeric NPs loaded with lutein have demonstrated long-term stability and sustained distribution within the ocular tissues. Swetledge et al. found that NPs were significantly absorbed, particularly in the choroid, and then rapidly eliminated.[75] Fenofibrate improves retinal degeneration and DR, although its solubility may limit therapy efficacy, as demonstrated by Khin et al. A water-soluble fenofibrate (FE)/cyclodextrin complex with increased solubility was developed employing polymers such as polyvinyl alcohol (PVA) and hydroxypropyl methylcellulose.[76] Naproxen-Eudragit RS100 NPs prepared using single emulsion technique showed lower crystallinity and slow drug release.[77]

Structure	Molecular formula	Molecular weight (Dalton/g/mol)	Charge	Role of polymer
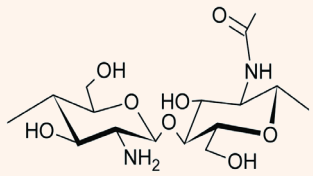	$C_{12}H_{24}N_2O_9$	3800–20,000 DA	positively charged	stabilizing NPs, improving ocular retention and inhibiting aggregation
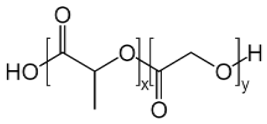	$(C_3H_6O_3)$ n.$(C_2H_4O_3)$ n	38,000–54,000 DA	negatively charged	drug penetration via ocular barriers is facilitated by PLGA NPs
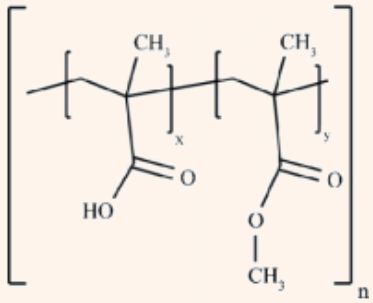	$C_{22}H_{39}ClN_2O_4$	32000 g/mol	positively charged	Eudragit RL 100 NPs increase the duration of medication residence by adhere to the ocular mucosa
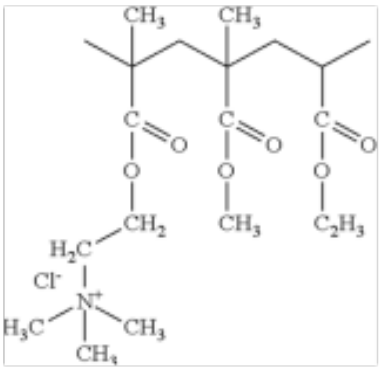	$C_{19}H_{34}ClNO_6$	407.9 g/mol	positively charged	high permeability, facilitating drug release
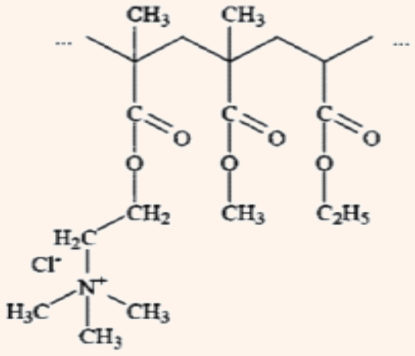	$C_{22}H_{39}ClN_2O_4$	32,000 g/mol	positively charged	sustained release

Natural polymers

There are numerous plant and animal sources of natural polymers. In addition, the cost is reasonable. Natural polymers are frequently biocompatible and nontoxic at a wide range of dosages. These can be synthesized using complex multi-step procedures or extracted from raw materials via laborious separation methods. Examples are albumin and chitosan.[78,79]

Synthetic polymers

Synthetic polymers are produced by polymerization procedures involving numerous monomer units and are rare in nature. They are often created utilizing modern growth technologies using petroleum-based raw materials. Due to their perfectly defined chemical structures, synthetic polymers allow for easier adjustment of their chemical and physical properties than natural polymers. Compared to organic materials, these artificial polymers offer greater control and versatility. Their tunability enables precise management of API release and they can be made to have mechanical properties comparable to those of biological tissues. Examples are PLA, poly(caprolactone), poly(acrylic acid), poly(vinyl alcohol), poly(cyanoacrylates), and PLGA NPs.[80,81]

Methods of preparation to develop polymeric nanoparticles

The various methods used to prepare the polymeric NPs are presented in Fig. 2. The type of medication contained within the polymeric NPs influences the specific delivery technique.[82] Typically, the 2 main strategies used involve the dispersion of existing polymers and the polymerization of monomers, which are both dual in nature.[83] Biological diluents are often used during the 1ststage of several polymer preparation techniques to aid the solubilization of the polymer.[84] The usage of these diluents can raise concerns about toxicity and risks to the environment. Furthermore, the final product must accommodate solvent residues. Monomer polymerization techniques make it possible to efficiently coat substances with polymeric NPs in a single reaction step. Regardless of the preparation process utilized, the end result is usually aqueous colloidal suspensions.[85]

Solvent evaporation

The primary method for producing polymeric NPs is solvent evaporation from a pre-formed polymer. This process generates nanospheres through an oil-in-water (o/w) emulsion. The organic phase is prepared by vigorously mixing or dissolving an active compound in an organic solvent. However, this can cause polymer degradation. Dichloromethane and chloroform were commonly used solvents in the past. Due to their toxicity, ethyl acetate has now become the preferred alternative.[86] In the initial stage, biological diluents are often used to solubilize the prepared polymers.[87] During the aqueous phase, the organic solution is mixed with a surfactant. This mixture is homogenized and ultrasonicated at high speeds to create suspended nanodroplets. As the polymer solution evaporates, NPs remain suspended in a stable emulsion. If the solvent is polar, evaporation occurs gradually under low pressure or with continuous magnetic stirring at room temperature. Once the solvent completely evaporates, NPs can be collected and purified by centrifugation. Freeze-drying is then used for long-term storage. This approach is effective and widely used for producing uniform polymeric nanospheres.[88]

Solvent diffusion

This approach combines an aqueous solution with a surfactant and a relatively water-miscible polymer solution containing a drug to form an oil-in-water (o/w) dispersion. To achieve kinetic equilibrium in a 2-stage process at room temperature, an organic solution – such as benzyl alcohol mixed with ethyl acetate – is used as the internal phase of a water-saturated colloid.[89] Significant dilution enhances solvent diffusion from the dispersed droplets into the external aqueous phase, promoting the formation of suspended particles. This method is widely employed to produce nanospheres or nanocapsules. In some cases, the final step can be eliminated through simple filtration or evaporation. The resulting NPs typically range in size from 80 nm to 900 nm. Adjustments to process parameters allow for control over particle size within this range. Although effective, this method may lead to partial diffusion of water-soluble drugs into the aqueous phase, potentially reducing drug encapsulation efficiency.[69]

Emulsification/reverse salting-out

Solvent diffusion techniques such as emulsification or reverse salting-out are commonly used to produce polymeric nanospheres. The salting-out method facilitates NP formation by removing hydrophilic solvents from the aqueous phase. The key difference lies in how an oil-in-water (o/w) emulsion is created. A water-miscible polymer solvent – such as ethanol or acetone – is combined with a salting-out agent and a colloidal stabilizer in the aqueous phase. Salting-out agents include electrolytes like magnesium chloride, calcium chloride and magnesium acetate ($Mg(CH_3COO)_2$), as well as non-electrolytes such as sucrose. Saturation of the aqueous medium reduces the miscibility between acetone and water. This enables the formation of 2 distinct solubility phases and supports o/w emulsion formation.[70] At room temperature, continuous stirring promotes stable emulsion development. Polymer precipitation occurs as the polymer diffuses from the organic solvent

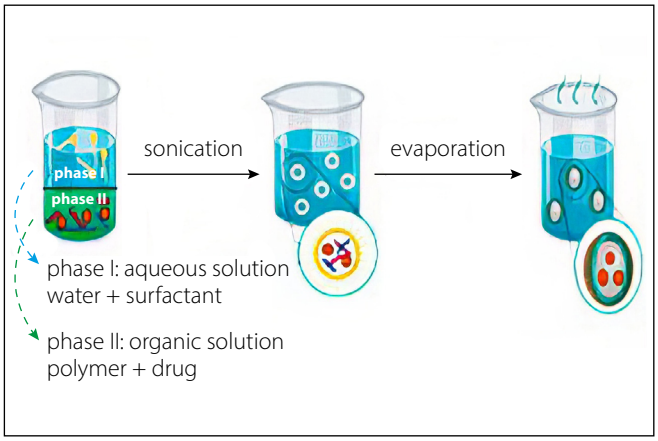

Solvent evaporation technique used for preparation of polymeric nanoparticles

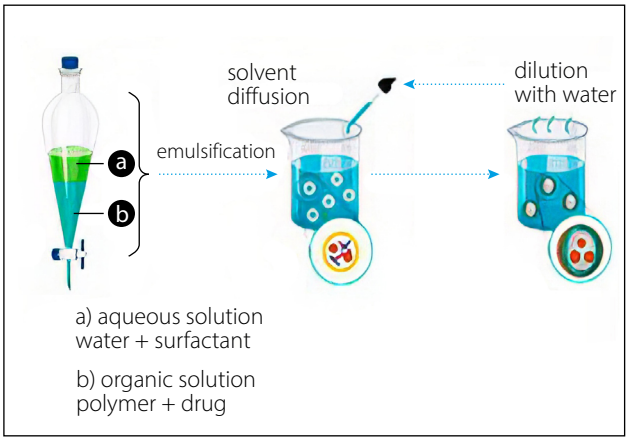

Solvent diffusion technique used for preparation of polymeric nanoparticles

POLYMERIC NANOPARTICLES

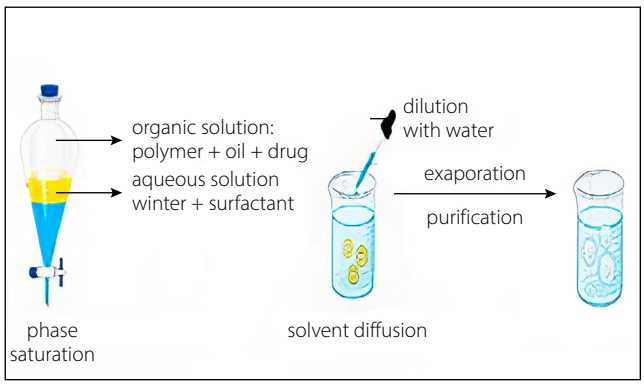

Emulsification / Reverse salting out technique used for preparation of polymeric nanoparticles

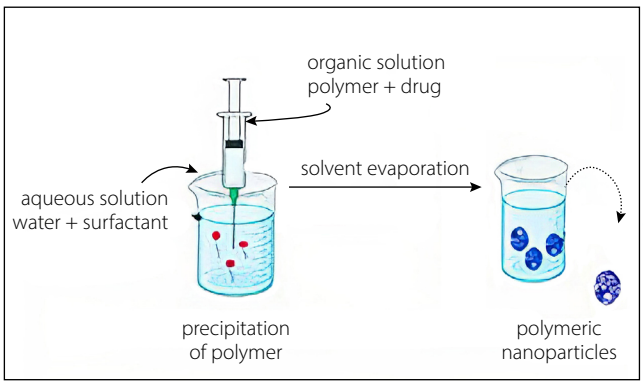

Nanoprecipitation technique used for preparation of polymeric nanoparticles

Fig. 2. Techniques for manufacturing polymeric nanoparticles

into the outer aqueous phase. This leads to nanosphere formation.[71] The resulting emulsion is then diluted with a defined amount of aqueous solution and deionized water. Filtration removes residual solvent and salting-out agents through cross-flow separation. Although this method simplifies processing, complete water solubility of the organic solvent is not required. The technique yields nanospheres ranging from 170 nm to 900 nm. By adjusting polymer concentration, average particle size can be fine-tuned between 200 nm and 500 nm.[72]

Nanoprecipitation

This approach, also known as the solvent displacement technique, involves 2 miscible solvents. A soluble organic solvent – such as acetone or acetonitrile – is used to dissolve the polymer and form the organic phase. Evaporation effectively removes the solvent, as it does not mix with water.[73,90–92] After solvent elimination, the polymer forms an interface in a lipophilic solution before being injected into the aqueous phase. This step is essential for NP formation. The polymer, dissolved in a moderately polar, water-soluble solvent, is slowly added to an aqueous medium under agitation, typically dropwise.[93]

As the polymer solution enters water, it rapidly diffuses and separates from water molecules. This promotes the immediate formation of NPs. Although the aqueous and organic phases typically interact simultaneously, procedural variations can still yield NPs.[94]

Surfactants play a crucial role in stabilizing the colloidal suspension during the process. Nanoparticles produced by the emulsification-solvent evaporation method often display uniform size and narrow size distribution compared to other methods.[95] Nanoprecipitation is a widely used method for producing nanospheres or nanocapsules, typically yielding polymeric NPs around 170 nm in diameter. This method involves dissolving or dispersing the active compound within the polymeric solution to form nanospheres. To form nanocapsules, the drug is first dissolved in oil and then emulsified into the organic polymeric phase before the internal stage begins.[96]

Characterization of polymeric nanoparticles

The physical properties of polymeric NPs vary depending on their composition, concentration, size, shape, surface qualities, crystallinity, and dispersion stage. The physical properties of polymeric NPs vary with their composition, concentration, size, shape, surface characteristics, crystallinity, and dispersion state; therefore, their comprehensive characterization is essential. Typically, a variety of techniques are employed to analyze these properties. One of the most frequently used by electron microscopy, electrophoresis, chromatography, near-infrared spectroscopy, dynamic light scattering (DLS), or photon correlation spectroscopy (PCS) and electrophoresis.[97,98] The examination of polymeric NPs is critical for finding difficulties with nanotoxicology and occupational exposure evaluation, both of which are required for regulating industrial processes and identifying health and safety risks.[99]

Morphology

Scanning and transmission electron microscopy (SEM and TEM) are commonly used to analyze the form or size of polymeric NPs, frequently in conjunction with cryofracture procedures. Transmission electron microscopy can distinguish between nanocapsules and nanospheres, as well as determine the thickness of the nanocapsules wall. Atomic force microscopy provides significant information on the surface morphology of NPs, revealing intricate topography, tiny cavities and pores.[100,101]

Particle size distribution

Polymeric NPs have an average size of 100–300 nm and a polydispersity of near 0. They can also be smaller than 50 nm or between 60 nm and 70 nm.[102] Size measurements are performed utilizing techniques such as dynamic or static light scattering. Quantitative composition, oil type and medicine dosage all have an effect on NP size. The DLS and SLS measurements can yield information on particle size distribution and aggregation state.[103]

Chemical composition and crystal structure

Chemical composition refers to the atomic elements and compounds found in NPs, which can be determined using single-particle elemental analysis methods.[104] Atomic absorption spectroscopy is a typical technique for measuring sample mass concentration by comparing the signal with calibration standards. Time-of-flight mass spectrometry is another method for determining the chemical composition of a single particle.[105] Crystal structure can be elucidated using powder XRD.[106]

Molar mass distribution of polymer

Drug-polymer interactions and polymer degradation have an impact on ingredient formulation due to their polymeric molecular dispersion. Size-exclusion chromatography and static light scattering are 2 regularly used techniques for this purpose.[107]

Surface area and chemistry

The surface area of NPs is critical for reactivity and ligand binding. Adsorption of inert gas is measured under various pressure settings to form one layer.[108] Nanoparticles

significantly affect solvent interactions due to the large number of atoms present on their surfaces. X-ray photoelectron spectroscopy and secondary ion mass spectroscopy are used to study the surface chemistry of these NPs.[109]

Zeta potential

The zeta potential is a critical characteristic that affects the surface charge of NPs. It is determined using Doppler techniques and influenced by factors such as functional group dissociation, ionic species adsorption and solvation effects. Polymeric NPs, such as those derived from poloxamers and other polymers, might influence zeta potential. A strong zeta potential is required to maintain the stability of colloidal suspensions.[110]

pH of suspensions

The stability of NP solutions can be better assessed through regular pH monitoring. Variations in pH may indicate the degradation of polymers, as evidenced by the condition of nanocapsules and nanospheres after 6 months of preservation.[111] This decrease in stability is related to carboxylic group ionization, hydrophobicity alterations and zeta potential changes, emphasizing the importance of pH monitoring in maintaining formulation integrity.[112]

Stability of polymeric NPs suspensions

During long-term storage, polymeric nanosuspensions are converted into colloidal suspensions due to slow deposition and Brownian motion.[113] Adsorption of active compounds and surfactants is one of the factors that influences their stability. Physicochemical factors such as particle size, zeta potential, polymer mass distribution, drug content, and pH can be used to assess their stability. However, industrial applications of polymeric NPs may be limited due to extended storage durations and low physicochemical stability.[114] To delay these concerns, drying methods like lyophilization or spray drying are recommended. Lyophilization removes water through sublimation, and spray drying facilitates the quick drying of droplets.[115]

Determination of the drug association

Nanoparticles' small size makes it difficult to distinguish between free and bound drug fractions, complicating the measurement of drug association with them. Drug concentration is measured using ultracentrifugation and ultrafiltration-centrifugation techniques.[116] Several factors influence the dose of pharmaceuticals in nanostructured systems, including the drug's physicochemical qualities, pH levels, polymer surface features, formulation order, oil type, and surfactants adsorbed onto the polymeric surface. Improving the surface characteristics of particles can result in various levels of drug association, which is critical for extending the drug's effects.[117] Drug adsorption isotherms on NP surfaces give information about drug distribution and association capacity. Detecting drug association mode is difficult since current techniques only evaluate the concentration of medicine coupled with NPs. Additional approaches include XRD or infrared spectroscopy.[118]

Pharmaceutical in vitro release kinetics

Drug release from polymeric NPs is determined by factors like desorption, matrix erosion, diffusion, or a combination of these mechanisms. Low-pressure filtration and ultrafiltration-centrifugation are 2 methods used to explain drug release from NPs. Drug release kinetics in nanospheres are typically exponential, whereas medication in nanocapsules has zero order kinetics when released via the polymeric membrane.[119]

In vitro and vivo toxicological studies

The use of NPs for drug delivery has several advantages, including increased stability and the capacity to encase active molecules. Nonetheless, the potential for nanotoxicity remains a major concern to be addressed.[120] Studies have shown that non-biodegradable and reversible polymer nanocarriers can be employed efficiently for ocular medication delivery. Biomimetic technology is used to develop more effective nanocarriers. Biodegradable synthetic polymers are widely used in medical applications. Examples include PLA and PLGA. These polymers are safe, biocompatible and show low immunogenicity and toxicity. Polymeric NPs, which are known for their high drug encapsulation efficiency and ease of manufacture, are widely employed in tissue engineering, drug delivery, biological sensors, and the development of biomimetic materials. Their possible applications are influenced by size, surface charge, hydrophilicity, hydrophobicity, and polymer type.[121]

The cytotoxicity of NPs is tested in vitro using colorimetric analysis. Jain and Thareja focused on PLGA NPs containing triterpenoids with possible anticancer capabilities and compares their effects on HepG2, Caco-2 and Y-79 cells. When the NPs were loaded with both natural and synthesized mixtures of oleanolic and ursolic acids, cell viability increased considerably.[122] Polyethylene glycol was added to the surface of dexibuprofen-loaded PLGA NPs to help them stay in the ocular mucosa longer. These nanospheres are less toxic to cells than free dexibuprofen and have been shown to be non-irritating in both in vitro and in vivo studies. Pranoprofen, another nonsteroidal anti-inflammatory drug (NSAID), has been improved by coating with PLGA nanospheres, which are non-cytotoxic to Y-79 cell lines. The use of polystyrene NPs in topical applications has shown that they accumulate at follicular apertures, resulting in excellent drug delivery with minimal toxicity. The discussion also covers biomimetic tactics like

cell membrane camouflage and functionalization. A new pH-responsive copolymer has been designed to produce biocompatible and biodegradable NPs for chemotherapeutic drug delivery. These nanosystems, known for their powerful anticancer properties, have been examined both in vitro and in vivo. They have a crosslinked bovine serum albumin shell that does not harm normal tissues.[123]

Applications of polymeric nanoparticles in ocular delivery

Polymeric NPs have gained significant interest in ocular medicine for their ability to provide regulated drug release, improved biodegradability and drug bioavailability. The use of these NPs in ocular therapeutics efficiently resolves difficulties such as quick drug clearance through tears and restricted drug absorption in ocular tissues. The following are

Table 3. Collective information of polymeric nanoparticles (NPs) used in ophthalmic application

Reference	Name of category	Name of API	Structure	Dosage form	Polymer used
124	antibacterial	ciprofloxacin	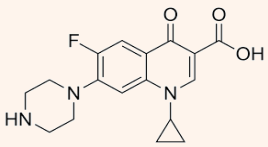	polymeric NPs	PLA
125	antibacterial	gemifloxacin	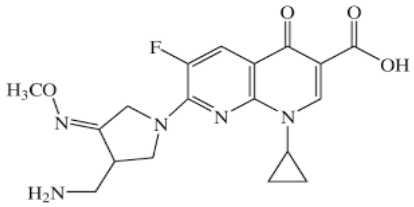	polymeric NPs	chitosan
126	antibacterial	moxifloxacin HCl	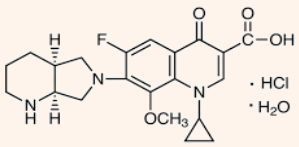	polymeric NPs	Eudragit® RL 100 and Kollidon® SR
127	antibacterial	moxifloxacin HCl	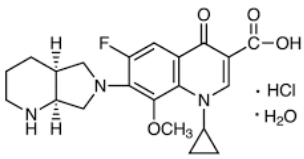	polymeric NPs	PLGA
128	antibacterial	levofloxacin	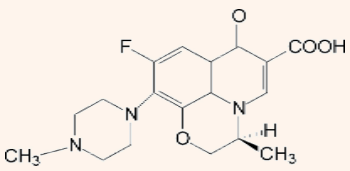	polymeric NPs	chitosan–PLGA
129	antibacterial	gatifloxacin	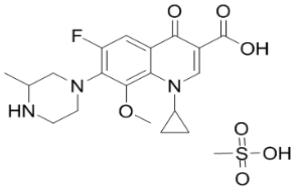	polymeric NPs	Eudragit RL and RS

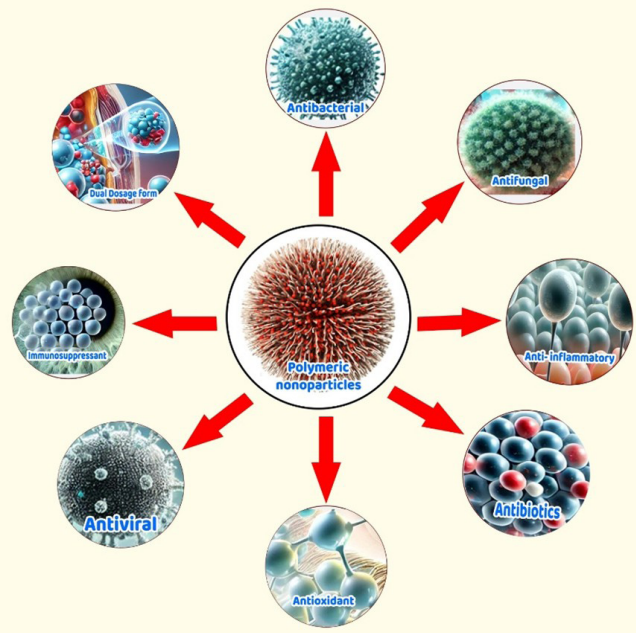

Fig. 3. Applications of polymeric nanoparticles in ocular delivery

Method of preparations	Surfactant used	Particle size	Zeta potential	Significance
nanoprecipitation	PVA	438–458 nm	−17 mV	preventing bacterial invasion
ionic gelation	Tween 20	158.4 nm	−15 mV	enhancement of precorneal retention
spray-drying	Span 60	400–450 nm	−18 mV	enhancement of corneal permeability
double emulsion (w/o/w) solvent evaporation	PVA, Tween 20	167.4–622.4 nm	10–40 mV	enhancement of bioavailability
single emulsion solvent evaporation	PVA	169.968 ±15.23 nm and 0.13 ±0.03 nm	49.54 ±2.43% and 11.29 ±2.13% mV	extended release
nanoprecipitation and double emulsion	Tween 80 PVA	410 nm and 68 nm	33 mV	increased bioavailability

Table 3. Collective information of polymeric nanoparticles (NPs) used in ophthalmic application

Reference	Name of category	Name of API	Structure	Dosage form	Polymer used
130	antibacterial	levofloxacin	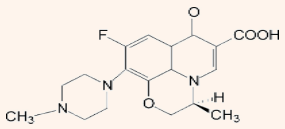	nanosuspension	PLGA
131	antibacterial	sparfloxacin	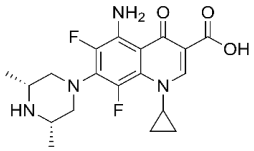	nanosuspension	PLGA
132	antibacterial	moxifloxacin	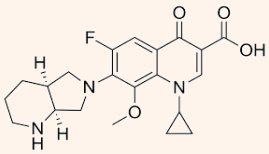	polymeric NPs	chitosan dextran sulfate
133	antibacterial	moxifloxacin Hcl	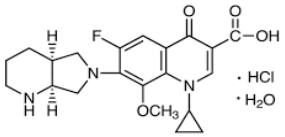	polymeric NPs	Eudragit RL 100
134	antifungal	voriconazole	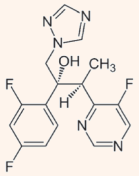	polymeric NPs	PLGA-PEG
135	antifungal	voriconazole	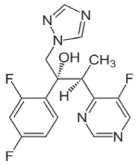	polymeric NPs	chitosan
136	antifungal	fluconazole	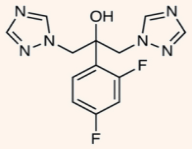	polymeric NPs	alginate/ chitosan
137	antifungal	natamycin	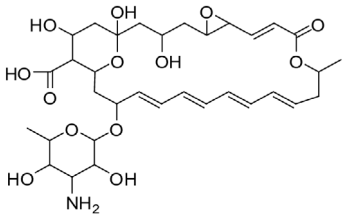	polymeric NPs	chitosan
138	antifungal	terconazole	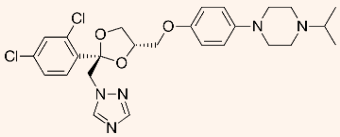	polymeric NPs	Eudragit RLPO®
139	antifungal	amphotericin B	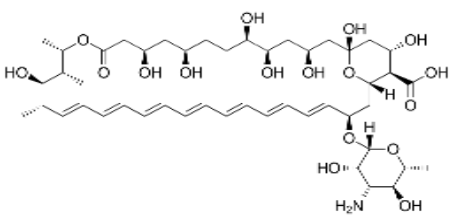	polymeric NPs	lecithin/ chitosan

Method of preparations	Surfactant used	Particle size	Zeta potential	Significance
nanoprecipitation	PVA	190–195 nm	–25 mV	prolonged retention
nanoprecipitation	PVA	180–190 nm	–22 mV	appropriate particle size
ionic gelation	PVA	279.18 ±15.63 nm	+31.23 ±1.32 mV	prolonged release profile
solvent displacement	PVA	below 200 nm	10–40 mV	good ocular retention property
emulsion/evaporation	PVA	361 ±68 nm	26.0 ±1.9 mV	effective at inhibiting the ***Candida albicans***
ionic gelation	Tween 20, Tween 80. sodium lauryl sulfate	160–500 nm	38–45 mV	sustains drug release
ionotropic pre-gelation	PVA	<390 nm	–20 mV	controlled drug release
ionic gelation	Tween-80 (v/v)	444:7 ±2:4 nm	22.6 mV	potent ability to inhibit fungi
nanoprecipitation	poloxamer 188	49.41–78.72 nm	(≥21.47) mV	enhancing ocular antimycotic activity
ionic gelation	Tween 80	161.9–230.5 nm	26.6–38.3 mV	better bioavailability

Table 3. Collective information of polymeric nanoparticles (NPs) used in ophthalmic application

Reference	Name of category	Name of API	Structure	Dosage form	Polymer used
140	non-steroidal anti-inflammatory drugs	dexibuprofen	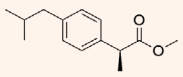	polymeric NPs	PLGA
141	non-steroidal anti-inflammatory drugs	aceclofenac	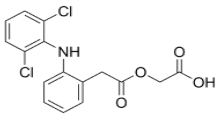	polymeric nanosuspensions	Eudragit RS 100
142	non-steroidal anti-inflammatory drugs	pranoprofen	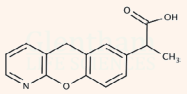	polymeric NPs	PLGA
143	non-steroidal anti-inflammatory drugs	diclofenac sodium	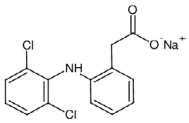	polymeric NPs	chitosan
144	non-steroidal anti-inflammatory drugs	aceclofenac	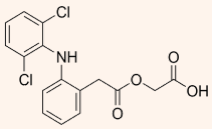	polymeric NPs	Eudragit RL 100-
145	non-steroidal anti-inflammatory drugs	diclofenac sodium	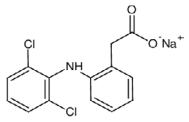	nanosuspension	Eudragit S100
146	anti-inflammatory drugs	triamcinolone acetonide	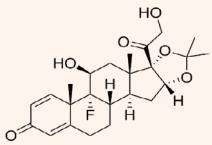	polymeric NPs	PLGA–chitosan
147	anti-inflammatory drugs	atorvastatin calcium	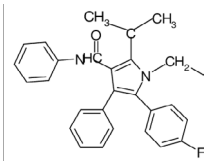	polymeric NPs	PLGA-CS
148	steroidal anti-inflammatory drugs	fluorometholone	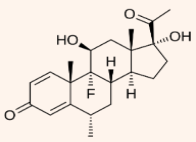	polymeric NPs	PEG-PLGA
149	steroidal anti-inflammatory drugs	fluorometholone	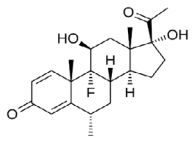	polymeric NPs	PLGA
150	steroidal anti-inflammatory drugs	triamcinolone acetonide	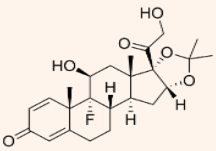	polymeric NPs	PLGA
151	steroidal anti-inflammatory drugs	pilocarpine HCl	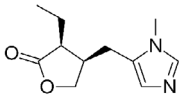	polymeric NPs	gelatine

Method of preparations	Surfactant used	Particle size	Zeta potential	Significance
solvent displacement	Tween 80®, PVA	below 200 nm	–15 mV	higher availability
nanoprecipitation	Tween	238.9 ±8 nm	40.3 ±3.8 mV	better patient safety
solvent displacement	PVA	350 nm	–7.41 mV and –8.5 mV	maximum encapsulation capacity
ionic gelation	Tween 80	130–190 nm	4–9 mV	increases bioavailability
nanoprecipitation	Tween 80	134.97 nm	30.5 mV	improves patient compliance
nanoprecipitation	poloxamer 188	172 nm	–23.7 mV and –6.07 mV	higher efficacy
emulsion-evaporation	PVA	195 nm	–22.5 mV	better penetration
single emulsion and solvent evaporation	PVA, Pluronic®F127	192.0±21.6 nm	17.4±5.62 mV	sustained action
nanoprecipitation	PVA	0.112 ±0.007 nm	–8.32 ±0.65 mV	better patient compliance
solvent displacement	poloxamer 188	below 200 nm	–30 mV	higher permeability at corneal level
emulsification/solvent diffusion	PVA	195 nm	–16.1 mV	better patient compliance
desolvation	PVA	110–220 nm	–6.2 mV	sustained action

Table 3. Collective information of polymeric nanoparticles (NPs) used in ophthalmic application

Reference	Name of category	Name of API	Structure	Dosage form	Polymer used
152	antibiotics	vancomycin	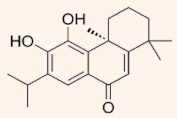	polymeric NPs	HA
153	antibiotics	daptomycin	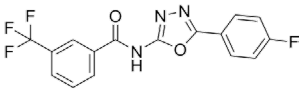	polymeric NPs	chitosan, sodium alginate
154	antibiotics	amikacin sulphate	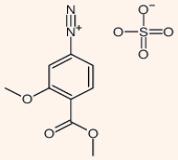	polymeric NPs/ nanosuspension	Eudragit RS100, Eudragit RL100
155	antibiotics	doxycycline	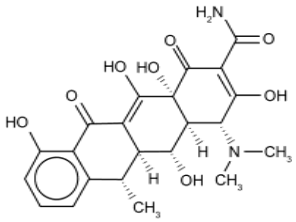	polymeric NPs	gellan gum
156	antibiotics	clarithromycin	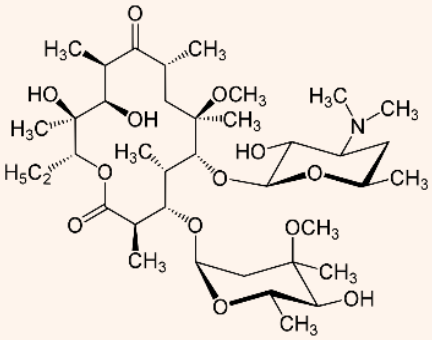	polymeric NPs	PLGA
157	antioxidant	rosmarinic acid	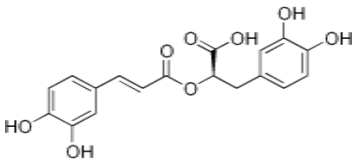	polymeric NPs	chitosan
158	antioxidant	lutein	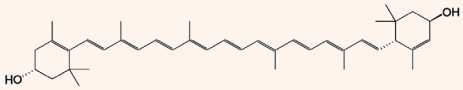	polymeric NPs	PLGA
159	antiviral	acyclovir	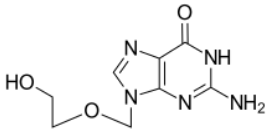	nanospheres	PLA
160	immunosuppressant	cyclosporin A	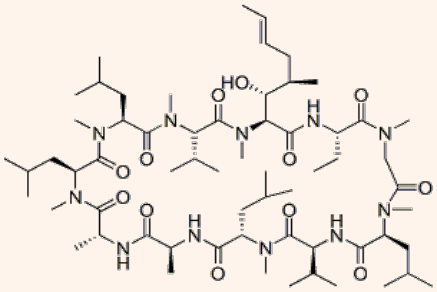	polymeric NPs	chitosan

Method of preparations	Surfactant used	Particle size	Zeta potential	Significance
emulsification and solvent evaporation	poloxamer 407	154 ±3 nm	26.4 ±3.3 mV	better penetration
ionotropic pre-gelation	Tween 80	393.0 ±31.3 nm	from −25.18 ±0.64 to −19.69 ±1.34 mV	maximum residence time
w/o/w emulsification solvent evaporation	PVA	149 ±16.2nm	25.69 ±1.4 mV	maximum penetration
emulsion cross-linking	PVA	383 ±4.2 nm	−22.6mV	sustained action
nano-precipitation	PVA	80.2 ±4.0 189 nm	−14.26 ±1.92 mV	for better absorption
ionic gelation	Pluronic F68	200–300 nm	28.2 ±2.2 mV	higher retention
emulsion evaporation	PVA,Tween-80	210.6 ±3.3 nm	6.7 ±0.3 mV	maximum photostability
solvent deposition	Brij 96, Pluronic F68, 3Triton X100, or Tween 80	200 nm	from −31.1 mV to −14.7 mV	better compliance
ionic gelation	Pluronic F68	293 nm	37 mV	longer extraocular release

Table 3. Collective information of polymeric nanoparticles (NPs) used in ophthalmic application

Reference	Name of category	Name of API	Structure	Dosage form	Polymer used
161	dual dosage form	sertaconazole	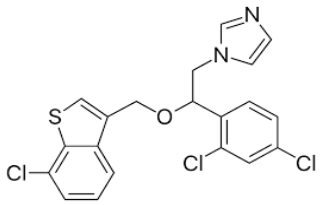	solid dispersion	PLGA
162	dual dosage form	fluconazole		gel	sodium alginate
163	dual dosage form	norfloxacin	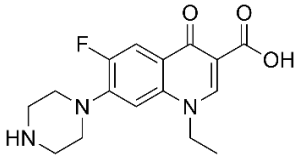	hydrogels	PLGA
164	dual dosage form	ofloxacin	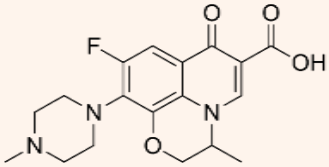	in situ gel	PCL
165	dual dosage form	fluconazole	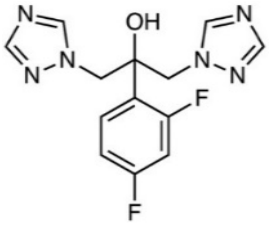	hydrogel	poly (caprolactone)
166	dual dosage form	fluoromethalone	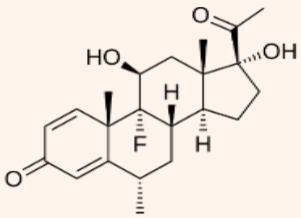	in situ gel	PLGA
167	dual dosage form	vancomycin	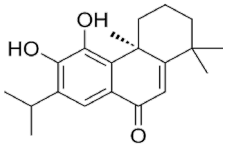	gel	Eudragit® RS100
168	dual dosage form	levofloxacin	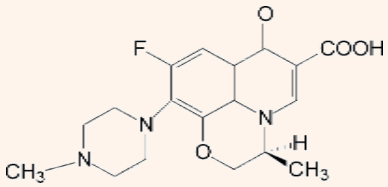	in situ gel	chitosan

PVA – polyvinyl alcohol; HCL – hydrochloride; PLGA – poly(lactic-co-glycolic) acid; PEG – polyethylene glycol; CS – chitosan; HCE – human corneasl epithelial; HA – hyaluronic acid; PCL – polycaprolactone.

Method of preparations	Surfactant used	Particle size	Zeta potential	Significance
nanoprecipitation	Tween 80	305.9 ±4.36 nm	22.57 ±0.23 mV	higher dissolution profile
antisolvent precipitation nanonization	sodium lauryl sulfate, Pluronic F-127	352 ±6.1 nm	–18.3 mV	higher corneal permeation
double-emulsion/solvent evaporation	Tween 80	392.02 nm and 190.51 nm	30.43 mV and –33.62 mV	prolonged drug release
emulsion solvent evaporation	Kolliphor P188	195.4 ±11.80 nm	55.4 ±3.07 mV	high penetration and absorption
solvent evaporation	Tween® 80 and polyvinyl alcohol	145 nm	28.23 mV	higher antifungal activity
solvent displacement	poloxamer 407	150.8 ±0.7 nm	–27.9 ±0.3 mV	high corneal residence
double emulsion (W/O/O), solvent evaporation	Span®80	155 nm	from –43 mV to +55 mV	smart carrier
ionotropic gelation	pluronic F-127	223.65 ±5.13 nm	±30 mV	non-irritant

some notable applications of polymeric NPs in eye therapy (Fig. 3, Table 3[124–168]).[169,170]

Antibacterial

A new treatment for bacterial keratitis, a condition that can cause to blindness and vision loss, has been developed using ciprofloxacin in conjunction with a mixture of glycol chitosan and PLA. The NPs obtained by Padaga et al. showed a significant antibacterial response against Pseudomonas aeruginosa and were effective in inhibiting bacterial quorum sensing. In vivo research demonstrated good ocular retention and a reduction in bacterial loads.[171]

Gemifloxacin (GM) has a longer residence time than the free drug in deep tissues and on the ocular surface. Eight types of GM NPs were created using the precipitation method triggered by sodium tripolyphosphate to produce chitosan polymer. The formulated NPs had an average entrapment efficiency of 46.6% and a cumulative release of 74.9%. Studies in rabbits showed a significant increase in GM concentration, improved trans corneal penetration and increased antibacterial effectiveness.[172] Moxifloxacin (MOX) hydrochloride is used to treat ocular infections, such as bacterial conjunctivitis. This drug is a fluoroquinolone antibiotic. It works by eliminating the microorganisms that cause conjunctivitis. Kırımlıoğlu et al. aimed to improve ocular absorption by increasing the carrier's interaction time with the ophthalmic membrane. Moxifloxacin hydrochloride was integrated into cationic Eudragit® RS 100 NPs via spray-drying technique. The formulations were characterized, and MOX was quantified using high-performance liquid chromatography (HPLC) analysis. The cytotoxicity tests found no negative effects after 24 h.[173]

Khan et al. investigated a NP-based approach to enhance ocular retention and drug bioavailability for the prolonged delivery of moxifloxacin (MOX). By utilizing PLGA matrix-forming polymers, the NPs were optimized for size, stability and polydispersity index. They found that the NPs exhibited high initial release rate and a prolonged drug release through diffusion, with a low clearance rate and elevated maximum plasma concentration (C_{max}), area under the curve (AUC) and mean residence time (MRT) in comparison to commercial eye drops. These results suggest that PLGA NPs significantly improve the bioavailability of MOX hydrochloride.[174]

Conjunctivitis is a common infection of the ocular surface that is normally treated with eye drops. Unfortunately, these drops may lose up to 95% of their medicament. A promising novel treatment uses PLGA NPs coated with chitosan and containing levofloxacin efficiently treat bacterial conjunctivitis. These NPs were evaluated concerning their size, drug absorption rates, entrapment efficiency, drug release profiles, ex vivo permeation, ophthalmic compatibility, antibacterial capabilities, and assessments utilizing binocular laser microscopy and gamma scintillation. The adjusted formulation demonstrated increased penetration, considerable antibacterial activity and an extended corneal residence duration.[175]

Gatifloxacin's ocular bioavailability was improved by embedding it in cationic polymeric NPs. The optimized formulation had a drug loading of 46%, acceptable levels of cytotoxicity and a sustained release rate. The underlying hypothesis is that these NPs increase GM's residence time.[176]

To overcome the challenges associated with drug delivery to the ocular region, the team developed and evaluated levofloxacin-encapsulated PLGA NPs, focusing on various characteristics such as ex vivo trans corneal permeability, zeta potential, in vitro drug release, and particle size. The NPs achieved a drug entrapment efficiency of nearly 85%, with an average particle size ranging from 190 nm to 195 nm. Furthermore, they demonstrated non-irritating characteristics, achieving an average score of 0.33 over a 24-h period in the hen's egg test-chorioallantoic membrane (HET-CAM).[177] Drugs with low ocular bioavailability, in contrast to conventional eye drops, face physiological barriers within the eye. To enhance ocular effectiveness, researchers are creating PLGA NPs to improve the distribution of sparfloxacin in the eye. These NPs exhibit a zeta potential of –22 mV and an average particle size ranging from 180 nm to 190 nm, making them suitable for ocular applications. Gupta et al. demonstrated significant retention in the precorneal area, remaining in the eye for a longer duration compared to standard commercial formulations.[178]

Moxifloxacin, a fourth-generation fluoroquinolone antibiotic, is commonly employed in the treatment of ocular infections such as keratitis and conjunctivitis. Its efficacy against Gram-negative bacteria is similar to that of ciprofloxacin and ofloxacin, while also demonstrating superior penetration into inflamed ocular tissues. Researchers have created nanoformulations encapsulating MOX to enhance ocular absorption, minimize side effects and improve patient adherence.[179]

Antifungal

Polymeric NPs are a viable approach for improving antifungal drug delivery in ocular applications, overcoming problems in getting antifungal medicines to the eye.

Cyclosporine A is used as an immunosuppressive, antiviral and anti-inflammatory medication to treat dry eye. Experimental results show that CsA can increase the antifungal activities of azoles, including voriconazole, by killing both planktonic cells and biofilms. Research of PLGA NPs discovered that voriconazole-loaded PLGA NPs did not significantly improve antifungal efficacy. However, PLGA NPs loaded with voriconazole and CsA displayed higher antifungal activity.[180]

Voriconazole, a triazole antifungal, is used to treat particular fungal infections and severe fungal illnesses. Mohammadzadeh et al. produced voriconazole-loaded chitosan

NPs utilizing ionic gelation and sodium tripolyphosphate to create a topical ocular delivery system. The NPs were investigated using XRD, DSC, SEM, and FTIR. A Box–Behnken design was devised, and the formulation showed substantial drug loading, no burst effect and a 48-h sustained drug release time, making it useful for eye delivery.[181]

Fluconazole's efficiency in treating infections can be enhanced by generating fluconazole-loaded polymeric NPs using a variety of polymers and processes. The NPs were created utilizing a twofold emulsion/solvent evaporation technique and ionotropic pre-gelation procedures. NP4 was chosen for in vitro release testing against a *C. albicans* resistant strain. This formulation displayed an initial fast release followed by a sustained release profile over a full day, resulting in a 20-fold reduction in fluconazole's minimum inhibitory concentration (MIC). As a result, fluconazole's antifungal potency against *C. albicans* increased significantly.[182]

To improve the antifungal properties of chitosan, emphasizing its potential for treating eye illnesses, these NPs were combined with sodium tripolyphosphate (CTS) and natamycin (NAT) to increase their inhibitory effects on *C. albicans*. The results suggested that NAT-NPs had a higher inhibitory concentration (IC50) and a wider area of inhibition against *C. albicans* than natamycin.[183] To improve the ocular distribution and antifungal activity of terconazole (TCZ) by creating cationic polymeric NPs containing TCZ. The NPs were evaluated using a variety of methodologies, including FTIR, entrapment efficiency testing and X-ray powder diffraction. They demonstrated prolonged antifungal activity for up to 24 h and were more effective against *C. albicans* than regular TCZ. Mohsen proposed that cationic polymeric NPs may be an efficient drug delivery strategy to increase the ocular antifungal effects of TCZ.[184]

Keratitis caused by fungi is the leading cause of blindness worldwide. Amphotericin-B is the primary treatment for fungal infections, although its low precorneal retention reduces its efficacy. To overcome this issue, Chhonker et al. developed lecithin/chitosan NPs that encapsulate amphotericin-B for long-term ocular administration. These NPs have enhanced antifungal activity against *Aspergillus fumigatus* and *C. albicans*, as well as higher bioavailability and precorneal residence duration.[185]

Non-steroidal anti-inflammatorys

Ocular inflammation is a common problem in ophthalmology and it is frequently treated with NSAIDS such as ibuprofen. However, these medicines have very low absorption in ocular tissues, with fewer than 5% being efficacious. Biodegradable polymeric PLGA NPs offer a viable alternative to traditional eye drops, with the goal of reducing side effects and increasing bioavailability. Solvent displacement procedures were used in conjunction with surfactants to create dexibuprofen-encapsulated formulations.[186]

Aceclofenac is a NSAID that can be used to treat ocular inflammation. It acts by inhibiting cyclooxygenase (COX) enzymes, which are involved in the formation of prostaglandins, a chemical messenger that contributes to inflammation and pain. The purpose of the study by Katara and Majumdar was to develop aceclofenac NPs using the direct precipitation method. These spherical NPs were shown to be suitable for intraocular delivery. They showed Higuchi square root release kinetics and a prolonged in vitro drug release profile, achieving a twofold increase in penetration compared to an aceclofenac water-based solution.[187]

Pranoprofen is an anti-inflammatory drug made of PLGA NPs that protects against strabismus and cataract surgery. It has been evaluated for cytotoxicity, corneal absorption, ocular compatibility and therapeutic efficacy, with no symptoms of toxicity.[188] Diclofenac sodium is a NSAID that is used topically to the eye to relieve inflammation, irritation and light sensitivity, especially following cataract extraction or refractive surgery. It works by inhibiting the production of specific chemicals that cause inflammation and pain. The goal of the study by Asasutjarit et al. was to improve the ocular bioavailability of diclofenac sodium (DC) by developing diclofenac sodium-trimethyl chitosan NPs (TMCNs) for use in ophthalmology. The ionic gelation process was used to generate DC-TMCNs with various compositions, enabling for evaluation of their physicochemical properties, drug release potential, risk of ocular irritation, and absorption in the eye. DC-TMCNs reached a zeta potential of +4 mV.[124]

Aceclofenac is a NSAID that can be used to treat ocular inflammation. Katara et al. developed formulation of aceclofenac NPs using Eudragit RL 100 resulted in a sustained in vitro release pattern consistent with Higuchi square root kinetics. This NP formulation increased drug penetration in excised corneas. It decreased lid closure scores in rabbits with arachidonic acid-induced ocular inflammation. It also reduced polymorphonuclear leukocyte migration in these rabbits. The formulation remained stable for over 2 years.[125]

Using a goat cornea-based experimental model, Ahuja et al. investigated how medicinal components alter diclofenac absorption. The oil-in-water emulsion solvent evaporation method was used to combine diclofenac sodium and Eudragit RS 100. These formulations exhibited a high zeta potential. They had an optimum particle size and efficient drug entrapment, and demonstrated a prolonged release of the medication in vitro without generating any discomfort in ocular tissues. The drug release mechanism was discovered as non-Fickian, with matrix diffusion control playing the key role.[126]

Steroids anti-inflammatory drugs

Steroidal anti-inflammatory medicines, often known as corticosteroids, are used in ophthalmology to treat eye irritation. They function by lowering the immune response and inflammation, which can be helpful in situations like uveitis and following surgeries like cataract extraction. Xing et al. aimed to improve the design of chitosan (CHT)-coated PLGA NPs containing triamcinolone acetonide (TA). The PLGA NPs infused with TA revealed potent anti-inflammatory activities, reduced levels of interleukin 6 (IL-6), alleviated inflammatory symptoms in rabbits, and demonstrated better transparency in aqueous humor compared to normal levels.[127] The ocular anti-inflammatory drug atorvastatin calcium was integrated into a polymeric NP to improve surface properties and allow for longer release. Four formulations were examined to assess their ocular irritation and efficacy in resolving inflammation caused by prostaglandin E1 (PGE1).[128] Nanoparticles made of PEG and PLGA, functionalized with cell-penetrating peptides and loaded with fluorometholone, have been developed for the treatment of eye irritation. These NPs revealed acceptable qualities for ocular administration and had anti-inflammatory effects in human corneal epithelial cells and mouse eyes, potentially providing a unique technique for managing ocular inflammatory disorders.[129]

Fluorometholone is an anti-inflammatory corticosteroid that is applied topically to the eyes to treat a variety of problems such as inflammation, allergies and postoperative recovery. It helps to minimize edema and redness in the eyes. Compared to some other corticosteroids, it is usually thought to have a lesser risk of elevating IOP. Gonzalez-Pizarro et al. aimed to produce and improve PLA NPs containing fluorometholone for the treatment of ocular inflammation. The resultant NPs, with an average particle size of less than 200 nm and a negative surface charge of –30 mV, were found to be acceptable for ocular applications. They showed greater corneal penetration and higher anti-inflammatory effects than current commercial medications, implying that they could be used as an effective alternative to traditional topical therapy.[130] To increase the efficacy of TA in the treatment of endotoxin-induced uveitis by using a modified emulsification/solvent diffusion approach, in vivo tests were conducted using PLGA NPs with a drug loading of 3.16%, and inflammatory parameters were measured in rabbit eyes. Furthermore, inflammatory mediators were assessed 3 h after injection.[131] Gelatin NPs containing hydrocortisone or pilocarpine HCl were created using the desolvation method. The pH affects particle size but does not modify their properties. Furthermore, a high level of pilocarpine HCl was successfully encapsulated within both types A and B gelatin particles, resulting in the formation of a compound.[132]

Antibiotics

A new formulation of vancomycin (VCM)-loaded N, N-dodecyl, methyl-polyethylenimine NPs integrated with HA, has been created to improve the treatment of bacterial endophthalmitis. The NPs showed high bactericidal activity and ocular compatibility, with a zeta potential of +26.4 ±3.3 mV and a 93% encapsulation rate for VCM. They were discovered to be non-irritating and non-toxic to emerging retinal pigment epithelia-19 (ARPE-19) cells, indicating that their use coupled with HA may provide further therapeutic benefits.[133] The use of mucous adhesive chitosan-loaded alginate (CS-ALG) NPs is a promising technique for providing daptomycin to the eye epithelium, potentially enhancing the treatment of bacterial Endophthalmitis by boosting drug permeability and retention in the eye.[134] In some studies on development of amikacin-loaded polymeric NPs, effective distribution of amikacin was observed. Sharma et al. examined characteristics such particle size, zeta potential and antibacterial effectiveness against *S. aureus*. These NPs were used to create tear films and showed compatibility with the Korsmeyer–Peppas model.[135]

Doxycycline is a tetracycline antibiotic. It treats illnesses through preventing the growth and spread of bacteria. Polymer-surfactant NPs containing doxycycline hydrochloride (DXY) were created to improve to improve the drug's penetration and retention time in the eye. These NPs were analyzed for their antibacterial characteristics and potential to induce eye irritation, demonstrating their safety and effectiveness for sustained delivery of ocular medicine.[136] Biodegradable NPs containing clarithromycin shown antibacterial activity against *S. aureus*. The NPs exhibited a constant size distribution and a spherical shape, indicating decreased drug crystallinity and the existence of noncovalent interactions.[137]

Antioxidants

Rosmarinic acid, a natural antioxidant found in plants such as rosemary, may provide significant benefits for eye health due to its antioxidant and anti-inflammatory effects. Chitosan NPs were used as natural carriers for rosmarinic acid, encapsulating extracts from *Satureja montana* and *Salvia officinalis*. Chitosan and sodium tripolyphosphate were combined in a 7:1 weight ratio at pH 5.8, resulting in NPs ranging in size from 200 nm to 300 nm. When delivered to human corneal cell lines and the retina pigment epithelium, the NPs showed no obvious cytotoxicity.[138] Lutein is a potent antioxidant and carotenoid that is essential for ocular health, notably in protecting the macula. It can help reduce inflammation, combat oxidative stress and possibly prevent or slow AMD. Carter et al. examined the use of lutein-loaded polymeric NPs as therapeutic delivery vehicles for ocular illnesses, including their stability and distribution. Their findings suggest that there

is significant absorption in ocular tissues, with the choroid having the highest uptake.[139]

Antiviral drugs

Acyclovir-containing nanosphere colloidal solutions were investigated as possible ocular medication delivery vehicles. Pegylated 1,2-distearoyl-3-phosphatidylethanolamine was added to PLA nanospheres. The ocular pharmacokinetics of acyclovir-loaded NPs were observed in vivo and compared to an aqueous suspension of the free medication. Giannavola et al. found that when the surfactant concentration grew, the average size and relative zeta potential of PLA nanospheres dropped. The PEG-coated nanospheres performed better than standard PLA nanospheres.[140]

Immunosuppressant

The current options of extraocular disease treatment is limited because of the difficulties in providing medications without harming intraocular structures or resulting in systemic drug exposure. De Campos et al. investigated the potential of chitosan NPs in new drug delivery methods for the ophthalmic mucus. Cyclosporin A was chosen for the model chemical. The NPs demonstrated high loading and CsA interaction efficiency, resulting in fast release in vitro and steady release in vivo.[141]

Dual dosage form

Polymeric NPs (PLGA NPs) of sertaconazole (STZ) has been used as delivery vehicles to increase ocular availability for the treatment of fungal keratitis. The nanoprecipitation process was employed to generate STZ-loaded PLGA NPs, which were then optimized using a 2^4-full factorial. The hydrodynamic size of PLGA NPs was increased by incorporating PEG 2000 in a solid dispersion containing sertaconazole. STZ-PEG2000-loaded PLGA NPs demonstrated a 2.5 increase in permeability through rabbit cornea and a fourfold decrease in MIC value against *C. albicans*.[142]

Developed and analyzed an improved formulation of fluconazole polymeric NPs, with a focus on its efficacy against a well-known *C. albicans* variety. These enhanced NPs were mixed into 2 different ophthalmic formulations. To assess the efficacy and safety of the produced product, Almehmady et al. looked into the ophthalmic formulations' rheological features, in vitro drug release, stability, and ocular delivery.[143] To improve norfloxacin (NFX) ocular absorption by creating hydrogels containing NFX-loaded NPs, they were created utilizing a double-emulsion/solvent evaporation technique with PLGA polymer. The selected NPs were spherical, had acceptable properties and showed promising antibacterial activity against *P. aeruginosa*. The hydrogels were thixotropic, pseudoplastic, spreadable, transparent, and produced better drug penetration and long-term release. The G3 and G4 systems showed encouraging antibacterial activity.[144]

Salama et al. focused on how nanotechnology and bioadhesive gel can potentially be used to create an ocular drug delivery system that reduces eye irritation. They highlighted the impact of formulation factors on drug entrapment efficiency, particle size, and polydispersity index. The optimized formulation LPCL-NP2 encapsulates ofloxacin in a spherical shape and the drug's amorphous form was confirmed with DSC analysis. The NP formulation was tested on rabbits with *Escherichia coli* infection and showed remarkable antibacterial effectiveness and low bacterial growth.[145] To increase fluconazole ocular penetration by creating and characterizing NPs by antisolvent precipitation nanonization, various surfactant concentrations were investigated and the ocular pharmacokinetics of a gel with a suitable drug NP composition was studied in rabbits. El Sayeh et al. found that NP formulations improved ocular diffusion findings. Formula F3 had the highest ex vivo release rate (100% after 6 h) and a narrower particle range (352 ±6.1 nm), with a zeta potential charge of –18.3 mV. The ocular gel containing fluconazole NPs improved ocular pharmacokinetic properties and increased medication corneal penetration.[146]

Thermosensitive gels have been developed to enhance ophthalmic anti-inflammatory efficacy by transforming into gels at corneal temperature and allowing appropriate release of PLGA NPs encapsulated with fluorometholone. These gels prevent initial drug release bursts and increase precorneal residence time, allowing for increased eye drop dosing. Gonzalez-Pizarro et al. showed that no formulation causes eye discomfort, indicating that they are effective for the acute and preventive control of ocular inflammatory disease.[147]

For improvement of ocular bioavailability, VCM-loaded polymeric nanoparticles were prepared and incorporated into chitosan-based gel by using double emulsion solvent evaporation technique. The Draize test confirmed that these formulations are non-irritating and suitable for ocular use. Microbiological susceptibility tests showed longer retention timeas and increased C_{max} levels and AUC. Consequently, VCM-loaded polymeric NPs are viable carriers for improving the distribution of VCM in ophthalmic applications.[148]

Levofloxacin, an antibacterial drug, was successfully encapsulated in chitosan NPs. Ameeduzzafar et al. used chitosan NPs to encapsulate levofloxacin, which proved to be an efficient treatment for eye infections. The NPs were created utilizing an ionic gelation process, which resulted in a high drug loading capacity and nanoscale particle size. The formulation was shown to be safe and non-irritating, with increased antibacterial activity against *S. aureus* and *P. aeruginosa*. The in situ gel approach for levofloxacin-coated chitosan NPs demonstrated beneficial outcomes.[149]

Expert opinion

In recent years, ophthalmology has made significant progress in resolving critical issues related to drug delivery to ocular tissues. Traditional ophthalmic dosage forms such as eye drops, ointments and gels frequently have low bioavailability and short drug retention time on the ocular surface, necessitating repeated administration and decreasing patient compliance. In response to these limitations, there has been a gradual shift to more modern drug delivery technologies, particularly colloidal formulations such as polymeric NPs. These nano-sized carriers have various advantages, including the capacity to encapsulate a wide range of medications, increased drug solubility and sustained and targeted delivery to ocular tissues. Despite these promising developments, employing polymeric NPs still faces a number of challenges, as evidenced by in vitro and in vivo studies, such as reproducibility, scalability and regulatory approval, which impede the seamless transition from laboratory research to clinical use.

Nonetheless, polymeric NPs continue to pique interest due to their distinct and advantageous features. These systems are built from a variety of natural and synthetic polymers, each with a particular viscosity grade and molecular weight that can be tuned to accomplish unique drug release profiles and therapeutic goals. By addressing these features, we can design dosage forms that are safe, biocompatible and exceptionally effective at delivering drug over long periods. Polymeric NPs, which are specifically designed for regulated and prolonged drug release, have the potential to reduce dose frequency while improving treatment outcomes for a variety of ocular diseases such as glaucoma, conjunctivitis, uveitis, and retinal disorders. Extensive preclinical research has focused on refining formulation properties such as particle size, surface charge and hydrophilicity in order to improve tissue penetration, reduce ocular irritation and extend medication retention time in the eye. Polymeric NPs have strong potential for ocular drug delivery. Their small particle size facilitates penetration through ocular barriers, while their inherent biocompatibility minimizes toxicity and patient discomfort.

Conclusions

This review emphasizes the considerable and growing promise of polymeric NPs in both the diagnosis and treatment of a wide range of ocular diseases. Over the years, polymeric NPs have emerged as innovative and highly versatile drug delivery systems that overcome many limitations associated with conventional ocular formulations. Their ability to offer previously unrecognized capabilities such as precise targeting, sustained drug release and improved therapeutic efficacy has created new opportunity for the management of challenging eye conditions. Polymeric NPs are particularly effective due to their small size, biocompatibility and the capacity to encapsulate a diverse range of therapeutic agents including hydrophilic and hydrophobic drugs by improving corneal permeability, prolonging residence time on the ocular surface and allowing for site-specific delivery. These nanocarriers significantly enhance drug bioavailability and therapeutic outcomes. In addition, polymeric NPs can be engineered to bypass ocular barriers and reach deeper tissues such as the posterior segment of the eye, thereby offering potential solutions for treating retinal diseases. Importantly, their sustained-release properties reduce the need for frequent administration, which not only improves patient compliance but also minimizes systemic side effects and toxicity. As a result, polymeric NPs represent a transformative advancement in ophthalmic drug delivery, offering a promising platform for developing next-generation therapies aimed at achieving long-term efficacy, safety and patient satisfaction.

Use of AI and AI-assisted technologies

Not applicable.

References

1. Hamidi M, Azadi A, Rafiei P. Hydrogel nanoparticles in drug delivery. *Adv Drug Deliv Rev*. 2008;60(15):1638–1649. doi:10.1016/j.addr.2008.08.002
2. Sahoo SK, Labhasetwar V. Nanotech approaches to drug delivery and imaging. *Drug Discov Today*. 2003;8(24):1112–1120. doi:10.1016/S1359-6446(03)02903-9
3. Sahoo S, Dilnawaz F, Krishnakumar S. Nanotechnology in ocular drug delivery. *Drug Discov Today*. 2008;13(3–4):144–151. doi:10.1016/j.drudis.2007.10.021
4. Vasir J, Reddy M, Labhasetwar V. Nanosystems in drug targeting: Opportunities and challenges. *Curr Nanosci*. 2005;1(1):47–64. doi:10.2174/1573413052953110
5. Barbu E, Verestiuc L, Nevell TG, Tsibouklis J. Polymeric materials for ophthalmic drug delivery: Trends and perspectives. *J Mater Chem*. 2006;16(34):3439. doi:10.1039/b605640g
6. Zimmer A, Kreuter J. Microspheres and nanoparticles used in ocular delivery systems. *Adv Drug Deliv Rev*. 1995;16(1):61–73. doi:10.1016/0169-409X(95)00017-2
7. Silva AM, Alvarado HL, Abrego G, et al. In vitro cytotoxicity of oleanolic/ursolic acids-loaded in PLGA nanoparticles in different cell lines. *Pharmaceutics*. 2019;11(8):362. doi:10.3390/pharmaceutics11080362
8. Ludwig A. The use of mucoadhesive polymers in ocular drug delivery. *Adv Drug Deliv Rev*. 2005;57(11):1595–1639. doi:10.1016/j.addr.2005.07.005
9. Shaikh N, Srishti R, Khanum A, et al. Vitreous hemorrhage: Causes, diagnosis and management. *Indian J Ophthalmol*. 2023;71(1):28–38. doi:10.4103/ijo.IJO_928_22
10. Singh M, Bharadwaj S, Lee KE, Kang SG. Therapeutic nanoemulsions in ophthalmic drug administration: Concept in formulations and characterization techniques for ocular drug delivery. *J Control Release*. 2020;328:895–916. doi:10.1016/j.jconrel.2020.10.025
11. Ahmed S, Amin MM, Sayed S. Ocular drug delivery: A comprehensive review. *AAPS PharmSciTech*. 2023;24(2):66. doi:10.1208/s12249-023-02516-9
12. Silva B, São Braz B, Delgado E, Gonçalves L. Colloidal nanosystems with mucoadhesive properties designed for ocular topical delivery. *Int J Pharm*. 2021;606:120873. doi:10.1016/j.ijpharm.2021.120873
13. Kels BD, Grzybowski A, Grant-Kels JM. Human ocular anatomy. *Clin Dermatol*. 2015;33(2):140–146. doi:10.1016/j.clindermatol.2014.10.006
14. Bachu R, Chowdhury P, Al-Saedi Z, Karla P, Boddu S. Ocular drug delivery barriers: Role of nanocarriers in the treatment of anterior segment ocular diseases. *Pharmaceutics*. 2018;10(1):28. doi:10.3390/pharmaceutics10010028

15. Ahmed S, Amin MM, El-Korany SM, Sayed S. Corneal targeted fenticonazole nitrate-loaded novasomes for the management of ocular candidiasis: Preparation, in vitro characterization, ex vivo and in vivo assessments. *Drug Deliv*. 2022;29(1):2428–2441. doi:10.1080/10717544.2022.2103600
16. Agrahari V, Mandal A, Agrahari V, et al. A comprehensive insight on ocular pharmacokinetics. *Drug Deliv Transl Res*. 2016;6(6):735–754. doi:10.1007/s13346-016-0339-2
17. Lee VHL, Robinson JR. Mechanistic and quantitative evaluation of precorneal pilocarpine disposition in albino rabbits. *J Pharm Sci*. 1979;68(6):673–684. doi:10.1002/jps.2600680606
18. Duvvuri S, Majumdar S, Mitra AK. Drug delivery to the retina: Challenges and opportunities. *Expert Opin Biol Ther*. 2003;3(1):45–56. doi:10.1517/14712598.3.1.45
19. Bourne RRA, Flaxman SR, Braithwaite T, et al. Magnitude, temporal trends and projections of the global prevalence of blindness and distance and near vision impairment: A systematic review and meta-analysis. *Lancet Glob Health*. 2017;5(9):e888–e897. doi:10.1016/S2214-109X(17)30293-0
20. Swetledge S, Jung JP, Carter R, Sabliov C. Distribution of polymeric nanoparticles in the eye: Implications in ocular disease therapy. *J Nanobiotechnol*. 2021;19(1):10. doi:10.1186/s12951-020-00745-9
21. Weinreb RN, Aung T, Medeiros FA. The pathophysiology and treatment of glaucoma: A review. *JAMA*. 2014;311(18):1901. doi:10.1001/jama.2014.3192
22. Bhagav P, Upadhyay H, Chandran S. Brimonidine tartrate-eudragit long-acting nanoparticles: Formulation, optimization, in vitro and in vivo evaluation. *AAPS PharmSciTech*. 2011;12(4):1087–1101. doi:10.1208/s12249-011-9675-1
23. Wadhwa S, Paliwal R, Paliwal SR, Vyas SP. Hyaluronic acid modified chitosan nanoparticles for effective management of glaucoma: Development, characterization and evaluation. *J Drug Target*. 2010;18(4):292–302. doi:10.3109/10611860903450023
24. Radwan SES, El-Moslemany RM, Mehanna RA, Thabet EH, Abdelfattah EZA, El-Kamel A. Chitosan-coated bovine serum albumin nanoparticles for topical tetrandrine delivery in glaucoma: In vitro and in vivo assessment. *Drug Deliv*. 2022;29(1):1150–1163. doi:10.1080/10717544.2022.2058648
25. Shahab MS, Rizwanullah Md, Alshehri S, Imam SS. Optimization to development of chitosan decorated polycaprolactone nanoparticles for improved ocular delivery of dorzolamide: In vitro, ex vivo and toxicity assessments. *Int J Biol Macromol*. 2020;163:2392–2404. doi:10.1016/j.ijbiomac.2020.09.185
26. Dubey V, Mohan P, Dangi JS, Kesavan K. Brinzolamide loaded chitosan-pectin mucoadhesive nanocapsules for management of glaucoma: Formulation, characterization and pharmacodynamic study. *Int J Biol Macromol*. 2020;152:1224–1232. doi:10.1016/j.ijbiomac.2019.10.219
27. Sánchez-López E, Egea MA, Davis BM, et al. Memantine-loaded PEGylated biodegradable nanoparticles for the treatment of glaucoma. *Small*. 2018;14(2):1701808. doi:10.1002/smll.201701808
28. Quinteros DA, Ferreira LM, Schaffazick SR, Palma SD, Allemandi DA, Cruz L. Novel polymeric nanoparticles intended for ophthalmic administration of acetazolamide. *J Pharm Sci*. 2016;105(10):3183–3190. doi:10.1016/j.xphs.2016.06.023
29. Warsi MH, Anwar M, Garg V, et al. Dorzolamide-loaded PLGA/vitamin E TPGS nanoparticles for glaucoma therapy: Pharmacoscintigraphy study and evaluation of extended ocular hypotensive effect in rabbits. *Colloids Surf B Biointerfaces*. 2014;122:423–431. doi:10.1016/j.colsurfb.2014.07.004
30. Lee RW, Nicholson LB, Sen HN, et al. Autoimmune and autoinflammatory mechanisms in uveitis. *Semin Immunopathol*. 2014;36(5):581–594. doi:10.1007/s00281-014-0433-9
31. Zhang L, Li Y, Zhang C, Wang Y, Song C. Pharmacokinetics and tolerance study of intravitreal injection of dexamethasone-loaded nanoparticles in rabbits. *Int J Nanomed*. 2009;4:175–183. doi:10.2147/ijn.s6428
32. Sakai T, Ishihara T, Higaki M, Akiyama G, Tsuneoka H. Therapeutic effect of stealth-type polymeric nanoparticles with encapsulated betamethasone phosphate on experimental autoimmune uveoretinitis. *Invest Ophthalmol Vis Sci*. 2011;52(3):1516. doi:10.1167/iovs.10-5676
33. Krishnaswami V, Kandasamy R, Alagarsamy S, Palanisamy R, Natesan S. Biological macromolecules for ophthalmic drug delivery to treat ocular diseases. *Int J Biol Macromol*. 2018;110:7–16. doi:10.1016/j.ijbiomac.2018.01.120
34. Luo Y, Yang L, Feng P, et al. Pranoprofen nanoparticles with poly(L-lactide)-b-poly(ethylene glycol)-b-poly(L-lactide) as the matrix toward improving ocular anti-inflammation. *Front Bioeng Biotechnol*. 2020;8:581621. doi:10.3389/fbioe.2020.581621
35. Adadi S, Jarnige K, Issaka Amidou R, Kfal Y, Tlamcani Z. *Candida* tropicalis fungal keratitis: A case report and literature review. *Cureus*. 2024;16(6):e62682. doi:10.7759/cureus.62682
36. Ahmed S, Amin MM, El-Korany SM, Sayed S. Pronounced capping effect of olaminosomes as nanostructured platforms in ocular candidiasis management. *Drug Deliv*. 2022;29(1):2945–2958. doi:10.1080/10717544.2022.2120926
37. Bhosale VA, Srivastava V, Valamla B, Yadav R, Singh SB, Mehra NK. Preparation and evaluation of modified chitosan nanoparticles using anionic sodium alginate polymer for treatment of ocular disease. *Pharmaceutics*. 2022;14(12):2802. doi:10.3390/pharmaceutics14122802
38. Cheung N, Mitchell P, Wong TY. Diabetic retinopathy. *Lancet*. 2010;376(9735):124-136. doi:10.1016/S0140-6736(09)62124-3
39. Ajlan RS, Silva PS, Sun JK. Vascular endothelial growth factor and diabetic retinal disease. *Semin Ophthalmol*. 2016;31(1–2):40–48. doi:10.3109/08820538.2015.1114833
40. Madjedi K, Pereira A, Ballios BG, et al. Switching between anti-VEGF agents in the management of refractory diabetic macular edema: A systematic review. *Surv Ophthalmol*. 2022;67(5):1364–1372. doi:10.1016/j.survophthal.2022.04.001
41. Liu J, Zhang X, Li G, et al. Anti-angiogenic activity of bevacizumab-bearing dexamethasone-loaded PLGA nanoparticles for potential intravitreal applications. *Int J Nanomed*. 2019;14:8819–8834. doi:10.2147/IJN.S217038
42. Mahaling B, Srinivasarao DA, Raghu G, Kasam RK, Bhanuprakash Reddy G, Katti DS. A non-invasive nanoparticle mediated delivery of triamcinolone acetonide ameliorates diabetic retinopathy in rats. *Nanoscale*. 2018;10(35):16485–16498. doi:10.1039/C8NR00058A
43. Zeng L, Ma W, Shi L, et al. Poly(lactic-co-glycolic acid) nanoparticle-mediated interleukin-12 delivery for the treatment of diabetic retinopathy. *Int J Nanomed*. 2019;14:6357–6369. doi:10.2147/IJN.S214727
44. Wong WL, Su X, Li X, et al. Global prevalence of age-related macular degeneration and disease burden projection for 2020 and 2040: A systematic review and meta-analysis. *Lancet Glob Health*. 2014;2(2):e106–e116. doi:10.1016/S2214-109X(13)70145-1
45. Thomas CJ, Mirza RG, Gill MK. Age-related macular degeneration. *Med Clin North Am*. 2021;105(3):473–491. doi:10.1016/j.mcna.2021.01.003
46. Varshochian R, Riazi-Esfahani M, Jeddi-Tehrani M, et al. Albuminated PLGA nanoparticles containing bevacizumab intended for ocular neovascularization treatment. *J Biomed Mater Res A*. 2015;103(10):3148–3156. doi:10.1002/jbm.a.35446
47. Pflugfelder SC, De Paiva CS. The pathophysiology of dry eye disease: What we know and future directions for research. *Ophthalmology*. 2017;124(11 Suppl):S4–S13. doi:10.1016/j.ophtha.2017.07.010
48. Li T, Tang J, Wu X, et al. Evaluating the efficacy of polyglycolic acid-loading tetrandrine nanoparticles in the treatment of dry eye. *Ophthalmic Res*. 2023;66(1):1148–1158. doi:10.1159/000533345
49. Wagh VD, Apar DU. Cyclosporine A-loaded PLGA nanoparticles for dry eye disease: In vitro characterization studies. *J Nanotechnol*. 2014;2014:683153. doi:10.1155/2014/683153
50. ElZomor H, Taha H, Aleieldin A, et al. High risk retinoblastoma: Prevalence and success of treatment in developing countries. *Ophthalmic Genet*. 2015;36(3):287–289. doi:10.3109/13816810.2015. 1016241
51. Pinelli F, Perale G, Rossi F. Coating and functionalization strategies for nanogels and nanoparticles for selective drug delivery. *Gels*. 2020;6(1):6. doi:10.3390/gels6010006
52. Das M, Sahoo SK. Folate decorated dual drug-loaded nanoparticle: role of curcumin in enhancing therapeutic potential of nutlin-3a by reversing multidrug resistance. *PLoS One*. 2012;7(3):e32920. doi:10.1371/journal.pone.0032920
53. Lane SS, Osher RH, Masket S, Belani S. Evaluation of the safety of prophylactic intracameral moxifloxacin in cataract surgery. *J Cataract Refract Surg*. 2008;34(9):1451–1459. doi:10.1016/j.jcrs.2008.05.034
54. Del Amo EM, Rimpelä AK, Heikkinen E, et al. Pharmacokinetic aspects of retinal drug delivery. *Prog Retin Eye Res*. 2017;57:134–185. doi:10.1016/j.preteyeres.2016.12.001
55. Gross A, Cestari DM. Optic neuropathy following retrobulbar injection: A review. *Semin Ophthalmol*. 2014;29(5–6):434–439. doi:10.3109/08820538.2014.959191

56. Urtti A, Salminen L. Minimizing systemic absorption of topically administered ophthalmic drugs. *Surv Ophthalmol*. 1993;37(6):435-456. doi:10.1016/0039-6257(93)90141-s
57. Janoria KG, Gunda S, Boddu SH, Mitra AK. Novel approaches to retinal drug delivery. *Exp Opin Drug Deliv*. 2007;4(4):371–388. doi:10.1517/17425247.4.4.371
58. Lang JC. Ocular drug delivery conventional ocular formulations. *Adv Drug Deliv Rev*. 1995;16(1):39–43. doi:10.1016/0169-409X(95)00012-V
59. Gaudana R, Ananthula HK, Parenky A, Mitra AK. Ocular drug delivery. *AAPS J*. 2010;12(3):348–360. doi:10.1208/s12248-010-9183-3
60. O'Brien Laramy MN, Nagapudi K. Long-acting ocular drug delivery technologies with clinical precedent. *Expert Opin Drug Deliv*. 2022;19(10):1285–1301. doi:10.1080/17425247.2022.2108397
61. Jumelle C, Gholizadeh S, Annabi N, Dana R. Advances and limitations of drug delivery systems formulated as eye drops. *J Control Release*. 2020;321:1–22. doi:10.1016/j.jconrel.2020.01.057
62. Araújo J, Gonzalez E, Egea MA, Garcia ML, Souto EB. Nanomedicines for ocular NSAIDs: Safety on drug delivery. *Nanomed Nanotechnol Biol Med*. 2009;5(4):394–401. doi:10.1016/j.nano.2009.02.003
63. Afarid M, Mahmoodi S, Baghban R. Recent achievements in nano-based technologies for ocular disease diagnosis and treatment: Review and update. *J Nanobiotechnol*. 2022;20(1):361. doi:10.1186/s12951-022-01567-7
64. Le Bourlais C, Acar L, Zia H, Sado PA, Needham T, Leverge R. Ophthalmic drug delivery systems: Recent advances. *Prog Retin Eye Res*. 1998;17(1):33–58. doi:10.1016/S1350-9462(97)00002-5
65. Tsai CH, Wang PY, Lin IC, Huang H, Liu GS, Tseng CL. Ocular drug delivery: Role of degradable polymeric nanocarriers for ophthalmic application. *Int J Mol Sci*. 2018;19(9):2830. doi:10.3390/ijms19092830
66. Ali Y, Lehmussaari K. Industrial perspective in ocular drug delivery. *Adv Drug Deliv Rev*. 2006;58(11):1258–1268. doi:10.1016/j.addr.2006.07.022
67. Machado S, Pacheco JG, Nouws HPA, Albergaria JT, Delerue-Matos C. Characterization of green zero-valent iron nanoparticles produced with tree leaf extracts. *Sci Total Environ*. 2015;533:76–81. doi:10.1016/j.scitotenv.2015.06.091
68. Soppimath KS, Aminabhavi TM, Kulkarni AR, Rudzinski WE. Biodegradable polymeric nanoparticles as drug delivery devices. *J Control Release*. 2001;70(1–2):1–20. doi:10.1016/S0168-3659(00)00339-4
69. Souto EB, Souto SB, Campos JR, et al. Nanoparticle delivery systems in the treatment of diabetes complications. *Molecules*. 2019;24(23):4209. doi:10.3390/molecules24234209
70. Quintanar-Guerrero D, Allémann E, Doelker E, Fessi H. Preparation and characterization of nanocapsules from preformed polymers by a new process based on emulsification-diffusion technique. *Pharm Res*. 1998;15(7):1056–1062. doi:10.1023/a:1011934328471
71. Vauthier C, Bouchemal K. Methods for the preparation and manufacture of polymeric nanoparticles. *Pharm Res*. 2009;26(5):1025–1058. doi:10.1007/s11095-008-9800-3
72. Mahalingam M, Krishnamoorthy K. Selection of a suitable method for the preparation of polymeric nanoparticles: Multi-criteria decision-making approach. *Adv Pharm Bull*. 2015;5(1):57–67. doi:10.5681/APB.2015.008
73. Crucho CIC, Barros MT. Polymeric nanoparticles: A study on the preparation variables and characterization methods. *Mater Sci Eng C Mater Biol Appl*. 2017;80:771–784. doi:10.1016/j.msec.2017.06.004
74. Kalam MA, Iqbal M, Alshememry A, Alkholief M, Alshamsan A. Development and evaluation of chitosan nanoparticles for ocular delivery of tedizolid phosphate. *Molecules*. 2022;27(7):2326. doi:10.3390/molecules27072326
75. Swetledge S, Carter R, Stout R, Astete CE, Jung JP, Sabliov CM. Stability and ocular biodistribution of topically administered PLGA nanoparticles. *Sci Rep*. 2021;11(1):12270. doi:10.1038/s41598-021-90792-5
76. Khin SY, Soe HMSH, Chansriniyom C, et al. Development of fenofibrate/randomly methylated β-cyclodextrin-loaded Eudragit® RL 100 nanoparticles for ocular delivery. *Molecules*. 2022;27(15):4755. doi:10.3390/molecules27154755
77. Adibkia K, Javadzadeh Y, Dastmalchi S, Mohammadi G, Niri FK, Alaei-Beirami M. Naproxen-eudragit RS100 nanoparticles: Preparation and physicochemical characterization. *Colloids Surf B Biointerfaces*. 2011;83(1):155–159. doi:10.1016/j.colsurfb.2010.11.014
78. Reshad RAI, Jishan TA, Chowdhury NN. Chitosan and its broad applications: A brief review. *J Clin Exp Invest*. 2021;12(4):em00779. doi:10.29333/jcei/11268
79. Kong M, Chen XG, Xing K, Park HJ. Antimicrobial properties of chitosan and mode of action: A state-of-the-art review. *Int J Food Microbiol*. 2010;144(1):51–63. doi:10.1016/j.ijfoodmicro.2010.09.012
80. Malafaya PB, Silva GA, Reis RL. Natural-origin polymers as carriers and scaffolds for biomolecules and cell delivery in tissue engineering applications. *Adv Drug Deliv Rev*. 2007;59(4–5):207–233. doi:10.1016/j.addr.2007.03.012
81. Cascone MG, Sim B, Sandra D. Blends of synthetic and natural polymers as drug delivery systems for growth hormone. *Biomaterials*. 1995;16(7):569–574. doi:10.1016/0142-9612(95)91131-H
82. Kumari A, Yadav SK, Yadav SC. Biodegradable polymeric nanoparticles based drug delivery systems. *Colloids Surf B Biointerfaces*. 2010;75(1):1–18. doi:10.1016/j.colsurfb.2009.09.001
83. Jawahar N, Meyyanathan S. Polymeric nanoparticles for drug delivery and targeting: A comprehensive review. *Int J Health Allied Sci*. 2012;1(4):217. doi:10.4103/2278-344X.107832
84. Pinto Reis C, Neufeld RJ, Ribeiro, AJ, Veiga F. Nanoencapsulation I. Methods for preparation of drug-loaded polymeric nanoparticles. *Nanomed Nanotechnol Biol Med*. 2006;2(1):8–21. doi:10.1016/j.nano.2005.12.003
85. Kamaly N, Yameen B, Wu J, Farokhzad OC. Degradable controlled-release polymers and polymeric nanoparticles: Mechanisms of controlling drug release. *Chem Rev*. 2016;116(4):2602–2663. doi:10.1021/acs.chemrev.5b00346
86. Desgouilles S, Vauthier C, Bazile D, et al. The design of nanoparticles obtained by solvent evaporation: A comprehensive study. *Langmuir*. 2003;19(22):95049510. doi:10.1021/la034999q
87. Bohrey S, Chourasiya V, Pandey A. Polymeric nanoparticles containing diazepam: Preparation, optimization, characterization, in-vitro drug release and release kinetic study. *Nano Convergence*. 2016;3(1):3. doi:10.1186/s40580-016-0061-2
88. De Jong WH, Borm PJA. Drug delivery and nanoparticles: Applications and hazards. *Int J Nanomed*. 2008;3(2):133–149. doi:10.2147/IJN.S596
89. Kumar S, Dilbaghi N, Saharan R, Bhanjana G. Nanotechnology as emerging tool for enhancing solubility of poorly water-soluble drugs. *BioNanoScience*. 2012;2(4):227–250. doi:10.1007/s12668-012-0060-7
90. Araújo J, Vega E, Lopes C, Egea MA, Garcia ML, Souto EB. Effect of polymer viscosity on physicochemical properties and ocular tolerance of FB-loaded PLGA nanospheres. *Colloids Surf B Biointerfaces*. 2009;72(1):48–56. doi:10.1016/j.colsurfb.2009.03.028
91. Govender T, Stolnik S, Garnett MC, Illum L, Davis SS. PLGA nanoparticles prepared by nanoprecipitation: Drug loading and release studies of a water soluble drug. *J Control Release*. 1999;57(2):171–185. doi:10.1016/s0168-3659(98)00116-3
92. Sánchez-López E, Egea MA, Cano A, et al. PEGylated PLGA nanospheres optimized by design of experiments for ocular administration of dexibuprofen: In vitro, ex vivo and in vivo characterization. *Colloids Surf B Biointerfaces*. 2016;145:241–250. doi:10.1016/j.colsurfb.2016.04.054
93. Sánchez-López E, Ettcheto M, Egea MA, et al. Memantine loaded PLGA PEGylated nanoparticles for Alzheimer's disease: In vitro and in vivo characterization. *J Nanobiotechnol*. 2018;16(1):32. doi:10.1186/s12951-018-0356-z
94. Salatin S, Barar J, Barzegar-Jalali M, Adibkia K, Kiafar F, Jelvehgari M. Development of a nanoprecipitation method for the entrapment of a very water soluble drug into Eudragit RL nanoparticles. *Res Pharm Sci*. 2017;12(1):1–14. doi:10.4103/1735-5362.199041
95. Martínez Rivas CJ, Tarhini M, Badri W, et al. Nanoprecipitation process: From encapsulation to drug delivery. *Int J Pharm*. 2017;532(1):66–81. doi:10.1016/j.ijpharm.2017.08.064
96. Bilati U, Allémann E, Doelker E. Nanoprecipitation versus emulsion-based techniques for the encapsulation of proteins into biodegradable nanoparticles and process-related stability issues. *AAPS PharmSciTech*. 2005;6(4):E594–E604. doi:10.1208/pt060474
97. Chidambaram M, Krishnasamy K. Modifications to the conventional nanoprecipitation technique: An approach to fabricate narrow-sized polymeric nanoparticles. *Adv Pharm Bull*. 2014;4(2):205–206. doi:10.5681/APB.2014.030
98. Carbone C, Martins-Gomes C, Pepe V, et al. Repurposing itraconazole to the benefit of skin cancer treatment: A combined azole-DDAB nanoencapsulation strategy. *Colloids Surf B Biointerfaces*. 2018;167:337–344. doi:10.1016/j.colsurfb.2018.04.031
99. Doktorovova S, Souto EB, Silva AM. Nanotoxicology applied to solid lipid nanoparticles and nanostructured lipid carriers: A systematic review of in vitro data. *Eur J Pharm Biopharm*. 2014;87(1):1–18. doi:10.1016/j.ejpb.2014.02.005

100. Andreani T, Kiill CP, De Souza ALR, et al. Effect of cryoprotectants on the reconstitution of silica nanoparticles produced by sol–gel technology. *J Therm Anal Calorim*. 2015;120(1):1001–1007. doi:10.1007/s10973-014-4275-4
101. Mathurin J, Pancani E, Deniset-Besseau A, et al. How to unravel the chemical structure and component localization of individual drug-loaded polymeric nanoparticles by using tapping AFM-IR. *Analyst*. 2018;143(24):5940–5949. doi:10.1039/C8AN01239C
102. Hickey JW, Santos JL, Williford JM, Mao HQ. Control of polymeric nanoparticle size to improve therapeutic delivery. *J Control Release*. 2015;219:536–547. doi:10.1016/j.jconrel.2015.10.006
103. Brar SK, Verma M. Measurement of nanoparticles by light-scattering techniques. *Trends Anal Chem*. 2011;30(1):4–17. doi:10.1016/j.trac.2010.08.008
104. Mourdikoudis S, Pallares RM, Thanh NTK. Characterization techniques for nanoparticles: Comparison and complementarity upon studying nanoparticle properties. *Nanoscale*. 2018;10(27):12871–12934. doi:10.1039/C8NR02278J
105. Lu M, Yang X, Yang Y, Qin P, Wu X, Cai Z. Nanomaterials as assisted matrix of laser desorption/ionization time-of-flight mass spectrometry for the analysis of small molecules. *Nanomaterials*. 2017;7(4):87. doi:10.3390/nano7040087
106. Yang Y, Jiang Y, Xu J, Yu J. Conducting polymeric nanoparticles synthesized in reverse micelles and their gas sensitivity based on quartz crystal microbalance. *Polymer*. 2007;48(15):4459–4465. doi:10.1016/j.polymer.2007.06.005
107. Stals PJM, Gillissen MAJ, Paffen TFE, et al. Folding polymers with pendant hydrogen bonding motifs in water: The effect of polymer length and concentration on the shape and size of single-chain polymeric nanoparticles. *Macromolecules*. 2014;47(9):2947–2954. doi:10.1021/ma500273g
108. Baer DR, Engelhard MH, Johnson GE, et al. Surface characterization of nanomaterials and nanoparticles: Important needs and challenging opportunities. *J Vac Sci Technol A*. 2013;31(5):050820. doi:10.1116/1.4818423
109. Simonet BM, Valcárcel M. Monitoring nanoparticles in the environment. *Anal Bioanal Chem*. 2009;393(1):17–21. doi:10.1007/s00216-008-2484-z
110. Honary S, Zahir F. Effect of zeta potential on the properties of nano-drug delivery systems: A review (part 1). *Trop J Pharm Res*. 2013;12(2):255–264. doi:10.4314/tjpr.v12i2.19
111. Al-Shaeli M, Benkhaya S, Al-Juboori RA, Koyuncu I, Vatanpour V. pH-responsive membranes: Mechanisms, fabrications, and applications. *Sci Total Environ*. 2024;946:173865. doi:10.1016/j.scitotenv.2024.173865
112. Hernández-Giottonini KY, Rodríguez-Córdova RJ, Gutiérrez-Valenzuela CA, et al. PLGA nanoparticle preparations by emulsification and nanoprecipitation techniques: Effects of formulation parameters. *RSC Adv*. 2020;10(8):4218–4231. doi:10.1039/C9RA10857B
113. Lazzari S, Moscatelli D, Codari F, Salmona M, Morbidelli M, Diomede L. Colloidal stability of polymeric nanoparticles in biological fluids. *J Nanopart Res*. 2012;14(6):920. doi:10.1007/s11051-012-0920-7
114. Heinz H, Pramanik C, Heinz O, et al. Nanoparticle decoration with surfactants: Molecular interactions, assembly and applications. *Surf Sci Rep*. 2017;72(1):1–58. doi:10.1016/j.surfrep.2017.02.001
115. Abdelwahed W, Degobert G, Stainmesse S, Fessi H. Freeze-drying of nanoparticles: Formulation, process and storage considerations. *Adv Drug Deliv Rev*. 2006;58(15):1688–1713. doi:10.1016/j.addr.2006.09.017
116. Joudeh N, Linke D. Nanoparticle classification, physicochemical properties, characterization, and applications: A comprehensive review for biologists. *J Nanobiotechnol*. 2022;20(1):262. doi:10.1186/s12951-022-01477-8
117. Wallace SJ, Li J, Nation RL, Boyd BJ. Drug release from nanomedicines: Selection of appropriate encapsulation and release methodology. *Drug Deliv Transl Res*. 2012;2(4):284–292. doi:10.1007/s13346-012-0064-4
118. Khan I, Saeed K, Khan I. Nanoparticles: Properties, applications and toxicities. *Arab J Chem*. 2019;12(7):908–931. doi:10.1016/j.arabjc.2017.05.011
119. Shen J, Burgess DJ. In vitro dissolution testing strategies for nanoparticulate drug delivery systems: Recent developments and challenges. *Drug Deliv Transl Res*. 2013;3(5):409–415. doi:10.1007/s13346-013-0129-z
120. Lee JH, Yeo Y. Controlled drug release from pharmaceutical nanocarriers. *Chem Eng Sci*. 2015;125:75–84. doi:10.1016/j.ces.2014.08.046
121. Maurya A, Singh AK, Mishra G, et al. Strategic use of nanotechnology in drug targeting and its consequences on human health: A focused review. *Interv Med Appl Sci*. 2019;11(1):38–54. doi:10.1556/1646.11.2019.04
122. Jain AK, Thareja S. In vitro and in vivo characterization of pharmaceutical nanocarriers used for drug delivery. *Artif Cells Nanomed Biotechnol*. 2019;47(1):524–539. doi:10.1080/21691401.2018.1561457
123. Lombardo D, Kiselev MA, Caccamo MT. Smart nanoparticles for drug delivery application: Development of versatile nanocarrier platforms in biotechnology and nanomedicine. *J Nanomater*. 2019;2019:1–26. doi:10.1155/2019/3702518
124. Asasutjarit R, Theerachayanan T, Kewsuwan P, Veeranodha S, Fuongfuchat A, Ritthidej GC. Development and evaluation of diclofenac sodium loaded-N-trimethyl chitosan nanoparticles for ophthalmic use. *AAPS PharmSciTech*. 2015;16(5):1013–1024. doi:10.1208/s12249-015-0290-4
125. Katara R, Majumdar DK. Eudragit RL 100-based nanoparticulate system of aceclofenac for ocular delivery. *Colloids Surf B Biointerfaces*. 2013;103:455–462. doi:10.1016/j.colsurfb.2012.10.056
126. Ahuja M, Dhake AS, Sharma SK, Majumdar DK. Diclofenac-loaded Eudragit S100 nanosuspension for ophthalmic delivery. *J Microencapsul*. 2011;28(1):37–45. doi:10.3109/02652048.2010.523794
127. Xing Y, Zhu L, Zhang K, Li T, Huang S. Nanodelivery of triamcinolone acetonide with PLGA-chitosan nanoparticles for the treatment of ocular inflammation. *Artif Cells Nanomed Biotechnol*. 2021;49(1):308–316. doi:10.1080/21691401.2021.1895184
128. Arafa MG, Girgis GN, El-Dahan MS. Chitosan-coated PLGA nano-particles for enhanced ocular anti-inflammatory efficacy of atorvastatin calcium. *Int J Nanomed*. 2020;15:1335–1347. doi:10.2147/IJN.S237314
129. Gonzalez-Pizarro R, Parrotta G, Vera R, et al. Ocular penetration of fluorometholone-loaded PEG-PLGA nanoparticles functionalized with cell-penetrating peptides. *Nanomedicine (Lond)*. 2019;14(23):3089–3104. doi:10.2217/nnm-2019-0201
130. Gonzalez-Pizarro R, Silva-Abreu M, Calpena AC, Egea MA, Espina M, García ML. Development of fluorometholone-loaded PLGA nanoparticles for treatment of inflammatory disorders of anterior and posterior segments of the eye. *Int J Pharm*. 2018;547(1–2):338–346. doi:10.1016/j.ijpharm.2018.05.050
131. Sabzevari A, Adibkia K, Hashemi H, et al. Polymeric triamcinolone acetonide nanoparticles as a new alternative in the treatment of uveitis: In vitro and in vivo studies. *Eur J Pharm Biopharm*. 2013;84(1):63–71. doi:10.1016/j.ejpb.2012.12.010
132. Vandervoort J, Ludwig A. Preparation and evaluation of drug-loaded gelatin nanoparticles for topical ophthalmic use. *Eur J Pharm Biopharm*. 2004;57(2):251–261. doi:10.1016/S0939-6411(03)00187-5
133. Cardoso JF, Perasoli FB, Almeida TC, et al. Vancomycin-loaded N,N-dodecyl,methyl-polyethylenimine nanoparticles coated with hyaluronic acid to treat bacterial endophthalmitis: Development, characterization and ocular biocompatibility. *Int J Biol Macromol*. 2021;169:330–341. doi:10.1016/j.ijbiomac.2020.12.057
134. Costa JR, Silva NC, Sarmento B, Pintado M. Potential chitosan-coated alginate nanoparticles for ocular delivery of daptomycin. *Eur J Clin Microbiol Infect Dis*. 2015;34(6):1255–1262. doi:10.1007/s10096-015--2344-7
135. Sharma UK, Verma A, Prajapati SK, Pandey H, Pandey AC. In vitro, in vivo and pharmacokinetic assessment of amikacin sulphate laden polymeric nanoparticles meant for controlled ocular drug delivery. *Appl Nanosci*. 2015;5(2):143–155. doi:10.1007/s13204-014-0300-y
136. Pokharkar V, Patil V, Mandpe L. Engineering of polymer–surfactant nanoparticles of doxycycline hydrochloride for ocular drug delivery. *Drug Deliv*. 2015;22(7):955–968. doi:10.3109/10717544.2014.893381
137. Mohammadi G, Nokhodchi A, Barzegar-Jalali M, et al. Physicochemical and anti-bacterial performance characterization of clarithromycin nanoparticles as colloidal drug delivery system. *Colloids Surf B Biointerfaces*. 2011;88(1):39–44. doi:10.1016/j.colsurfb.2011.05.050
138. Da Silva SB, Ferreira D, Pintado M, Sarmento B. Chitosan-based nanoparticles for rosmarinic acid ocular delivery: In vitro tests. *Int J Biol Macromol*. 2016;84:112–120. doi:10.1016/j.ijbiomac.2015.11.070
139. Carter RT, Swetledge S, Navarro S, Liu CC, Ineck N, Lewin AC, Sabliov CM. The impact of lutein-loaded poly (lactic-co-glycolic acid) nanoparticles following topical application: An in vitro and in vivo study. *PLoS One*. 2024;*19*(8):1–21. doi:10.1371/journal.pone.0306640
140. Giannavola C, Bucolo C, Maltese A, et al. Influence of preparation conditions on acyclovir-loaded poly-d,l-lactic acid nanospheres and effect of PEG coating on ocular drug bioavailability. *Pharm Res*. 2003;20(4):584–590. doi:10.1023/a:1023290514575

141. De Campos AM, Sánchez A, Alonso MJ. Chitosan nanoparticles: A new vehicle for the improvement of the delivery of drugs to the ocular surface: Application to cyclosporin A. *Int J Pharm*. 2001;224(1–2):159–168. doi:10.1016/S0378-5173(01)00760-8
142. Eleraky NE, Attia MA, Safwat MA. Sertaconazole-PLGA nanoparticles for management of ocular keratitis. *J Drug Deliv Sci Technol*. 2024;95:105539. doi:10.1016/j.jddst.2024.105539
143. Almehmady AM, El-Say KM, Mubarak MA, et al. Enhancing the antifungal activity and ophthalmic transport of fluconazole from PEGylated polycaprolactone-loaded nanoparticles. *Polymers (Basel)*. 2022;15(1):209. doi:10.3390/polym15010209
144. Gebreel RM, Edris NA, Elmofty HM, Tadros MI, El-Nabarawi MA, Hassan DH. Development and characterization of PLGA nanoparticle-laden hydrogels for sustained ocular delivery of norfloxacin in the treatment of *pseudomonas* keratitis: An experimental study. *Drug Des Dev Ther*. 2021;15:399–418. doi:10.2147/DDDT.S293127
145. Salama AH, AbouSamra MM, Awad GEA, Mansy SS. Promising bioadhesive ofloxacin-loaded polymeric nanoparticles for the treatment of ocular inflammation: Formulation and in vivo evaluation. *Drug Deliv Transl Res*. 2021;11(5):1943–1957. doi:10.1007/s13346-020-00856-8
146. El Sayeh F. Abou El Ela A, Abbas Ibrahim M, Alqahtani Y, Almomen A, Sfouq Aleanizy F. Fluconazole nanoparticles prepared by antisolvent precipitation technique: Physicochemical, in vitro, ex vivo and in vivo ocular evaluation. *Saudi Pharm J*. 2021;29(6):576–585. doi:10.1016/j.jsps.2021.04.018
147. Gonzalez-Pizarro R, Carvajal-Vidal P, Halbault Bellowa L, Calpena AC, Espina M, García ML. In-situ forming gels containing fluorometholone-loaded polymeric nanoparticles for ocular inflammatory conditions. *Colloids Surf B Biointerfaces*. 2019;175:365–374. doi:10.1016/j.colsurfb.2018.11.065
148. Yousry C, Elkheshen SA, El-laithy HM, Essam T, Fahmy RH. Studying the influence of formulation and process variables on vancomycin-loaded polymeric nanoparticles as potential carrier for enhanced ophthalmic delivery. *Eur J Pharm Sci*. 2017;100:142154. doi:10.1016/j.ejps.2017.01.013
149. Ameeduzzafar, Imam SS, Abbas Bukhari SN, Ahmad J, Ali A. Formulation and optimization of levofloxacin loaded chitosan nanoparticle for ocular delivery: In-vitro characterization, ocular tolerance and antibacterial activity. *Int J Biol Macromol*. 2018;108:650–659. doi:10.1016/j.ijbiomac.2017.11.170
150. Silva NC, Silva S, Sarmento B, Pintado M. Chitosan nanoparticles for daptomycin delivery in ocular treatment of bacterial endophthalmitis. *Drug Deliv*. 2015;22(7):885–893. doi:10.3109/10717544.2013.858195
151. Losa C, Calvo P, Castro E, Vila-Jato JL, Alonso MJ. Improvement of ocular penetration of amikacin sulphate by association to poly(butylcyanoacrylate) nanoparticles. *J Pharm Pharmacol*. 1991;43(8):548–552. doi:10.1111/j.2042-7158.1991.tb03534.x
152. De Paiva CS, Corrales RM, Villarreal AL, et al. Corticosteroid and doxycycline suppress MMP-9 and inflammatory cytokine expression, MAPK activation in the corneal epithelium in experimental dry eye. *Exp Eye Res*. 2006;83(3):526–535. doi:10.1016/j.exer.2006.02.004
153. Lotfipour F, Valizadeh H, Mohammadi G, et al. Antibacterial activity of clarithromycin loaded PLGA nanoparticles. *Pharmazie*. 2012;67(1):63–68. doi:10.1691/ph.2012.1052
154. Vieira LC, Moreira CPDS, Castro BFM, et al. Rosmarinic acid intravitreal implants: A new therapeutic approach for ocular neovascularization. *Planta Med*. 2020;86(17):1286–1297. doi:10.1055/a-1223-2525
155. Misra R, Sahoo SK. Antibacterial activity of doxycycline-loaded nanoparticles. *Methods Enzymol*. 2012;509:61–85. doi:10.1016/B978-0-12-391858-1.00004-6
156. Fresta M, Fontana G, Bucolo C, Cavallaro G, Giammona G, Puglisi G. Ocular tolerability and in vivo bioavailability of poly(ethylene glycol) (PEG)-coated polyethyl-2-cyanoacrylate nanosphere-encapsulated acyclovir. *J Pharm Sci*. 2001;90(3):288–297. doi:10.1002/1520-6017(200103)90:3<288::aid-jps4>3.0.co;2-5
157. Başaran E, Yenilmez E, Berkman MS, Büyükköroğlu G, Yazan Y. Chitosan nanoparticles for ocular delivery of cyclosporine A. *J Microencapsul*. 2014;31(1):49–57. doi:10.3109/02652048.2013.805839
158. Tavakoli N, Taymouri S, Saeidi A, Akbari V. Thermosensitive hydrogel containing sertaconazole loaded nanostructured lipid carriers for potential treatment of fungal keratitis. *Pharm Dev Technol*. 2019;24(7):891–901. doi:10.1080/10837450.2019.1616755
159. Kakkar S, Singh M, Mohan Karuppayil S, et al. Lipo-PEG nano-ocular formulation successfully encapsulates hydrophilic fluconazole and traverses corneal and non-corneal path to reach posterior eye segment. *J Drug Target*. 2021;29(6):631–650. doi:10.1080/1061186X.2020.1871483
160. Kumar M, Upadhyay P, Pathak K. Norfloxacin loaded pH triggered nanoparticulate in situ gel for extraocular bacterial infections: Optimization, ocular irritancy and corneal toxicity. *Int J Pharm Res*. 2016;15(1):3–22. doi:10.22037/ijpr.2016.1795
161. Taghe S, Mirzaeei S. Preparation and characterization of novel, mucoadhesive ofloxacin nanoparticles for ocular drug delivery. *Braz J Pharm Sci*. 2019;55:e17105. doi:10.1590/s2175-97902019000117105
162. Aldosari BN, Ibrahim MA, Alqahtani Y, Abou El Ela AESF. Formulation and evaluation of fluconazole nanosuspensions: In vitro characterization and transcorneal permeability studies. *Saudi Pharm J*. 2024;32(7):102104. doi:10.1016/j.jsps.2024.102104
163. Shokoohi-Rad S, Daneshvar R, Jafarian-Shahri M, Rajaee P. Comparison between betamethasone, fluorometholone and loteprednol etabonate on intraocular pressure in patients after keratorefractive surgery. *J Curr Ophthalmol*. 2018;30(2):130–135. doi:10.1016/j.joco.2017.11.008
164. Tong WY, Tan WN, Kamarul Azizi MA, et al. Nanoparticle-laden contact lens for controlled release of vancomycin with enhanced antibiotic efficacy. *Chemosphere*. 2023;338:139492. doi:10.1016/j.chemosphere.2023.139492
165. Coneac G, Vlaia V, Olariu I, et al. Development and evaluation of new microemulsion-based hydrogel formulations for topical delivery of fluconazole. *AAPS PharmSciTech*. 2015;16(4):889–904. doi:10.1208/s12249-014-0275-8
166. Wang TZ, Guan B, Liu XX, Ke LN, Wang JJ, Nan KH. A topical fluorometholone nanoformulation fabricated under aqueous condition for the treatment of dry eye. *Coll Surf B Biointerfaces*. 2022;212:112351. doi:10.1016/j.colsurfb.2022.112351
167. Yousry C, Fahmy RH, Essam T, El-Laithy HM, Elkheshen SA. Nanoparticles as tool for enhanced ophthalmic delivery of vancomycin: A multidistrict-based microbiological study, solid lipid nanoparticles formulation and evaluation. *Drug Dev Pharm*. 2016;42(11):1752-1762. doi:10.3109/03639045.2016.1171335
168. Abdullah S, Thiab S, A. Al-Masud A, Marzoog Al-Sharafa M, Ardakani A. Carrageenan matrix for sustained levofloxacin delivery: Formulation strategies and dual evaluation approaches. *J Pharm Innov*. 2025;20(4):142. doi:10.1007/s12247-025-10043
169. Palanikumar L, Al-Hosani S, Kalmouni M, et al. pH-responsive high stability polymeric nanoparticles for targeted delivery of anticancer therapeutics. *Commun Biol*. 2020;3(1):95. doi:10.1038/s42003-020--0817-4
170. Zielińska A, Carreiró F, Oliveira AM, et al. Polymeric nanoparticles: Production, characterization, toxicology and ecotoxicology. *Molecules*. 2020;25(16):3731. doi:10.3390/molecules25163731
171. Padaga SG, Bhatt H, Ch S, et al. Glycol chitosan-poly(lactic acid) conjugate nanoparticles encapsulating ciprofloxacin: A mucoadhesive, antiquorum-sensing and biofilm-disrupting treatment modality for bacterial keratitis. *ACS Appl Mater Interfaces*. 2024;16(15):18360–18385. doi:10.1021/acsami.3c18061
172. Hassan HAFM, Ali AI, ElDesawy EM, ElShafeey AH. Pharmacokinetic and pharmacodynamic evaluation of gemifloxacin chitosan nanoparticles as an antibacterial ocular dosage form. *J Pharm Sci*. 2022;111(5):1497–1508. doi:10.1016/j.xphs.2021.12.016
173. Kırımlıoğlu GY, Özer S, Büyükköroğlu G, Yazan Y. Moxifloxacin hydrochloride-loaded Eudragit® RL 100 and Kollidon® SR based nanoparticles: Formulation, in vitro characterization and cytotoxicity. *Comb Chem High Throughput Screen*. 2021;24(3):328–341. doi:10.2174/1386207323666200428091945
174. Khan F, Nasir F, Iqbal Z, et al. Improved ocular bioavailability of moxifloxacin HCl using PLGA nanoparticles: Fabrication, characterization, in-vitro and in-vivo evaluation. *Iran J Pharm Res*. 2021;20(3):592–608. doi:10.22037/ijpr.2021.114478.15054
175. Zafar A, Khan N, Alruwaili NK, et al. Improvement of ocular efficacy of levofloxacin by bioadhesive chitosan-coated PLGA nanoparticles: Box–Behnken design, in-vitro characterization, antibacterial evaluation and scintigraphy study. *Iran J Pharm Res*. 2020;19(1):292–311. doi:10.22037/ijpr.2019.15318.13016

176. Duxfield L, Sultana R, Wang R, et al. Development of gatifloxacin-loaded cationic polymeric nanoparticles for ocular drug delivery. *Pharm Dev Technol*. 2016;21(2):172–179. doi:10.3109/10837450.2015.1091839
177. Gupta H, Aqil M, Khar RK, Ali A, Bhatnagar A, Mittal G. Biodegradable levofloxacin nanoparticles for sustained ocular drug delivery. *J Drug Target*. 2011;19(6):409–417. doi:10.3109/1061186X.2010.504268
178. Gupta H, Aqil M, Khar RK, Ali A, Bhatnagar A, Mittal G. Sparfloxacin-loaded PLGA nanoparticles for sustained ocular drug delivery. *Nanomed Nanotechnol Biol Med*. 2010;6(2):324–333. doi:10.1016/j.nano.2009.10.004
179. Kaskoos R. Investigation of moxifloxacin loaded chitosan-dextran nanoparticles for topical instillation into eye: In-vitro and ex-vivo evaluation. *Int J Pharm Investig*. 2014;4(4):164. doi:10.4103/2230-973X.143114
180. Martín V, De La Haba RR, López-Cornejo P, et al. Synergistic antifungal activity against *Candida albicans* between voriconazole and cyclosporine a loaded in polymeric nanoparticles. *Int J Pharm*. 2024;664:124593. doi:10.1016/j.ijpharm.2024.124593
181. Mohammadzadeh S, Shahsavari S, Karimian F, Hashemi SJ, Akbari Javar H, Mollabagher H. Development and characterization of optimized sustained release voriconazole-loaded chitosan nanoparticles for ocular delivery. *J Part Sci Technol*. 2021;7(1):1–10. doi:10.22104/jpst.2021.4769.1183
182. Saleh N, Elshaer S, Girgis G. Biodegradable polymers-based nanoparticles to enhance the antifungal efficacy of fluconazole against *Candida albicans*. *Curr Pharm Biotechnol*. 2022;23(5):749–757. doi:10.2174/1389201022666210708105142
183. Liu Y, Cui X, Zhao L, Zhang W, Zhu S, Ma J. Chitosan nanoparticles to enhance the inhibitory effect of natamycin on *Candida albicans*. *J Nanomater*. 2021;2021:6644567. doi:10.1155/2021/6644567
184. Mohsen AM. Cationic polymeric nanoparticles for improved ocular delivery and antimycotic activity of terconazole. *J Pharm Sci*. 2022;111(2):458–468. doi:10.1016/j.xphs.2021.09.019
185. Chhonker YS, Prasad YD, Chandasana H, et al. Amphotericin-B entrapped lecithin/chitosan nanoparticles for prolonged ocular application. *Int J Biol Macromol*. 2015;72:1451–1458. doi:10.1016/j.ijbiomac.2014.10.014
186. Sánchez-López E, Esteruelas G, Ortiz A, et al. Dexibuprofen biodegradable nanoparticles: One step closer towards a better ocular interaction study. *Nanomaterials*. 2020;10(4):720. doi:10.3390/nano10040720
187. Katara R, Sachdeva S, Majumdar DK. Design, characterization, and evaluation of aceclofenac-loaded Eudragit RS 100 nanoparticulate system for ocular delivery. *Pharm Dev Technol*. 2019;24(3):368–379. doi:10.1080/10837450.2018.1486424
188. Cañadas C, Alvarado H, Calpena AC, et al. In vitro, ex vivo and in vivo characterization of PLGA nanoparticles loading pranoprofen for ocular administration. *Int J Pharm*. 2016;511(2):719–727. doi:10.1016/j.ijpharm.2016.07.055